Lecture Notes in Physics 889

Huey-Wen Lin
Harvey B. Meyer *Editors*

Lattice QCD for Nuclear Physics

Springer

Lecture Notes in Physics

Volume 889

The Lecture Notes in Physics

The series Lecture Notes in Physics (LNP), founded in 1969, reports new developments in physics research and teaching-quickly and informally, but with a high quality and the explicit aim to summarize and communicate current knowledge in an accessible way. Books published in this series are conceived as bridging material between advanced graduate textbooks and the forefront of research and to serve three purposes:

- to be a compact and modern up-to-date source of reference on a well-defined topic
- to serve as an accessible introduction to the field to postgraduate students and nonspecialist researchers from related areas
- to be a source of advanced teaching material for specialized seminars, courses and schools

Both monographs and multi-author volumes will be considered for publication. Edited volumes should, however, consist of a very limited number of contributions only. Proceedings will not be considered for LNP.

Volumes published in LNP are disseminated both in print and in electronic formats, the electronic archive being available at springerlink.com. The series content is indexed, abstracted and referenced by many abstracting and information services, bibliographic networks, subscription agencies, library networks, and consortia.

Proposals should be sent to a member of the Editorial Board, or directly to the managing editor at Springer:

Christian Caron
Springer Heidelberg
Physics Editorial Department I
Tiergartenstrasse 17
69121 Heidelberg/Germany
christian.caron@springer.com

More information about this series at
http://www.springer.com/series/5304

Huey-Wen Lin • Harvey B. Meyer
Editors

Lattice QCD for Nuclear Physics

Springer

Editors
Huey-Wen Lin
Department of Physics
University of Washington
Seattle
Washington
USA

Harvey B. Meyer
Institute of Nuclear Physics
Johannes Gutenberg-Universität Mainz
Mainz
Germany

ISSN 0075-8450 ISSN 1616-6361 (electronic)
Lecture Notes in Physics
ISBN 978-3-319-08021-5 ISBN 978-3-319-08022-2 (eBook)
DOI 10.1007/978-3-319-08022-2
Springer Cham Heidelberg New York Dordrecht London

Library of Congress Control Number: 2014956267

Printed on acid-free paper

Springer is part of Springer Science+Business Media (www.springer.com)

Foreword

The development of quantum chromodynamics over the past few decades as the accepted theory of the strong interactions has transformed almost every aspect of nuclear physics. Many major experimental nuclear physics programs being conducted today at national laboratories in the USA are directly related to QCD, including determination of the internal structure of hadrons and the nature of confinement at Jefferson Laboratory, the properties of the quark gluon plasma at Brookhaven, and the measurement of the neutron electric dipole moment at Oak Ridge National Laboratory. Even in more traditional nuclear structure studies, such as anticipated at the rare isotope beam facility (FRIB) under construction at Michigan State University, the theoretical framework often used today consists of overlapping techniques, with mean field and energy density functionals being used for the heaviest nuclei, shell models for the intermediate mass, numerical solutions of the Schrödinger equation for light nuclei—and underlying all that, the fundamental inter-nucleon interactions based on an effective field theory for QCD, which itself is increasingly informed by direct computation from lattice QCD.

There are various techniques for making theoretical progress in QCD: perturbation theory for high energy collisions, phenomenological effective field theories for low energy processes, and innovative models such as the color glass condensate for low-x physics. However, much of the physics of interest to nuclear physics must be computed nonperturbatively and so for many applications, lattice QCD is the ideal method.

We are now living in a "golden age" for lattice QCD as applied to nuclear physics. This is due to the confluence of increased hardware speed, as well as enormous progress in the past decade in improving computational algorithms. Just as important, though, is the increased awareness among nuclear physicists that we are on the threshold of finally being able to use lattice QCD to accurately answer many of the outstanding questions in nuclear physics. As lattice QCD becomes one of the most potent tools for theorists to unlock the secrets of the nucleus, it becomes increasingly important to train young scientists in the subject. Thus it is with great

pleasure that the INT has hosted this summer school in lattice QCD, and with great anticipation of what this new generation of scientists will eventually teach us.

Seattle, WA, USA David B. Kaplan
April 2014

Preface

Perhaps the most fascinating aspect of the strong interaction of particle physics is the wealth of qualitatively different regimes it exhibits. Modern nuclear physics deals with phenomena typically occurring at energy, momentum, temperature, or density scales between a few MeV and a few GeV. A relatively new goal in the field is to connect nuclear phenomena directly to the fundamental theory of the strong interaction, quantum chromodynamics. QCD has only a few free parameters, and it is remarkable that so much can, in principle, be predicted from so little.

In certain regimes, such as low-energy nuclear few-body systems, effective field theories provide a systematic approach. QCD can then be used to determine their low-energy parameters and to test their range of validity. But certain observables, like the spectrum of excited hadrons and the charge distributions of the nucleon, or the transition from the hadronic phase of QCD to a plasma phase at high temperatures, have no obvious simpler description in terms of effective degrees of freedom. A systematic treatment then involves the full complexity of QCD.

Lattice QCD provides a framework to handle the theory of the strong interaction from first principles in a wide range of energies relevant to nuclear physics. It is a discretized formulation of QCD on a spacetime lattice which preserves its SU(3) gauge symmetry. The latter is key to its ability of handling the theory in its non-perturbative regime. Numerical techniques and high-performance computing are an essential part of lattice QCD. The success of lattice QCD calculations depends thus on its practitioners being proficient both in quantum field theory and in programming and numerical methods.

In the summer school held at the Institute for Nuclear Theory in Seattle, 6–24 August 2012 (http://www.int.washington.edu/PROGRAMS/12-2c/), a series of courses were delivered, aimed at giving graduate students not only an overall understanding of lattice gauge theory, but also at covering in detail how one applies lattice gauge theory to the calculation of key quantities in nuclear physics. The list of lectures held at the school is given hereafter. State-of-the-art algorithms for generating gauge ensembles and fermion propagators were covered. Students performed numerical exercises on using lattice QCD code, analyzing and fitting

data, and on utilizing new hardware, such as graphics processing units (GPUs) and the CUDA environment. In this book you will find the contents of the lectures on the most central physics topics written up. We hope that they provide an accessible and solid introduction to nuclear physics applications in lattice QCD for graduate students and any interested physicist.

Seattle, WA, USA — Huey-Wen Lin
Mainz, Germany — Harvey B. Meyer
April 2014

Contents

Contributors

K.U. Can Department of Physics, Tokyo Institute of Technology, Meguro, Tokyo, Japan

Carleton DeTar Department of Physics and Astronomy, University of Utah, Salt Lake City, UT, USA

William Detmold Center for Theoretical Physics, Massachusetts Institute of Technology, Cambridge, MA, USA

A. Kusno Department of Physics, College of William and Mary, Williamsburg, VA, USA

Huey-Wen Lin Department of Physics, University of Washington, Seattle, WA, USA

E.V. Mastropas Department of Physics, College of William and Mary, Williamsburg, VA, USA

Harvey B. Meyer PRISMA Cluster of Excellence, Institut für Kernphysik and Helmholtz Institut Mainz, Johannes Gutenberg-Universität Mainz, Mainz, Germany

Sinéad M. Ryan School of Mathematics, Trinity College, Dublin, Ireland

Brian C. Tiburzi Department of Physics, The City College of New York, New York, NY, USA

Graduate School and University Center, The City University of New York, New York, NY, USA

RIKEN BNL Research Center, Brookhaven National Laboratory, Upton, NY, USA

James M. Zanotti CSSM, School of Chemistry and Physics, The University of Adelaide, Adelaide, SA, Australia

Chapter 1
Lattice QCD: A Brief Introduction

H.B. Meyer

Abstract A general introduction to lattice QCD is given. The reader is assumed to have some basic familiarity with the path integral representation of quantum field theory. Emphasis is placed on showing that the lattice regularization provides a robust conceptual and computational framework within quantum field theory. The goal is to provide a useful overview, with many references pointing to the following chapters and to freely available lecture series for more in-depth treatments of specifics topics.

1.1 Introduction and Scope

Lattice QCD is a framework in which the strong interactions can be studied from first principles, from low to high energy scales. It is a mature subject started in 1974 [1]. Deep inelastic experiments had shown that in reactions involving a very high momentum transfer, weakly coupled quarks appear as the prominent degrees of freedom at the interaction point. The asymptotic states of the theory, however, were clearly bound states of quarks called hadrons. Lattice QCD provided for the first time a framework in which this apparent dichotomy could be addressed. However, due to the complexity of non-perturbative phenomena at low energies, it is only with the advent of supercomputers that the approach acquired the potential of being quantitatively predictive [2]. By now, lattice QCD is an important source of information for tests of the Standard Model, where it provides results for various hadronic matrix elements that are complementary to those obtained using phenomenological approaches. It has also become a viable basis for calculations of nuclear few-body quantities (see chapter "Nuclear Physics from Lattice QCD"), and for the exploration of part of the QCD phase diagram (chapter "High Temperature and Density in Lattice QCD").

The goal of this introduction is to give a concise overview of the theoretical basis on which the lattice QCD calculations described in the following chapters

H.B. Meyer (✉)
PRISMA Cluster of Excellence, Institut für Kernphysik and Helmholtz Institut Mainz, Johannes Gutenberg-Universität Mainz, D-55099 Mainz, Germany
e-mail: meyerh@kph.uni-mainz.de

H.-W. Lin, H.B. Meyer (eds.), *Lattice QCD for Nuclear Physics*, Lecture Notes in Physics 889, DOI 10.1007/978-3-319-08022-2_1

rest. Several textbooks are available [3–6] for more detailed introductions. Quantum field theory has many facets, and those that are of central importance in lattice QCD are not necessarily the ones most emphasized in standard QFT textbooks, which are mostly concerned with the perturbative calculation of the scattering amplitudes. The presentation is meant to help the interested reader orient himself in the subject, and also to provide the young practitioner with a minimum background to embark on a lattice calculation. A number of excellent lecture series on more specific topics are freely available on the arXiv preprint server, and often I refer the reader to them. The reader is assumed to have had some exposure to the path integral formulation of quantum field theory, and to have some familiarity with the basics of strong interaction physics.

1.2 The Lattice Formulation of Quantum Field Theory

In this section we introduce lattice field theory as a way to 'discretize' continuum field theories. The Euclidean path integral is introduced, but the discussion remains largely at the classical level; quantum effects are treated in the next sections. We treat the cases of the scalar, Dirac spinor and (non-Abelian) gauge fields.

1.2.1 Scalar Field Theory

In this chapter we will be working entirely in d-dimensional Euclidean space; the scalar product of two vectors reads $a \cdot b = a_\mu \delta_{\mu\nu} b_\nu = a_\mu b_\mu$ and there is no distinction between covariant and contravariant indices.

The Euclidean partition function for a real scalar field ϕ reads

$$Z = \int D\phi \ \exp(-S[\phi]) \tag{1.1}$$

with the measure formally defined as $D\phi = \prod_x d\phi(x)$. In continuum field theory, the action in d spacetime dimensions is defined as

$$S[\phi] = \int d^d x \ \left(\frac{1}{2} (\partial_\mu \phi(x))^2 + \frac{1}{2} m^2 \phi^2 + \frac{1}{4!} \lambda \phi^4 \right). \tag{1.2}$$

The parameter m corresponds to the mass of the scalar particle and λ to the strength of its self-interaction. The path integral measure needs to be given a precise meaning, since the partition function (1.1) involves an integral over an accountable number of degrees of freedom. If a perturbative treatment of the theory is desired, propagators and Feynman rules can nonetheless be derived and the corresponding momentum integrals can be regulated using dimensional regularization.

The lattice regularization provides an intuitive way of rendering the number of degrees of freedom countable and all correlation functions finite. The limit of the lattice spacing going to zero can be taken once the (renormalized) correlation functions have been calculated; it is referred to as the 'continuum limit'. Here the interactions do not have to be treated perturbatively.

We will restrict ourselves to four-dimensional cubic lattices,

$$\Lambda = \left\{ x \in \mathbb{R}^d \;\middle|\; x = a\,n,\; n \in \mathbb{Z}^d \right\}. \tag{1.3}$$

The length a is referred to as the lattice spacing. A lattice field $\phi(x)$ is the assignment of a real number to every point on the lattice.

We write unit vectors in the four directions as $\hat{\mu}$, $\mu = 0, 1, \ldots d$. In order to formulate an action for the lattice field theory, it is natural to introduce the discretized forward and backward derivatives

$$\partial_\mu \phi(x) = \frac{1}{a}(\phi(x + a\hat{\mu}) - \phi(x)), \qquad \partial^\star_\mu \phi(x) = \frac{1}{a}(\phi(x) - \phi(x - a\hat{\mu})), \tag{1.4}$$

as well as the symmetric derivative $\tilde{\partial}_\mu = \frac{1}{2}(\partial_\mu + \partial^\star_\mu)$. Discretizing the continuum action in the same way one would discretize differential equations, (making the simplest choices) we arrive at

$$S[\phi] = a^d \sum_x \left(\frac{1}{2}(\partial_\mu \phi(x))^2 + \frac{1}{2} m^2 \phi(x)^2 + \frac{1}{4!}\lambda \phi(x)^4 \right). \tag{1.5}$$

Exercises

1. Show that the finite-difference operators ∂_μ, ∂^*_ν all commute.
2. Show the following properties of the forward and backward derivatives:

$$\partial_\mu(\chi(x)\psi(x)) = \partial_\mu \chi(x)\, \psi(x) + \chi(x)\partial_\mu \psi(x) + a\partial_\mu \chi(x)\partial_\mu \psi(x), \tag{1.6}$$

$$a^d \sum_x \chi(x)\partial_\mu \phi(x) = -a^d \sum_x \partial^*_\mu \chi(x)\, \phi(x). \tag{1.7}$$

3. Show that in the $\lambda \to \infty$ limit, the scalar lattice action reduces to the Ising model

$$S_{\text{Ising}} = -\kappa \sum_x \sigma(x)\sigma(x + a\hat{\mu}) \tag{1.8}$$

with the rescaled field $\sigma(x)$ taking values in $\mathbb{Z}_2 = \{+1, -1\}$. Remember that additive constants in the action do not influence correlation functions and can be dropped.

4. Generalize the lattice treatment of the scalar field theory to a complex scalar field, and to a two-component complex scalar field. The latter case is the relevant model for the Standard Model Higgs.

1.2.1.1 Analysis in Momentum Space

It is worth recalling the representation of lattice fields in momentum space, perhaps familiar to the reader from condensed matter physics. If we set

$$\tilde{\phi}(p) = a^d \sum_x e^{-ipx} \phi(x), \tag{1.9}$$

then clearly $\tilde{\phi}(p + \frac{2\pi}{a} n) = \tilde{\phi}(p)$ for $n \in \mathbb{Z}^d$. The independent momenta are therefore restricted to the Brillouin zone,

$$\mathcal{B} = \left\{ p \in \mathbb{R}^d \;\middle|\; |p_\mu| \le \frac{\pi}{a} \right\} \tag{1.10}$$

and the position-space field can be written as

$$\phi(x) = \int_{\mathcal{B}} \frac{d^d p}{(2\pi)^d} \, e^{ipx} \, \tilde{\phi}(p). \tag{1.11}$$

This representation shows very clearly that the lattice thus introduces a momentum cutoff of order $\frac{1}{a}$, since higher-momentum modes do not appear in Eq. (1.11).

Exercises

1. Show that in momentum space the forward and backward derivatives operators act multiplicatively with the factors

$$\partial_\mu \quad \longrightarrow \quad \tfrac{1}{a}(e^{iap_\mu} - 1), \tag{1.12}$$

$$\partial^*_\mu \quad \longrightarrow \quad \tfrac{1}{a}(1 - e^{-iap_\mu}), \tag{1.13}$$

$$\tilde{\partial}_\mu \quad \longrightarrow \quad i\,\mathring{p}_\mu, \tag{1.14}$$

$$\triangle \equiv \sum_\mu \partial^*_\mu \partial_\mu \quad \longrightarrow \quad -\hat{p}^2, \tag{1.15}$$

   where

$$\mathring{p}_\mu \equiv \tfrac{1}{a} \sin(ap_\mu), \qquad \hat{p}_\mu \equiv \tfrac{2}{a} \sin(\tfrac{1}{2} ap_\mu). \tag{1.16}$$

2. Show that the propagator is given by

$$\langle \phi(x)\phi(y)\rangle = \int_{\mathcal{B}} \frac{d^d p}{(2\pi)^d} \frac{e^{ip(x-y)}}{\hat{p}^2 + m^2} \tag{1.17}$$

$$= \int_{-\pi/a}^{\pi/a} \frac{d^{d-1}\boldsymbol{p}}{(2\pi)^{d-1}} \frac{e^{-\Omega_{\boldsymbol{p}}|x_0-y_0|+i\,\boldsymbol{p}(\boldsymbol{x}-\boldsymbol{y})}}{\frac{2}{a}\sinh(a\Omega_{\boldsymbol{p}})} \tag{1.18}$$

with $\Omega_{\boldsymbol{p}} = \frac{2}{a}\,\mathrm{asinh}(\frac{a}{2}\sqrt{\hat{\boldsymbol{p}}^2 + m^2})$. The second equality is best established using contour integration (see Sect. 1.2.2.2).

1.2.1.2 Symmetries

A very important aspect of any regularization is, how much symmetry of the original action (1.2) it preserves. More precisely, the question is which of the discrete symmetries and which of the continuous symmetry generators are preserved. It is clear that translations, rotations and boosts are no longer continuous symmetries of the lattice action. This is a general downside of the lattice regularization: it breaks space-time symmetries, i.e. the Poincaré group, and only a discrete subgroup remain as a symmetry. Recalling that Noether's theorem applies to continuous symmetries, this implies that on the lattice we cannot expect to find four conserved currents associated with space-time symmetries (the energy-momentum tensor). Fortunately this does not represent an obstacle to most calculations, for reasons explained below.

Exercise Give the list of symmetries of the complex scalar field theory on the lattice. Apart from Poincaré symmetry, have any other symmetries of the continuum theory been broken by the regularization? Give the expression of the conserved current associated with the U(1) symmetry transformation

$$\phi'(x) = e^{i\alpha}\phi(x), \qquad (\phi^*)'(x) = \phi^*(x)e^{-i\alpha}. \tag{1.19}$$

1.2.2 Fermions

From here on, we consider field theories in four spacetime dimensions. In the continuum Euclidean theory, the action for a Dirac fermion of mass m reads

$$S_{\mathrm{f}}[\psi,\bar{\psi}] = \int d^4x\ \bar{\psi}(x)(\gamma_\mu\partial_\mu + m)\psi(x) \tag{1.20}$$

where all four 4×4 matrices γ_μ are hermitian and satisfy $\{\gamma_\mu, \gamma_\nu\} = 2\delta_{\mu\nu}$. Correspondingly, the propagator, which coincides with the Green's function of $(\gamma_\mu \partial_\mu + m)$, reads

$$\langle \psi(x)\bar{\psi}(y)\rangle = \int \frac{d^4p}{(2\pi)^4} \frac{e^{ip(x-y)}}{i\not{p}+m} \tag{1.21}$$

with $\not{p} \equiv p_\mu \gamma_\mu$. Via Wick's theorem, n-point functions can be expressed as a sum of products of propagators with appropriate minus signs.

The original Wilson formulation of fermions on the lattice assigns a Dirac spinor $\psi(x)$ to every lattice site $x \in \Lambda$. The corresponding action [1] reads

$$S_{\mathrm{f}}[\psi, \bar{\psi}] = a^4 \sum_x \bar{\psi}(x)(D_{\mathrm{w}} + m)\psi(x), \tag{1.22}$$

$$D_{\mathrm{w}} = \sum_\mu \left(\gamma_\mu \tilde{\partial}_\mu - a\partial^*_\mu \partial_\mu\right). \tag{1.23}$$

The first-order derivatives are discretized symmetrically in the first term, but an additional term proportional to the lattice Laplacian operator has been added. It is clear that the first-order derivatives alone would not couple neighbouring points, thereby not attributing a large action to certain high-momentum modes; this feature would lead to unwanted additional long-range degrees of freedom called 'doublers'. The doubling problem is fixed by the addition of the Laplacian term. A more precise analysis will be given below in momentum space.

Exercises

1. Verify that the following transformations are symmetries of the Wilson action:
   Parity:

$$\psi(x) \to \gamma_0 \psi(x_0, -\boldsymbol{x}), \qquad \bar{\psi}(x) \to \bar{\psi}(x_0, -\boldsymbol{x})\gamma_0\,; \tag{1.24}$$

   Euclidean time reversal: with $\gamma_5 \equiv \gamma_0\gamma_1\gamma_2\gamma_3$,

$$\psi(x) \to \gamma_0\gamma_5 \psi(-x_0, \boldsymbol{x}), \qquad \bar{\psi}(x) \to \bar{\psi}(-x_0, \boldsymbol{x})\gamma_5\gamma_0\,; \tag{1.25}$$

   Charge conjugation[1]:

$$\psi(x) \to (\bar{\psi}(x)\gamma_0\gamma_2)^\top, \qquad \bar{\psi}(x) \to (\gamma_0\gamma_2\psi(x))^\top. \tag{1.26}$$

[1] This transformation law applies for certain representations of the Dirac matrices, e.g.

$$\gamma_0 = \begin{pmatrix} 0 & 1 \\ 1 & 0 \end{pmatrix}, \qquad \gamma_i = \begin{pmatrix} 0 & -i\sigma^i \\ i\sigma^i & 0 \end{pmatrix}$$

with σ^i the Pauli matrices.

2. Give the expression of the conserved current associated with the U(1) symmetry transformation

$$\psi'(x) = e^{i\alpha}\psi(x), \qquad \bar{\psi}'(x) = \bar{\psi}(x)e^{-i\alpha}. \tag{1.27}$$

3. With respect to the obvious scalar product of lattice fermion fields, show that the Wilson-Dirac operator satisfies the γ_5-hermiticity relation

$$D_{\mathrm{w}}^{\dagger} = \gamma_5 D_{\mathrm{w}} \gamma_5. \tag{1.28}$$

1.2.2.1 Path-Integral Representation of Correlation Functions

Wick's theorem for fermionic n-point functions (see for instance [7], Sec. 4.2.2) has a representation in terms of a path integral over Grassmann variables. Let us recall how this works. Let $\eta_1, \ldots, \eta_n$ and $\bar{\eta}_1, \ldots, \bar{\eta}_n$ be anticommuting generators of a Grassmann algebra. Let also ζ and $\bar{\zeta}$ be n-component vectors of anticommuting variables and A an $n \times n$ c-number matrix. If the 'integration' rules are defined as

$$\int d\eta_i = \int d\bar{\eta}_i = 0, \tag{1.29}$$

$$\int d\eta_i \, \eta_j = \int d\bar{\eta}_i \, \bar{\eta}_j = \delta_{ij}, \tag{1.30}$$

$$\int d\eta_i \, \bar{\eta}_j = \int d\bar{\eta}_i \, \eta_j = 0, \tag{1.31}$$

then the Gaussian integral for the generating functional

$$Z[\zeta, \bar{\zeta}] \equiv \int d\eta_1 \ldots d\eta_n \, d\bar{\eta}_1 \ldots d\bar{\eta}_n \tag{1.32}$$
$$\exp\Big(- \sum_{i,j} (\bar{\eta}_i A_{ij} \eta_j) + \sum_i (\bar{\eta}_i \zeta_i + \bar{\zeta}_i \eta_i) \Big)$$

is given by

$$Z[\zeta, \bar{\zeta}] = c \cdot \det(A) \, \exp\Big(\sum_{i,j} \bar{\zeta}_i (A^{-1})_{ij} \zeta_j \Big). \tag{1.33}$$

Note that the determinant appears in the numerator rather than in the denominator. Applying this machinery to a lattice fermion field ($\eta_i := \psi_\alpha(x)$, $A := D_{\mathrm{w}} + m$), one obtains the following 'path-integral' representation of the lattice n-point functions,

$$\langle \psi(x_1) \ldots \psi(x_n) \, \bar{\psi}(y_1) \ldots \bar{\psi}(y_n) \rangle \tag{1.34}$$
$$= \frac{1}{Z[0,0]} \int D[\psi] D[\bar{\psi}] \, \psi(x_1) \ldots \psi(x_n) \, \bar{\psi}(y_1) \ldots \bar{\psi}(y_n) \, \exp(-S_{\mathrm{f}}[\psi, \bar{\psi}])$$

with

$$D[\psi] = \prod_{\alpha,x} d\psi_\alpha(x), \qquad D[\bar{\psi}] = \prod_{\alpha,x} d\bar{\psi}_\alpha(x). \tag{1.35}$$

Since Wick's theorem gives all correlation functions in terms of the propagator, only the latter remains to be specified. Using Eq. (1.14, 1.15), the expression for the propagator is easily found,

$$\langle \psi(x)\bar{\psi}(y)\rangle = \int_{\mathcal{B}} \frac{d^4p}{(2\pi)^4} \frac{e^{ip(x-y)}}{i\sum_\mu (\mathring{p}_\mu \gamma_\mu) + \frac{1}{2}a\hat{p}^2 + m}. \tag{1.36}$$

The spectrum of a theory is given by the location of the poles in its two-point functions. To find the poles, we first rewrite the momentum-space propagator as

$$\frac{1}{i\sum_\mu (\gamma_\mu \mathring{p}_\mu) + \frac{1}{2}a\hat{p}^2 + m} = \frac{-i\sum_\mu (\gamma_\mu \mathring{p}_\mu) + \frac{1}{2}a\hat{p}^2 + m}{\mathring{p}^2 + (\frac{1}{2}a\hat{p}^2 + m)^2}. \tag{1.37}$$

Exercises

1. Show that

$$\mathring{p}_\mu^2 = \hat{p}_\mu^2 - \frac{1}{4}a^2\hat{p}_\mu^4. \tag{1.38}$$

2. Use this identity to write the denominator of Eq. (1.37) as

$$\mathring{p}^2 + (\tfrac{1}{2}a\hat{p}^2 + m)^2 = \alpha(\boldsymbol{p})\hat{p}_0^2 + \sigma(\boldsymbol{p}), \tag{1.39}$$

$$\alpha(\boldsymbol{p}) \equiv 1 + am + \frac{1}{2}a^2\hat{\boldsymbol{p}}^2, \tag{1.40}$$

$$\sigma(\boldsymbol{p}) \equiv m^2 + (1+am)\hat{\boldsymbol{p}}^2 + \frac{1}{2}a^2\sum_{k<l}\hat{p}_k^2\hat{p}_l^2. \tag{1.41}$$

3. Conclude that the poles of the propagator are located at $p_0 = \pm i\omega_{\boldsymbol{p}}$ with

$$\omega_{\boldsymbol{p}} \equiv \frac{2}{a}\,\mathrm{asinh}\left(\frac{a}{2}\sqrt{\sigma(\boldsymbol{p})/\alpha(\boldsymbol{p})}\right) = \sqrt{m^2 + \boldsymbol{p}^2} + \mathrm{O}(a). \tag{1.42}$$

1.2.2.2 The Propagator in the Time-Momentum Representation

A representation of correlation functions that is particularly useful in lattice QCD is the mixed time-momentum representation $(x_0, \boldsymbol{p})$. The reason is that it allows for a spectral interpretation in terms of energy eigenstates of definite overall momentum $\boldsymbol{p}$. Having located the poles of the propagator, its time-momentum representation

can be obtained by a contour integration using the residue theorem. We choose a rectangular contour with one side coinciding with the segment $[-\pi/a, \pi/a]$ on the real axis, and long vertical sides going up for $x_0 - y_0 > 0$. The contributions from the vertical sides of the rectangle cancel each other, and the contribution from the horizontal side at large Im p_0 is exponentially small; therefore, the $\int_{-\pi/a}^{\pi/a}$ integral is entirely given by the residue of the integrand at the pole $p_0 = +i\omega_{\boldsymbol{p}}$,

$$\langle \psi(x)\bar{\psi}(y)\rangle \overset{x_0>y_0}{=} \int_{-\pi/a}^{\pi/a} \frac{d^3\boldsymbol{p}}{(2\pi)^3} e^{-\omega_{\boldsymbol{p}}(x_0-y_0)} e^{i\,\boldsymbol{p}\cdot(\boldsymbol{x}-\boldsymbol{y})} \rho(\boldsymbol{p}), \tag{1.43}$$

$$\rho(\boldsymbol{p}) \;=\; \left\{ \frac{-i\gamma_\mu \mathring{p}_\mu + \frac{1}{2}a\hat{p}^2 + m}{\alpha(\boldsymbol{p})(-i)\frac{\partial \hat{p}_0^2}{\partial p_0}} \right\}_{p_0 = i\omega_{\boldsymbol{p}}} . \tag{1.44}$$

Explicitly, the result is

$$\langle \psi(x)\bar{\psi}(y)\rangle \overset{x_0\neq y_0}{=} \int_{-\pi/a}^{\pi/a} \frac{d^3\boldsymbol{p}}{(2\pi)^3} \frac{e^{-\omega_{\boldsymbol{p}}|x_0-y_0|+i\,\boldsymbol{p}\cdot(\boldsymbol{x}-\boldsymbol{y})}}{2\mathcal{E}_{\boldsymbol{p}}} \cdot \tag{1.45}$$
$$\left(\mathrm{sign}(x_0-y_0)\frac{1}{a}\sinh(a\omega_{\boldsymbol{p}})\gamma_0 - i\boldsymbol{\gamma}\cdot\mathring{\boldsymbol{p}} + \frac{1}{2}a\hat{\boldsymbol{p}}^2 + m - \frac{a\sigma(\boldsymbol{p})}{2\alpha(\boldsymbol{p})} \right).$$

with $\mathcal{E}_{\boldsymbol{p}}$ defined in Eq. (1.47). The case $x_0 < y_0$ is treated analogously and can be checked by using relation (1.28).

Exercises

1. Show that

$$\rho(\boldsymbol{p}) = \frac{1}{2\mathcal{E}_{\boldsymbol{p}}} \left(\frac{1}{a}\sinh(a\omega_{\boldsymbol{p}})\gamma_0 - i\boldsymbol{\gamma}\cdot\mathring{\boldsymbol{p}} + \frac{1}{2}a\hat{\boldsymbol{p}}^2 + m - \frac{a\sigma(\boldsymbol{p})}{2\alpha(\boldsymbol{p})} \right), \tag{1.46}$$

$$\mathcal{E}_{\boldsymbol{p}} \equiv \frac{\alpha(\boldsymbol{p})}{a}\sinh(a\omega_{\boldsymbol{p}}). \tag{1.47}$$

2. For the case $x_0 = y_0$, show by direct calculation of the p_0 integral that

$$\langle \psi(x)\bar{\psi}(y)\rangle \overset{x_0=y_0}{=} \int_{-\pi/a}^{\pi/a} \frac{d^3\boldsymbol{p}}{(2\pi)^3} \frac{e^{i\,\boldsymbol{p}\cdot(\boldsymbol{x}-\boldsymbol{y})}}{2\mathcal{E}_{\boldsymbol{p}}} \cdot \tag{1.48}$$
$$\left(-i\boldsymbol{\gamma}\cdot\mathring{\boldsymbol{p}} + \frac{1}{2}a\hat{\boldsymbol{p}}^2 + m + \frac{2\mathcal{E}_{\boldsymbol{p}} - a\sigma(\boldsymbol{p})}{2\alpha(\boldsymbol{p})} \right).$$

3. Verify, using Eqs. (1.48) and (1.45), that the propagator satisfies

$$(D_{\mathrm{w}} + m)\langle \psi(x)\bar{\psi}(y)\rangle = \frac{1}{a^4}\delta_{x,y}. \tag{1.49}$$

1.2.3 Gauge Fields

We start by recalling a few properties of gauge fields in the continuum. The fermion theory (1.20) has a global U(1) symmetry. If the single fermion field is replaced by an N-tuplet (corresponding to N 'colors'), the global symmetry becomes $U(N)$. Here we will focus on the SU(N) subgroup. Promoting the latter symmetry to a local one requires introducing gauge fields $A_\mu(x) = A^a_\mu(x)T^a \in \mathrm{su}(N)$ belonging to the Lie algebra. We will use traceless hermitian generators T^a, normalized according to $\mathrm{Tr}\{T^aT^b\} = \frac{1}{2}\delta^{ab}$ and satisfying the commutation relations $[T^a, T^b] = if^{abc}T^c$. The structure constants f^{abc} are real and totally antisymmetric. With $\Lambda(x) \in SU(N)$, the gauge-transformed fields are defined as

$$\psi^\Lambda(x) = \Lambda(x)\psi(x), \qquad \bar\psi^\Lambda(x) = \bar\psi(x)\Lambda(x)^{-1}, \tag{1.50}$$

$$A^\Lambda_\mu(x) = \Lambda(x)A_\mu(x)\Lambda(x)^{-1} + i\,\Lambda(x)\partial_\mu\Lambda(x)^{-1}. \tag{1.51}$$

The covariant derivative of the fermion field

$$D_\mu\psi(x) = (\partial_\mu - iA_\mu(x))\psi(x) \tag{1.52}$$

then transforms like $\psi(x)$ and the fermion action

$$S_\mathrm{f}[\psi,\bar\psi] = \int d^4x\ \bar\psi(x)(\gamma_\mu D_\mu + m)\psi(x) \tag{1.53}$$

is gauge invariant. The field strength tensor

$$G_{\mu\nu} = G^a_{\mu\nu}T^a \equiv \partial_\mu A_\nu - \partial_\nu A_\mu - i[A_\mu, A_\nu] \tag{1.54}$$

(or equivalently $G^a_{\mu\nu} = \partial_\mu A^a_\nu - \partial_\nu A^a_\mu + f^{abc}A^b_\mu A^c_\nu$) transforms covariantly,

$$G^\Lambda_{\mu\nu}(x) = \Lambda(x)G_{\mu\nu}(x)\Lambda(x)^{-1}. \tag{1.55}$$

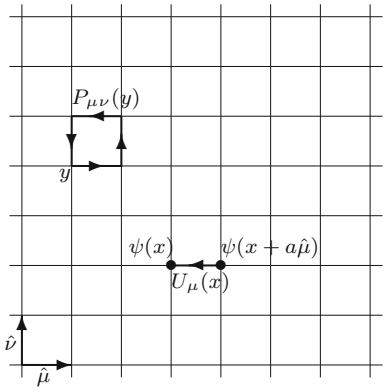

Fig. 1.1 Geometric interpretation of the dynamical variables $\psi(x)$ and $U_\mu(x)$ on a cubic spacetime lattice. The product $U_\mu(x)\psi(x+a\hat\mu)$ transforms in the same way as $\psi(x)$ under the gauge transformation (1.50). The plaquette defined in Eq. (1.64) is also displayed

In particular, the gauge action

$$S_{\rm g}[A] = \frac{1}{2g_0^2}\int d^4x\ {\rm Tr}\{G_{\mu\nu}(x)G_{\mu\nu}(x)\} \tag{1.56}$$

is gauge invariant.

The logic to be followed is similar on the lattice. We consider a gauge transformation acting on a lattice fermion field as in Eq. (1.50). The *raison d'être* of the gauge field is to make finite-difference operators gauge covariant. Specifically, if $U_\mu(x) \in SU(N)$ is a variable which transforms as

$$U_\mu^\Lambda(x) = \Lambda(x)U_\mu(x)\Lambda(x+a\hat{\mu})^{-1}, \tag{1.57}$$

then

$$\nabla_\mu\psi(x) \equiv \frac{1}{a}\left(U_\mu(x)\psi(x+a\hat{\mu}) - \psi(x)\right). \tag{1.58}$$

transforms like $\psi(x)$ itself (see Fig. 1.1). Because of its role in the finite-difference operator, $U_\mu(x)$ is naturally associated with the 'link' joining the points x and $x + a\hat{\mu}$. It is therefore referred to as a 'link variable'. Similarly,

$$\nabla_\mu^*\psi(x) \equiv \frac{1}{a}\left(\psi(x) - U_\mu(x-a\hat{\mu})^{-1}\psi(x-a\hat{\mu})\right). \tag{1.59}$$

also transforms like $\psi(x)$.

From the classical point of view that the lattice action ought to be a discretization of the continuum action, the question of the relation between the link variable $U_\mu(x)$ and the continuum gauge field $A_\mu(x)$ poses itself. To answer this question we recall the definition of a Wilson line. If $x(s)$ is a path from $x(0) = y$ to $x(1) = z$, the Wilson line for a given gauge field is defined by a path-ordered exponential,

$$U([A];z,y) = \mathcal{P}\exp\left(i\int_0^1 ds\,\frac{{\rm d}x_\mu}{{\rm d}s}\,A_\mu(x(s))\right) \tag{1.60}$$

$$\equiv 1 + \sum_{n=1}^{\infty} i^n \int_0^1 ds_1 \int_0^{s_1} ds_2 \ldots \int_0^{s_{n-1}} ds_n\,\frac{{\rm d}x_{\mu_1}}{{\rm d}s_1}\ldots\frac{{\rm d}x_{\mu_n}}{{\rm d}s_n}\cdot \tag{1.61}$$

$$\cdot\ A_{\mu_1}(x(s_1))\ldots A_{\mu_n}(x(s_n)).$$

A crucial property of the Wilson is its transformation under a gauge transformation (1.51) of the field $A_\mu(x)$,

$$U([A^\Lambda];z,y) = \Lambda(z)U([A];z,y)\Lambda(y)^{-1}. \tag{1.62}$$

Comparing this transformation law to Eq. (1.57), we conclude that the link variable can (at the classical level) be thought of as the straight Wilson line going from $x + a\hat{\mu}$ to x, defined on the continuum gauge field.

Exercises

1. Show that $U_t \equiv U([A]; x(t), y)$ satisfies $(\partial_t + \dot{x}_\mu(t)A_\mu(x(t)))U_t = 0$ with $U_0 = 1$.
2. Prove that $U([A]; z, y) \in \mathrm{SU}(N)$. Hint: show that $\partial_t(U_t^\dagger U_t) = 0$.
3. Prove relation (1.62). Hint: show that $\Lambda(z(t))U([A]; z(t), y)\Lambda(y)^{-1}$ satisfies the differential equation in Exercise (1) for the gauge transformed field A^Λ.

1.2.4 Lattice QCD

Given the transformation property (1.58) of the covariant derivative, the following fermion action is gauge invariant,

$$S_{\mathrm{f}}[\psi, \bar{\psi}, U] = a^4 \sum_x \bar{\psi}(x)(D_{\mathrm{w}} + m_0)\psi(x), \tag{1.63}$$

$$D_{\mathrm{w}} = \sum_\mu (\gamma_\mu \tilde{\nabla}_\mu - a\nabla_\mu \nabla_\mu^*)$$

with ∇_μ, ∇_μ^* and $\tilde{\nabla}_\mu$ respectively the forward, backward and symmetrized covariant derivatives, $\tilde{\nabla}_\mu = \frac{1}{2}(\nabla_\mu + \nabla_\mu^*)$. More generally, operators such as

$$\bar{\psi}(x)\gamma_\mu\psi(x), \qquad \bar{\psi}(x)\gamma_\mu\nabla_\nu\psi(x), \quad \text{and} \quad \bar{\psi}(z)U_{\mu_1}(z)\ldots U_{\mu_n}(y - a\hat{\mu}_n)\psi(y),$$

where a quark and an antiquark field are joined by a product of link variables along a given path, are gauge invariant.

Gauge invariant operators made solely of the link variables are easily constructed. The gauge transformation of a Wilson line returning to its starting point, $U([A]; y, y)$ is a similarity transformation (see Eq. (1.57)), and therefore the trace of the loop is gauge invariant. The simplest non-trivial Wilson loop on the lattice is the *plaquette*

$$P_{\mu\nu}(x) = U_\mu(x)U_\nu(x + a\hat{\mu})U_\mu(x + a\hat{\nu})^{-1}U_\nu(x)^{-1}. \tag{1.64}$$

The trace $\mathrm{Tr}\{P_{\mu\nu}(x)\}$ is gauge invariant. For a long-wavelength classical continuum field $A_\mu(x)$, it must therefore be possible to represent it as a linear combination of local gauge invariant operators with appropriate powers of the lattice spacing

a to get the dimensions right. The lowest-dimensional non-trivial gauge invariant operator is $\mathrm{Tr}\{G_{\mu\nu}(x)G_{\rho\sigma}(x)\}$. A straightforward calculation then shows that

$$P_{\mu\nu}(x) = N - \frac{1}{2}a^4 \mathrm{Tr}\{G_{\mu\nu}(x)G_{\mu\nu}(x)\} + \ldots \tag{1.65}$$

The simplest lattice action for the gauge fields is thus

$$S_\mathrm{g}[U] = \frac{2}{g_0^2}\sum_x \sum_{\mu<\nu} \mathrm{Re}\,\mathrm{Tr}\{1 - P_{\mu\nu}(x)\}. \tag{1.66}$$

The total action

$$S[U,\psi,\bar{\psi}] = S_\mathrm{f}[U,\psi,\bar{\psi}] + S_\mathrm{g}[U] \tag{1.67}$$

can thus be regarded (for $N = 3$) as a discretization of the continuum QCD action. For every quark flavor $u, d, s, c \ldots$, a term (1.63) is added to the action with the appropriate (bare) quark mass.

The details of the action (1.67) appear quite arbitrary, however, the precise form of the action should not matter—in a sense specified in Sect. 1.3—in the regime where the correlation lengths are much longer than the lattice spacing. For instance, another widely used type of fermion action is the Kogut-Susskind or 'staggered' action [8,9]. See [10] for a description of staggered fermions as they are used today.

Exercise How do the discrete symmetries C, P and T act on the lattice gauge fields for the action (1.67)?

1.2.4.1 The Path Integral

So far we have presented a lattice action for the fermion and gauge fields. In order to fully formulate the quantum theory, we need to specify the integration measure in the path integral. While this was done in Sect. 1.2.2.1 for the fermions, the definition of the measure

$$D[U] = \prod_{x,\mu} dU_\mu(x) \tag{1.68}$$

still needs to be given. With an integration measure in hand, expectation values are defined as[2]

$$\langle \mathcal{O}_1 \ldots \mathcal{O}_n \rangle = \frac{1}{Z}\int D[U] \int D[\psi]D[\bar{\psi}]\, \mathcal{O}_1 \ldots \mathcal{O}_n \;\exp(-S[U,\psi,\bar{\psi}]). \tag{1.69}$$

[2]The partition function Z is chosen such that $\langle 1 \rangle = 1$.

The measure is required to be '$SU(N)$ invariant'; that is

$$\int dU\ f(UV) = \int dU\ f(VU) = \int dU\ f(U) \qquad \forall\, V \in SU(N). \tag{1.70}$$

An immediate consequence of this property is the following. Suppose we calculate the expectation value of $\mathcal{O}[\psi, \bar{\psi}, U]$. The latter operator can be decomposed into irreducible representations of the SU(N) symmetry group associated with any given point x. It then follows from Eq. (1.70) and the gauge invariance of the action that all the non-singlet contributions vanish. A further crucial observation is that gauge-fixing is not required for the path integral to make sense, because the volume of the gauge group is finite,

$$\int \prod_x d\Lambda(x) = 1. \tag{1.71}$$

An explicit form for the measure is given in the exercise below.

Exercises If $U \in \mathrm{SU}(N)$ is parametrized by $t_1, \ldots t_n$, $n \equiv N^2 - 1$, let

$$g_{ij} \equiv -2\,\mathrm{Tr}\left\{(U^{-1}\tfrac{\partial}{\partial t_i}U)\ (U^{-1}\tfrac{\partial}{\partial t_j}U)\right\} \tag{1.72}$$

1. Verify that g_{ij} is a positive-definite metric on SU(N).
2. Let

$$dU = c\ dt_1 \ldots dt_n\ \sqrt{\det(g)} \tag{1.73}$$

   with c chosen such that $\int dU = 1$. Show that the measure is independent of the parametrization.
3. Show that property (1.70) is satisfied.

1.3 The Approach to the Continuum and Renormalization

We give an overview of how the weak-coupling expansion is set up in the lattice regularization. A systematic and rigorous derivation of the expansion can be found in [11]; many explicit formulae are given in [12]; and a general strategy for numerical perturbative computations was first given in [13]. We then discuss the renormalization group, the approach to the continuum and the 'improvement' of the lattice theory.

1.3.1 The Weak-Coupling Expansion

The perturbative expansion is based on the idea that for g_0 very small, the path integral should be dominated by the fields that minimize the action. Perturbation theory is then a saddle point expansion around such field configurations. The gauge fields minimizing $S_g[U]$ are of the form $U_\mu(x) = \Lambda(x)\Lambda(x + a\hat{\mu})^{-1}$ and are thus gauge-equivalent to the 'unit-configuration' $U_\mu(x) = 1\ \forall \mu, x$. The small fluctuations of the link variables are then parametrized by a gauge potential,

$$U_\mu(x) = \exp(ig_0 a A_\mu(x)), \qquad A_\mu(x) = A^a_\mu(x) T^a. \tag{1.74}$$

If the plaquette entering the action is expanded in the $A_\mu(x)$,

$$P_{\mu\nu}(x) \equiv \exp(ig_0 a^2 G_{\mu\nu}(x)), \qquad G_{\mu\nu}(x) = G^a_{\mu\nu}(x) T^a, \tag{1.75}$$

then one finds

$$S_g[U] = \frac{a^4}{4} \sum_x G^a_{\mu\nu}(x) G^a_{\mu\nu}(x) + \mathrm{O}(g_0^2), \tag{1.76}$$

$$G_{\mu\nu}(x) = \partial_\mu A_\nu(x) - \partial_\nu A_\mu(x) + \mathrm{O}(g_0). \tag{1.77}$$

The relations familiar from continuum field theory are thus recovered, with the derivatives replaced by finite differences. One can also show that the Jacobian of the change of integration variables is of the form

$$dU_\mu(x) = \Big(\prod_{a=1}^{N^2-1} dA^a_\mu(x) \Big) \Big(1 + \frac{g_0^2 N}{12} a^2 A^b_\nu(x) A^b_\nu(x) + \dots \Big). \tag{1.78}$$

Although the lattice QCD path integral exists even prior to gauge fixing, an important aspect of perturbation theory is to factor out the integration over the gauge group. One can show that the condition $\partial^*_\mu A_\mu = 0$ is equivalent to the condition that the variation $\epsilon \partial_\omega A_\mu(x)$ of the field $A_\mu(x)$ under any infinitesimal gauge transformation $\Lambda(x) = 1 + i\epsilon\omega(x)$ is orthogonal to $A_\mu(x)$ itself[3]; it is thus a natural gauge-fixing condition. The result of the procedure is that the perturbative expansion of an observable $\mathcal{O}$ is given by the functional integral

$$\langle \mathcal{O} \rangle = \frac{1}{Z} \int D[U] D[c] D[\bar{c}]\, \mathcal{O}[U]\, \exp(-S_{\mathrm{tot}}[A, c, \bar{c}]), \tag{1.79}$$

[3] With respect to the scalar product $(A, B) = a^4 \sum_{x,\mu,a} A^a_\mu(x) B^a_\mu(x)$.

where c and $\bar{c}$ are Fadeev-Popov ghosts, and

$$S_{\rm tot}[A,c,\bar{c}] = S_{\rm g}[U] + S_{\rm gf}[A] + S_{\rm FP}[A,c,\bar{c}], \tag{1.80}$$

$$S_{\rm FP}[A,c,\bar{c}] = a^4 \sum_x \bar{c}^a(x) \triangle_{\rm FP}^{ab} c^b(x), \tag{1.81}$$

$$S_{\rm gf}[A] = \frac{\lambda_0 a^4}{2} \sum_x \partial_\mu^* A_\mu^a(x) \partial_\nu^* A_\nu^a(x). \tag{1.82}$$

It is understood that $U_\mu(x) = \exp(ig_0 a A_\mu(x))$ and that the integration measure is given by Eq. (1.78), and the Fadeev-Popov operator is given by $\triangle_{\rm FP}\omega(x) \equiv g_0 \partial_\mu^* \, \partial_\omega A_\mu(x)$.

The gauge-fixed action leads to Feynman rules in the usual way. The gauge-field and ghost propagators read

$$\langle A_\mu^a(x) A_\nu^b(y)\rangle = \delta^{ab} \int_{\mathcal{B}} \frac{d^4p}{(2\pi)^4} \frac{e^{i(p(x-y)+\frac{1}{2}ap_\mu - \frac{1}{2}ap_\nu)}}{\hat{p}^2} \cdot \left(\delta_{\mu\nu} - (1-\lambda_0^{-1})\frac{\hat{p}_\mu \hat{p}_\nu}{\hat{p}^2}\right), \tag{1.83}$$

$$\langle c^a(x) c^b(y)\rangle = \delta^{ab} \int_{\mathcal{B}} \frac{d^4p}{(2\pi)^4} \frac{e^{ip(x-y)}}{\hat{p}^2}. \tag{1.84}$$

In the continuum formulation, a momentum cutoff can be problematic in gauge theories since the modes that are cut off depend on the gauge. The way the lattice regularization preserves the consequences of gauge invariance (BRS symmetry [14]) while introducing a momentum cutoff is that more and more vertices appear at higher orders.

The fermions also lead to Feynman rules as in the continuum; the propagator was given in Eq. (1.36), and the quark-quark-gluon vertex is given by

$$ig_0 (T^a)_{ij} \left(\gamma_\mu \cos(\tfrac{1}{2}a(p+p')_\mu) - i \sin(\tfrac{1}{2}a(p+p')_\mu)\right), \tag{1.85}$$

with p the incoming momentum of a quark with color index j and p' the outgoing momentum of the other quark line.

The vertices rapidly become algebraically complex to write down. It soon becomes essential to employ an automated way of generating the Feynman rules [13], see [15] for an overview of recent results obtained in this way. High-order lattice perturbation theory has been used to determine the strong coupling constant [16].

1.3.2 The Renormalization Group

Lattice QCD (see Eqs. (1.63), (1.66), (1.67)) can formally be viewed as a four-dimensional classical statistical mechanics system. Thus removing the cutoff from the quantum field theory, i.e. taking the continuum limit, can be viewed as the approach to a second order phase transition where all correlation lengths in lattice units[4] diverge. First the values of the parameters for which this happens must be found. We consider initially the case of the pure-gauge theory.

For illustration, we consider one particular observable that may be computed in perturbation theory, the rectangular Wilson loop

$$\mathcal{L}_\mu(x,d) \equiv U_\mu(x)U_\mu(x+a\hat{\mu})\dots U_\mu(x+(d-a)\hat{\mu}), \tag{1.86}$$

$$W_{\mu\nu}(x,d,d') \equiv \mathcal{L}_\mu(x,d)\mathcal{L}_\nu(x+d\,\hat{\mu},d')\mathcal{L}_\mu(x+d'\hat{\nu},d)^{-1}\mathcal{L}_\nu(x,d')^{-1} \tag{1.87}$$

As we shall see in Sect. 1.4.1, if we define a *static potential* $V(R)$ via

$$\langle W_{0k}(x,R,T)\rangle \overset{T\to\infty}{=} c(R)\exp(-TV(R)) + \dots, \tag{1.88}$$

it has the interpretation of the potential energy between two quarks in the limit where the latter become infinitely massive. To remove an ultraviolet-divergent additive constant, we consider the 'static force' $F(R) \equiv -\frac{\partial V}{\partial R}$. Computationally, the force also depends on the bare coupling and the lattice spacing.[5] A one-loop calculation in the pure SU(N) gauge theory yields the result

$$F(R,g_0,a) \overset{R\gg a}{=} \frac{C_F}{4\pi R^2}\left(g_0^2 + \frac{11N}{24\pi^2}g_0^4(\log(R/a)+c) + \mathrm{O}(g_0^6)\right) \tag{1.89}$$

with $C_F = (N^2-1)/(2N)$ and c a numerical constant. Now, we expect the force at a fixed separation R to reach a finite limit when $a \to 0$. The form (1.89) clearly shows that this is only possible if g_0 is adjusted as a function of a. How exactly it must be adjusted can be worked out by requiring that F actually be independent of a,

$$0 = a\frac{d}{da}F(R,g_0(a),a) = \left(a\frac{\partial}{\partial a} - \beta(g_0)\frac{\partial}{\partial g_0}\right)F(R,g_0,a)\Big|_{g_0=g_0(a)}, \tag{1.90}$$

with

$$\beta(g_0) \equiv -a\frac{\partial g_0}{\partial a}. \tag{1.91}$$

[4] The correlation lengths λ are defined by the fall-off of correlation functions, $C(x) \sim \exp(-|x|/\lambda)$.

[5] Dimensional analysis implies $F(R,g_0,a) = \frac{1}{a^2}\hat{F}(R/a,g_0)$.

Inserting the one-loop expression (1.89) into Eq. (1.90), one finds

$$\beta(g_0) = -b_0 g_0^3, \qquad b_0 = \frac{11N}{48\pi^2}. \tag{1.92}$$

The definition (1.91) of $\beta(g_0)$ can now be read as a differential equation for g_0. The negative value of the beta function means that g_0 must be made smaller in order to reduce the lattice spacing. The asymptotic solution of the differential equation is

$$g_0^2 = -\frac{1}{b_0 \log(a\mu)} + \dots \tag{1.93}$$

This is the expression of the 'asymptotic freedom' property of QCD at the level of the bare regularized theory. Note that an arbitrary mass scale μ had to be introduced. Its appearance is sometimes referred to as dimensional transmutation.

More generally, consider first the pure SU(N) gauge theory in perturbation theory. The bare parameters of the theory, g_0 and λ_0, as well as the momentum-space bare n-point correlation functions $G_0(p_1, \dots, p_n)$ of the gauge potential A_μ^a, can be traded for renormalized parameters g, λ and renormalized correlation functions $G(p_1, \dots, p_n)$. The latter have a finite continuum limit; they are well-defined functions of the external momenta, g, λ and a renormalization scale μ that is introduced when defining the finite-part of correlation functions. One could say that the divergences have been absorbed into the bare parameters. The latter can be adjusted as a function of the lattice spacing in such a way that g, μ and λ stay constant as $a \to 0$. The bare coupling g_0 can then be expressed as a function of $a\mu$ and a renormalized coupling g. For instance, a renormalized coupling based on the static force may be introduced by setting

$$F(R) = \frac{C_F g^2(R)}{4\pi R^2} \qquad \text{(defines } g(R)\text{)}. \tag{1.94}$$

The perturbative result (1.89) then shows that

$$g^2(r) = g_0^2 + \frac{11N}{24\pi^2} g_0^4 \log(\bar{r}/a) + \mathrm{O}(g_0^6), \qquad \bar{r} \equiv r\, \exp(c). \tag{1.95}$$

In the presence of fermions, the coefficient of the beta function is modified,

$$b_0 = \frac{11N - 2N_\mathrm{f}}{48\pi^2}. \tag{1.96}$$

Thus asymptotic freedom remains a property of the theory as long as $N_\mathrm{f} < \frac{11}{2}N$. In addition to g_0 and λ_0, the fermion masses need to be renormalized. While in the continuum theory, chiral symmetry prevents the appearance of an additive correction to the masses, the explicit breaking of chiral symmetry by the Wilson action (see Sect. 1.5.2) means that a tuning of the bare mass m_0 to a 'critical' value m_c is

necessary in order to reach the point where the renormalized quark mass $\overline{m}$ vanishes. One writes

$$\overline{m} = Z_m(m_0 - m_c). \tag{1.97}$$

In the statistical-mechanics language, $g_0 = 0$ corresponds to a free-field theory and the critical point is thus a Gaussian one. However, the quantities that are of interest from the quantum field theory point of view are typically ratios of correlation lengths corresponding (at the non-perturbative level) to ratios of hadron masses.

1.3.3 The Continuum Limit and Universality

We have so far looked at a specific discretization of the continuum action, the Wilson action. There is a degree of arbitrariness in the choice of the discretization. However, the continuum limit is *universal*, as implied by the theory of critical phenomena. Ratios of correlation lengths associated with source fields of different quantum numbers do not depend on the details of the action. Only the list of long-wavelength modes, the dimensionality of space and the symmetries of the action matter.

As far as the quantum field theory is concerned, the property of universality implies in particular that if physical renormalization conditions are imposed (e.g. a momentum-subtraction scheme, or the renormalized coupling defined from the static $\bar{Q}Q$ force), the results will be exactly the same as if dimensional regularization had been used. If a renormalization scheme is used which is tied up with the regularization (such as minimal subtraction), the results differ by a finite renormalization of the parameters $(g, \bar{m}, \lambda)$ and the fields. We refer the reader to [17] for an in-depth discussion of renormalization.

In practical calculations it is important to know at what rate the continuum limit is approached. An important framework to analyze this question was developed by Symanzik [18]. The idea is to write down an effective (continuum) theory for the long-wavelength[6] degrees of freedom of the lattice fields. The effective theory is non-renormalizable, but comes with a clear power-counting scheme. The lowest-order Lagrangian, if all goes according to plan, is the continuum QCD Lagrangian. All higher-dimensional operators consistent with the symmetries of the lattice action contribute, however their coefficients are suppressed by powers of the lattice spacing. The discussion is thus analogous to the low-energy description of beyond the Standard Model physics if one identifies a^{-1} with the scale of 'new physics'. One unusual aspect is that here not only Lorentz-scalar operators can appear, due to the breaking of Lorentz symmetry by the lattice regulator.

[6]Compared to the lattice spacing.

In the language of the Symanzik effective field theory, the dimension-three operator $\bar{\psi}\psi$ must be included with a coefficient of order $1/a$ for the case of the Wilson action. This statement is equivalent to the additive renormalization of the quark mass in Eq. (1.97). However, direct inspection of the symmetries shows that no other operators of dimension $d < 5$ appear that are not already included in the naive continuum limit of the Wilson action. This is the real reason why Wilson lattice QCD is a valid regularization of QCD. The discretization of the continuum QCD action in a classical way was, in retrospect, only a useful guide. However, this procedure did allow for the setup of the perturbative expansion in a relatively standard way.[7]

From a practical point of view, the most important prediction of Symanzik's analysis applied to the Wilson action is that the continuum limit is approached asymptotically with a correction term of $\mathrm{O}(a)$ multiplying a power series in $\log(a)$. In the pure gauge theory, the corrections are of order a^2. It should be emphasized that the approach to the continuum is predictable because of asymptotic freedom. Since the continuum limit is at $g_0 = 0$, the scaling dimension of operators is in first approximation equal to their naive engineering dimension.

1.3.4 Improvement

In practice, the approach to the continuum with $\mathrm{O}(a)$ corrections can lead to large systematic uncertainties on the final results, since it is computationally very costly to reduce the lattice spacing. Therefore, a strategy has been developed to accelerate the approach to the continuum [20, 21].

One way to formulate the problem is the following. One wants to tune the coefficients of certain operators in the lattice theory such that in the action of the Symanzik effective theory, the coefficients of the dimension-five operators vanish. This condition guarantees for instance that the spectrum (masses and dispersion relations of hadrons) approaches its continuum limit with $\mathrm{O}(a^2)$ corrections (up to logarithms).

The symmetries of continuum QCD and the equations of motion can be used to reduce the list of dimension-five operators in the Symanzik effective theory. Then these operators are carried over in 'discretized' form to the lattice theory. It turns out that, apart from a rescaling of the gauge action and the quark mass term, the only new term appearing is the 'Pauli' or 'clover' term,

$$S \to S + \frac{i}{4} c_{\mathrm{sw}} a^5 \sum_x \bar{\psi}(x) \sigma_{\mu\nu} \hat{G}_{\mu\nu} \psi(x). \tag{1.98}$$

[7] Recently, the use of a gauge action with no obvious classical continuum limit, but respecting the same symmetries as the Wilson gauge action has been studied [19].

Here $\sigma_{\mu\nu} = \frac{i}{2}[\gamma_\mu, \gamma_\nu]$ and $\hat{G}_{\mu\nu}$ is a lattice-site centered discretization [20] of the field strength tensor $G_{\mu\nu}$. A condition to determine the value of the coefficient $c_{\rm sw}$ that will eliminate the $\mathrm{O}(a)$ effects is provided by requiring that the PCAC relation (see Sect. 1.5.1.1) be satisfied under different kinematic conditions [22]. In imposing the condition, one must take into account that also composite operators such as the axial current receive improvement terms.

1.4 Observables

In order to illustrate the way lattice QCD is used, we describe three types of observables: the Wilson loop, the hadron spectrum and the chiral condensate.

1.4.1 The Wilson Loop and Its Interpretation

Apart from local operators, extended gauge-invariant operators such as

$$\mathcal{O}_r(x) = \bar{Q}(x)\mathcal{L}_1(x,r)Q'(x+r\boldsymbol{e}_1), \tag{1.99}$$

$$\tilde{\mathcal{O}}_r(x) = \bar{Q}'(x+r\boldsymbol{e}_1)\mathcal{L}_1(x,r)^{-1}Q(x), \tag{1.100}$$

can be used to probe mesons with different quantum numbers. Here Q and Q' are meant to represent different quark flavors. It is interesting to consider the two-point function $\langle\tilde{\mathcal{O}}_r(x+t\boldsymbol{e}_0)\,\mathcal{O}_r(x)\rangle$ in the limit where the quark mass goes to infinity.

For a large quark mass, the quark propagator in a given background gauge field can be expanded in a geometric series,

$$(D_{\rm w}+m)^{-1} = \frac{1}{m}\sum_{n=0}^{\infty}\left(\frac{-D_{\rm w}}{m}\right)^n. \tag{1.101}$$

Since $D_{\rm w}$ only couples nearest neighbours, $(D_{\rm w}^n\psi)(x)$ vanishes for $\frac{1}{a}\sum_{\mu=0}^{3}|x_\mu| > n$ if $\psi(x) = u\delta_{0,x}$ is a source field located at the origin, u being a 12-component colored spinor. For $x = (x_0, \mathbf{0})$ with $x_0 > 0$, the leading contribution

$$((D_{\rm w}+m)^{-1}\psi)(x) = \frac{\exp(-x_0\log(am))}{2m}\,\mathcal{L}_0(0,x_0)\,(1+\gamma_0)\,u \cdot(1+\mathrm{O}((am)^{-2})) \tag{1.102}$$

is determined by the Wilson line joining the origin to x.

Thus, if we perform the Wick contractions for the correlator $\langle \mathcal{O}_r(x)\, \tilde{\mathcal{O}}_r(0)\rangle$, we obtain a Wilson loop,

$$\begin{aligned}\langle \tilde{\mathcal{O}}_r(x + t\boldsymbol{e}_0)\, \mathcal{O}_r(x)\rangle &= c\ \exp(-2x_0 \log(am))\ \mathrm{Tr}\,\{W_{01}(x, r, t)\} \\ &\sim \exp(-tV(r)),\end{aligned} \tag{1.103}$$

with c a constant. Writing the expectation value of the Wilson loop as the two-point function of $\bar{Q}Q$ operators with static quarks separated by a distance r suggests the interpretation anticipated in Eq. (1.88), namely, that it falls off exponentially in Euclidean time, with an exponent given by the meson energy. The latter consists of the (divergent) quark self-energies and the r-dependent interaction energy, or 'static potential'. The quark self-energies drop out in the force $F(r) = -\frac{\partial V}{\partial r}$. The latter is often used in practice as a way of 'setting the scale', most commonly by defining the reference length r_0 through the condition $r_0^2 F(r_0) = 1.65$ [23]. The physical value of r_0 is about 0.50 fm [24].

1.4.1.1 The Strong-Coupling Expansion

The Wilson loop was originally proposed as an order parameter for the confinement of quarks [1]. If all quarks are made very massive, the potential energy between any two quarks has either an area law, $\langle W_{0k}(0, r, t)\rangle \sim \exp(-\sigma rt)\rangle$, or a perimeter law, $\langle W_{0k}(0, r, t)\rangle \sim \exp(-m(r + t))\rangle$. According to the interpretation derived in Sect. 1.4.1, the two cases distinguish respectively between the static force $F(r)$ going to a non-vanishing or vanishing value at long distances.

The strong-coupling expansion is, in a sense, particularly natural on the lattice, and simpler than the weak-coupling expansion. In this context it is customary to introduce the parameter

$$u \equiv \frac{1}{g_0^2} \tag{1.104}$$

and to expand the partition functions and observables in powers of β. The Haar measure plays a central role. Consider a single link variable U. The only non-vanishing integrals of a monomial in components of U and U^* up to order 2 included are

$$\int dU = 1, \qquad \int dU\, U_{ij} U^*_{lk} = \frac{1}{N}\delta_{il}\delta_{jk}. \tag{1.105}$$

In addition, there is the 'baryon-like' contribution

$$\int dU\, U_{i_1 j_1} \ldots U_{i_N j_N} = \frac{1}{N}\epsilon_{i_1 \ldots i_N}\, \epsilon_{j_1 \ldots j_N}. \tag{1.106}$$

To compute the partition function

$$Z_u = \int DU \;\; \exp\Big(u \sum_{x,\mu,\nu} \mathrm{Tr}\,\{P_{\mu\nu}(x)\}\Big), \tag{1.107}$$

we write

$$\begin{aligned} \exp\Big(u \sum_{x,\mu,\nu} \mathrm{Tr}\,\{P_{\mu\nu}(x)\}\Big) &= \prod_p \exp(u\mathrm{Tr}\,\{P_p\}) \\ &= \sum_{\{n_p\}} u^{\sum_p n_p} \prod_p \frac{1}{n_p!} \mathrm{Tr}\,\{P_p\}^{n_p}, \end{aligned} \tag{1.108}$$

where $p \equiv (x, \mu, \nu)$ is the label of an oriented plaquette. Diagrammatically, in order to compute the order u^n we must lay down n tiles on the cubic faces of the lattice.

Consider then the expectation of a Wilson loop,

$$\langle W_{0k}(0, r, t)\rangle = \frac{1}{Z_u} \int DU \; W_{0k}(0, r, t) \; \exp\Big(u \sum_{x,\mu,\nu} \mathrm{Tr}\,\{P_{\mu\nu}(x)\}\Big). \tag{1.109}$$

The Wilson loop contains at most a single power of any link variable. In view of Eq. (1.105), each link variable must be 'saturated' by a corresponding factor of the link variable coming from the expansion of the exponential. Let $A = rt/a^2$. The first non-trivial contribution appears at order u^A and comes when the entire surface of the Wilson loop is 'tiled' with plaquettes from the action. The integral then gives

$$\langle W_{0k}(0, r, t)\rangle \sim u^A. \tag{1.110}$$

Thus we have obtained an area law with

$$a^2\sigma = -\log u, \qquad u \to 0. \tag{1.111}$$

Similarly, the mass gap m_G of the pure gauge theory (corresponding to a 'glueball') can be computed by considering the plaquette-plaquette correlator, $\sum_{i,j=1}^{3} \langle P_{ii}(t, \mathbf{0}) P_{jj}(0)\rangle \sim \exp(-m_G t)$. The result is in leading order

$$am_G = -4 \log u, \qquad u \to 0. \tag{1.112}$$

The reader is invited to consult [3] for a systematic discussion of the strong-coupling expansion.

1.4.1.2 Quark Confinement

That the theory exhibits linear confinement in the strong coupling regime $g_0^2 \gg 1$ does not mean that this feature is present near the continuum limit ($g_0^2 \ll 1$). As a case in point, the 'compact' formulation of U(1) gauge theory admits a phase transition at a bare coupling of order unity, beyond which the static potential is of the Coulomb type. All numerical evidence points to a finite string tension σ in the continuum limit of SU($N \geq 2$) gauge theory; see for instance [25, 26]. Quite a bit can be inferred, however, by assuming that the linear potential survives the continuum limit, and that the relevant effective degrees of freedom of a large Wilson loop are the two transverse fluctuations of a two-dimensional sheet in four dimensions [27, 28]. An effective bosonic string theory has been developed based on this picture, yielding an expansion of the static potential in powers of $1/r$,

$$V(r) = \mu + \sigma r - \frac{\pi}{12r} + \ldots \tag{1.113}$$

The effective string theory makes even stronger predictions for the corrections to the linear potential at large r; see [29] and references therein. These sharp predictions still remain to be fully tested by numerical simulations, but there is good numerical evidence that the static potential follows the prediction (1.113). Moreover, the spectrum predicted by the Nambu-Goto string action provides an excellent description of the low-lying (closed-string) states [30].

1.4.2 Hadron Spectroscopy

Here we will adopt a continuum notation and consider that we are in the infinite-volume, continuum Euclidean theory. The main purpose of this section is to show that the spectrum of stable hadrons can be extracted from the long-distance behavior of Euclidean correlation functions. An explicit analytic continuation of the correlation functions to Minkowski space is not required.

For concreteness we will consider the simplest case of the pion. From Eq. (1.18), we saw that the energy of a scalar particle could be read off from the large Euclidean time of the propagator in the time-momentum representation. The form of the free-field propagator, however, generalizes to (even non-perturbatively) interacting field theories via the Källen-Lehmann spectral representation. The Heisenberg representation, continued to Euclidean time, reads

$$\hat{\phi}(x) = e^{H|x_0| - i\boldsymbol{P}\cdot\boldsymbol{x}}\, \hat{\phi}(0)\, e^{-H|x_0| + i\boldsymbol{P}\cdot\boldsymbol{x}} \tag{1.114}$$

Suppose we use as an interpolating operator $\hat{\phi}(x) = \bar{d}\gamma_5 u$ and write

$$\langle 0|\hat{\phi}(x)|\boldsymbol{p}\rangle = \sqrt{\phi_\pi}\, e^{-E_{\boldsymbol{p}}|x_0| + i\boldsymbol{p}\cdot\boldsymbol{x}}. \tag{1.115}$$

Then define

$$G(x_0, \boldsymbol{p}) \equiv \int d^3x \; e^{-i\,\boldsymbol{p}\cdot\boldsymbol{x}} \langle 0|\hat{\phi}(x)\hat{\phi}(0)^\dagger|0\rangle = \int d^3x \; e^{-i\,\boldsymbol{p}\cdot\boldsymbol{x}} \; \langle \phi(x)\phi(0)^\dagger\rangle. \tag{1.116}$$

Inserting a complete set of states of total momentum $\boldsymbol{p}$, and taking into account the fact that the next states above the pion form a continuum of three-pion states,[8]

$$1 = \int \frac{d^3\boldsymbol{p}}{(2\pi)^3 2E_{\boldsymbol{p}}} |\boldsymbol{p}\rangle\langle\boldsymbol{p}| + (\text{projector onto states of energy} > 3m_\pi). \tag{1.117}$$

we have

$$G(x_0, \boldsymbol{p}) \overset{|x_0|\to\infty}{=} \phi_\pi \, \frac{e^{E_{\boldsymbol{p}}|x_0|}}{2E_{\boldsymbol{p}}} + \mathrm{O}(e^{-3m_\pi|x_0|}). \tag{1.118}$$

A typical operator that couples to the nucleon is (here $C = \gamma_0\gamma_2$)

$$\chi_\alpha(x) = \epsilon_{abc}(u^{a\,\top} C\,\gamma_5 d^b) u^a_\alpha(x). \tag{1.119}$$

However, often operators are used that do not transform as a Dirac spinor under boosts. In that case the other symmetries can still be used to constrain the possible form of the two-point function. One can decompose

$$C_2(x_0, \boldsymbol{p})_{\alpha\beta} \equiv \int d^3x \; e^{-i\,\boldsymbol{p}\cdot\boldsymbol{x}} \langle \chi_\alpha(x)\bar{\chi}_\beta(0)\rangle \tag{1.120}$$

$$= (C_2^+(x_0, \boldsymbol{p}) + C_2^-(x_0, \boldsymbol{p}))_{\alpha\beta}, \tag{1.121}$$

with

$$C_2^+(x_0, \boldsymbol{p}) \equiv \tfrac{1}{2}(1+\gamma_0) C_2(x_0, \boldsymbol{p}) \tag{1.122}$$

$$= \tfrac{1}{2}(1+\gamma_0)\Big(\mathcal{F}(x_0, \boldsymbol{p}^2) - i\,\mathcal{G}(x_0, \boldsymbol{p}^2)\; \boldsymbol{p}\cdot\boldsymbol{\gamma}\Big),$$

$$C_2^-(x_0, \boldsymbol{p}) \equiv \tfrac{1}{2}(1-\gamma_0) C_2(x_0, \boldsymbol{p}) \tag{1.123}$$

$$= \tfrac{1}{2}(1-\gamma_0)\Big(\mathcal{F}(-x_0, \boldsymbol{p}^2) - i\,\mathcal{G}(x_0, \boldsymbol{p}^2)\; \boldsymbol{p}\cdot\boldsymbol{\gamma}\Big).$$

Charge conjugation implies that $\mathcal{G}$ is even in x_0. Spectral positivity implies that $\gamma_0 C_2$ is a Hermitian, positive-definite matrix. Thus, the functions $\mathcal{F}$ and $\mathcal{G}$ are real and must satisfy

$$-\mathcal{F}(x_0, \boldsymbol{p}^2)\; \mathcal{F}(-x_0, \boldsymbol{p}^2) \geq \boldsymbol{p}^2 \mathcal{G}(x_0, \boldsymbol{p}^2)^2, \tag{1.124}$$

$$\mathrm{sign}(x_0)\,(\mathcal{F}(x_0, \boldsymbol{p}^2) - \mathcal{F}(-x_0, \boldsymbol{p}^2)) \geq 0. \tag{1.125}$$

[8] One-particle states are normalized according to $\langle \boldsymbol{p}'|\boldsymbol{p}\rangle = (2\pi)^3 2E_{\boldsymbol{p}}\delta(\boldsymbol{p}-\boldsymbol{p}')$.

At zero momentum, $C_2^+(x_0, \mathbf{0})$ receives contributions only from positive-parity baryons, while $C_2^-(x_0, \mathbf{0})$ only couples to negative-parity baryons (see the transformation of spinors under parity, Eq. (1.24)). Thus, one may extract the proton mass m_p from the long-distance part of the projected correlator

$$\mathrm{Tr}\,\{C_2^+(x_0, \mathbf{0})\} \sim |\chi_\mathrm{p}|^2 \exp(-m_\mathrm{p} x_0), \qquad x_0 \to +\infty, \tag{1.126}$$

where the trace acts on the spin indices. Many more aspects of spectroscopy calculations are covered in chapter "Lattice Methods for Hadron Spectroscopy".

1.4.3 Spontaneous Chiral Symmetry Breaking and Low-Energy Constants

In view of the special role of the pions in QCD as pseudo-Goldstone bosons associated with the spontaneous breaking of chiral symmetry, both their masses and couplings to the axial current are of interest. Consider the case where two degenerate quark flavors, up and down, are very light and let $\psi = (u, d)^\top$. Current-algebra relations imply the Gell-Mann–Oakes–Renner (GMOR) relation

$$F_\pi^2 m_\pi^2 \overset{m\to 0}{=} 2m\,\Sigma, \qquad \Sigma = -\frac{1}{2}\lim_{m\to 0}\lim_{V\to 0}\langle\bar{\psi}\psi\rangle, \tag{1.127}$$

giving the leading-order dependence of the pion mass in terms of the quark mass. The pion decay constant F_π is defined by (the axial current A_μ^a is defined in Eq. (1.143) below)

$$\langle 0|A_\mu^a(0)|\pi^b\rangle = ip_\mu\,\delta^{ab} F_\pi, \tag{1.128}$$

and its value (92.2 MeV) is extracted from the weak decay $\pi^- \to \mu^-\bar{\nu}_\mu$. In lattice QCD it can be extracted for instance from the two-point function

$$\int d^3x\ \langle A_0^a(x) A_0^b(0)\rangle \overset{|x_0|\to\infty}{=} \frac{\delta^{ab}}{2} F_\pi^2 m_\pi\ \exp(-m_\pi|x_0|). \tag{1.129}$$

The GMOR relation (1.127) can be used to estimate the chiral condensate Σ, knowing m_π and F_π for a range of small quark masses. However, the condensate can also be extracted in an independent way. Consider the average spectral density of the Dirac operator,

$$\rho(\lambda, m) = \frac{1}{V}\sum_{k=1}^{\infty}\langle\delta(\lambda - \lambda_k)\rangle. \tag{1.130}$$

The Banks-Casher relation [31] gives the condensate as the density of modes of the Dirac operator around the origin in the chiral limit,

$$\lim_{\lambda\to 0}\lim_{m\to 0}\lim_{V\to\infty}\rho(\lambda,m)=\frac{\Sigma}{\pi}. \tag{1.131}$$

This relation has been used as a way to compute the chiral condensate in the chiral limit [32]. Other methods exist as well,[9] and a recent average given by the FLAG2 report [34] is

$$\Sigma^{1/3}=270(7)\,\mathrm{MeV} \tag{1.132}$$

in QCD with two flavors. The GMOR relation is found to be a good approximation well beyond the physical values of the light-quark masses. The level of accuracy reached in lattice calculations is however such that low-energy constants that appear at higher orders in chiral perturbation theory are being determined with competitive accuracy [34].

1.5 Theory Topics for the Lattice Practitioner

We give an introduction to a few theory topics which are, on one hand, of general interest for aspiring quantum field theorists, and which on the other hand have proved important in practical lattice calculations.

1.5.1 Ward Identities

Suppose that the Euclidean action $S[\psi,\bar{\psi},U]$ is invariant under a global transformation of the fields. Promoting the transformation to a local one generates interesting relations among correlation functions. As an example in lattice QCD with the Wilson action, consider then the local transformation

$$\psi'(x)=e^{i\alpha(x)}\psi(x),\qquad \bar{\psi}'(x)=\bar{\psi}(x)e^{-i\alpha(x)}. \tag{1.133}$$

One finds, for an infinitesimal transformation,

$$S[\psi',\bar{\psi}',U]=S[\psi,\bar{\psi},U]+\delta S[\psi,\bar{\psi},U], \tag{1.134}$$

[9] At the time of writing, the Yang-Mills gradient flow provides probably the most efficient way to compute the chiral condensate with precision [33].

$$\delta S[\psi,\bar{\psi},U] = i\ a^4 \sum_x \partial_\mu \alpha(x) J_\mu(x) + \mathrm{O}(\alpha^2), \tag{1.135}$$

with

$$J_\mu(x) = \tfrac{1}{2}\big(\bar{\psi}(x+a\hat{\mu})(1+\gamma_\mu)U_\mu^\dagger(x)\psi(x) \\ -\bar{\psi}(x)(1-\gamma_\mu)U_\mu(x)\psi(x+a\hat{\mu})\big), \tag{1.136}$$

while the integration measure is left invariant. If $\mathcal{O}$ is an observable which transforms according to

$$\mathcal{O}[\psi',\bar{\psi}',U] = \mathcal{O}[\psi,\bar{\psi},U] + \delta\mathcal{O}[\psi,\bar{\psi},U] + \mathrm{O}(\alpha^2), \tag{1.137}$$

then

$$\langle\mathcal{O}\rangle = \int DU\, D\psi' D\bar{\psi}'\ \mathcal{O}[\psi',\bar{\psi}',U]\ \exp(-S[\psi',\bar{\psi}',U]) \tag{1.138}$$

$$= \int DU\ \underbrace{D\psi' D\bar{\psi}'}_{=D\psi D\bar{\psi}}\ (\mathcal{O}[\psi,\bar{\psi},U] + \delta\mathcal{O}[\psi,\bar{\psi},U]) \\ \exp(-S[\psi,\bar{\psi},U] - \delta S[\psi,\bar{\psi},U]) \tag{1.139}$$

$$= \langle\mathcal{O}\rangle + \langle\delta\mathcal{O} - \mathcal{O}\delta S\rangle + \mathrm{O}(\alpha^2).$$

We conclude

$$\langle\delta\mathcal{O}\rangle = \langle\mathcal{O}\delta S\rangle. \tag{1.140}$$

For instance, for $\mathcal{O} = J_\nu(y)$, we have $\delta\mathcal{O} = -ia\partial_\nu\alpha(y)S^{(\nu)}(y)$,

$$S^{(\nu)}(y) = \tfrac{1}{2}\big(\bar{\psi}(y+a\hat{\nu})(1+\gamma_\nu)U_\nu(y)^{-1}\psi(y) \\ +\bar{\psi}(y)(1-\gamma_\nu)U_\nu(y)\psi(y+a\nu)\big). \tag{1.141}$$

It can be thought of as a point-split discretization of the continuum scalar operator $\bar{\psi}\psi$. Now choosing $\alpha(x) = \epsilon\, e^{ikx}$, we finally obtain the relation [35]

$$a^4 \sum_{x,\mu} \hat{k}_\mu \Big\langle J_\nu(y) J_\mu(x) \Big\rangle e^{ik(x-y+\frac{a}{2}\hat{\mu}-\frac{a}{2}\hat{\nu})} = -a\hat{k}_\nu\, \langle S^{(\nu)}(y)\rangle. \tag{1.142}$$

This relation tells us that the longitudinal part of the polarization tensor is a pure contact term, and specifies the latter for the present regularization of QCD.

1.5.1.1 Chiral Ward Identities

The consequences of the global continuous symmetries of QCD can be elegantly worked out as Ward identities in the continuum Euclidean path integral (cf. [21], Sec. 4); the results are equivalent to those derived in the algebra of currents acting on the Hilbert space of the quantum states.

Perhaps the most important use of Ward identities in lattice QCD is to impose renormalization and/or improvement conditions on composite operators. The Ward identities can be derived in the continuum theory, and as long as on-shell correlation functions[10] are considered, they can be imposed in the lattice theory, thus providing renormalization conditions for certain local operators.

As an important example, consider QCD with a doublet of degenerate quark flavors, represented by a field $\psi(x) = (u(x), d(x))^\top$ (there may be more flavors in addition). The isovector axial current and pseudoscalar density read

$$A^a_\mu(x) = \bar{\psi}\gamma_\mu\gamma_5\frac{\tau^a}{2}\psi(x), \qquad P^a(x) = \bar{\psi}(x)\gamma_5\frac{\tau^a}{2}\psi(x), \tag{1.143}$$

where τ^a are the Pauli matrices acting in flavor space. For instance, the identity of the partially conserved axial current (PCAC) for QCD with a doublet of degenerate quark flavors

$$\partial_\mu A^a_\mu(x) = 2mP^a(x), \tag{1.144}$$

valid in all on-shell correlation functions, is used to define the quark mass m in Wilson lattice QCD, as well as to determine the finite renormalization of the axial current [21, 36, 37]. Equation (1.144) also shows that the renormalization of the quark mass m is known once the axial current and the pseudoscalar density are renormalized, see [38].

Similar to the axial current, the energy-momentum tensor requires a finite renormalization in order to satisfy the Ward identities of translation invariance. See e.g. [39] for the use of continuum Ward identities to renormalize the energy-momentum tensor in lattice field theory.

1.5.2 Chiral Symmetry on the Lattice

One drawback of the Wilson-Dirac operator (1.63) is that it does not preserve chiral symmetry: in the massless continuum theory, the action is invariant under the variation

$$\delta\psi(x) = \gamma_5\psi(x), \qquad \delta\bar{\psi}(x) = \bar{\psi}(x)\gamma_5 \tag{1.145}$$

[10] By 'on-shell correlation function', we mean that all operators involved are located at a physical distance from each other. By focusing on these, we avoid the discussion of contact terms, which in general are regularization-dependent.

of the fields. This property follows from the fact that, at vanishing quark mass, the Dirac operator anticommutes with γ_5. The Laplacian term in the Wilson-Dirac operator clearly spoils this property.

This is no coincidence, as the Nielsen-Ninomiya theorem [40–42] implies that chiral symmetry cannot be realized in this form on the lattice. We give here a particularly simple version of the theorem quoted in [43]. If $S = a^4 \sum_x \bar{\psi}(x) D \psi(x)$ is the free-fermion action, and $De^{ipx}u = \tilde{D}(p)e^{ipx}u$ for u a constant spinor and $\tilde{D}(p)$ a 4×4 matrix, then the following four properties cannot be realized simultaneously:

i. $\tilde{D}(p)$ is analytic and periodic in p_μ with a period $2\pi/a$;
ii. $\tilde{D}(p) = i\gamma_\mu p_\mu + \mathrm{O}(ap^2)$ at small momenta;
iii. $\tilde{D}(p)$ is invertible at all momenta that are non-vanishing mod $2\pi/a$;
iv. D anticommutes with γ_5.

As an example in one dimension, consider the case $\tilde{D}(p) = \frac{1}{a}\gamma_1 \sin(p_1 a)$. It satisfies the one-dimensional analogue of the conditions (i), (ii) and (iv) above, but violates (iii). The presence of a second zero of $\tilde{D}(p)$ within the Brillouin zone at $p_1 = \pi/a$ is a consequence of the existence of a zero at the origin, and that by periodicity it must cross zero again with the same slope at $p_1 = 2\pi/a$ [44].

However one can show that a modified 'chiral' transformation [43],

$$\delta\psi(x) = \gamma_5(1 - \tfrac{1}{2}aD)\psi(x), \qquad \delta\bar{\psi}(x) = \bar{\psi}(x)(1 - \tfrac{1}{2}aD)\gamma_5, \tag{1.146}$$

is indeed a symmetry of the action if the following 'Ginsparg-Wilson' relation [45] is satisfied by the Dirac operator,

$$\gamma_5 D + D\gamma_5 = aD\gamma_5 D. \tag{1.147}$$

In term of the propagator, this relation reads

$$\langle \psi(x)\bar{\psi}(y)\rangle\, \gamma_5 + \gamma_5\, \langle \psi(x)\bar{\psi}(y)\rangle = a^{-3}\gamma_5 \delta_{x,y}, \tag{1.148}$$

which shows that the ordinary chiral symmetry is realized on the mass shell. An explicit lattice Dirac operator that satisfies Eq. (1.147) is the 'overlap' operator [46]

$$D = \frac{1}{a}(1 - A(A^\dagger A)^{-1/2}), \qquad A = 1 - aD_{\mathrm{w}}. \tag{1.149}$$

It also satisfies the conditions (i), (ii) and (iii) above. The analyticity of $\tilde{D}(p)$ for real momenta implies the locality of D on a range of the order a.

The realization of a form of chiral symmetry on the lattice has important consequences. In particular, relation (1.147) implies that the 'topological charge' Q defined as

$$Q = a^4 \sum_x q(x), \qquad q(x) \equiv -\frac{a}{2}\mathrm{Tr}\,\{\gamma_5 D(x,x)\}, \tag{1.150}$$

is equal to the index $\mathrm{Tr}\{\gamma_5 P_0\}$ of the Dirac operator [47], where P_0 is the projector onto the subspace of its zero modes.

We refer the reader to Sec. 5 of [48] and to [49, 50] for accessible and more complete introductions to the subject of chiral symmetry and lattice fermions. In particular, lattice domain wall fermions [51–53] are a widely used formulation of chiral fermions.

1.5.3 Topology of the Gauge Field

Let D be a Dirac operator obeying the Ginsparg-Wilson relation (1.147). Then Q provides a definition of the topological charge obeying the index theorem. Its cumulants can be rewritten in such a way that, by power counting, no short-distance singularities appear. A universal (i.e. regularization-independent) definition of the cumulants of the topological charge can then be given [54]. In particular, the topological susceptibility χ_t can be written

$$\chi_t \equiv \frac{1}{V}\langle Q^2\rangle = m_1 \dots m_5 \int d^4x_1 \dots d^4x_4 \left\langle P_{31}(x_1) S_{12}(x_2) S_{23}(x_3) P_{54}(x_4) S_{45}(0)\right\rangle_{\mathrm{conn}} \tag{1.151}$$

with $P_{rs}(x) = \bar{\psi}_r(x)\gamma_5\psi_s(x)$, $S_{rs}(x) = \bar{\psi}_r(x)\psi_s(x)$ respectively the pseudoscalar and scalar density with respect to quark flavors r and s.

Direct calculations of the topological susceptibility based on the overlap Dirac operator (see Eq. (1.150)) have been performed in SU(3) gauge theory; as an example, we quote [55]

$$r_0^4 \chi_t = 0.059 \pm 0.003. \tag{1.152}$$

(the reference length r_0 was defined at the end of Sect. 1.4.1). Other ways of estimating χ_t motivated by semi-classical arguments yield comparable results (see, for instance, [56, 57]).

1.5.4 Recursive Finite-Size Technique: Linking Vastly Different Length Scales

Consider a renormalized coupling $g^2(\mu)$. We saw an example defined via the force between two static quarks, Eq. (1.95), where $\mu = 1/r$. At standard simulation parameters, the smallest lattice spacing for which a linear system size of several fm can be accomodated is about 0.05 fm. However, in order to make contact

with perturbation theory in a completely controlled way, it is desirable to compute the renormalized coupling at distances as small as 0.002 fm. It is clear that the large hierarchy between the distances typical of non-perturbative physics and the regime where perturbation theory becomes quantitatively accurate requires a special treatment.

Probably the only strategy that addresses this issue in a completely satisfactory way is the 'recursive finite-size technique' or 'step-scaling'. The general idea is that the inverse size of the system $1/L$ itself plays the role of the renormalization scale μ. This means that the confinement scale ~ 0.5 fm need not be accomodated in a calculation of the renormalized coupling at a large renormalization scale. A second key point is that attention must be paid to avoid zero modes of the quark and the gluon fields in the perturbative regime. The latter can cause serious problems with the stability and ergodicity of simulations. One set of boundary conditions that removes all zero modes is the set implemented in the Schrödinger functional [58]. There may well be other useful choices [59]. The Schrödinger functional has been used extensively to compute the running coupling [60–63] and has also proved very useful in formulating renormalization conditions for various local operators; see, for instance, [38, 64].

The idea of relating a quantity at high energy scales to the same quantity at small energy scales in multiple manageable steps in order to avoid a large hierarchy of scales is also used in other contexts. One of them is the calculation of the QCD equation of state at high temperatures [65, 66].

1.6 Importance Sampling Monte-Carlo Methods: Basic Ideas

In this section we describe the ideas behind the numerical methods that are used in practical calculations. First consider, for concreteness, the case of the pure gauge theory, Eq. (1.66). The first idea is to interpret

$$p[U] = \frac{1}{Z} D[U] \exp(-S_{\mathrm{g}}[U]) \tag{1.153}$$

as a normalized probability distribution on the space of all gauge fields. The second idea is to generate a representative sample of field 'configurations' $\{U_1, \ldots, U_{N_c}\}$, meaning that the fraction of the number of configurations belonging to a domain $\mathcal{D}$ of field space is given by

$$\int_{\mathcal{D}} D[U]\, p[U],$$

with an error of order $N_c^{-1/2}$. Third, the path-integral expectation value of observables can be estimated according to

$$\langle \mathcal{O}[U] \rangle = \frac{1}{N_c} \sum_{i=1}^{N_c} \mathcal{O}[U_i] + \mathrm{O}(N_c^{-1/2}). \tag{1.154}$$

One thus needs a method of generating the probability distribution (1.153). Usually, a complicated probability distribution must be generated iteratively; a Markov chain is a general method that achieves this. The chain starts from an initial configuration and then visits a sequence of configurations according to a given transition probability. General criteria exist that guarantee that the configurations visited after a sufficient number of iterations are indeed distributed according to the desired probability distribution [67]. For the state-of-the-art update rule, see, for instance, Sec. 2.3 of [67] and Appendix B of [68] and references therein.

The way fermions are treated in virtually all current lattice calculations is by integrating them out, yielding the determinant of the Dirac operator in the numerator of the path integral (see Eqs. (1.32–1.33)). The determinant can be treated as part of the probability distribution $p[U]$, provided it is positive on all gauge-field configurations. The γ_5 hermiticity of the Dirac operator implies that the determinant is real. For a doublet of mass-degenerate quarks, the square of the determinant is thus positive. For the other quark flavors, chiral symmetry, if realized on the lattice, guarantees that the determinant is positive; for non-chiral discretizations, the eigenvalues appear to all be positive with a substantial spectral gap, so that the property holds in practice.

The state-of-the-art algorithm to generate the distribution of gauge fields including the effect of the quarks is the hybrid Monte-Carlo algorithm [69], with its many important refinements of the last decade or so [67, 70, 71]. The generated sample of gauge-field configurations (an 'ensemble') is stored on disk, so that observables can be calculated on the configurations at a later stage. As an example, the two-point function of quark bilinears $\mathcal{O}(x) = \bar{u}(x)\Gamma u(x)$, $\mathcal{O}'(x) = \bar{u}(x)\Gamma' u(x)$ (with Γ, Γ' matrices acting on the spin degrees of freedom) are evaluated as

$$\begin{aligned} \langle \mathcal{O}(x)\, \mathcal{O}'(y) \rangle = \frac{1}{N} \sum_{i=1}^{N_c} \Big(& - \mathrm{Tr}\big\{ \Gamma D^{-1}([U_i]; x, y) \Gamma' D^{-1}([U_i]; y, x) \big\} \\ & + \mathrm{Tr}\big\{ \Gamma D^{-1}([U_i]; x, x) \big\}\, \mathrm{Tr}\big\{ \Gamma' D^{-1}([U_i]; y, y) \big\} \Big) + \mathrm{O}(N_c^{-1/2}), \end{aligned} \tag{1.155}$$

where D is the lattice Dirac operator in a given gauge field and the traces are taken with respect to color and spin indices.

1.7 Outlook

I hope that the introduction given here provides a useful overview of the most important concepts and methods in lattice QCD. It is a theoretically sound quantum field theoretic framework, and, with the steady increase in computing power and the improvement of algorithms, it makes predictions that have a high phenomenological impact [34, 72]. It has also had an influence on the way other problems are approached, for instance in the simulation of theories that may represent strongly coupled extensions of the Standard Model [73] and, more distantly, in theories describing a gas of strongly interacting fermions [74–76]. The following chapters give a far more detailed account of nuclear physics applications of lattice QCD.

Chapter 2
Lattice Methods for Hadron Spectroscopy

Sinéad M. Ryan

Abstract Lattice hadron spectroscopy is crucial to inform and direct a new generation of experiments. Useful calculations require control of both statistical and systematic uncertainties. In these lectures selected methods for lattice hadron spectroscopy are discussed in detail. The lectures aim to describe all aspects of a calculation from quark propagation to fitting and interpreting data. After some motivation for lattice spectroscopy, the path integral approach and construction of correlation functions are discussed. There are detailed discussions of techniques for quark propagators, including new developments in calculations of all-to-all propagators. Lattice and continuum symmetries are contrasted and techniques for spin identification in lattice calculations are discussed in some detail. Design and construction of optimal operators as well as fitting and systematic errors are addressed. Finally, open problems and challenges are described focusing on resonances and scattering states.

2.1 Introduction

The nonperturbative spectrum of mesons and baryons built from light and heavy quarks provides a fascinating arena in which to study the strong interaction. Indeed many of the most recently discovered hadrons have unexpected properties and their discovery has reignited theoretical and phenomenological interest in spectroscopy. Within the Standard Model (SM), to separate electroweak physics from strong-interaction effects we must first understand the hadon spectrum. Meanwhile beyond the SM, models of electroweak symmetry breaking, such as technicolour, may require nonperturbative techniques at the TeV scale which are similar to the techniques developed for spectroscopy at GeV scales. To understand therefore the new puzzling states which have been observed and to probe the physics at LHC energies better techniques for spectroscopy will be crucial and will help us to understand the nature of masses and transitions.

S.M. Ryan (✉)
School of Mathematics, Trinity College, Dublin 2, Ireland
e-mail: ryan@maths.tcd.ie

H.-W. Lin, H.B. Meyer (eds.), *Lattice QCD for Nuclear Physics*, Lecture Notes in Physics 889, DOI 10.1007/978-3-319-08022-2_2

While the quark model has provided a useful framework in which to understand the structure of mesons and baryons it is limited to just a subset of the states which QCD in principle allows. Lattice QCD offers the prospect of nonperturbative, systematically-improvable model-independent calculations of hadron masses and mixing (as well of course as a wealth of other properties of QCD). In these lectures we will review some approaches and discuss new methods to address the significant challenges which remain in the era of dynamical calculations at realistic quark masses.

2.1.1 Notation and Basics

The objects of interest are formed from constituent quarks and antiquarks to make bound states of mesons and baryons as well as molecular and multiquark states, hybrid states and glueballs. In QCD the fundamental constituents are the quarks (in six flavours) and gluons. The fields of the lagrangian are combined in colourless combinations forming bound states.

The quark model is a useful classification of hadrons in terms of their valence quarks—the quarks (q) and antiquarks ($\bar{q}$) that give the quantum numbers of the hadrons. States in the continuum are classified by the quantum numbers: J, the total angular momentum; P, the parity and C, charge conjugation. Recall that $|L-S| \leq J \leq |L+S|$ and in the quark model naming scheme, $n^{2S+1}L_J$, the values of L are $L = \{0, 1, \ldots\}$ and $S = \{0, 1\}$. The parity is defined by $P = (-1)^{(L+1)}$ and charge conjugation is $C = (-1)^{(L+S)}$. The latter is a good quantum number for $q\bar{q}$ states with the same quark and antiquark flavour e.g. charmonium but not for example for heavy-light mesons, $D_{(s)}$, $B_{(s)}$, nor for baryons.

2.1.1.1 Mesons

Mesonic states are composed of two spin-half fermions, and described by ${}^{2S+1}L_J$ in quark model notation with $S = 0$ for antiparallel quark spins and $S = 1$ when the quark spins are parallel.

States in the quark model follow a "natural spin-parity" series with $P = (-1)^J$ and so have $S = 1$ and thus $CP = +1$. With these conditions, the allowed states have $J^{PC} = 0^{-+}, 0^{++}, 1^{--}, 1^{+-}, 2^{--}, 2^{-+}, \ldots$. However, states with $P = (-1)^J$ but $CP = -1$ are forbidden in a $q\bar{q}$ model of mesons, meaning that the states $J^{PC} = 0^{+-}, 0^{--}, 1^{-+}, 2^{+-}, 3^{-+}, (\text{even})^{+-}, (\text{odd})^{-+}, \ldots$ which are allowed by QCD cannot be accommodated in a simple quark model picture and must therefore be more than a simple bound state of a quark and antiquark. These are the "exotic" states of QCD.

2.1.1.2 Baryons

In this case there are three quarks in colourless combination (with baryon number $B = 1$), J is half-integer and in particular C is not a good quantum number so that states are classified by J^P. The spin-statistics theorem tells us that a baryon wavefunction must be antisymmetric under the exchange of any two quarks. Since all hadrons are colour neutral, the combinations of colour indices of the three quarks must be antisymmetric and the remaining labels: flavour, spin and spatial structure must be in totally symmetric combinations,

$$|\mathrm{qqq}\rangle_A = |\mathrm{colour}\rangle_A \otimes |\mathrm{space, spin, flavour}\rangle_S . \tag{2.1}$$

The possible states are then

$$|\mathrm{qqq}\rangle_A = |\mathrm{colour}\rangle_A \otimes \begin{matrix} [|\mathrm{space}\rangle_S \otimes |\mathrm{spin}\rangle_A \otimes |\mathrm{flavour}\rangle_A]_S \\ [|\mathrm{space}\rangle_S \otimes |\mathrm{spin}\rangle_S \otimes |\mathrm{flavour}\rangle_S]_S \end{matrix} \tag{2.2}$$

and a linear combination

$$\begin{aligned} |\mathrm{qqq}\rangle_A = {} & \alpha |\mathrm{colour}\rangle_A \otimes [|\mathrm{space}\rangle_S \otimes |\mathrm{spin}\rangle_A \otimes |\mathrm{flavour}\rangle_A]_S \\ & + \beta |\mathrm{colour}\rangle_A \otimes [|\mathrm{space}\rangle_S \otimes |\mathrm{spin}\rangle_S \otimes |\mathrm{flavour}\rangle_S]_S . \end{aligned}$$

with $\alpha^2 + \beta^2 = 1$. An outstanding question in baryon spectroscopy is that of missing states. For three quarks (u, d, s) there is an (approximate) $SU(3)$ flavour symmetry and a decomposition in flavour given by

$$3 \otimes 3 \otimes 3 = 10_S \oplus 8_M \oplus 8_M \oplus 1_A, \tag{2.3}$$

where A is antisymmetric, S is symmetric and M is mixed. The decuplet is symmetric in flavour and the two octets have a mixed symmetry and since they are related by a unitary transformation describe the same states. This analysis predicts many more states than observed by experiments, a phenomenon known as the missing resonance problem.

2.1.1.3 Gluonic Excitations: Hybrids and Glueballs

In addition to the mesons and baryons discussed above in terms of quark degrees of freedom, QCD allows for a richer spectrum of states when we take into account the gluonic degrees of freedom. We can formulate color-neutral states of pure glue, called glueballs and states in which excitations of the gluonic field in a hadron form so-called hybrids.

Theoretical discussions of glueballs focus on states made from two or three gluons and as for the conventional mesons and baryons these states are color neutral and have integer angular momentum. The two-gluon states will have $J = 0$ (scalar or pseudo-scalar) or $J = 2$ (tensor). Three-gluon states can have $J = 1$ (vector) or $J = 3$.

Glueballs will mix with ordinary mesons and are therefore difficult to identify unambiguously in experiments. There is a considerable history of lattice calculations of glueballs. A pioneering quenched calculation mapped the spectrum of states in great detail [77]. However, unquenched calculations must also take into account the allowed mixing with ordinary mesons and are consequently more technically challenging. See for example [78] and references therein.

2.1.2 Current and Future Experiments

Before we delve into the details of lattice hadron spectrum calculations it is worthwhile to review briefly some of the experimental activity underway. There is significant new effort being devoted to understanding the light and charm spectra and to answering the questions:

1. Are there resonances that do not fit the quark model?
2. Are there gluonic excitations in these spectra?
3. What structure does confinement lead to?

2.1.2.1 Current Status

Since the early 2000s there has been a renaissance in charmonium spectroscopy. The unexpected discovery of new narrow structures above the open charm threshold by Belle and Babar led to substantial renewed interest in what was believed to be a well-understood sector. There has been much speculation about the nature of the so-called "X,Y,Z" states including possible molecular and hybrid states. Intriguingly the $Z^{\pm}(4430)$ is a charged state and so cannot be a simple $c\bar{c}$ meson. However, very little is definitively known and as yet no clear picture has emerged. BESIII continues to take data, with an aim to accumulate 10^8 to 10^9 J/Ψ and Ψ' decays. These states decay primarily by $c\bar{c}$ annhilation and hadronisation to light mesons. The experiment has reported new states including the $X(1835)$, $X(2120)$ and $X(2370)$ [79]. However, no quantum number assignments have been made yet and both independent confirmation and measurement of the quantum numbers is essential.

2.1.2.2 Planned Experiments

The GlueX experiment at the Hall D facility at JLab plans to have first physics results in 2015. The primary goal is the search for and study of gluonic excitations in the meson spectrum, produced in γp collisions. Photoproduction of exotic hybrids is expected to be particularly effective, while also allowing an extensive study of the conventional spectrum. As well as discovery, GlueX should in principle be able to confirm the existence of new states seen at BESIII, through a complementary production mode and in addition measure or confirm the measurement of quantum numbers. Using their proposed kaon identification system GlueX will additionally be able to study baryons, including excited Ξ baryons.

The PANDA experiment at the Facility for Antiproton and Ion Research (FAIR) which is under construction at GSI in Darmstadt will collide antiprotons with a fixed target. The hadron spectroscopy program at PANDA includes a search for gluonic excitations: glueballs and hybrids and charmonium spectroscopy: in particular of states above threshold. The goal is to find the missing D and F wave states in charmonium and to understand the nature of the X, Y, Z states. PANDA will also study the D meson spectrum, again to address the question of unexplained states which do not fit into the quark model picture for heavy-light systems. A comprehensive programme of baryon spectroscopy is also planned—in particular for strange and charmed baryons.

In principle, lattice QCD can provide a complementary approach as well discrimating between models and providing guidance for experimental searches to address these questions by identifying properties of states in the continuum limit of the theory and by going beyond precision ground state spectroscopy to compute scattering and resonance widths. To achieve this we need new tools: techniques for statistical precision, even at high spin; methods for operator construction and spin identification on the lattice; new methods for resonance and isoscalar physics; control of the relevant extrapolations ($m_q \to m_{\text{physical}}, V \to \infty, a \to 0$). A discussion of recent progress to address some of these issues will be the main topic of these lectures. The topics I cover are not exhaustive but will I hope give a flavour of the progress being made, what you might expect to see in the near future and how to judge the relative merits of such calculations. There are many excellent textbooks, reviews and lecture notes available including this not exhaustive list [3, 5, 6, 21, 80–86].

2.1.3 Lattice Hadron Spectroscopy

An important goal for lattice calculations is a determination of the low-energy spectrum of quarks and gluons from the QCD Lagrangian

$$\mathcal{L}_{\text{QCD}} = -\frac{1}{4} F^a_{\mu\nu} F^{a\mu\nu} + \sum_f \bar{\Psi}_f \left(i \gamma^\mu D_\mu - m_f \right) \Psi_f, \tag{2.4}$$

where the index f represents flavour and the covariant derivative D_μ is defined

$$D_\mu = \partial_\mu - ig\left(\frac{1}{2}\lambda^a\right)A^a_\mu. \tag{2.5}$$

In such calculations there are just two input parameters, the coupling g and the bare mass m_f. The continuum theory is recovered by simulating at or extrapolating to physical values of the light quark masses and in the limits $a \to 0$ and $V \to \infty$.

At the Lattice conference in 2011, Hoelbling [87] reviewed progress in lattice spectroscopy, described in Fig. 2.1. The plots show that many lattice collaborations are now making simulations with $N_f \geq 2$, at light quark masses and large volumes. In these lectures I will not discuss fermion discretisations, chiral extrapolations or the details of simultations at or close to the physical point. Note that recent results for the low-lying spectrum of hadrons in the light sector show internal consistency between different lattice fermion formulations and impressive agreement with experimental results [88–92].

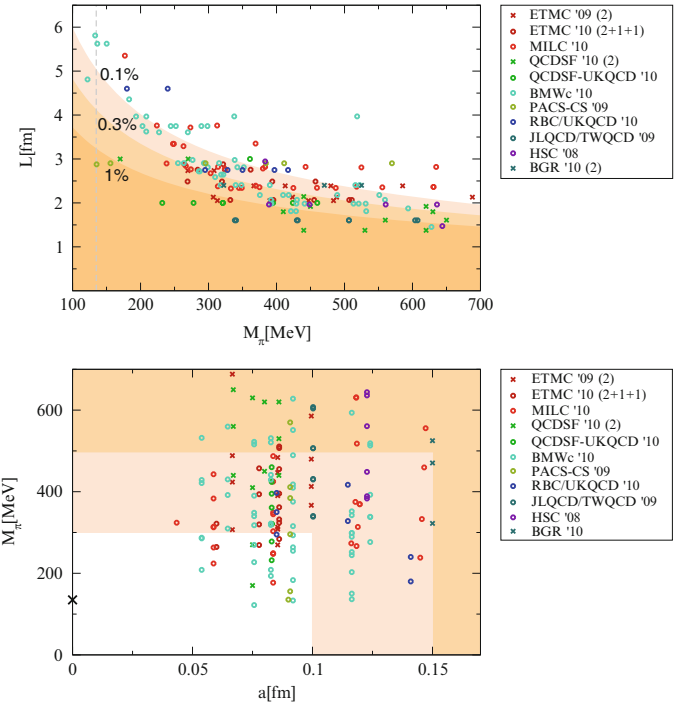

Fig. 2.1 The landscape of recent dynamical lattice calculations, from Hoelbling's review. The left plot shows the lattice extent L vs the pion mass. The physical pion mass is at the dashed line and the shading represents the relative error on the pion mass from 1 to 0.1 %. The right plot shows the pion mass, M_π vs the lattice spacing, a. The physical point is marked with a cross and the shading from dark to light indicates the more desirable parameter space for calculations

2.1.4 Correlators in a Euclidean Field Theory

Recall that in a Euclidean field theory, physical observables $\mathcal{O}$ are evaluated as an expectation value over the relevant degrees of freedom

$$\langle \mathcal{O} \rangle = \frac{1}{Z} \left\{ \int \mathcal{D}U \, \mathcal{D}\Psi \, \mathcal{D}\bar{\Psi} \, \mathcal{O} \, e^{-S_{QCD}} \right\} . \tag{2.6}$$

The quark fields are Grassmann and are integrated out analytically, giving (with $N_f = 2$)

$$\langle \mathcal{O} \rangle = \frac{1}{Z} \left\{ \int \mathcal{D}U \, \mathrm{det} M^2 \, \mathcal{O} \, e^{-S_G} \right\} , \tag{2.7}$$

where S_G is the gauge action. The expectation value is then calculated by importance sampling of gauge fields and averaging over these ensembles. Typically, in hadron spectroscopy we are in interested in two-point correlation functions built from interpolating operators, which are functions of the fields Ψ. A simple example is a local meson operator $\mathcal{O}(x) = \bar{\Psi}_a(x) \Gamma \Psi_b(x)$, where Γ is an element of the Dirac algebra with possible displacements and a, b are flavour indices.

The two-point function is then

$$C(\boldsymbol{x}, t) = \langle \mathcal{O}(x) \mathcal{O}^\dagger(0) \rangle = \langle \bar{\Psi}_a(x) \Gamma \Psi_b(x) \bar{\Psi}_b(0) \Gamma^\dagger \Psi_a(0) \rangle, \tag{2.8}$$

where I note that $x \equiv (t, \boldsymbol{x}); t \geq 0$.

Using Wick's theorem to contract the quark fields replaces the fields with propagators in the expression for the correlation function

$$\begin{aligned} C(\boldsymbol{x}, t) = &- \langle \mathrm{Tr} \left(M_a^{-1}(0, x) \Gamma M_b^{-1}(x, 0) \Gamma^\dagger \right) \rangle \\ &+ \delta_{ab} \langle \mathrm{Tr} \left(\Gamma M_a^{-1}(x, x) \right) \mathrm{Tr} \left(\Gamma^\dagger M_a^{-1}(0, 0) \right) \rangle. \end{aligned} \tag{2.9}$$

The trace is taken over spin and colour indices, which have been suppressed here for clarity. $M^{-1}_{(a,b)}$ is the quark propagator.

Now, for flavour non-singlets (with $a \neq b$) the second term above vanishes and the two-point correlation function can be written

$$C(\boldsymbol{x}, t) = \langle \mathrm{Tr} \left(\gamma_5 M_a^{-1}(x, 0)^\dagger \gamma_5 \Gamma M_b^{-1}(x, 0) \Gamma^\dagger \right) \rangle. \tag{2.10}$$

To arrive at this expression we have also used γ_5 hermiticity, namely that $M^{-1}(x, y) = \gamma_5 M^{-1}(y, x)^\dagger \gamma_5$, to rewrite the correlator in terms of propagators from the origin to all sites. These are the *point (to all) propagators* traditionally used in lattice calculations. In one final step we consider correlators in momentum space at zero momentum,

$$C(\boldsymbol{p},t) = \sum_{\boldsymbol{x}} e^{i\,\boldsymbol{p}\cdot\boldsymbol{x}}\, C(\boldsymbol{x},t) \tag{2.11}$$

$$\text{and}\;\; C(t) = C(\boldsymbol{p}=0,t) = \sum_{\boldsymbol{x}} C(\boldsymbol{x},t).$$

It is useful to bear in mind from what we have seen above that the fermion fields in the lagrangian are present in calculations of the fermion determinant and contribute to the integral over the gauge fields, while those fermion fields in measurements are manifest in calculations of the propagators. The integral over gauge fields is done using importance sampling and is not the subject of these lectures. We will however see more about techniques to determine the quark propagators.

For hadron spectroscopy the goal is to extract the energy of (colourless) states of QCD. This information is encoded in the two-point correlation functions which are discussed above and which I now write as

$$C(t) = \langle \phi_i(t) | \phi_j^\dagger(0) \rangle, \tag{2.12}$$

where, ϕ_i and $\phi_j^\dagger$ are operators acting on the quark fields to create a state at time $t = 0$ and annihilate it at a later time t. Using the Euclidean time evolution of such operators, $\phi(t) = e^{Ht}\phi e^{-Ht}$ and inserting a complete set of states allows us to write the correlator as

$$C(t) = \sum_{n=0}^{\infty} \frac{|\langle \phi | n \rangle|^2}{2m_n} e^{-E_n t}, \tag{2.13}$$

and note also that we are working in the low-temperature limit of QCD where $\beta = 1/kT = L_t$ is large. From Eq. (2.13) it is easy to see that in the large time limit the exponential fall-off of the correlator gives the ground state energy, E_0, namely $\lim_{t\to\infty} C(t) = Ze^{-E_0 t}$. The usual procedure then is to fit correlators to an exponential and extract the ground state energy from the data at large times. A useful quantity in this respect is the effective mass, which can be defined as

$$a_t m_{\text{effective}} = -\log\left(\frac{C(t)}{C(t-1)}\right). \tag{2.14}$$

The effective mass should plateau at large time separations as the ground state exponential dominates in the correlator. This is illustrated in Fig. 2.2 which shows a single correlator and corresponding effective mass for the J/Ψ meson, determined on a $12^3 \times 128$ anisotropic lattice. Note that for operators $\phi_i = \phi_j$ in Eq. (2.12) the correlation function is positive definite and the effective mass converges monotonically from above.

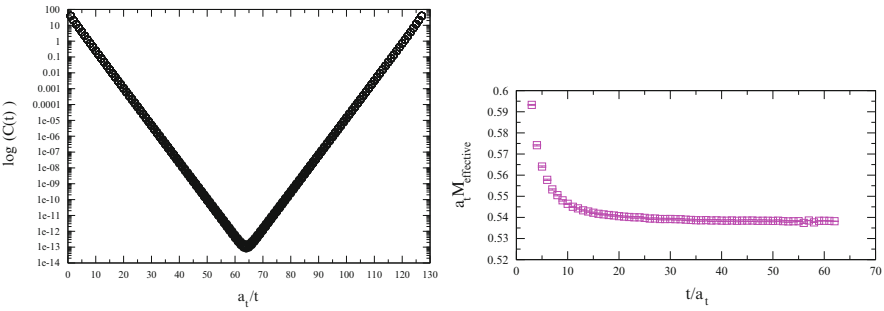

Fig. 2.2 The left plot is a log plot of the correlator data, which is symmetric about the midpoint of the lattice for mesons under periodic boundary conditions. The right plot is the corresponding effective mass, determined using Eq. (2.14). Note that the data reach a plateau and remain constant from approximately timeslice twenty-five. At earlier times, excited state contamination in the form of additional exponentials is clearly visible

Now, it is clear from Eq. (2.13) that the correlation function contains information on all states that can be created by the operators used. However, the technique described above reliably gives the ground state while excited states, which would require more exponentials and more free parameters in a fit, very quickly become unreliable.

A different approach, designed to allow access to these excited states in a lattice calculation is the variational method, which I will return to in Sect. 2.4.2.3. The idea is that if we can measure a matrix of correlation functions

$$C_{ij}(t) = \langle 0|\phi_i(t)\phi_j^\dagger(0)|0\rangle, \tag{2.15}$$

for all i, j and solve a generalised eigenvalue problem $\mathbf{C}(t)\underline{v} = \lambda\mathbf{C}(t_0)\underline{v}$, then the eigenvalues λ are related to the state energies by

$$\lim_{(t-t_0)\to\infty} \lambda_k = e^{-E_k t} + \mathcal{O}\left(e^{-\Delta E_n t}\right). \tag{2.16}$$

For this method to be practical we need (i) a good basis set of operators that resembles the states of interest and (ii) all elements of this correlation matrix measured [93]. In Sect. 2.4 we will look in more detail at the different approaches to operator construction which facilitate the variational approach.

2.2 Some New (and Old) Ideas for Making Measurements

To improve the precision and range of calculations that lattice methods can tackle let us take a closer look at quark propagators: the hadronic building blocks. In the previous section we saw that using time translational invariance and for flavour non-singlets a so-called point-to-all propagator can be calculated. The main advantage

of these propagators is that their calculation does not require vast computing resources. However, this comes at a hefty cost. Using point propagators restricts the accessible physics, making calculations of flavour singlets, where $a = b$ in Eq. (2.9) (e.g. the η') and condensates impossible as these objects need propagators with sources everywhere in space. From a practical point of view point propagators restrict the interpolating basis used since a new inversion is needed for every operator that is not restricted to a single lattice point. Finally, from a philosophical point of view the point propagator entangles the propagator calculation and operator construction in a non-trivial way.

In this section I will discuss some different approaches used to calculate quark propagators: smeared point propagators, all-to-all propagators and distillation. Please see the references for a fuller description of these and other methods.

2.2.1 Smearing

Recall that hadrons are extended objects $\mathcal{O}(1)$ fm whilst so far we have discussed the calculations of hadronic properties in terms of point-like propagators and interpolating fields. These may have small overlap with the state of interest, as determined by the amplitude $\mathcal{Z}_n = \langle \phi | n \rangle$ appearing in Eq. (2.13). Improvements can be made by optimising the projection onto the state of interest using "smearing": one uses an extended operator (for example of the form $\bar{q}^{(1)}_{\mathbf{x}} \Gamma \phi_{\mathbf{x},\mathbf{y}} q^{(2)}_{\mathbf{y}}$) where the function $\phi_{\mathbf{x},\mathbf{y}}$ is chosen to resemble a wavefunction. Essentially this works since the ground state wavefunction is smooth with no nodes.

This idea has been realised using Coulomb gauge fixing [94, 95] and by using iterative gauge-covariant smearing of the quark fields. This amounts to replacing

$$\Psi(\boldsymbol{x}, t) = \sum_{\boldsymbol{y}} \mathcal{G}(\boldsymbol{x}, \boldsymbol{y}, U(t)), \Psi(\boldsymbol{y}, t), \tag{2.17}$$

where the function $\mathcal{G}$ is the (Gaussian) smearing function given by $\mathcal{G}(\boldsymbol{x}, \boldsymbol{y}, U(t)) = (1 + \kappa_s H)^{n_\sigma}$ and H is frequently the lattice covariant Laplacian in three dimensions. Examples of iterative smearing procedures include Jacobi smearing [96] and Wuppertal smearing [97].

In addition, the gauge noise in a Monte-Carlo calculation can be significantly reduced by smearing the link, (U) fields that appear in $\mathcal{G}$. Again, there are different approaches here including APE [98], HYP [99] and stout smearing [100].

Distillation [101], which will be more thoroughly discussed in Sect. 2.2.2.1 in the context of methods for all-to-all propagators can also be thought of as a variation or re-definition of smearing.

2.2.2 All to All Propagators

Let us turn now to consider methods for determining the quark propagator from all sites on the lattice to all sites. As already mentioned, point propagators restrict the accessible physics and we would like a robust method to go beyond this. To compute all elements of the quark propagator however would require full knowledge of the inverse and this is prohibitively expensive. Recall that the lattice representation of the Dirac operator is a large but sparse matrix and if we are satisfied with an unbiased estimator of all elements then sparse matrix methods can be used. Stochastic estimation should be acceptable—after all we are already using it to generate the gauge fields. We will also discuss later in this lecture the crucial role of variance reduction in these stochastic estimations.

To begin, we consider a spectral representation of the fermion matrix, $Q = \gamma_5 M$. This has the advantage that Q is hermitian and so its eigenvalues are easier to compute. If the eigenvalues and eigenvectors $\{\lambda^{(i)}, v^{(i)}\}$ of Q can be computed then

$$Q = \sum_{i=1}^{N} \lambda^{(i)} v^{(i)} \otimes v^{*(i)} \quad \text{and so} \quad Q^{-1} = \sum_{i=1}^{N} \frac{1}{\lambda^{(i)}} v^{(i)} \otimes v^{*(i)}. \tag{2.18}$$

Unfortunately, finding even a small subset of eigenvectors is computationally expensive and so one is generally forced to truncate this representation for $N_{ev} \ll N$. This truncated sum now violates reflection positivity and must be corrected.

Let us go back and reconsider the fermion matrix, Q, by writing instead a stochastic representation of this matrix. This proceeds in the usual way: an ensemble of random independent noise vectors, $\{\eta_{[1]}, \eta_{[2]}, \ldots, \eta_{[N_r]}\}$ is generated with the property

$$\langle\langle \eta_{[r]}(x) \otimes \eta_{[r]}(y)^\dagger \rangle\rangle = \delta_{x,y}, \tag{2.19}$$

where the angle brackets indicate the expectation value over the distribution of noise vectors. Z_4 is a good choice, noting that each component of the noise vectors has modulus 1, ie. $\eta^{i\alpha}(x)^* \eta^{i\alpha}(x) = 1$ (with no summation), where i, j are colour indices and α, β label spin.

The solution vectors, $\Psi_{[r]}$ are obtained in the usual way

$$\Psi_{[r]}(x) = Q^{-1} \eta_{[r]}(y), \tag{2.20}$$

In this approach the quark propagator from any point x to any point y is written

$$Q^{-1}(y,x)^{ij}_{\alpha\beta} = \langle\langle \Psi_{[r]} \otimes \eta^\dagger_{[r]} \rangle\rangle^{ij}_{\alpha\beta} = \lim_{N_r \to \infty} \frac{1}{N_r} \sum_{r}^{N_r} \Psi^{i\alpha}_{[r]}(y) \eta^{j\beta}_{[r]}(x)^\dagger. \tag{2.21}$$

For N_r different sources the variance falls like $1/\sqrt{N_r}$ and it would be useful to find methods that do better than this.

Exercise Verify that Eq. (2.21) indeed provides the inverse of the matrix Q by multiplying the equation on both sides with Q.

2.2.2.1 Variance Reduction by Dilution

In stochastic methods variance reduction is critical and it is useful to ask if the variance can be reduced below what has been mentioned. I will present one successful approach, called "dilution".

Recall that the exact propagator can be computed with a finite (but large) amount of effort, namely by using point-propagators methods with Kronecker delta sources everywhere on the lattice. This suggests a trick. We break the vector space of the quark fields V into d smaller sub-spaces, $V = V_1 \oplus V_2 \oplus \ldots$ spanned by subsets of the basis vectors. This partitioning, called dilution, is arbitrary.

We can look at this in more detail. Dilute the noise vector η in some set of variables so that $\eta = \sum_j \eta^{(j)}$. For spectroscopy where temporal correlations are relevant an important example is time dilution which we can write as

$$\eta(\boldsymbol{x}, t) = \sum_{j=0}^{N_t-1} \eta^{(j)}(\boldsymbol{x}, t) \tag{2.22}$$

and $\eta^{(j)}(\boldsymbol{x}, t) = 0$ unless $t = j$. Each diluted source is inverted, yielding N_d pairs of vectors $\{\Psi^{(j)}, \eta^{(j)}\}$. An estimator of Q^{-1} with a single noise source is then

$$\sum_{i=0}^{N_d-1} \Psi^{(i)}(\boldsymbol{x}, t) \otimes \eta^{(i)}(\boldsymbol{x}_0, t_0)^\dagger. \tag{2.23}$$

In the so-called "homeopathic limit" of dilution with a noise vector for each time, space, colour and spin component, the exact propagator is recovered in a finite number of steps. This of course is not practical in current simulations; however, the path through dilution space may be optimised so that the gauge field noise dominates for a manageable number of inversions.

It is also possible to incorporate dilution with the stochastic estimation in a hybrid method. Essentially the steps are: calculate N_{ev} eigenvalues and eigenvectors of Q exactly and determine $Q^{-1}_{N_{ev}}$; use the stochastic method with dilution to correct the truncation. There are further details and a discussion of further optimisation in [102].

So, how does this dilution method compare with point propagators? The left pane of Fig. 2.3 shows the correlator for a light pseudoscalar determined on a $12^3 \times 24$ lattice at $\beta = 5.7$ with Wilson fermions and 75 gauge field configurations. The right pane shows an effective mass plot for three different states (the 1^{+-}, ρ and π)

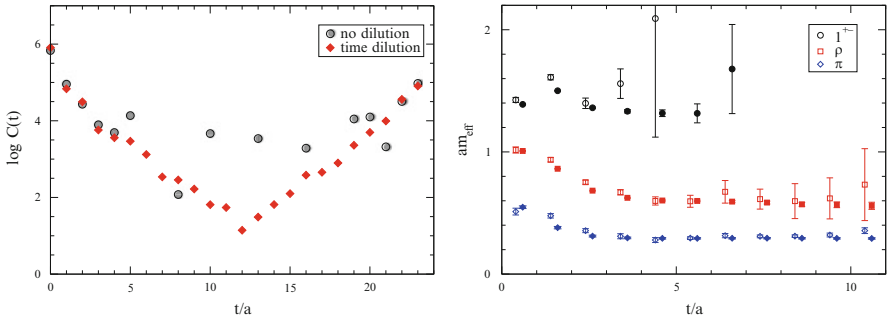

Fig. 2.3 The left pane is a log plot of the correlator, as described in the text, comparing the point propagators with all-to-all propagators calculated using time dilution. The right pane shows the effective masses of three states again comparing the statistical precision of point and all-to-all propagators

determined on the same ensembles. Both plots are taken from [102]. The light quarks are relatively heavy with $m_\pi/m_\rho = 0.50$. One hundred eigenvectors were determined and dilution in time, space even-odd[1] and spin was implemented (in the right-hand plot). The plots shows an impressive improvement in the statistical precision with which the correlator and effective masses are determined when using dilution (in time only) compared to traditional point sources.

2.2.3 *Distillation*

I will briefly describe a rather different approach to the determination of quark propagation, termed "distillation" [101]. Essentially the method is a redefinition of smearing (as described above) which as we will see leads to rather dramatic improvements in statistical precision and the range of accessible hadronic physics.

Consider a smeared quark field, $\tilde{\Psi}$ derived from the "raw" quark field, Ψ in the path integral by $\tilde{\Psi}(t) = \Box[U(t)]\Psi(t)$. The general expression for a (e.g. mesonic) creation operator is then

$$\mathcal{O}_M(t) = \overline{\tilde{\Psi}}(t)\Gamma\tilde{\Psi}(t), \tag{2.24}$$

where Γ is an operator in position, spin, colour space and the aim of smearing is to improve the overlap onto the state of interest.

[1] A cubic, or hypercubic, lattice may be divided into sublattices of "even" and "odd" sites, sometimes also referred to as checkerboarding. A lattice point, $x \in \mathbb{Z}^4$ is even or odd depending or whether the sum of its coordinates x_μ is even or odd. For details see for example the textbooks referenced.

Let us look in more detail at the smearing operator $\Box$. Smearing is known to be very effective in building an operator that projects onto a low-lying hadronic state and a popular (gauge-covariant) algorithm is Gaussian smearing. A linear operator is applied,

$$\Box_J = \exp\left(\sigma\nabla^2\right), \tag{2.25}$$

In this example ∇^2 is a lattice representation of the three-dimensional gauge-covariant laplace operator on the source time-slice.

$$\nabla^2_{x,y} = 6\delta_{x,y} - \sum_{i=1}^{3} U_i(x)\delta_{x+\hat{\imath},y} + U_j^\dagger(x-\hat{\imath})\delta_{x-\hat{\imath},y}. \tag{2.26}$$

Correlation functions built from such smeared operators then look like

$$\mathrm{Tr}\Box_J M^{-1}\Box_J M^{-1}\Box_J \ldots. \tag{2.27}$$

The key observation is that the Gaussian smearing operator acts as a projection operator on the space of coloured scalar fields on a time-slice ie $N_S \times N_c$. This is nicely seen by looking at the eigenvalues of the operator ∇^2 as shown in Fig. 2.4, taken from [101]. In brief then, distillation defines smearing to be explicitly a very low-rank operator, ie $N_\mathcal{D} \ll N_S \times N_c$. The distillation operator is

$$\Box(t) = V(t)V^\dagger(t), \tag{2.28}$$

and $V^a_{\underline{x},c}(t)$ is an $N_\mathcal{D} \times (N_S \times N_c)$ matrix. One is free to choose a definition of $\Box$ and in studies to date it has been defined as $\Box_\triangle$ the projection operator into $\mathcal{D}_\triangle$, the space spanned by the lowest eigenmodes of the three-dimensional laplacian. This operator is idempotent so $\Box^2_\triangle = \Box_\triangle$ and it is also easy to see that $\lim_{N_\mathcal{D}\to(N_S\times N_C)} \Box_\triangle = 1$. Note however that this choice for ∇^2 is not unique. It does preserve lattice symmetries being translation, parity and charge-conjugation symmetric. It is $O(3)$ symmetric and as discussed in [101] is close to $SO(3)$ symmetric.

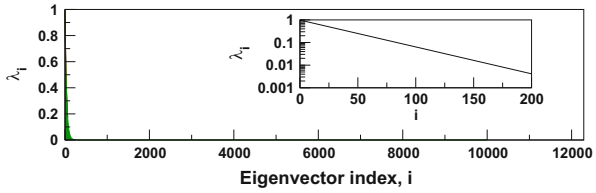

Fig. 2.4 The eigenvalues of a Gaussian smearing operator. The main pane is the raw data, barely visible while the inset shows the first 200 modes on a log scale. Only the first $\mathcal{O}(100)$ modes are significant. The data are determined on a 16^3 spatial volume

If we now consider an isovector meson two-point function

$$C_{\text{meson}}(t_1 - t_0) = \langle\langle \bar{u}(t_1)\Box_{t_1}\Gamma_{t_1}\Box_{t_1} d(t_1)\bar{d}(t_0)\Box_{t_0}\Gamma_{t_0}\Box_{t_0} u(t_0)\rangle\rangle, \tag{2.29}$$

then integrating over the quark fields yields

$$\begin{aligned} C_{\text{meson}}(t_1 - t_0) = & \\ & \langle \text{Tr}_{\{\underline{x},\sigma,c\}} \left(\Box_{t_1}\Gamma_{t_1}\Box_{t_1} M^{-1}(t_1,t_0)\Box_{t_0}\Gamma_{t_0}\Box_{t_0} M^{-1}(t_0,t_1)\right)\rangle. \end{aligned} \tag{2.30}$$

Now, substituting the low-rank distillation operator for $\Box$ reduces this to a much smaller trace, written

$$C_{\text{meson}}(t_1 - t_0) = \langle \text{Tr}_{\sigma,\mathcal{D}} \left[\phi(t_1)\tau(t_1,t_0)\phi(t_0)\tau(t_0,t_1)\right]\rangle, \tag{2.31}$$

where both $\phi^{\alpha,a}_{\beta,b}$ and $\tau^{\alpha,a}_{\beta,b}$ are $(N_\sigma \times N_\mathcal{D}) \times (N_\sigma \times N_\mathcal{D})$ matrices and

$$\phi(t) = V^\dagger(t)\Gamma_l V(t); \quad \tau(t,t') = V^\dagger M^{-1}(t,t')V(t'). \tag{2.32}$$

In the low-rank space, all elements of the reduced quark propagator are now accessible in a reasonable amount of compute time. As well as the reduction in compute time, distillation offers a second advantage: the separation of operator construction from quark propagation. Note that in Eq. (2.31) the function $\tau(t,t')$, known as the *perambulator*, contains the information on quark propagation while the $\phi(t)$ describe the source and sink operators and determine the quantum numbers of the state to be constructed. The perambulators may be calculated and stored to be combined *a posteriori* with any number of source and sink operators. In addition, the number of eigenvalues used in $\Box$ may also be increased *a posteriori* without starting a calculation from scratch.

Distillation has proved particularly successful for calculations of isoscalar mesons, which traditionally have been difficult if not impossible to determine with precision. Figure 2.5 is taken from [103] and shows the disconnected contributions to the two-point correlation function, denoted $\mathcal{D}$ for the $\bar{\Psi}\gamma_5\Psi$ operator in the light meson sector together with the connected contributions, $\mathcal{C}$. Figure 2.6 shows the corresponding isoscalar spectrum of light mesons.

While distillation offers a new avenue for precision spectroscopy it is not suitable for all hadronic physics. A particular example includes the strangeness content of the nucleon for which the standard all-to-all algorithms must be used.

In addition, the cost of distillation grows rapidly with the spatial volume of the lattice. $N_\mathcal{D}$ scales with N_S and to maintain a constant resolution in the distillation space the cost of a calculation scales with V^2. Table 2.1 illustrates the cost scaling as a function of volume for mesons and baryons. However, the method has been successfully used on volumes up to 24^3 with $N_\mathcal{D} = 128$ for a range of physics.

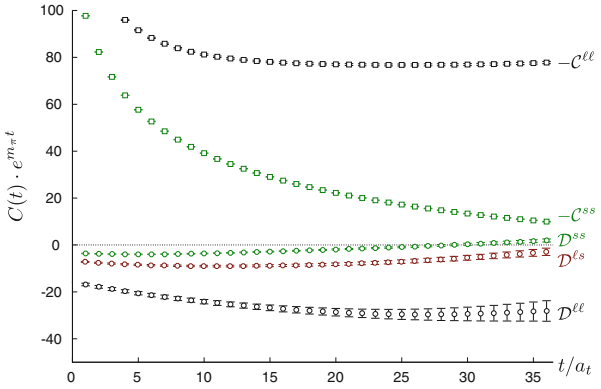

Fig. 2.5 Distillation allows for precision calculation of disconnected contributions. The plot shows the connected as well as disconnected contributions, determined using distillation. Note the statistical precision and persistence of the signal for the disconnected diagrams

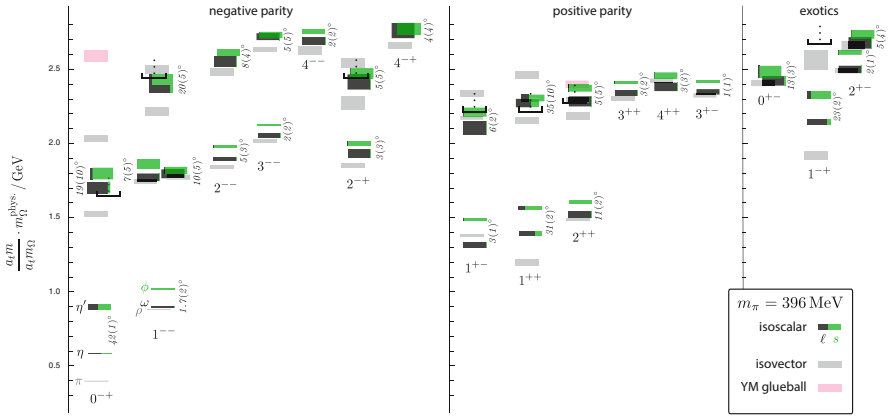

Fig. 2.6 The light meson isoscalar spectrum from the Hadron Spectrum Collaboration

Table 2.1 The cost scaling of distillation from inversions to contractions for mesons and baryons

Fermion solutions	Construct τ	$\mathcal{O}(N_S^2)$
Operator constructions	Construct ϕ	$\mathcal{O}(N_S^2)$
Meson contractions	$\text{Tr}[\phi\tau\phi\tau]$	$\mathcal{O}(N_S^3)$
Baryon contractions	$\bar{B}\tau\tau\tau B$	$\mathcal{O}(N_S^4)$

One solution, to mitigate the cost of distillation with increasing volume, is once again to use stochastic estimation techniques, together with distillation called stochastic LapH [104]. A stochastic identity matrix is constructed in the distillation space $\mathcal{D}$ by introducing a vector η with $N_\mathcal{D}$ elements and

$$E[\eta_i] = 0 \quad \text{and} \quad E[\eta_i \eta_j^*] = \delta_{ij}. \tag{2.33}$$

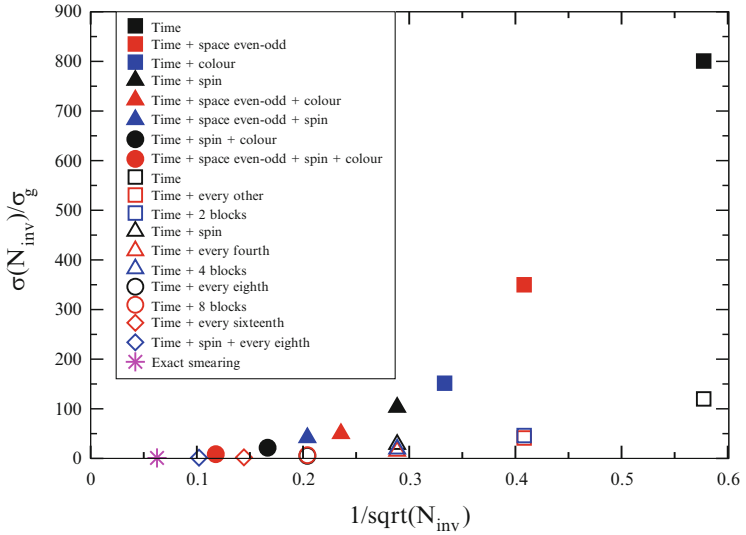

Fig. 2.7 The ratio of the standard deviation from different stochastic estimators to the exact LapH estimate on time slice 5 for a nucleon correlator. Filled symbols denoted noise introduced on the entire lattice, open symbols use the "stochastic LapH" method outlined here

The distillation operator is then

$$\square = E[V\eta\eta^\dagger V^\dagger] = E[WW^\dagger]. \tag{2.34}$$

Of course this introduces noise into the computations and variance reduction once again becomes important. A good approach, as we saw earlier, is then to use dilution as before to "thin out" the stochastic noise. One can use $N_\mathcal{D}$ orthogonal projectors to make a variance-reduced estimator of $I_\mathcal{D} = E[WW^\dagger] = \sum_{k=1}^{N_\eta} E[V\mathcal{P}_k\eta\eta^\dagger\mathcal{P}_k V^\dagger]$ with $W_k = V\mathcal{P}_k\eta$ a $N_\eta \times (N_S \times N_C)$ matrix. Figure 2.7, taken from [105] demonstrates the improvements achieved using different dilution strategies for noise in distillation space for a baryon correlator compared to noise introduced across the entire lattice.

2.2.4 Interim Summary

In this section we have discussed methods to calculate quark propagation and make measurements. In this context it is useful to note that smearing and distillation are both rotationally symmetric operations and so do not change the quantum numbers of the states being determined. Algorithms which address the exponential fall in signal-to-noise in correlators and which reduce the cost of making measurements

are crucial. This is especially true for precision spectroscopy, the determination of exotic states and isoscalar mesons and for a strategy to include multi-hadron states in lattice calculations.

Exercise Do the linear algebra to derive Eqs. (2.30–2.31).

2.3 Lattice Symmetries and Classifying States

In continuum QCD observable states are classified according to angular momentum and parity, J^P which label the irreducible representations (irreps) of the relevant symmetry group: the improper rotation group $O(3)$. These irreps include bosonic (single-valued) and fermionic (double-valued) representations and in addition, the projection of angular momentum onto some axis, J_z labels rows of the representation.

On a spatially isotropic lattice the continuous rotational symmetry is broken and the relevant symmetry group is O_h, the cubic point group. Eigenstates of the lattice hamiltonian then transform under irreps of O_h and lattice states are classified by these irreps (Λ^P) rather than by J^P. A manifestation of this symmetry breaking is that continuum states with the same J^P but different J_z values are in general separated across lattice irreps. It is important then to design operators which couple strongly to lattice eigenstates, i.e. which project into the irreps of O_h.

Now, let us consider the symmetry group of the cube in more detail. The correct group to consider is O the octahedral group which is dual to a cube. There are 24 rotational (orientation-preserving/proper) symmetries and 48 if one includes combinations of reflection and rotation. This leads us to consider the cubic point group $O_h = O \otimes \{I, I_s\}$. O has five conjugacy classes (O_h has 10) and the number of conjugacy classes gives the number of irreps. Using Schur's lemma for a group G and irreps Γ_i of G,

$$|G| = \sum_i \dim(\Gamma_i)^2, \tag{2.35}$$

and a short calculation shows that for O we get: $24 = 1^2 + 1^2 + 2^2 + 3^2 + 3^2$ the dimensions of the five irreps of O labelled A_1, A_2, E, T_1, T_2 respectively. The extension to O_h includes the 24 improper rotations (spatial inversions) of O such that

$$I_s \begin{pmatrix} x \\ y \\ z \end{pmatrix} \to \begin{pmatrix} -x \\ -y \\ -z \end{pmatrix}. \tag{2.36}$$

The number of group elements is now 48 with 10 irreps labelled

$$A_{1g}, A_{1u}, A_{2g}, A_{2u}, E_g, E_u, T_{1g}, T_{1u}, T_{2g}, T_{2u}$$

and the (g, u) label the even ($g$erade) and odd ($u$ngerade) behaviour under spatial inversion.

For baryons one considers O^D, the double cover of O. This 48-element group is obtained from O by including a negative identity (corresponding to rotations through 2π). Therefore O^D is the group through which the identity is recovered after rotation through 4π. It has eight single-valued irreps, five of which correspond to irreps of O. The three new irreps are G_1, G_2, H and once again, using Schur's lemma we get $24 = \sum_i \Gamma_i^2 = 2^2+2^2+4^2$ giving us the dimensions of the additional irreps $(2, 2, 4$ respectively).

Having briefly covered the properties of the relevant symmetry groups for mesons and baryons in lattice QCD the next section will discuss how a connection is made between the states identified in a lattice calculation and their continuum counterparts. I have not discussed group theory in detail and refer the reader to the many excellent textbooks some of which are listed here: [106–109].

2.3.1 Connecting Lattice and Continuum Groups

In this discussion, I will focus on O and meson states for simplicity, the procedure for the double cover group, O^D and baryons is the same.

In $SO(3)$ there are an infinite number of irreps (J values) whereas for O, as we have just seen, there are just five irreps. Therefore there is not a one-to-one mapping between the irreps but rather lattice irreps may contain many states from different continuum irreps. To identify which continuum states can occur in a particular lattice irrep we note firstly that O is a subgroup of $SO(3)$. By restricting the irreps of $SO(3)$ labelled by J to rotations allowed on a lattice we generate representations that are reducible ie J is reducible under O or O_h. This procedure is called subduction and using the relationship

$$n_J^{(\alpha)} = \frac{1}{N_G} \sum_k n_k \chi_k^{(\alpha)} \chi_k^{(J)}, \tag{2.37}$$

it is possible to find the multiplicity of the irreps of $SO(3)$ in O. Note that in Eq. (2.37) χ is the character of a representation, N_G is the order of the group and n_k is the dimension of the kth representation. Table 2.2 gives an example of this subduction process for continuum states up to $J = 4$. In principle then, to identify say a $J = 2$ state, results from the E and T_2 irreps at finite lattice spacing should be extrapolated to the continuum where for a particular state the results should agree. This is an expensive procedure, requiring simulations to be

Table 2.2 The results of subduction showing the relationship between the continuum and lattice irreps, up to $J = 4$. Note that as discussed in the text a continuum spin may be appear in a number of lattice irreps making spin identification for states with $J > 1$ complicated

	A_1	A_2	E	T_1	T_2
$J = 0$	1				
$J = 1$				1	
$J = 2$			1		1
$J = 3$		1		1	1
$J = 4$	1		1	1	1
$\vdots$	$\vdots$	$\vdots$	$\vdots$	$\vdots$	$\vdots$

repeated at multiple lattice spacings. Even if this were feasible it is not guaranteed to yield an unambiguously determined state. Consider the following example in the charmonium system. From Table 2.2 we see that a spin four state, 4^{++} should appear, at finite a, in the A_1, E, T_1, T_2 irreps. However, in charmonium there is also a near-degenerate triplet of P waves with quantum numbers $(0^{++}, 1^{++}, 2^{++})$ which are distributed across the same irrep pattern, namely A_1, E, T_1, T_2. In a lattice calculation, even after extrapolation to the continuum limit, it would be extremely difficult, if not impossible, to disentangle a radial excitation of this triplet from the 4^{++} ground state without some additional information. Before I discuss how to tackle this problem let me briefly mention the group theory of two particles in a box. This, of course, is relevant once states above threshold are considered where multi-hadron operators must be included. In general, for mesons in flight the relevant symmetry group is reduced to the little group of allowed cubic rotations that leave the momentum invariant. There is a detailed description in [110, 111].

2.4 Building Operators and Extracting Energies

In this chapter we have spent some time looking at different methods for quark propagation. Now, we will discuss operator construction and how to extract energies from the correlation functions determined in a lattice calculation. The meson and baryon operators are generally of the form $\mathcal{O} = \bar{\Psi}_{i\alpha}(\boldsymbol{x}, t)\Gamma_{\alpha\beta}\Psi_{i\beta}(\boldsymbol{x}, t)$ and $\mathcal{O} = \epsilon^{abc}(\Psi^a(\boldsymbol{x}, t)\Gamma\Psi^b(\boldsymbol{x}, t))\Psi^c(\boldsymbol{x}, t)$.

The simplest operators we can consider are colour-singlet local fermion bilinears such as $\mathcal{O}_\pi = \bar{d}\gamma_5 u$ and $\mathcal{O}_\rho = \bar{d}\gamma_i u$ for mesons and $\mathcal{O}_N = \epsilon^{abc}(u^a C\gamma_5 d^b)u^c$ and $\mathcal{O}_\Delta = \epsilon^{abc}(u^a C\gamma_\nu d^b)u^c$ for baryons. The local operators written here give access to states with $J = 0, 1, \frac{1}{2}, \frac{3}{2}$. While one can choose different Dirac structures Γ the spin and parity of the hadrons will put constraints on the number of operators that

can be constructed. To study higher-spin states with $J > 1$ (mesons) and $J > 3/2$ (baryons) additional operators must be used. In addition we would like many more operators that all transform irreducibly under some irrep, enabling a variational analysis.

One approach, using smearing techniques described in Sect. 2.2.1 is to use smearing functions of different widths. Combining these sources can generate nodes in the wavefunctions to better overlap with (radially) excited states. See for example [112] for a discussion and results.

Another approach (and one which can be combined with different smearings) is to use extended operators. Recall that lattice operators are bilinears, with path-ordered products between the quark (and the anti-quark) fields. Different offsets, connecting paths and spin contractions give different projections into lattice irreps. Further simple examples are given in Fig. 2.8 for mesons and in Fig. 2.9, taken from [113], for baryons. In this way one can make arbitrarily complicated operators to access high-spin states and to allow for a variational analysis. An early success of this approach was a determination of the Yang-Mills glueball spectrum [77]. QCD is a non-abelian gauge theory and so allows bound states of pure glue. In this case the interpolating fields are purely gluonic and built from Wilson loops, as shown in Fig. 2.10. The spectrum which was extracted using these operators is also shown in Fig. 2.10. Note that states with spin up to $J = 3$ were determined.

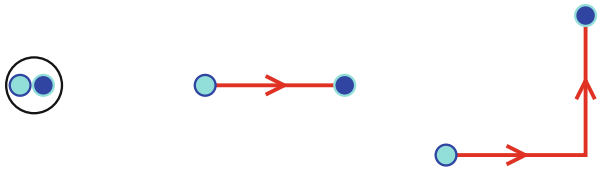

Fig. 2.8 Meson operators. Written in full these are $\mathcal{O}_{\alpha\beta} = \sum_x \bar{\Psi}_\alpha(x)\Psi_\beta(x)$, $\mathcal{O}^i_{\alpha\beta} = \sum_x \bar{\Psi}_\alpha(x)U_i(x)\Psi_\beta(x+\hat{\imath})$, $\mathcal{O}^{ij}_{\alpha\beta} = \sum_x \bar{\Psi}_\alpha(x)U_i(x)U_j(x+\hat{\imath}\Psi_\beta(x+\hat{\imath}-\hat{\jmath})$ respectively

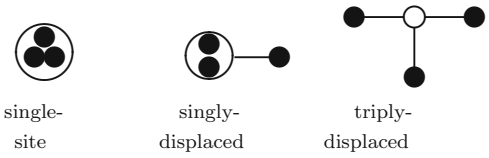

Fig. 2.9 Three different prototype extended baryon operators. The *hollow circle* is the reference site

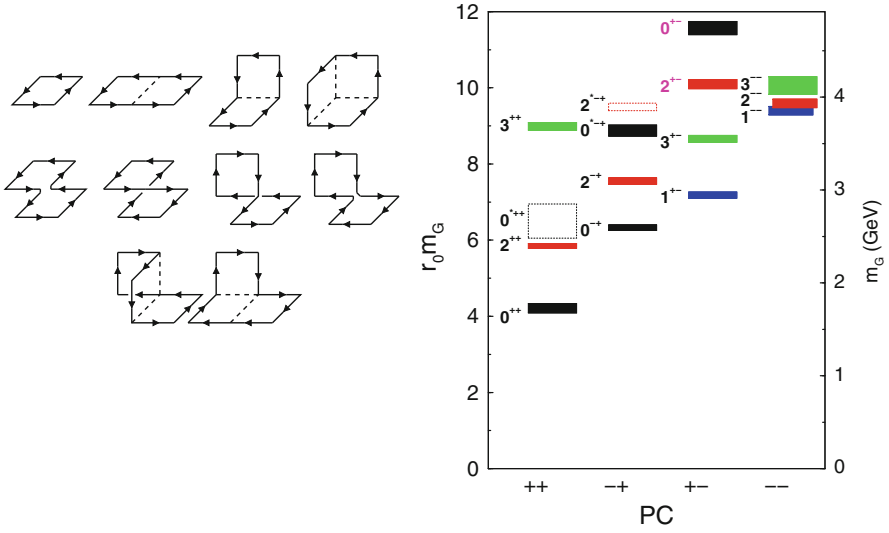

Fig. 2.10 A selection of operators for glueball spectroscopy. These were used in a variational calculation to determine the (quenched) glueball spectrum shown in the right plot

2.4.1 Constructing Good Operators

We have seen how operators of arbitrary complexity can be calculated to access, in principle, high-spin states. However, it is useful to ask what makes a "good" operator in order to maximise the statistical precision and to ensure reliable state identification at finite lattice spacing. A useful list of properties for operators includes

1. have definite momentum and transform under the symmetries of a lattice irrep
2. the basis of operators used should have a good overlap with the states of interest (eigenvectors of the variational method) which are, or are close to being, linearly independent
3. not noisy ie produce a correlator with acceptable statistical precision over a reasonable number of timeslices

On the last point we have seen how to improve statistical precision using smearing and distillation as well as noise reduction in all-to-all propagators using e.g. dilution.

Now, recall that in an earlier lecture we discussed the relationship between lattice and continuum irreps. If we now rewrite Table 2.2 we see that a correlator, $C(t) = \langle 0|\phi(t)\phi^{\dagger}(0)|0\rangle$, contains in principle information about all (continuum) spin states that appear in a lattice irrep, Λ^{PC} (Table 2.3).

The objective is to build a basis of good operators according to the bullet points listed earlier in this section. There are different approaches to optimising lattice operators and I present one here [114].

Table 2.3 The relationship between lattice and continuum irreps, determined by subduction. The table illustrates that lattice operators that transform according to a lattice irrep will contain information about more than one continuum spin state

Lattice irrep, Λ	Dimension	Continuum irreps, J
A_1	1	$0, 4, \ldots$
A_2	1	$3, 5, \ldots$
E	2	$2, 4, \ldots$
T_1	3	$1, 3, \ldots$
T_2	4	$2, 3, \ldots$
G_1	3	$\frac{1}{2}, \frac{7}{2}, \ldots$
G_2	3	$\frac{5}{2}, \frac{7}{2}, \ldots$
H	4	$\frac{3}{2}, \frac{5}{2}, \ldots$

We begin by considering continuum operators built from n derivatives of the form

$$\phi = \bar{\Psi} \Gamma \left(D_{i1} D_{i2} D_{i3} \ldots D_{in} \right) \Psi. \tag{2.38}$$

Construct irreps of $SO(3)$ and then subduce these representations into O_h. Now replace the derivatives with lattice finite differences such that

$$D_j \Psi(x) \to \frac{1}{a} \left(U_j(x) \Psi(x + \hat{\jmath} - U_j^{\dagger}(x - \hat{\jmath}) \Psi(x - \hat{\jmath}) \right), \tag{2.39}$$

where we note that on a discrete lattice, covariant derivatives become finite displacements of quark fields connected by links.

The final step is the empirical observation, with for example a more detailed discussion in [115], that the overlaps $\mathcal{Z} = \langle 0 | \phi^{\Lambda^{PC}} | J^{PC(\Lambda)} \rangle$ in the different lattice irreps subduced from a common continuum irrep are the same up to rotation-breaking effects.

To see this explicitly let us consider an operator for the $J^{PC} = 2^{++}$ meson. Recall from Table 2.2 that a spin two state will be split across the T_2 and E lattice irreps. In the continuum an operator that creates a state with 2^{++} quantum numbers is

$$\phi_{ij} = \bar{\Psi} \left(\gamma_i D_j + \gamma_j D_i - \frac{2}{3} \delta_{ij} \gamma \cdot D \right) \Psi. \tag{2.40}$$

Following the recipe described above we substitute gauge-covariant lattice finite differences for D. By subduction we find that

$$\begin{aligned} \phi^{T_2} &= \{ \phi_{12}, \phi_{23}, \phi_{31} \}, \\ \phi^{E} &= \left\{ \frac{1}{\sqrt{2}} (\phi_{11} - \phi_{22}), \frac{1}{\sqrt{6}} (\phi_{11} + \phi_{22} + \phi_{33}) \right\}. \end{aligned}$$

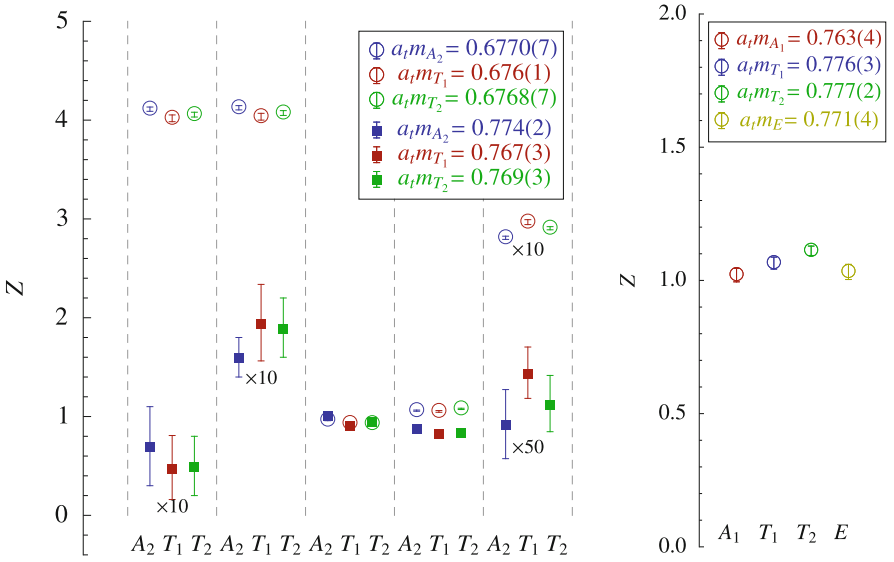

Fig. 2.11 An example of the agreement of overlaps of lattice operators from different irreps which have been subduced from the same continuum operator. For more details see [116] and references therein

States determined from variational analyses in these two different irreps should then agree in the continuum limit and at finite a be reasonably close, assuming (hopefully) small discretisation effects. A second tool at finite a is to examine the operator overlaps $\mathcal{Z}$ for the signature of continuum symmetry

$$\mathcal{Z} = \langle 0|\phi^{(T_2)}|2^{++(T_2)}\rangle = \langle 0|\phi^{(E)}|2^{++(E)}\rangle, \tag{2.41}$$

up to rotation-breaking effects. This approach has been followed by the Hadron Spectrum Collaboration to good effect. Figure 2.11 taken from [116] shows this operator overlap analysis for spin three and spin four states in charmonium. In each case there is very good agreement across the relevant irreps (A_2, T_1, T_2 for $J = 3$ and A_1, T_1, T_2, E for $J = 4$).

2.4.2 *Fitting Data to Extract Energies*

Hadron energies are determined from 2-point correlation functions. We begin by considering a simple correlator of the form

$$C(\boldsymbol{p}, t) = \sum_{\boldsymbol{x}} e^{i\,\boldsymbol{p}\cdot\boldsymbol{x}}\, \langle \mathcal{O}(\boldsymbol{x}, t)\mathcal{O}^{\dagger}(\boldsymbol{0}, t)\rangle, \tag{2.42}$$

where $\mathcal{O}$ is a single interpolating operator for the hadron of interest. Recall that by inserting a complete set of energy eigenstates $|n\rangle$ and assuming a discrete energy spectrum as $t \to \infty$ and for hadrons at rest

$$C(t) \to \frac{1}{2E_n} |\langle 0|\mathcal{O}|n_0\rangle|^2 \; e^{-E_0 t}, \tag{2.43}$$

where n_0 is the lightest state that couples to $\mathcal{O}$ and has energy E_0.

Again, recall that a useful quantity for this analysis is the *effective mass*

$$a_t M_{\text{eff}}(t) = \ln\left(\frac{C(t)}{C(t+1)}\right) \overset{t\to\infty}{\longrightarrow} \text{constant}, \tag{2.44}$$

and an alternative definition appropriate for mesons, under periodic boundary conditions, uses the hyperbolic cosine and is given by

$$a_t M_{\text{eff}}(t) = \cosh^{-1}\left(\frac{C(t+1) + C(t-1)}{2C(t)}\right). \tag{2.45}$$

At large time separations on the lattice the ground state dominates and the effective mass should plateau at this energy. Of course the onset and length of the plateau will depend on $\mathcal{O}$. The hadron mass is extracted from fits to correlator data in this plateau region. Such fits require some finesse however since statistical errors grow exponentially with t (except in the case of the pion) and fitting too far out in the temporal extent increases the statistical uncertainty.

Figure 2.12 shows a typical effective mass plot—in this case for the vector J/Ψ charmonium state. The cyan box highlights the plateau region, at large times, where the effective mass converges to the ground state. In this region the correlator data is fitted to the expected form, $C(t) = Ae^{-E_0 t}$ using, for example, a χ^2 minimisation algorithm with A and E_0 free parameters and for some "reasonable" choice of time

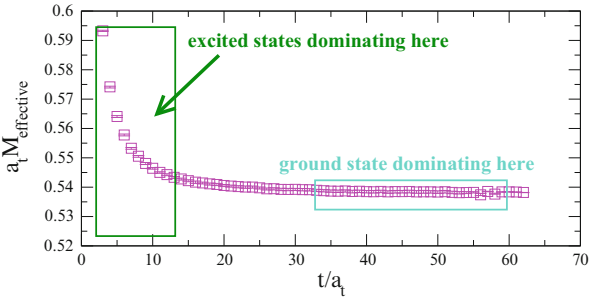

Fig. 2.12 The same plot as in Fig. 2.2 now with the plateau region and the region of excited state contamination highlighted

range. Statistical errors on the fitted energy can be determined using bootstrap or jackknife (described later). The plot also shows a region where excited state energies are significant and a single-exponential fit would not be reasonable.

2.4.2.1 Resampling Techniques

Bootstrap and Jackknife are examples of what is known as resampling and both are used extensively to estimate statistical errors in lattice calculations.

The jackknife method was introduced by Quenouille in 1949 to estimate the bias of an estimator and later further refined by Tukey (who also gave us the FFT) in 1957. Consider a set of N measurements, and remove the first leaving a jackknifed set of $N-1$ resampled measurements. Repeat the analysis (in our case the exponential fits) on this reduced set, giving parameters $\alpha_{J(1)}$. The resampling is repeated, discarding the second measurement etc to get a set of parameters $\alpha_{J(i)},\ i = 1, \ldots, N$. The statistical error is then estimated from averages over the resampled set

$$\sigma_J^2 = \frac{(N-1)}{N} \sum_{i=1}^{N} \left(\alpha_{J(i)} - \alpha\right)^2, \tag{2.46}$$

where α is the result from fitting the full dataset.

The second resampling technique is the bootstrap method, developed by Efron in the late 1970s. In this case a new dataset is created by drawing N datapoints, with replacement, from the original dataset of size N. Replacement means that a configuration may appear twice in a sample; thus you do not get the original set each time but a set with a random fraction of the original points with some appearing multiple times. As for the jackknife method, the analysis is repeated on each set.

2.4.2.2 Notes on Fitting

When fitting correlator data to exponentials a good fit can be characterised by a few measures

1. the fit should be stable with respect to the choice of time range in the plateau region. In particular, it should be stable with respect to small changes in t_{min}, the minimum timeslice included in the fit.
2. the fit should include a reasonable range in t. The number of points included will of course depend on the temporal extent and resolution of the lattice.
3. the energy extracted should be stable if additional exponentials are added to the fitting function.
4. for correlated fits, a good $\chi^2/N_{\text{d.o.f.}}$, typically of order one when this quantity can be reliably determined.
5. "reasonable" statistical errors on the fitted mass.

Within the lattice QCD community there are some well-established quantities which are used to describe the quality of fits, including

1. a sliding window plot: the fitted mass is plotted as a function of t_{min}. A plateau region in this plot means the fitted mass is stable as a function of t_{min}.
2. a fit histogram: the idea is to design a quantity that monitors the behaviour of a good fit as described above. An example is to plot $QN_{\text{d.o.f.}}/(\Delta m)$ for each $(t_{\text{min}}, t_{\text{max}})$ with $Q = \Gamma[(\text{interval} - N_{\text{param}})/2, \chi^2/2]$ and choose the $(t_{\text{min}}, t_{\text{max}})$ that maximises this quantity.
3. χ-by-eye: always a good idea to check fit ranges do look reasonable on the effective mass plots.

The analysis discussed so far is focused on determinations of ground state energies. Looking again at the sample effective mass plot, shown in Fig. 2.12, it is clear that while a single exponential dominates at large times, at short time separations there are contributions from higher excited states in the form of additional exponentials in the correlation function

$$C(t) = Ae^{-E_0 t} + Be^{-E_1 t} + \ldots. \tag{2.47}$$

A two-exponential fit with parameters A, B, E_0, E_1 may allow for a determination of E_1, the energy of the first excited state. A reasonable approach since the regions where E_0 and E_1 are distinct is to fit for E_0 as described, and freeze its value in a fit for E_1. However, these two exponential fits can be very unstable and a different approach is needed especially to extract energies above just the first excited state. There are a number of techniques for this including Bayesian analysis; χ^2-histogram analysis and a variational analysis. I will discuss the latter in more detail.

2.4.2.3 A Little More on Variational Analysis

We have already seen the basics of a variational analysis and is described in [117, 118] and [93]. In a brief recap we consider a basis of operators $\mathcal{O}_i$ for $i = 1, \ldots, N$ in a given lattice irrep. Form a matrix of correlators

$$C_{ij}(t) = \langle \mathcal{O}_i(t) \mathcal{O}_j^\dagger(0) \rangle, \tag{2.48}$$

and treat this system as a generalised eigenvalue problem

$$C(t)\mathbf{v}_n(t, t_0) = \lambda_n(t, t_0) C(t_0) \mathbf{v}_n(t, t_0), \tag{2.49}$$

where t_0 is a reference timeslice which you choose. The vectors $\mathbf{v}_n$ diagonalise $C(t)$ and for finite N one can show that a generalised effective mass is

$$E_n^{\text{eff}}(t, t_0) = -\partial_t \log \lambda_n(t, t_0) = E_n + O(e^{-\Delta E_n t}). \tag{2.50}$$

The eigenvalues λ_n that are solved for in the GEVP and ordered such that $\lambda_1(t) > \lambda_2(t) > \ldots \lambda_N(t)$ at large t. The λ_i are then related to the energies of the states in the irrep and these energies can be extracted from fits to the "principal correlators". When using jackknife or bootstrap techniques the eigenvectors resulting from the GEVP should be also be monitored to maintain a consistent ordering in the samples. Note that the procedure depends on the choice of reference timeslice, t_0. In an analysis this parameter should be varied to test the robustness of results. In particular, if the value of t_0 is too small then states with energies larger than that of interest, say E_n will contaminate the results. This is especially true if there is just a small energy gap to E_{n+1} and in this case a large distance in t will be needed to resolve a plateau. Values of t_0 too large may result in numerical instabilities.

2.4.2.4 Anisotropic Lattices

Let me make a brief comment here on the utility of anisotropic lattices for hadron spectroscopy. If we can build a good basis of operators we have seen how we can extract energies for low-lying states from the correlator at short distances. The lattice correlator can only be sampled at discrete values of t and signal can fall quickly for a massive state, while the statistical noise does not. A brute force approach to reduce the lattice spacing in all directions is a costly solution to this problem. Nevertheless one can mitigate the cost by reducing the temporal lattice spacing, a_t whilst keeping the spatial mesh coarse. This is an anisotropic lattice.

Of course, the anisotropic lattice reduces the symmetries of the theory from the hypercubic to the cubic point group and for example, the dimension four operators on the lattice are split

$$\begin{aligned} \mathrm{Tr} F_{\mu\nu} F_{\mu\nu} &\rightarrow \left\{ \mathrm{Tr} F_{ij} F_{ij}, \mathrm{Tr} F_{i0} F_{i0} \right\} \\ \bar{\Psi} \gamma_\mu D_\mu \Psi &\rightarrow \left\{ \bar{\Psi} \gamma_i D_i \Psi, \bar{\Psi} \gamma_0 D_0 \Psi \right\} . \end{aligned}$$

Note that on the $3 \oplus 1$ anisotropic lattice described here the spatial symmetries are unchanged from the isotropic case and the group theory and operator construction discussions from earlier sections are unchanged.

There is a cost to this approach however. The space-time symmetry breaking introduces extra bare parameters in the lagrangian, arising from the so-called aspect ratio, $\xi = a_s/a_t$, which must be tuned to restore Euclidean rotational invariance in the continuum limit. For QCD one can think of this as demanding that quarks and gluons "feel" the same anisotropy. This requires an *a priori* tuning of parameters. In dynamical QCD where the fermions contribute through the determinant term in the path integral two physical conditions, one in the gauge sector and one in the fermion sector, must be simultaneously satisfied. A typical example uses the sideways potential and the pion dispersion relation. Each time the lattice spacing (temporal or

spatial) is changed the tuning must be repeated. In addition taking a continuum limit is challenging as one should consider the temporal and spatial spacings separately. Nevertheless, the anisotropic lattice as proved extremely effective for resolving precisely the energy levels of hadrons from light to heavy.

2.4.3 A Lattice Error Budget

In this section I have not discussed the standard systematic uncertainties which must be accounted for in a lattice calculation. These effect all lattice calculations, not specifically hadronic quantities and have also been discussed elsewhere at this School. They include lattice artefacts: which require an extrapolation to the continuum limit, $a \to 0$; finite volume effects: in spectroscopy energy measurements can be distorted by the finite box. A rule of thumb is that $m_\pi L > 3$ is reasonable for many quantities; unphysically heavy pions: simulations at the physical point are now a reality but most calculations still rely on chiral extrapolation to reach physical up and down quark masses. Chiral perturbation theory (ChPT) is used to guide these extrapolations but an open question is whether chiral corrections are reliably described by ChPT; Fitting uncertainties: the choice of fit range and t_0 and how to choose these quantities has been discussed above.

2.5 Current Challenges

In this final section I would like to discuss some challenges for lattice hadron spectroscopy. I will focus on one topic: resonances and scattering. The most recent progress on this (and other topics in spectroscopy) has been described in plenary and parallel sessions at Lattice 2013 [119].

2.5.1 Resonances and Scattering States

In this chapter we have assumed that all particles in the spectrum are stable, and that quark bilinears or three-quark operators are a reliable way to reproduce the states of interest. However, the majority of states are not stable and are in fact resonances or scattering states. A resonance is a state that forms for example when colliding two particles and which then decays quickly to scattering states. Resonances respect conservation laws: if the isospin of the colliding particles is $\frac{3}{2}$ then the resonance must have isospin $\frac{3}{2}$ (a Δ resonance). They are usually indicated by a sharp peak in a cross-section as a function of the centre-of-mass energy of the collision.

A challenge for lattice QCD is to distinguish and describe resonances and scattering states. The difficulty for lattice calculations lies in the Maiani-Testa no-go theorem [120]. Recall that importance sampling in Monte-Carlo simulations relies on having a path integral with positive definite probability measure, which is the motivation for the Wick rotation to Euclidean space. However, the Maiani-Testa theorem states that in general, scattering matrix (S-matrix) elements cannot be extracted from infinite-volume Euclidean-space correlation functions. In Minkowski space the S-matrix elements are complex functions, above kinematic thresholds. However, in a Monte-Carlo calculation (in Euclidean space) these matrix elements are real and there is no distinction between the $|in\rangle$ and $|out\rangle$ states and information about the phase due to final-state interactions is lost. Lüscher showed how information about elastic scattering can be inferred from the volume-dependence of the spectrum. The formalism for the relativistic (elastic) case in a cubic box for a system at rest is described in [117, 121] and was subsequently extended to moving frames in [122–124].

This has led to renewed progress in recent years in studies of scattering states and resonances which has been enabled by some of the new techniques described in these lectures. In particular, to be able to determine volume-dependence reliably it is crucial to have precise data and unambiguous spin-identification so that two-hadron states can be distinguished from nearby excited states.

2.5.1.1 The Lüscher Formalism

In general, on a finite lattice with periodic boundary conditions the hadron momenta are quantised: $\underline{p} = \frac{2\pi}{L}\{n_x, n_y, n_z\}$, with $n_i \in \{0, 1, 2, \ldots L-1\}$, and the energy spectrum is a set of discrete levels, classified by $\underline{p}$. The allowed energies, for a particle of mass m are

$$E = \sqrt{m^2 + \left(\frac{2\pi}{L}\right)^2 N^2}, \quad \text{where} \quad N^2 = n_x^2 + n_y^2 + n_z^2. \tag{2.51}$$

The density of states in such systems will increase with energy since there are more momenta combinations for a given N^2 e.g. both $(3, 0, 0)$ and $(2, 2, 1)$ correspond to $N^2 = 9$. It is also of course possible to construct a system with zero total angular momentum from two hadrons with back-to-back momentum, $\underline{p}$ and $-\underline{p}$.

A brief example is given by the $\rho \to \pi\pi$ system. The energy levels of two non-interacting pions in a periodic box of length L are

$$E = 2\sqrt{m_\pi^2 + p^2}, \quad p = \frac{2\pi|\boldsymbol{n}|}{L} \tag{2.52}$$

where as usual $\boldsymbol{n}$ has components $n_i \in \mathbb{Z}$. Considering the interacting case, the energy levels are

$$E = 2\sqrt{m_\pi^2 + p^2}, \quad p = \left(\frac{2\pi}{L}\right) q \tag{2.53}$$

where q is no longer constrained to originate from a quantised momentum mode. Therefore the energy eigenvalues will deviate from the noninteracting case. These deviations contain information about the underlying strong interaction and yield resonance information via the Lüscher formalism described by

$$\delta(p) = -\phi(q) + \pi n, \tag{2.54}$$

where

$$\tan\phi(q) = -\frac{\pi^{3/2} q}{Z_{00}(1; q^2)} \quad \text{and} \quad q = \frac{pL}{2\pi}. \tag{2.55}$$

As usual, p_n is defined for level n with energy E_n from the dispersion relation $E_n = 2\sqrt{m^2 + p_n^2}$. The Z_{00} is a generalised Zeta function given by [125]

$$Z_{jm}(s, q^2) = \sum_{n \in \mathbb{Z}^3} \frac{r^j Y_{jm}(\theta, \phi)}{(n^2 - q^2)^s}. \tag{2.56}$$

Once the phase shift is determined and for a well-defined resonance, one can fit a Breit-Wigner to extract the resonance width Γ_ρ and mass m_ρ,

$$\frac{p^3}{E} \cot\delta(p) = -\frac{p_\rho^3}{m_\rho^2 \Gamma_\rho}(E^2 - m_\rho^2), \qquad p_\rho = \frac{1}{2}\sqrt{m_\rho^2 - 4m_\pi^2}. \tag{2.57}$$

To extract these energy shifts one needs good operators for both single-hadron and multi-hadron states. Distillation has proved a crucial tool in this regard. Our example, $\rho \to \pi\pi$, is in isospin one, and in principle this involves disconnected diagrams which, as already discussed, add additional complexity to lattice calculations. One can learn a lot however, by looking at the simpler $I = 2$, $\pi\pi$ system. The Hadron Spectrum Collaboration has produced a detailed study of this system including many operators to map out the phase shift in great detail. Figure 2.13 shows the energy shifts in $I = 2$ $\pi\pi$ scattering from [126]. The phase shift (for $l = 0$, the lowest wave and $l = 2$) has been calculated for many different momenta and different volumes as shown in Fig. 2.14. More recently [127], the $I = 1$ phase shift has been mapped out in great detail and a resonance width and mass extracted. There are already similar calculations in the open charm sector both with much fewer momenta points or lower statistics [128, 129]. More can be expected in the

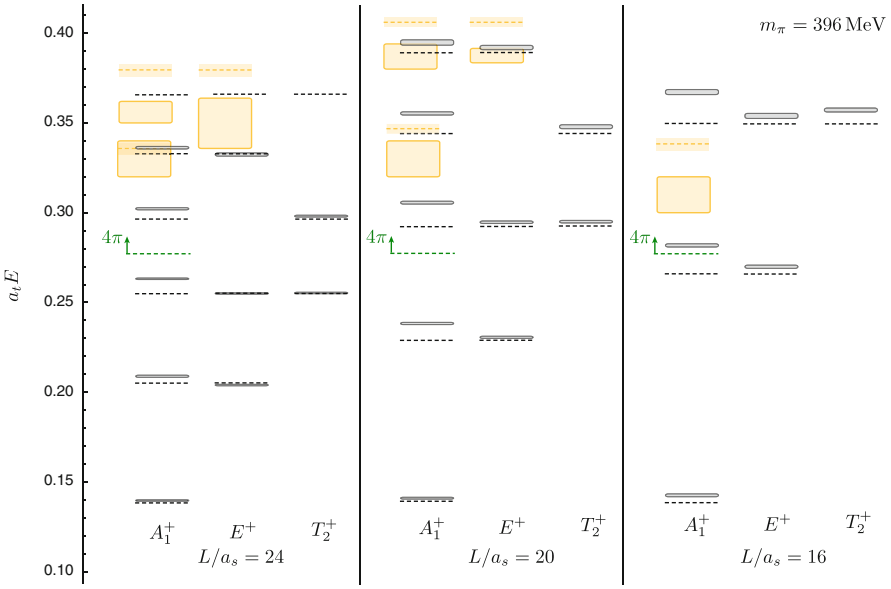

Fig. 2.13 Energy shifts in $I = 2$ for three volumes and three lattice irreps. *Solid black lines* are the energy levels extracted from a variational analysis. The *dashed lines* are the expected non-interacting levels and the *orange boxes* are possible $\pi\pi^*$ scattering states

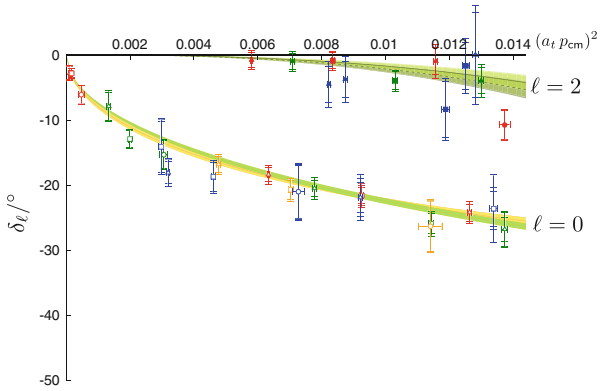

Fig. 2.14 The phase shift in $I = 2$, for $l = 0$ and $l = 2$ at a pion mass of 396MeV

near future and new theoretical frameworks in scattering [130] hint at interesting prospects for further results.

2.6 Summary

There is much exciting work in spectroscopy that I have been unable to cover in these lectures and I refer the reader to the proceedings of recent Lattice conferences for further details. I chose to focus on methods, both old and new, for the basic building blocks of spectroscopy and hopefully described their applications as well as some of the attendant pitfalls. Lattice hadron spectroscopy is progressing rapidly at the moment and new ground-breaking calculations and methods are emerging. We can also expect many new discoveries and data for existing and planned experiments in the next ten years. The challenge is for lattice calculations to keep pace!

Acknowledgements I would like to thank the organisers for an enjoyable and stimulating school and the INT for support for my visit. I have also been supported by the Science Foundation Ireland through the award of grant number 11-RFP.1-PHY-3201 and by the Research Executive Agency (REA) of the European Union under Grant Agreement number PITN-GA-2009-238353 (ITN STRONGnet).

Chapter 3
Hadron Structure on the Lattice

K.U. Can, A. Kusno, E.V. Mastropas, and J.M. Zanotti

Abstract The aim of these lectures will be to provide an introduction to some of the concepts needed to study the structure of hadrons on the lattice. Topics covered include the electromagnetic form factors of the nucleon and pion, the nucleon's axial charge and moments of parton and generalised parton distribution functions. These are placed in a phenomenological context by describing how they can lead to insights into the distribution of charge, spin and momentum amongst a hadron's partonic constituents. We discuss the techniques required for extracting the relevant matrix elements from lattice simulations and draw attention to potential sources of systematic error. Examples of recent lattice results are presented and are compared with results from both experiment and theoretical models.

3.1 Introduction

The proton was believed to be a point-like particle until the measurement of its magnetic moment by Nobel-Prize laureate Otto Stern in 1933. The significant deviation of the measured value $\mu_p \approx 2.5\mu_N$ from the unit nuclear magneton $\mu_N = e/2M_N$, where M_N is the nucleon mass, provided first evidence for the composite nature of the proton. The latest CODATA value now indicates that $\mu_p = 2.792847356(23)\mu_N$. Our modern understanding is that the nucleon is not a point-like particle but a colour-singlet bound state of the fundamental building blocks of hadronic matter: quarks and gluons. It is a challenge, however, to understand

K.U. Can (✉)
Department of Physics, H-27, Tokyo Institute of Technology, Meguro, Tokyo 152-8551 Japan
e-mail: utku.can@th.phys.titech.ac.jp

A. Kusno • E.V. Mastropas
Department of Physics, College of William and Mary, P.O. Box 8795, Williamsburg VA 23187-8795, USA
e-mail: akusno@email.wm.edu; emastropas@email.wm.edu

J.M. Zanotti
CSSM, School of Chemistry and Physics, The University of Adelaide, Adelaide SA 5005, Australia
e-mail: james.zanotti@adelaide.edu.au

H.-W. Lin, H.B. Meyer (eds.), *Lattice QCD for Nuclear Physics*, Lecture Notes in Physics 889, DOI 10.1007/978-3-319-08022-2_3

how these constituents are distributed inside the nucleon and how they combine to give the nucleon its fundamental properties. We can immediately think of questions like: being a charge neutral object, does the neutron have a charged core in analogy with an atom or is the charge distributed homogeneously? How do the constituents combine to form the different hadrons? And can we find unravel the spin structure of the proton?

The electromagnetic current is the perfect probe for investigating the charge and magnetisation distributions of the nucleon, whereas the axial-vector current can resolve the spin structure. For instance, it is still a mystery as to how much of the spin of the proton is carried by quarks and gluons. Deep-inelastic scattering experiments, for example, indicate that only $1/3$ of the proton's spin is carried by quarks and antiquarks [131,132]. This problem was originally known as the "proton-spin crisis" and demonstrates that questions still remain as to the fundamental structure of hadrons.

Experimental probes of nucleon electromagnetic structure are based on electron-proton scattering processes, since QED is a well-understood theory, and its small fine-structure constant allows perturbative calculations. From the experimental point of view it is also easy to accelerate electrons and tune their energies to desired values. The electron-proton scattering processes can be considered in two categories: elastic and deep-inelastic scattering.

In these lecture notes, we will first introduce some of the phenomenological quantities used to assist in our understanding of nucleon structure and some of the experimental processes used to determine them. We then turn our attention to studying some of the techniques used to study these same quantities on the lattice, together with some detailed examples for the more common calculations. We will finish by placing the lattice methods in context by highlighting a couple of recent results and comparing them to experimental determinations.

3.2 Experimental Probes

3.2.1 Elastic $e-p$ Scattering

In elastic electron-nucleon scattering, the electron interacts with the nucleon via photons and leaves the nucleon intact but with recoil. This process is dominated by single-photon exchange, and it is possible to map out the charge and magnetisation-density distributions of the nucleon by varying the momentum transferred to the nucleon target. If we consider the nucleon to be a point-like particle, we can describe the interaction cross section of this process with the Mott formula:

$$\left(\frac{d\sigma}{d\Omega}\right)_{\text{point}} = \frac{(Z\alpha)^2 E^2}{4k^2 \sin^4(\theta/2)} \left(1 - \frac{k^2}{E^2} \sin^2(\theta/2)\right), \tag{3.1}$$

where Z is the atomic (proton) number, α is the fine-structure constant, E and k are the energy and momentum of the incoming electron, and θ is the scattering angle described as $q^2 = -4EE' \sin^2(\theta/2)$, with E' the outgoing electron energy and q the transfer momentum. However, experimental data shows a clear deviation from the point-like cross section, indicating that the nucleon has some internal structure. So it is necessary to reconsider the cross-section formula and include a term that depends on q^2,

$$\frac{d\sigma}{d\Omega} = \left(\frac{d\sigma}{d\Omega}\right)_{\text{point}} \left|F(q^2)\right|^2 . \tag{3.2}$$

3.2.1.1 Rosenbluth Formula

We will attempt to rewrite the cross section starting from the S-matrix. For simplicity, we will consider only the tree-level diagram, however, since the fine-structure constant is small and one-photon exchange diagrams dominate the process. This was expected to be a safe approximation, but in fact it is now known that the inclusion of two-photon exchange effects are vital (see, e.g., [133]), especially at large q^2; nonetheless, we will not consider these here. The S-matrix is given by

$$\begin{aligned} S &= (2\pi)^4 \delta^4(k + P - P' - k')\bar{u}(k')(-ie\gamma^\mu)u(k)\frac{-i}{q^2}\left\langle P'|(ie)J_\mu|P\right\rangle \\ &= -i(2\pi)^4 \delta^4(k + P - P' - k')\mathcal{M}\,, \end{aligned} \tag{3.3}$$

where the Dirac-delta function ensures energy-momentum conservation, $\bar{u}(k')$ and $u(k)$ are the fermion spinor fields with four-momenta k and k', $(-ie\gamma^\mu)$ is the electron-photon vertex, and $\langle P'|(ie)J_\mu|P\rangle$ the photon-nucleon vertex. In the second step we have introduced the invariant amplitude $\mathcal{M}$,

$$\mathcal{M} = \frac{1}{q^2}\bar{u}(k')(-ie\gamma^\mu)u(k)\langle P'|(ie)J_\mu|P\rangle. \tag{3.4}$$

The electromagnetic current is

$$J^\mu = \sum_i e_i \bar{\psi}_i \gamma^\mu \psi_i\,, \tag{3.5}$$

where the index i sums over all quark flavours with $m_q \ll m_p$, namely the up, down and strange quarks. The cross section in terms of invariant amplitude can be written as

$$d\sigma = \frac{E'}{2EM^2}\frac{1}{1 + \frac{2E}{M}\sin^2(\theta/2)}|\mathcal{M}|^2\frac{d\Omega}{(2\pi)^2}\,, \tag{3.6}$$

where E' is the energy of the scattered electron, and we write the squared invariant amplitude in terms of leptonic and hadronic tensors:

$$|\mathcal{M}|^2 = \frac{e^4}{Q^4} \ell^{\mu\nu} W_{\mu\nu} \,. \tag{3.7}$$

Here $-q^2 = Q^2$, the leptonic tensor is defined as

$$\ell^{\mu\nu} = \bar{u}(k')\gamma^\mu u(k)\bar{u}(k)\gamma^\nu u(k'), \tag{3.8}$$

and the hadronic tensor as

$$W^{\mu\nu} = \left\langle P|J^\nu|P'\right\rangle \langle P'|J^\mu|P\rangle \,. \tag{3.9}$$

The above hadronic matrix element between nucleon states is defined by two Lorentz-invariant form factors (FFs),

$$\langle P'|J^\mu(\boldsymbol{q})|P\rangle = \bar{u}(P')\left[\gamma^\mu F_1(q^2) + i\sigma^{\mu\nu}\frac{q_\nu}{2M}F_2(q^2)\right]u(P), \tag{3.10}$$

with $\sigma^{\mu\nu} = \frac{i}{2}[\gamma^\mu, \gamma^\nu]$ and M being the mass of the nucleon. F_1 and F_2 are referred to as the Dirac and Pauli form factors, respectively. Using the fact that both tensors are symmetric and conserved (i.e. $q^\mu \ell_{\mu\nu} = q^\mu W_{\mu\nu} = 0$), the elastic scattering cross-section in the lab frame can be written as

$$\frac{d\sigma}{d\Omega} = \sigma_{\text{Mott}}\left[\frac{G_E^2(Q^2) + \tau G_M^2(Q^2)}{1+\tau} + 2\tau G_M^2(Q^2)\tan^2\frac{\theta}{2}\right], \tag{3.11}$$

where we have defined the Sachs electric and magnetic FFs,

$$\begin{aligned} G_E(Q^2) &= F_1(Q^2) - \tau F_2(Q^2), \\ G_M(Q^2) &= F_1(Q^2) + F_2(Q^2), \end{aligned} \tag{3.12}$$

in terms of F_1 and F_2 and the factor $\tau = Q^2/4M^2$. Rewriting the cross section in terms of the virtual photon's longitudinal polarisation $\epsilon = (1 + (1 + \tau)2\tan^2(\theta/2))^{-1}$, we end up with the Rosenbluth formula,

$$\frac{d\sigma}{d\Omega} = \frac{\sigma_{\text{Mott}}}{1+\tau}\left[G_E^2(Q^2) + \frac{\tau}{\epsilon}G_M^2(Q^2)\right] \,. \tag{3.13}$$

So we see that it is possible to extract the electric and magnetic form factors from the slope and intercept of a curve fitted to the experimental cross section plotted as a function of scattering angle at fixed momentum transfer Q^2. This is known as the Rosenbluth separation technique. We note from Eq. (3.13), however, that the

coefficient of G_E is suppressed at large Q^2, and hence the cross section is dominated by G_M in this domain. Therefore, it is harder to extract information on G_E^2 at large momentum transfers.

3.2.1.2 Polarisation Transfer

Given the shortcomings of the Rosenbluth separation technique in extracting accurate results for the electric form factor at large Q^2, it is clear that there is a need for new experimental methods. The need for polarisation-transfer techniques was pointed out in several papers [134–137]. With advances in experimental techniques such as highly polarised and high-luminosity electron beams, polarised targets (e.g ^{1}H, ^{2}H, ^{3}He) and large and efficient neutron detectors, the polarisation-transfer experiments began to give us more insight about the nucleon's structure.

It is possible to obtain the ratio G_E^p/G_M^p from the elastic scattering of longitudinally polarised electrons from unpolarised protons in terms of the transferred polarisation components perpendicular (P_t) and parallel (P_l) to the recoil proton's momentum in the scattering plane [135, 137],

$$\frac{G_E^p}{G_M^p} = -\frac{P_t}{P_l}\frac{E+E'}{2M}\tan\left(\frac{\theta}{2}\right), \tag{3.14}$$

where E and E' are the incident and scattered electron energy, respectively, and θ is the electron scattering angle.

A recent analysis by the JLab Hall-A Collaboration [138] showed that, unlike the conventional Rosenbluth-method estimation which provided $\mu_p G_E^p/G_M^p \approx 1$, the proton form-factor ratio clearly deviates from unity. Figure 3.1 from [138] shows the behaviour of this ratio.

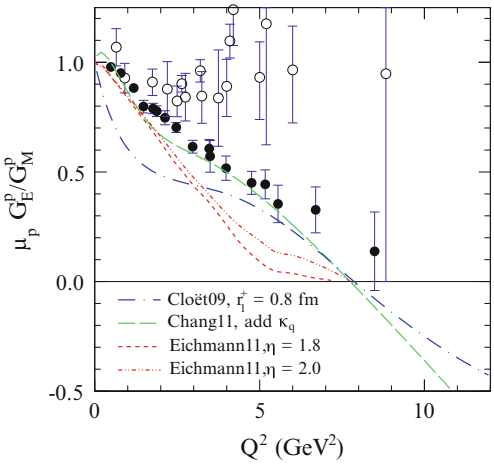

Fig. 3.1 Experimental data with fitted predictions based on Dyson-Schwinger equation calculations. *Empty circles* indicate the unpolarised, whereas the *filled ones* are obtained from polarisation-transfer experiments. Figure from [138]

It is evident that the G_E^p falls faster than G_M^p, and their Q^2 dependences differ. If the planned experiments forming part of the JLab upgrade[1] find the slope of the linear fall stays unchanged, then it might lead to the conclusion that G_E^p changes sign. One last note is that the discrepancy between the Rosenbluth and polarisation-transfer methods is believed to be due to the two-photon exchange (TPE) radiative corrections to the cross-section measurements. A broad discussion about TPE can be found in [133] and references therein.

3.2.1.3 Physical Interpretation

The physical interpretation of the electric and magnetic form factors is that for small Q^2, or in the limit $M \to \infty$ such that $Q^2 \ll M^2$, we can assume that the initial- and final-state nucleons are fixed at the same location and that they have the same internal structure. We then have the physical interpretation that the Fourier transforms of the form factors lead to density distributions. However, since M is finite, one should consider nucleon recoil effects with increasing Q^2. In this case, the initial and final nucleon states no longer have the same momentum, thus their wavefunctions differ (i.e. there is a relative Lorentz contraction), and it is no longer possible to have a probability or density interpretation [139].

One method for circumventing this issue is to consider the Breit frame where the initial and final momenta of the nucleon have the same magnitude. In this case, the initial- and final-state nucleon wavefunctions are sampled in the same frame, and we recover our density-distribution interpretation.

An alternative frame that also retains the density-distribution interpretation of form factors in a model-independent way is given by the infinite-momentum frame where the parton (quark) charge density in transverse space is given as a two-dimensional Fourier transformation of F_1,

$$\rho(b) = \int \frac{d^2\mathbf{q}_\perp}{(2\pi)^2} e^{-i\mathbf{b}_\perp \cdot \mathbf{q}_\perp} F_1(Q^2 = \mathbf{q}_\perp^2), \tag{3.15}$$

where $\mathbf{q}_\perp$ and $\mathbf{b}_\perp$ are the momentum transfer and distance of the quark to the center of momentum, respectively, of a fast-moving nucleon in the longitudinal direction.

Pursuing the spatial density interpretation, we can expand the Fourier transform of such a distribution, which allows us to write the electric form factor as

$$G_E(Q^2) = \int d^3\mathbf{x}\, e^{i\mathbf{x}\cdot\mathbf{q}} \rho(\mathbf{x}) \simeq 1 - \frac{1}{6} Q^2 \langle r^2 \rangle + \ldots \tag{3.16}$$

[1] See for instance, http://www.jlab.org/exp_prog/12GEV_EXP/.

The charge radius of the nucleon is then defined by

$$\langle r^2 \rangle = -6 \left. \frac{dG_E(Q^2)}{dQ^2} \right|_{Q^2=0} . \tag{3.17}$$

We note here that there has been a lot of recent activity surrounding $r = \sqrt{\langle r_E^2 \rangle}$. Electron-proton scattering experiments found that the rms charge radius of the proton is $r = 0.875(8)(6)$ fm, in good agreement with the atomic-hydrogen Lamb-shift experiments and QED calculations [140]. Recent muonic-hydrogen Lamb-shift measurements, however, indicate $r = 0.84184(67)$ fm, showing a 5σ difference [141], which has yet to be resolved.

3.2.2 Deep-Inelastic Scattering

In the previous section, we saw how elastic electron-proton scattering can provide a framework in which to determine the electromagnetic form factors of the proton. While elastic scattering occurs at small enough energies so that the final proton would stay intact, we now consider an experimental process that occurs with high enough energy that the proton is "smashed" into many fragments. This is known as deep-inelastic scattering (DIS). The DIS process is dominated by a single quark in the nucleon which is "knocked out" by a virtual photon (see Fig. 3.2).

As in case of elastic scattering, let us start with the expression for the S-matrix for deep-inelastic scattering:

$$S = (2\pi)^4 \delta^4(k + P - P' - k') \bar{u}(k')(-ie\gamma^\mu) u(k) \frac{-i}{q^2} \langle X | (ie) J^\mu | P \rangle . \tag{3.18}$$

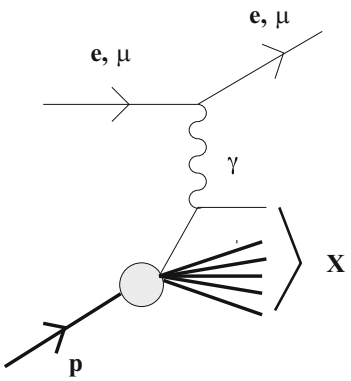

Fig. 3.2 Deep-inelastic scattering

We have here conservation of momentum $\delta^4(k + P - P' - k')$, a leptonic piece $\bar{u}(k')(-ie\gamma^\mu)u(k)$ which can be calculated in perturbation theory, and a hadronic piece $\langle X|(ie)J^\mu|P\rangle$. After smashing the initial proton with the probe, it is going to break up into many fragments, and for an inclusive process we need to include in the hadronic piece all possible final states, which we label X. The inclusive cross section can be written in the following form:

$$\frac{d\sigma}{d\Omega dE} = \frac{\alpha^2}{Q^4}\frac{E'}{E}\ell_{\mu\nu}W^{\mu\nu}. \tag{3.19}$$

Here $\ell_{\mu\nu}$ is the leptonic tensor, $W^{\mu\nu}$ is the hadronic tensor which itself is a square of the matrix element from Eq. (3.18), and we have here a sum over all possible final states

$$W_{\mu\nu} = \frac{1}{4\pi}\sum_X \langle P|J_\mu|X\rangle\langle X|J_\nu|P\rangle(2\pi)^4\delta^4(P + q - P_X). \tag{3.20}$$

Since the final states are summed over, the hadronic tensor $W^{\mu\nu}$ only depends on the initial proton momentum P and photon momentum q. Using Lorentz symmetry, parity and time-reversal invariance and current conservation, we can express this hadronic tensor in terms of two invariant tensors

$$\begin{aligned} W_{\mu\nu} = {} & W_1\left(-g^{\mu\nu} + \frac{q^\mu q^\nu}{q^2}\right) \\ & + \frac{W_2}{M^2}\left(P^\mu - q^\mu\frac{(P\cdot q)}{q^2}\right)\left(P^\nu - q^\nu\frac{(P\cdot q)}{q^2}\right), \end{aligned} \tag{3.21}$$

where W_1 and W_2 are the so-called structure functions of the proton which depend on two variables: the 4-momentum transfer squared

$$Q^2 = -q^2, \tag{3.22}$$

and the energy transferred to the nucleon by the scattering electron

$$\nu = \frac{P\cdot q}{M}. \tag{3.23}$$

The early data from SLAC indicated that these structure functions W_1 and W_2 are nearly independent of Q^2 when plotted as a function of the dimensionless combination

$$x = -\frac{q^2}{2P\cdot q} = \frac{Q^2}{2M\nu}. \tag{3.24}$$

This effect is known as Bjorken scaling, and x is called the Bjorken scaling variable, although as we will discuss later, small scaling violations are observed at small x.

3.2.2.1 Parton Model

If we work at fixed x, the limit of $Q^2 \to \infty$ is known as the Bjorken limit. The effect of Bjorken scaling in this limit led Feynman to introduce the "parton model". According to his idea, the inelastic electron-proton scattering is a sum of elastic scatterings of the electron on free partons within the proton (the term parton refers to any particle with no internal structure). A key factor for investigating the proton substructure is the wavelength of the probe

$$\lambda \sim \frac{1}{\sqrt{Q^2}}, \tag{3.25}$$

and, of course, at large momentum transfer we are going to have higher resolution; Fig. 3.3 represents it diagrammatically. If Q^2 is small (i.e. the wavelength is large), then the probe will only resolve the proton as a whole, but if we increase the value of Q^2 (decrease the wavelength of the probe), this means that we will be able to resolve quantities inside of the hadron, so the probe will "see" quarks rather than a proton. This picture is also valid for a fast-moving nucleon, i.e. the infinite-momentum frame.

In the Bjorken limit, one defines the functions

$$F_1(x) = \lim_{Q^2 \to \infty} W_1(Q^2, \nu), \tag{3.26}$$

$$F_2(x) = \lim_{Q^2 \to \infty} \frac{\nu}{M} W_2(Q^2, \nu). \tag{3.27}$$

And in Feynman's parton model, the structure functions are sums of the parton densities f_i constituting the proton:

$$F_1(x) = \frac{1}{2} \sum_i e_i^2 f_i(x), \tag{3.28}$$

$$F_2(x) = x \sum_i e_i^2 f_i(x)\,, \tag{3.29}$$

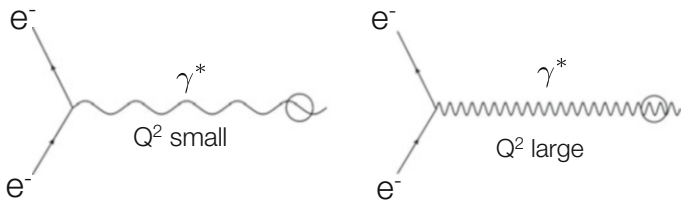

Fig. 3.3 Large momentum transfer leads to higher resolution. The left diagram represents resolving a proton at small Q^2, while the right diagram has a Q^2 high enough for investigating proton substructure (quarks)

where for quarks, the charge e_i is also included. f_i is the probability that the struck parton, i, carries a fraction, x, of the proton momentum, and is called a parton distribution function (PDF). Since the total probability must be 1, we have

$$\sum_i \int_0^1 dx\, x f_i(x) = 1. \tag{3.30}$$

Results from DIS tell us that the fraction of the nucleon momentum carried by the quarks $\int dx\, xq(x)$ is only about 50 % (here $q(x) = f_q(x)$). This gives us an idea that gluons must play a very important role in the structure of the nucleon by carrying roughly half of its momentum. In fact, much of our knowledge about QCD and the structure of the nucleon has been derived from DIS experiments. They told us that there are two up and one down valence quarks with electric charge $2/3$ and $-1/3$ in the proton; the number of quarks is infinite because the integral over parton densities $\int dx\, q(x)$ does not seem to converge, so there is an infinite number of quark-antiquark pairs living inside of the proton.

3.2.2.2 Parton Distribution Functions

Let us take a look at how these PDFs might look. For a point nucleon (i.e. if we consider the nucleon as a single parton with no internal structure which carries all momentum), F_2 is a delta function at $x = 1$ (Fig. 3.4). If the nucleon is made up of three quarks which equally share the momentum, then each quark carries $1/3$ of the momentum, and we will have a delta function at $1/3$, as in Fig. 3.5. If the three quarks are interacting, which means that they are exchanging some gluons, then they can share momentum. So the PDF is going to be smeared around the peak of $1/3$ (see Fig. 3.6). Finally, we should consider the case with sea quarks. Here, one quark emits a gluon which turns into quark-antiquark pair, and then all valence quarks in $q\bar{q}$ loop must have lower x than the original quark. Therefore, in Fig. 3.7 we should see an enhancement at small x.

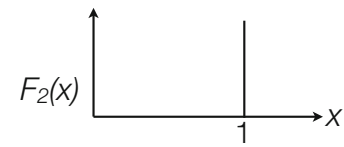

Fig. 3.4 PDF for a point nucleon

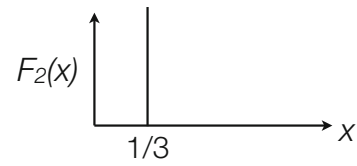

Fig. 3.5 PDF for a nucleon with three quarks

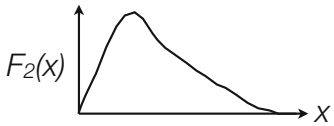

Fig. 3.6 PDF for three interacting quarks

Fig. 3.7 Enhancement at small x for the nucleon with sea quarks

The proton contains two up and one down quarks which are termed "valence" quarks: $u_v(x)$, $d_v(x)$. It is possible that a valence quark radiates a gluon which then turns into a quark-antiquark pair which are termed "sea" quarks, and we are going to call PDFs associated with $u_s(x)$, $d_s(x)$, $s_s(x)$. Then we can write the proton and neutron structure functions as following (ignoring heavy quarks):

$$F_2^p(x) = x\left\{\frac{4}{9}\left[u^p(x)+\bar{u}^p(x)\right]+\frac{1}{9}\left[d^p(x)+\bar{d}^p(x)\right]+\frac{1}{3}\left[s^p(x)+\bar{s}^p(x)\right]\right\}, \tag{3.31}$$

$$F_2^n(x) = x\left\{\frac{4}{9}\left[u^n(x)+\bar{u}^n(x)\right]+\frac{1}{9}\left[d^n(x)+\bar{d}^n(x)\right]+\frac{1}{3}\left[s^n(x)+\bar{s}^n(x)\right]\right\}, \tag{3.32}$$

where total PDF of any particular flavour in Eqs. (3.31), (3.32) is

$$q \equiv q_v + q_s. \tag{3.33}$$

Under isospin flip $u \leftrightarrow d$ and $p \leftrightarrow n$, assuming charge symmetry means that the distribution of the up quarks in the proton is the same as distribution of the down quarks in the neutron:

$$u(x) \equiv u^p(x) = d^n(x), \tag{3.34}$$

and the distribution of the down quarks in the proton is the same as the distribution of the up quarks in the neutron:

$$d(x) \equiv d^p(x) = u^n(x). \tag{3.35}$$

If we also assume that different flavours (u, d, s) of the quarks occur with equal probability in the sea, then we can write down this total contribution S:

$$S \equiv u_s = \bar{u}_s = d_s = \bar{d}_s = s_s = \bar{s}_s. \tag{3.36}$$

So we can now write the proton and neutron structure functions in terms of the valence u in the proton and the valence d in the proton, and a sea quark contribution:

$$F_2^p(x) = x\left\{\frac{1}{9}\left[4u_v(x) + d_v(x)\right] + \frac{4}{3}S(x)\right\}, \tag{3.37}$$

$$F_2^n(x) = x\left\{\frac{1}{9}\left[4d_v(x) + u_v(x)\right] + \frac{4}{3}S(x)\right\}. \tag{3.38}$$

We expect that at small x ($x \ll 1$) the sea quarks should dominate, so that

$$\frac{F_2^n}{F_2^p} \to 1, \tag{3.39}$$

while at large x ($x \to 1$) the valence quarks should dominate (and $u_v(x) > d_v(x)$ since there are two up versus one down valence quarks in the proton), then

$$\frac{F_2^n}{F_2^p} \to \frac{1}{4}. \tag{3.40}$$

And this is exactly what is seen in DIS experiment results.

Recall the momentum sum rule:

$$\sum_i \int_0^1 dx\, x f_i(x) = 1, \tag{3.41}$$

but electron-proton DIS experiments find the light-quark contributions to be roughly

$$\int dx\, x[u(x) + \bar{u}(x)] \approx 0.36, \tag{3.42}$$

$$\int dx\, x[d(x) + \bar{d}(x)] \approx 0.18. \tag{3.43}$$

This tells us that almost half of the proton momentum is carried by electrically neutral partons. These experiments were repeated by using neutrino scattering, and they indicated that these neutral partons do not interact weakly (i.e. are not quarks), therefore the missing momentum has to be carried by gluons. The need for inclusion of gluons in the parton model is also evidenced by the scaling violations at finite Q^2 discussed in Sect. 3.2.2.

3.2.3 Neutron Beta Decay

We all know that free neutrons are unstable: they are stable inside nuclei, but if a neutron exists outside of the nucleus, then it has a lifetime of approximately 15 min. This is because it can decay to a proton by the weak interaction

$$n \to pe^{-}\bar{\nu}_e\,, \tag{3.44}$$

emitting a W boson which in turn decays into an electron and electron antineutrino.

Neutron decay is the simplest way of studying the weak interaction. The decay rate of the neutron is proportional to the matrix element of the weak $V-A$ current:

$$\begin{aligned}\langle p(p',s')|(V_\mu - A_\mu)|n(p,s)\rangle = \\ \bar{u}_p(p',s')\Big\{\gamma_\mu f_1(q^2) + i\frac{\sigma_{\mu\nu}q^\nu}{2M}f_2(q^2) + \frac{q_\mu}{2M}f_3(q^2) \\ -\left[\gamma_\mu\gamma_5 g_1(q^2) + i\frac{\sigma_{\mu\nu}q^\nu}{2M}\gamma_5 g_2(q^2) + \frac{q_\mu}{2M}\gamma_5 g_3(q^2)\right]\Big\}u_n(p,s).\end{aligned} \tag{3.45}$$

Because of the tiny mass difference between the proton and the neutron

$$M_n - M_p \simeq 1.3\ \text{MeV}\,, \tag{3.46}$$

the momentum transfer here is so small that all the terms proportional to q may be dropped, and we only need to consider to first order the contribution from the f_1 and g_1 terms. By convention, we call the value of f_1 at zero momentum g_V, and the corresponding value of g_1, g_A:

$$g_V = f_1(0), \quad g_A = g_1(0). \tag{3.47}$$

According to the conserved vector current (CVC) hypothesis, which says that the vector part of this weak $V-A$ current is the same as the vector part of the electromagnetic current, under isospin symmetry this $f_1(0)$, or g_V, will give us the charge of the system, which is one ($g_V = 1$). There also exists the so-called Adler-Weisberger relation which predicts $g_A = 1.26$. So how do we extract g_A from experiment? The decay rate for a neutron at rest and with spin pointing in the $\boldsymbol{s}_n$ direction is given by

$$\frac{dR}{dp_e d\Omega_e d\Omega_{\bar{\nu}}} = \frac{G_F^2|V_{ud}|^2}{(2\pi)^5}\left[\alpha + \beta\boldsymbol{v}_e\cdot\boldsymbol{v}_{\bar{\nu}} + \gamma\boldsymbol{s}_n\cdot\boldsymbol{v}_e + \delta\boldsymbol{s}_n\cdot\boldsymbol{v}_{\bar{\nu}}\right]p_e^2(E_{\max}-E_e)^2. \tag{3.48}$$

Here $\boldsymbol{v}_e$ and $\boldsymbol{v}_{\bar{\nu}}$ are the velocities of the final electron and electron antineutrino, respectively, G_F is Fermi constant, and V_{ud} is a CKM matrix element. E is the energy of the electron, p_e is the momentum of the electron, and $E_{\max}$ is the

difference between the neutron and proton masses, which provides a bound on the energy spectrum of the electron:

$$E_{\max} = M_n - M_p \simeq 1.3 \text{ MeV}. \tag{3.49}$$

So the decay rate is defined then in terms of the quantities α, β, γ and δ described as functions of g_V and g_A:

$$\begin{aligned} \alpha &= g_V^2 + 3g_A^2, & \beta &= g_V^2 - g_A^2, \\ \gamma &= 2(g_A g_V - g_A^2), & \delta &= 2(g_A g_V + g_V^2), \end{aligned} \tag{3.50}$$

allowing us to extract g_A from this experiment. We can see that even for an unpolarised neutron (in this case the γ and δ terms are zero, and we only have the α and β terms which are expressed in terms of squares of g_A and g_V), we can define $|g_A/g_V|$ through an accurate determination of the angular correlation between the outgoing electron and electron antineutrino. To determine the sign of g_A, spin-dependent measurements are required; in other words, we want at least one of the γ or δ terms to be nonzero since they are proportional to a single power of g_A. Current best determination of $|g_A/g_V|$ provided by Particle Data Group (PDG2012) gives $|g_A/g_V| = 1.2701(25)$.

3.2.3.1 Axial Form Factor

Considering the general case of the matrix element of the weak $V-A$ current, away from $q^2 = 0$, will give us access to the form factors as functions of q^2. If we consider only the axial-vector part of the weak current between the neutron and proton states from Eq. (3.45), we find

$$\begin{aligned} \langle p(p',s')|A^\mu(\boldsymbol{q})|n(p,s)\rangle = \bar{u}_p(p',s')\Big[&\gamma^\mu\gamma_5 G_A(q^2) + i\sigma^{\mu\nu}\gamma_5 \frac{q_\nu}{2M} G_T(q^2) \\ &+ \gamma_5 \frac{q^\mu}{2M} G_P(q^2)\Big] u_n(p,s). \end{aligned} \tag{3.51}$$

Similarly to Eq. (3.10) for electromagnetic form factors, this is written in terms of Lorentz invariant form factors. The first term, which we call now $G_A(q^2)$, is the axial form factor, the third term, $G_P(q^2)$, is the induced pseudoscalar form factor, and the second term, the tensor form factor G_T, vanishes if charge symmetry assumed, $u_p = d_n$. The partially conserved axial current relation (PCAC) tells us that the divergence of the matrix element of the axial-vector current is proportional to m_π^2 which, as we go to chiral limit, should vanish:

$$\partial_\mu A^\mu \propto m_\pi^2 \xrightarrow{m_q \to 0} 0\,, \tag{3.52}$$

i.e. the axial current is only conserved in the chiral limit. This is, in general, not true for Eq. (3.51). However if G_P has a pion pole

$$G_P(q^2) \to \frac{4M_N f_\pi g_{\pi NN}(q^2)}{-q^2 + m_\pi^2}, \tag{3.53}$$

and G_A takes the following form in terms of $g_{\pi NN}$ and the pion decay constant f_π

$$M_N G_A(q^2) = f_\pi g_{\pi NN}(q^2), \tag{3.54}$$

then the matrix element in Eq. (3.51) satisfies the PCAC relation. Then at $q^2 = 0$ we get the so-called Goldberger-Treiman relation

$$M_N g_A = f_\pi g_{\pi NN}. \tag{3.55}$$

3.2.3.2 Axial Charge g_A

As discussed above, the axial charge is defined as the value of the axial form factor at $q^2 = 0$, $g_A = G_A(q^2 = 0)$. This presents an ideal quantity for benchmark lattice calculations of nucleon structure. The fact that it is defined at zero momentum guarantees that calculations are statistically clean. This is also an isovector quantity since this matrix element between the proton and neutron with a $\bar{u}d$ current is related under charge symmetry to the $u - d$ proton matrix element

$$\langle p|\bar{u}\gamma^\mu\gamma^5 d|n\rangle = \langle p|\bar{u}\gamma^\mu\gamma^5 u - \bar{d}\gamma^\mu\gamma^5 d|p\rangle, \tag{3.56}$$

and therefore, disconnected contributions cancel. So in principle it should be possible to perform precision lattice calculations of g_A which can be compared to the experimental value.

3.3 Determining Matrix Elements on the Lattice

Here we outline the procedure required for calculating matrix elements such as those in Eqs. (3.51) and (3.10). We start with introducing lattice three-point functions and the sequential-source technique used for calculating them. We then show how to extract the relevant matrix elements from these three-point functions through constructing ratios of lattice three- and two-point functions.

3.3.1 Lattice Three-Point Functions

We start our discussion by introducing the lattice nucleon three-point function

$$G(t,\tau;p,p') = \sum_{\boldsymbol{x_2},\boldsymbol{x_1}} e^{-i\,\boldsymbol{p'}\cdot(\boldsymbol{x_2}-\boldsymbol{x_1})} e^{-i\,\boldsymbol{p}\cdot\boldsymbol{x_1}} \Gamma_{\beta\alpha} \cdot \\ \cdot \langle \Omega | T\{\chi_\alpha(\boldsymbol{x_2},t)\mathcal{O}(\boldsymbol{x_1},\tau)\bar{\chi}_\beta(0)\}|\Omega\rangle\,, \tag{3.57}$$

which is also illustrated in Fig. 3.8, where a particle is created at $t = 0$ by the creation operator $\bar{\chi}_\beta(0)$, interacts with the generic current $\mathcal{O}(\boldsymbol{x_1},\tau)$ at some Euclidean time τ and is annihilated at some time t by the annihilation operator $\chi_\alpha(\boldsymbol{x_2},t)$. In our case the creation (annihilation) operator has the quantum numbers of the proton. A time-ordered product ensures that everything happens in correct order. The $\Gamma_{\beta\alpha}$ matrix is the spin-projection operator, Ω represents the vacuum state and, finally, the Fourier transform projects the particle to a definite momentum state. Inserting a complete set of states $I = \sum_{B^{(\prime)},p^{(\prime)},s^{(\prime)}} |B^{(\prime)},p^{(\prime)},s^{(\prime)}\rangle\langle B^{(\prime)},p^{(\prime)},s^{(\prime)}|$ before and after the current operator and exploiting the translational invariance $\chi(\boldsymbol{x},t) = e^{\hat{H}t} e^{-i\,\hat{\boldsymbol{P}}\cdot\boldsymbol{x}} \chi(0) e^{i\,\hat{\boldsymbol{P}}\cdot\boldsymbol{x}} e^{-\hat{H}t}$, we find

$$G(t,\tau;p,p') = \sum_{B,B'}\sum_{s,s'} e^{-E_{B'}(\boldsymbol{p'})(t-\tau)} e^{-E_B(\boldsymbol{p})\tau} \Gamma_{\beta\alpha} \times \\ \left\langle \Omega \left| \chi_\alpha(0) \right| B',p',s' \right\rangle \left\langle B',p',s' \left| \mathcal{O}(\boldsymbol{q}) \right| B,p,s \right\rangle \left\langle B,p,s \left| \bar{\chi}_\beta(0) \right| \Omega \right\rangle\,, \tag{3.58}$$

where $E_B(\boldsymbol{p})$ denotes the energy of the baryon B with momentum $\boldsymbol{p}$. As the Euclidean time evolves, $0 \ll \tau \ll t$, excited states are exponentially suppressed and the ground-state proton dominates

$$G(t,\tau;p,p') = \sum_{s,s'} e^{-E_{p'}(t-\tau)} e^{-E_p\tau} \Gamma_{\beta\alpha} \times \\ \left\langle \Omega \left| \chi_\alpha(0) \right| N(p',s') \right\rangle \left\langle N(p',s') \left| \mathcal{O}(\boldsymbol{q}) \right| N(p,s) \right\rangle \left\langle N(p,s) \right| \bar{\chi}_\beta(0) \left| \Omega \right\rangle\,, \tag{3.59}$$

where we have simplified our notation and E_p now denotes the energy of the proton with momentum $p = |\boldsymbol{p}|$.

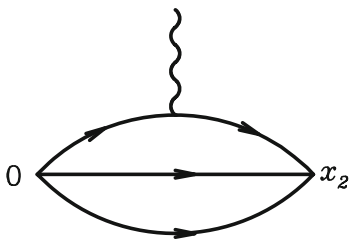

Fig. 3.8 Quark-flow diagram for a proton three-point function described in Eq. (3.57)

3.3.1.1 Three-Point Functions at the Quark Level

We now wish to derive a form for a lattice three-point function in terms of quark propagators. We will start with the simple case of the pion for which we will use the standard interpolating operator

$$\chi(x) = \bar{d}(x)\gamma_5 u(x), \tag{3.60}$$

where $\bar{d}(x)$ and $u(x)$ are the quark fields and γ_5 gives the correct quantum numbers for a pseudoscalar meson. Inserting the local current operator,

$$\mathcal{O}(x) = \bar{q}(x)\Gamma q(x), \tag{3.61}$$

where Γ stands for any combination of γ-matrices and derivatives (e.g. γ_μ for the electromagnetic current), the three-point function of pion is then

$$\begin{aligned} G(t,\tau;p,p') = \sum_{\boldsymbol{x_2},\boldsymbol{x_1}} & e^{-i\,\boldsymbol{p'}\cdot(\boldsymbol{x_2}-\boldsymbol{x_1})} e^{-i\,\boldsymbol{p}\cdot\boldsymbol{x_1}} \\ & \left\langle \Omega \left| T\left\{ -\bar{d}(x_2)\gamma_5 u(x_2)\bar{u}(x_1)\Gamma u(x_1)\bar{u}(0)\gamma_5 d(0)\right\}\right| \Omega\right\rangle , \end{aligned} \tag{3.62}$$

where we are first considering the u-quark contribution to the full three-point function. Writing the colour (Latin) and Dirac (Greek) indices explicitly,

$$\begin{aligned} G(t,\tau;p,p') = & \sum_{\boldsymbol{x_2},\boldsymbol{x_1}} e^{-i\,\boldsymbol{p'}\cdot(\boldsymbol{x_2}-\boldsymbol{x_1})} e^{-i\,\boldsymbol{p}\cdot\boldsymbol{x_1}} \times \\ & \left\langle \Omega | T\{ -\bar{d}^a_\beta(x_2)\gamma^5_{\beta\gamma} u^a_\gamma(x_2)\bar{u}^b_\rho(x_1)\Gamma_{\rho\delta} u^b_\delta(x_1)\bar{u}^c_\xi(0)\gamma^5_{\xi\alpha} d^c_\alpha(0)\} | \Omega \right\rangle, \end{aligned} \tag{3.63}$$

we now perform all possible Wick contractions,

$$\begin{aligned} G(t,\tau;p,p') = & \sum_{\boldsymbol{x_2},\boldsymbol{x_1}} e^{-i\,\boldsymbol{p'}\cdot(\boldsymbol{x_2}-\boldsymbol{x_1})} e^{-i\,\boldsymbol{p}\cdot\boldsymbol{x_1}} \times \\ & \left\{ S^{ca}_{d\alpha\beta}(0,x_2)\gamma^5_{\beta\gamma} S^{ab}_{u\gamma\rho}(x_2,x_1)\Gamma_{\rho\delta} S^{bc}_{u\delta\xi}(x_1,0)\gamma^5_{\xi\alpha} \right. \\ & \left. - S^{ca}_{d\alpha\beta}(0,x_2)\gamma^5_{\beta\gamma} S^{ac}_{u\gamma\xi}(x_2,0)\gamma^5_{\xi\alpha} S^{bb}_{u\delta\rho}(x_1,x_1)\Gamma_{\rho\delta} \right\}, \end{aligned} \tag{3.64}$$

where S_q stands for the quark propagator. Then we take the Dirac and colour traces to obtain

$$\begin{aligned} G(t,\tau;p,p') = & \sum_{\boldsymbol{x_2},\boldsymbol{x_1}} e^{-i\,\boldsymbol{p'}\cdot(\boldsymbol{x_2}-\boldsymbol{x_1})} e^{-i\,\boldsymbol{p}\cdot\boldsymbol{x_1}} \\ & \left\{ \mathrm{Tr}[S_d(0,x_2)\gamma_5 S_u(x_2,x_1)\Gamma S_u(x_1,0)\gamma_5] \right. \\ & \left. - \mathrm{Tr}[S_d(0,x_2)\gamma_5 S_u(x_2,0)\gamma_5]\,\mathrm{Tr}[S_u(x_1,x_1)\Gamma] \right\}, \end{aligned} \tag{3.65}$$

and using the γ_5-hermiticity, $S^\dagger(x,0) = \gamma_5 S(0,x)\gamma_5$, we end up with

$$\begin{aligned} G(t,\tau;p,p') = \sum_{\boldsymbol{x_2},\boldsymbol{x_1}} & e^{-i\,\boldsymbol{p'}\cdot(\boldsymbol{x_2}-\boldsymbol{x_1})} e^{-i\,\boldsymbol{p}\cdot\boldsymbol{x_1}} \\ & \Big\{ \mathrm{Tr}[S_d^\dagger(x_2,0) S_u(x_2,x_1) \Gamma S_u(x_1,0)] \\ & - \mathrm{Tr}[S_d^\dagger(x_2,0) S_u(x_2,0)]\,\mathrm{Tr}[S_u(x_1,x_1)\Gamma] \Big\} . \end{aligned} \tag{3.66}$$

We can a similar result for the d-quark contribution $\bar{d}\,\Gamma\, d$, which, however, in the isospin limit is identical to that for the u-quark. The first term of Eq. (3.66) stands for the usual connected diagram whereas the $S_u(x_1,x_1)$ in second term indicates a quark loop and a disconnected diagram.

So in this case we have found that there are two dominant terms needed to calculate the full pion three-point function; however, due to the number of quark fields, it gets complicated when we consider the proton.

The interpolating operator of proton is

$$\chi_\alpha(x) = \epsilon^{abc} \left(u^{Ta}(x) C\gamma_5 d^b(x)\right) u^c_\alpha(x) , \tag{3.67}$$

leading to the three-point function for, e.g., the u-quark current insertion,

$$\begin{aligned} G_\Gamma(t,\tau;p,p') = & \sum_{\boldsymbol{x_2},\boldsymbol{x_1}} e^{-i\,\boldsymbol{p'}\cdot(\boldsymbol{x_2}-\boldsymbol{x_1})} e^{-i\,\boldsymbol{p}\cdot\boldsymbol{x_1}} \Gamma \epsilon^{abc} \epsilon^{a'b'c'} \times \\ & \Big\langle \Omega \Big| T \Big\{ \Big(u^{Ta}(x_2) C\gamma_5 d^b(x_2)\Big) u^c_\alpha(x_2) \bar{u}(x_1) \mathcal{O} u(x_1) \bar{u}^{c'}(0) \cdot \\ & \Big(\bar{d}^{b'}(0) C\gamma_5 \bar{u}^{Ta'}(0)\Big) \Big\} \Big| \Omega \Big\rangle , \end{aligned} \tag{3.68}$$

where C is the charge-conjugation operator. After all possible connected Wick contractions we can write this three-point function in terms of up and down pieces,

$$G_\Gamma(t,\tau;p,p') = q_u C^u_\Gamma(t,\tau;p,p') + q_d C^d_\Gamma(t,\tau;p,p'), \tag{3.69}$$

where for the electromagnetic current we have explicitly included the electric charges of the up and down quarks ($q_{u,d}$), and $C^u_\Gamma(t,\tau;p,p')$ and $C^d_\Gamma(t,\tau;p,p')$ are defined as

$$\begin{aligned} C^{u,d}_\Gamma(t,\tau;p,p') \equiv & \sum_{\boldsymbol{x_1}} e^{-i\,\boldsymbol{q}\cdot\boldsymbol{x_1}} \times \\ & \Big\langle \mathrm{Tr}\Big[\Sigma^{u,d}_\Gamma(\boldsymbol{0},0;\boldsymbol{x_1},\tau;\boldsymbol{p'},t) \mathcal{O}(\boldsymbol{x_1},\tau) S(\boldsymbol{x_1},\tau;0) \Big] \Big\rangle , \end{aligned} \tag{3.70}$$

where $\boldsymbol{q} = \boldsymbol{p}' - \boldsymbol{p}$ is the momentum transfer. The $\Sigma_\Gamma^{u,d}$ term is the combination of propagators shown in Fig. 3.9 and written as

$$\Sigma_\Gamma^{u,d}(\mathbf{0}, 0; \boldsymbol{x_1}, \tau; \boldsymbol{p}', t) = \sum_{\boldsymbol{x_2}} S_\Gamma^{u,d}(\boldsymbol{x_2}, t; \mathbf{0}, 0; \boldsymbol{p}') S(\boldsymbol{x_2}, t; \boldsymbol{x_1}, \tau), \tag{3.71}$$

where S_Γ^u and S_Γ^d are

$$\begin{aligned} S_\Gamma^{u;a'a}(\boldsymbol{x_2}, t; \mathbf{0}, 0; \boldsymbol{p}') &= e^{-i\,\boldsymbol{p}'\cdot\boldsymbol{x_2}} \epsilon^{abc} \epsilon^{a'b'c'} \times \\ &\Big\{ \tilde{S}^{d;bb'}(\boldsymbol{x_2}, t; \mathbf{0}, 0) S^{u;cc'}(\boldsymbol{x_2}, t; \mathbf{0}, 0) \Gamma \\ &+ \mathrm{Tr_D}\left[\tilde{S}^{d;bb'}(\boldsymbol{x_2}, t; \mathbf{0}, 0) S^{u;cc'}(\boldsymbol{x_2}, t; \mathbf{0}, 0) \right] \Gamma \\ &+ \Gamma S^{u;bb'}(\boldsymbol{x_2}, t; \mathbf{0}, 0) \tilde{S}^{d;cc'}(\boldsymbol{x_2}, t; \mathbf{0}, 0) \\ &+ \mathrm{Tr_D}\left[\Gamma S^{u;bb'}(\boldsymbol{x_2}, t; \mathbf{0}, 0) \right] \tilde{S}^{d;cc'}(\boldsymbol{x_2}, t; \mathbf{0}, 0) \Big\}, \end{aligned} \tag{3.72}$$

$$\begin{aligned} S_\Gamma^{d;a'a}(\boldsymbol{x_2}, t; \mathbf{0}, 0; \boldsymbol{p}') &= e^{-i\,\boldsymbol{p}'\cdot\boldsymbol{x_2}} \epsilon^{abc} \epsilon^{a'b'c'} \times \\ &\Big\{ \tilde{S}^{u;bb'}(\boldsymbol{x_2}, t; \mathbf{0}, 0) \tilde{\Gamma} \tilde{S}^{u;cc'}(\boldsymbol{x_2}, t; \mathbf{0}, 0) \\ &+ \mathrm{Tr_D}\left[\Gamma S^{u;bb'}(\boldsymbol{x_2}, t; \mathbf{0}, 0) \right] \tilde{S}^{u;cc'}(\boldsymbol{x_2}, t; \mathbf{0}, 0) \Big\}, \end{aligned} \tag{3.73}$$

and we have defined $\tilde{S} \equiv C\gamma_5 S \gamma_5 C$. We also note that $\mathrm{Tr_D}$ indicates a trace of Dirac indices, while the colour indices are still explicit.

Now that we have expressed the three-point function in terms of quark propagators, we can calculate it by computing and contracting the propagators. However, because of the $S(\boldsymbol{x_2}, t; \boldsymbol{x_1}, \tau)$ propagator and the presence of sums over $\boldsymbol{x_1}$, $\boldsymbol{x_2}$ we can not calculate the quantities given in Eq. (3.70) directly. The workaround is to use the sequential-source technique in which we first compute the ordinary propagators $S(x, 0)$ and then construct the sources $S_\Gamma^{u;a'a}$ or $S_\Gamma^{d;a'a}$, as described in Eqs. (3.72)

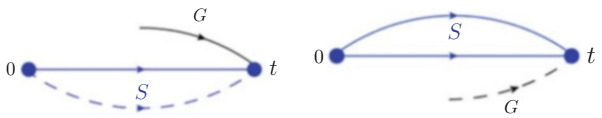

Fig. 3.9 Diagrammatic view of the Σ_Γ term for up (*left*) and down (*right*) quark contributions. The blue S combination corresponds to the $S_\Gamma^{u,d}(\boldsymbol{x_2}, t; \mathbf{0}, 0; \boldsymbol{p}')$ piece and the black G stands for $S(\boldsymbol{x_2}, t; \boldsymbol{x_1}, \tau)$. *Solid (dashed) lines* indicate $u(d)$-quark propagators

and (3.73). The sequential propagator $\Sigma_{\Gamma}^{u,d}(\mathbf{0}, 0; \boldsymbol{x_1}, \tau; \boldsymbol{p}', t)$ is then computed via a second inversion by solving the linear system of equations

$$\sum_{x_1} M(x_2, x_1)\gamma_5 \Sigma_{\Gamma}^{\dagger u,d}(\mathbf{0}, 0; \boldsymbol{x_1}, \tau; \boldsymbol{p}', t) = \gamma_5 S_{\Gamma}^{\dagger u,d}(\boldsymbol{x_2}, t; \mathbf{0}, 0; \boldsymbol{p}'). \tag{3.74}$$

Contracting the sequential propagator with the operator $\mathcal{O}(\boldsymbol{x_1}, \tau)$ and an ordinary propagator from source to current $S(\boldsymbol{x_1}, 0)$, we can construct the three-point function as in Eq. (3.70).

With this approach we have inverted the sequential propagator through the sink by fixing the final-state particle and sink momentum. This allows us to investigate the momentum dependence of the form factors for different insertion currents, since the sum over $\boldsymbol{x_1}$ is performed last. Alternatively, we could have chosen to invert the sequential source through the current, leaving the choice of final-state particle free; however, we would need separate a inversion for each choice of $\boldsymbol{q}$ and operator. The advantage of this method, however, is that the choice of quark sector, hadron boost and polarisation are all free to be determined after the sequential propagator has been calculated. Further information can be found in [142]. Choosing between these two approaches depends on what we are interested in computing. Mapping out the q^2-dependence of various form factors for a single hadronic state would be suited to choosing the "sequential source through the sink" method, as described in Eqs. (3.70)–(3.74), while comparing results for a single operator for a number of different hadronic states would be more suited to the "sequential source through the current method".

3.3.2 Extracting Matrix Elements

Recall the nucleon three-point function given in Eq. (3.57). Since we are interested in determining the matrix element $\langle N(p', s') | \mathcal{O}(\boldsymbol{q}) | N(p, s) \rangle$, we should somehow cancel the exponential time-dependent factors and wavefunction amplitudes, i.e. $\langle \Omega | \chi_\alpha(0) | N(p', s') \rangle$ and $\langle N(p, s) | \bar{\chi}_\beta(0) | \Omega \rangle$, which are, in general, momentum dependent. For this purpose we will use the nucleon two-point function,

$$G_2(t, \boldsymbol{p}) = \sum_s e^{-E_p t} \Gamma_{\beta\alpha} \langle \Omega | \chi_\alpha | N(p, s) \rangle \left\langle N(p, s) \left| \bar{\chi}_\beta \right| \Omega \right\rangle, \tag{3.75}$$

and consider the combination of the nucleon three- and two-point functions

$$R(t, \tau; \boldsymbol{p}', \boldsymbol{p}; \mathcal{O}) = \frac{G_\Gamma(t, \tau; \boldsymbol{p}', \boldsymbol{p}; \mathcal{O})}{G_2(t, \boldsymbol{p}')} \left[\frac{G_2(\tau, \boldsymbol{p}') G_2(t, \boldsymbol{p}') G_2(t - \tau, \boldsymbol{p})}{G_2(\tau, \boldsymbol{p}) G_2(t, \boldsymbol{p}) G_2(t - \tau, \boldsymbol{p}')} \right]^{\frac{1}{2}}. \tag{3.76}$$

With periodic or anti-periodic boundary conditions in time, the two-point function in Eq. (3.75) can be written in terms of nucleon spinors

$$G_2(t,\boldsymbol{p}) = \sum_s \frac{\sqrt{Z^{\text{snk}}(\boldsymbol{p})\bar{Z}^{\text{src}}(\boldsymbol{p})}}{2E_{\boldsymbol{p}}} \text{Tr}\left[\bar{u}(\boldsymbol{p},s)\Gamma u(\boldsymbol{p},s)\right]\left[e^{-E_p t} + e^{-E'_p(T-t)}\right] + \nu\text{-spinor terms with opposite parity,} \tag{3.77}$$

where the $Z^{\text{src(snk)}}$ is the wavefunction overlap with the proton at the source (sink) and T is the lattice time extent. Using the relation for spinors in Euclidean space

$$\sum_s u(\boldsymbol{p},s)\bar{u}(\boldsymbol{p},s) = -i\not{p} + m\ , \tag{3.78}$$

together with the projection matrix $\Gamma_4 = (1+\gamma_4)/2$, to maximise the overlap with the positive-parity forward-propagating state we get

$$G_2(t,\boldsymbol{p}) = \sqrt{Z^{\text{snk}}(\boldsymbol{p})\bar{Z}^{\text{src}}(\boldsymbol{p})}\left[\left(\frac{E_p+m}{E_p}\right)e^{-E_p t} + \left(\frac{E'_p+m'}{E'_p}\right)e^{-E'_p(T-t)}\right]. \tag{3.79}$$

Similarly, for the three-point function, when $0 \ll \tau \ll t \ll \frac{1}{2}T$, we get

$$G_\Gamma(t,\tau;\boldsymbol{p}',\boldsymbol{p};\mathcal{O}) = \sqrt{Z^{\text{snk}}(\boldsymbol{p}')\bar{Z}^{\text{src}}(\boldsymbol{p})}F(\Gamma,\mathcal{J})e^{-E_{p'}(t-\tau)}e^{-E_p\tau}, \tag{3.80}$$

where

$$F(\Gamma,\mathcal{J}) = \frac{1}{4}\text{Tr}\left[\left(\gamma_4 - i\frac{\boldsymbol{p}'\cdot\boldsymbol{\gamma}}{E_{p'}} + \frac{m}{E_{p'}}\right)\mathcal{J}\left(\gamma_4 - i\frac{\boldsymbol{p}\cdot\boldsymbol{\gamma}}{E_p} + \frac{m}{E_p}\right)\right]. \tag{3.81}$$

The nucleon matrix elements we are interested in will now have the form

$$\langle N(p',s')|\mathcal{O}(\boldsymbol{q})|N(p,s)\rangle = \bar{u}(p',s')\mathcal{J}u(p,s), \tag{3.82}$$

where we have labeled the combination of gamma matrices and Lorentz-invariant form factors sandwiched between two nucleon spinors generically as $\mathcal{J}$. For example, for the electromagnetic current we have

$$\mathcal{J} = \gamma^\mu F_1(Q^2) + i\sigma^{\mu\nu}\frac{q_\nu}{2M}F_2(Q^2)\ . \tag{3.83}$$

3.3.2.1 Example 1: Form Factors

As an example, if we choose the unpolarised projection matrix Γ_4, the electromagnetic current as our operator, and $\boldsymbol{p} = \boldsymbol{p}' = \mathbf{0}$, then the term proportional to $F_2(Q^2)$ in Eq. (3.83) vanishes and we have

$$\langle N(p',s')|J^{\mu}(0)|N(p,s)\rangle = \bar{u}(p',s')\gamma^{\mu}u(p,s)F_1(Q^2=0)\,. \tag{3.84}$$

Hence we are in a position to determine $F_1(Q^2 = 0)$.

First of all, we should remember that this matrix element is defined in Minkowski space while we work in Euclidean space, so we need to Euclideanise it using relations for transforming Minkowski gamma matrices to Euclidean gamma matrices, and we also need to transform our momenta:

$$\gamma_0^M = \gamma_4^E, \quad \gamma_i^M = -i\,\gamma_i^E, \quad p_4^E = ip_0^M \equiv iE(\boldsymbol{p}), \quad p_i^E = -p_i^M\,. \tag{3.85}$$

After Euclideanisation we can see that the matrix element (3.10) can be written in the form

$$\begin{aligned}\langle N(p',s')|\bar{q}\gamma_{\mu}^E q|N(p,s)\rangle = \bar{u}(p',s')\gamma_{\mu}^E u(p,s)F_1(Q^2) \\ +\bar{u}(p',s')\frac{\sigma_{\mu\nu}^E q_{\nu}^E}{2M}u(p,s)F_2(Q^2),\end{aligned} \tag{3.86}$$

which looks very similar to Eq. (3.10), except for a factor of i in the second term. Recalling that in our current example $q_{\nu}^E = 0$, we can rewrite this as

$$\langle N(p',s')|\bar{q}\gamma_{\mu}^E q|N(p,s)\rangle = \bar{u}(p',s')\gamma_{\mu}^E u(p,s)F_1(Q^2=0)\,, \tag{3.87}$$

and Eq. (3.83) reduces to

$$\mathcal{J} = \gamma^{\mu}F_1(Q^2=0)\,, \tag{3.88}$$

which we can substitute into Eq. (3.81). If we insert the time component and the spatial components of the vector of gamma matrices separately, we will get (after taking the trace) the following:

$$F(\Gamma_4,\gamma_4) = \frac{1}{2E_{\boldsymbol{p}}E_{\boldsymbol{p}'}}\left[(E_{\boldsymbol{p}}+m)(E_{\boldsymbol{p}'}+m)+\boldsymbol{p}'\cdot\boldsymbol{p}\right]\,, \tag{3.89}$$

$$F(\Gamma_4,\gamma_i) = \frac{-i}{2E_{\boldsymbol{p}}E_{\boldsymbol{p}'}}\left[(E_{\boldsymbol{p}}+m)\boldsymbol{p}'+(E_{\boldsymbol{p}'}+m)\boldsymbol{p}\right]. \tag{3.90}$$

If we now take the specific case relevant to our example where both source and sink momenta are zero ($\boldsymbol{p}' = \boldsymbol{p} = 0$), then we will get

$$F(\Gamma_4, \gamma_4) = 2\, F_1(Q^2 = 0)\,, \tag{3.91}$$

while the spatial components vanish

$$F(\Gamma_4, \gamma_i) = 0\,. \tag{3.92}$$

Now we can go back to the ratio of three- and two-point functions (Eq. (3.76)) and, after working it through, we will find that it simply provides the factor $\sqrt{\frac{E_{p'} E_p}{(E_{p'}+m)(E_p+m)}}$ in terms of energies and mass, times the function $F(\Gamma, \mathcal{J}(\boldsymbol{q}))$:

$$R(t, \tau; \boldsymbol{p}', \boldsymbol{p}; \mathcal{O}) = \sqrt{\frac{E_{p'} E_p}{(E_{p'} + m)(E_p + m)}} F(\Gamma, \mathcal{J}(\boldsymbol{q})) \quad \left\{ 0 \ll \tau \ll t \ll \frac{1}{2} T \right\}\,. \tag{3.93}$$

And if we look, again, at our very specific case:

$$\Gamma_4 = \frac{1}{2}(1 + \gamma_4), \quad \mathcal{O} = V_4 \equiv \gamma_4, \quad \boldsymbol{p}' = \boldsymbol{p} = 0, \tag{3.94}$$

then the ratio in Eq. (3.93) will give us directly F_1 at $Q^2 = 0$:

$$R(t, \tau; \boldsymbol{p}', \boldsymbol{p}; \mathcal{O}) = F_1(q^2 = 0). \tag{3.95}$$

We can also choose certain combinations of parameters and kinematics which provide access to the Sachs form factors,

$$R(t, \tau; 0, \boldsymbol{p}; \gamma_4, \Gamma_4) = K \left(F_1(q^2) - \frac{E_p - M}{2M} F_2(q^2) \right) = K\, G_E(q^2), \tag{3.96}$$

$$R(t, \tau; 0, \boldsymbol{p}; \gamma_i, \Gamma_4) = -iK \frac{q_i}{E_p + M} G_E(q^2), \tag{3.97}$$

$$R(t, \tau; 0, \boldsymbol{p}; \gamma_i, \Gamma_j) = -iK \epsilon_{ijk} \frac{q_k}{E_p + M} G_M(q^2), \tag{3.98}$$

where $K = \sqrt{(E_p + M)/(2E_p)}$ and $\Gamma_j = i(1 + \gamma_4)\gamma_5\gamma_j/2$. In Fig. 3.10 we show some results from [143] for the ratio in Eq. (3.96) for several choices of momentum transfer. As we can clearly see, the ratio decreases in size as we increase the momentum transfer, indicating that the form factor $G_E(q^2)$ falls as a function of q^2.

More generally, we can consider all combinations that contribute at a fixed q^2, construct a set of simultaneous equations and solve for the two unknowns, $F_1(q^2)$

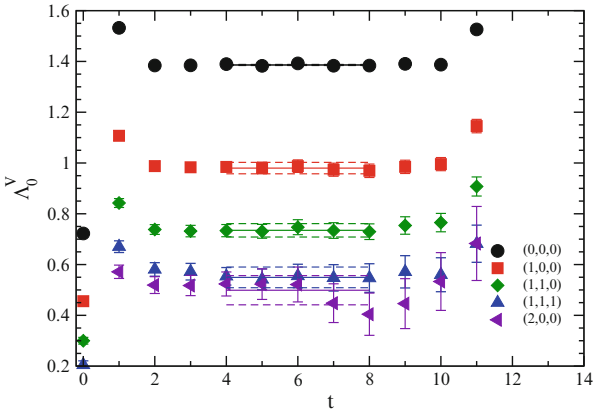

Fig. 3.10 Ratio of three- and two-point functions from Eq. (3.96) from [143]

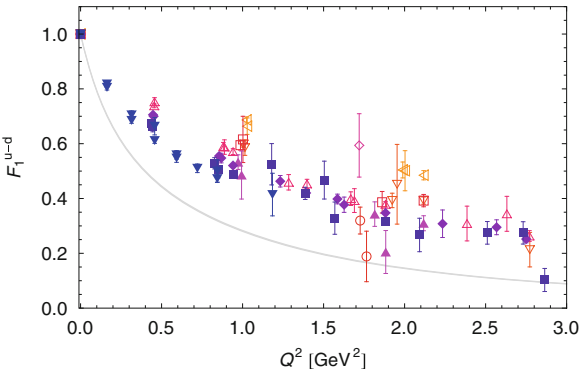

Fig. 3.11 $F_1^{(u-d)}(q^2)$ for several values of 250 MeV $< m_\pi <$ 1.5 GeV from [144]

and $F_2(q^2)$. As an example, we show in Fig. 3.11 some lattice results for $F_1(q^2)$ from [144] for a range of pion masses 250 MeV $< m_\pi <$ 1.5 GeV compared to a parameterisation of experimental data denoted by the shaded band [145]. As can be seen, the lattice results lie above the experimental band, although this is now known to be due to the large pion masses used in many lattice simulations [146].

3.3.2.2 Example 2: g_A

In order to compute the nucleon axial charge, g_A, we need access to the matrix element given in Eq. (3.51) in the forward ($q^2 = 0$) limit,

$$\langle p|\bar{u}\gamma^\mu\gamma^5 d|n\rangle = \bar{u}(p',s')\gamma^\mu\gamma^5 u(p,s)g_A\,. \tag{3.99}$$

As we did in the previous section for the electromagnetic form factors, we wish to isolate this matrix element from the lattice three-point function (Eq. (3.57)). In other words, we wish to determine the matrix element Eq. (3.82) for the particular case where the operator $\mathcal{O}$ is the axial current and the Dirac structure on the right-hand side of Eq. (3.99) shows that in this particular case $\mathcal{J}$ in Eq. (3.82) is simply

$$\mathcal{J} = \gamma_\mu \gamma_5 \, g_A \, . \tag{3.100}$$

We can now substitute this into $F(\Gamma, \mathcal{J})$ defined in Eq. (3.81). For unpolarised gamma nucleons, i.e. $\Gamma = \Gamma_{\text{unpol}}$, we find

$$F(\Gamma_{\text{unpol}}, \gamma_4\gamma_5) = 0, \quad F(\Gamma_{\text{unpol}}, \gamma_i\gamma_5) = 0. \tag{3.101}$$

Obviously, we need a different choice of projection matrix. In order to polarise our nucleon states so that they have definite spin in a particular direction $\boldsymbol{s}$, we will need to use the spin-projectors

$$\Gamma_{\text{pol}} = \frac{1}{2}(1+\gamma_4) i\gamma_5 \boldsymbol{\gamma}\cdot\boldsymbol{s} \, . \tag{3.102}$$

Re-evaluating $F(\Gamma, \mathcal{J})$ in Eq. (3.81) with this choice, we find for time and spatial components of the axial current

$$F(\Gamma_{\text{pol}}, \gamma_4\gamma_5) = -\frac{1}{2E_{\boldsymbol{p}}E_{\boldsymbol{p}'}}\left[(E_{\boldsymbol{p}}+m)\boldsymbol{p}'\cdot\boldsymbol{s} + (E_{\boldsymbol{p}'}+m)\boldsymbol{p}\cdot\boldsymbol{s}\right], \tag{3.103}$$

$$F(\Gamma_{\text{pol}}, \gamma_i\gamma_5) = \frac{i}{2E_{\boldsymbol{p}}E_{\boldsymbol{p}'}}\left[(E_{\boldsymbol{p}}+m)(E_{\boldsymbol{p}'}+m)\boldsymbol{s} + \right. \tag{3.104}$$

$$\left. (\boldsymbol{p}'\cdot\boldsymbol{s})\boldsymbol{p} + (\boldsymbol{p}\cdot\boldsymbol{s})\boldsymbol{p}' - (\boldsymbol{p}'\cdot\boldsymbol{p})\boldsymbol{s}\right]_i \, ,$$

which now depend not only on the energy and momenta of the nucleon states, but also on the direction of its spin.

In particular, we notice that for the spatial component (Eq. (3.104)) we have terms that are proportional directly to $\boldsymbol{p}$ and $\boldsymbol{p}'$, but there is also a term $(E_{\boldsymbol{p}} + m)(E_{\boldsymbol{p}'} + m)\boldsymbol{s}$ which is not proportional to momentum but proportional to the nucleon's energy and the direction of its spin. So even in the case when both $\boldsymbol{p}$ and $\boldsymbol{p}'$ are zero we have a nonzero contribution

$$F(\Gamma_{\text{pol}}, \gamma_i\gamma_5) = 2i s_i, \tag{3.105}$$

and g_A can be determined by choosing the direction of axial current to be the same as the direction of nucleon polarisation. For example, if we choose the polarisation of the nucleon to be in the z-direction, then we need to compute lattice three-point functions with

$$\Gamma_{\text{pol}} = \Gamma_3 = \frac{1}{2}(1+\gamma_4) i\gamma_5\gamma_3, \quad \mathcal{O} = \bar{q}\gamma_3\gamma_5 q \, . \tag{3.106}$$

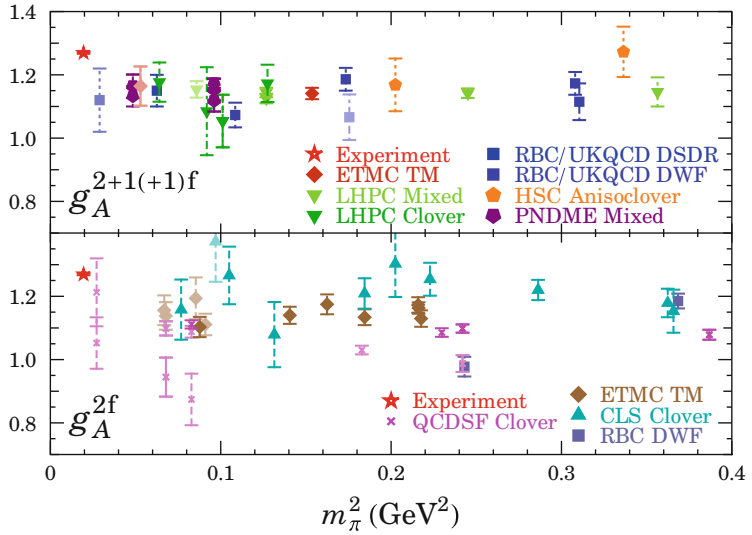

Fig. 3.12 Summary of lattice calculations of g_A by H.-W. Lin [147]

With these particular choice of kinematics ($\boldsymbol{p} = \boldsymbol{p}' = \mathbf{0}$), the ratio defined in Eq. (3.76) simplifies to provide a direct determination of g_A

$$R(t,\tau;\mathbf{0},\mathbf{0};\gamma_3\gamma_5,\Gamma_3) = \frac{G_{\Gamma_3}(t,\tau;\mathbf{0},\mathbf{0};\gamma_3\gamma_5)}{G_2(t,\mathbf{0})} = ig_A\,, \tag{3.107}$$

Due to its status as a benchmark calculation for nucleon structure simulations, g_A has been heavily investigated on the lattice. In Fig. 3.12 we show a summary of calculations by several lattice collaborations compiled by H.-W. Lin [147] in 2012. It is clear that there is broad agreement between the many different groups, with the bulk of the results lying about 10 % below the experimental value. This discrepancy has attracted much attention recently with several arguments such as excited state contamination [148] and finite volumes effects [149] being put forward as explanations. We will not go into a discussion regarding these issues here.

3.3.3 Moments of Structure Functions

In order to proceed towards lattice calculations of matrix elements relevant to structure functions, we need to consider what is called the moments of the structure functions. Moments are integrals with respect to the momentum fraction x, weighted with some power of x, and as we increase this power, this increases the moment, e.g.

$$\int_0^1 dx\, x^{n-2} F_2(x, Q^2) = E^{\mathcal{S}}_{F_2;\nu_n}(M^2/Q^2, g^{\mathcal{S}}) \nu_n^{\mathcal{S}}(M) + \mathcal{O}(1/Q^2). \tag{3.108}$$

These moments can be separated at some renormalisation scale M in a scheme $\mathcal{S}$ into a perturbative part, which is called a Wilson coefficient (E) and calculable in perturbation theory, and a nonperturbative part which we label ν_n, where n is the power of the moment. These ν_n come from forward proton matrix elements of local operators, and hence are amenable to lattice calculations

$$\left\langle N(p,s') \left| \mathcal{O}_q^{\{\mu_1 \ldots \mu_n\}} \right| N(p,s) \right\rangle = 2\bar{u}(p,s') \nu_n^{(q)} p^{\{\mu_1 \ldots \mu_n\}} u(p,s), \tag{3.109}$$

where $\{\ldots\}$ indicates symmetrisation of indices and the subtraction of traces.

Expressions similar to Eq. (3.108) exist for moments of other structure functions:

- unpolarised: $F_1/F_2/F_3 \leftrightarrow \nu_n$,
- polarised: $g_1 \leftrightarrow a_n$, $g_2 \leftrightarrow a_n - d_n$,
- and transversity: $h_1 \leftrightarrow h_n$.

As our first example, we consider an operator $\mathcal{O}$ which contains a gamma matrix, similar to the electromagnetic current, and one or more covariant derivatives, where the number of derivatives depends on moment we are looking at

$$\mathcal{O}_q^{\{\mu_1 \ldots \mu_n\}} = (i)^{n-1} \bar{q} \gamma^{\mu_1} \overleftrightarrow{D}^{\mu_2} \ldots \overleftrightarrow{D}^{\mu_n} q, \tag{3.110}$$

$$\overleftrightarrow{D} = \frac{1}{2}\left(\overrightarrow{D} - \overleftarrow{D}\right). \tag{3.111}$$

On the lattice the covariant derivatives take their usual definitions by a finite difference

$$(\overrightarrow{D}_\mu \psi)(x) = \frac{1}{2}\left[U_\mu(x)\psi(x + a\hat{\mu}) - U_\mu^\dagger(x - a\hat{\mu})\psi(x - a\hat{\mu})\right], \tag{3.112}$$

$$(\overline{\psi}\, \overleftarrow{D}_\mu)(x) = \frac{1}{2}\left[\overline{\psi}(x + a\hat{\mu})U_\mu^\dagger(x) - \overline{\psi}(x - a\hat{\mu})U_\mu(x - a\hat{\mu})\right]. \tag{3.113}$$

The terms $\mathcal{O}(1/Q^2)$ in Eq. (3.108) are higher-twist contributions, which are suppressed at large Q^2. So our operators $\mathcal{O}$ here are all of twist two and provide the dominant contribution in the deep-inelastic (large-Q^2) limit.

Similarly, for the moments of polarised structure functions we consider a polarised nucleon state and the matrix element is now dependent on the orientation of the nucleon spin, s^μ,

$$\left\langle N(p,s') \left| \mathcal{O}_q^{5;\{\mu_1 \ldots \mu_n\}} \right| N(p,s) \right\rangle = \bar{u}(p,s') \frac{a_{n-1}^{(q)}}{n+1} s^{\{\mu_1} p^{\mu_2} \ldots p^{\mu_n\}} u(p,s). \tag{3.114}$$

Here the operator contains a γ_5, so this is the axial version of Eq. (3.110)

$$\mathcal{O}_q^{5;\{\mu_1\ldots\mu_n\}} = (i)^{n-1}\bar{q}\gamma^{\mu_1}\gamma^5\overleftrightarrow{D}^{\mu_2}\ldots\overleftrightarrow{D}^{\mu_n}q. \tag{3.115}$$

3.3.3.1 Moments of PDFs

The interpretation of v_n in terms of moments of PDFs $q(x)$ is

$$v_n^{(q)} = \int_0^1 dx\, x^{n-1}\left(q(x) + (-1)^n\bar{q}(x)\right) = \langle x^{n-1}\rangle_q\,, \tag{3.116}$$

where $q(x)$ ($\bar{q}(x)$) is the probability to find a quark (antiquark) with momentum fraction x. Similarly, in the polarised case we have a_n which are simply the moments of polarised PDFs:

$$a_n^{(q)} = 2\int_0^1 dx\, x^n\left(\Delta q(x) + (-1)^n\Delta\bar{q}(x)\right) = 2\langle x^n\rangle_{\Delta q}\,. \tag{3.117}$$

$\Delta q(x)$ here are written as

$$\Delta q(x) = q_+(x) - q_-(x), \tag{3.118}$$

where $q_+(x)$ ($q_-(x)$) is the "probability" of finding a quark with momentum fraction x and the direction of the helicity equal (opposite) to that of the proton. In particular,

$$\frac{1}{2}a_0^{(q)} = \langle 1\rangle_{\Delta q} = \Delta q \tag{3.119}$$

is the fraction of the nucleon spin carried by quarks of flavour q. Also, the axial charge g_A is just

$$g_A = \Delta u - \Delta d. \tag{3.120}$$

3.3.3.2 Operators

As we have seen, on the lattice we need to consider twist-2 operators. We start their definitions by first noting that by changing to Euclidean space from Minkowski space we replace the Lorentz group by the orthogonal group $\mathcal{O}(4)$. We also work in discrete space-time which reduces this to the hypercubic group $H(4) \subset \mathcal{O}(4)$, and since $H(4)$ is finite, mixings are possible [150]. In order to reduce operator mixing, it is useful to use certain operator combinations which reside in certain irreducible representations of $H(4)$. For example, if we look at v_2 there are two

different irreducible representations we can form that have different combinations of indices:

$$\mathcal{O}_{v_{2a}} = \mathcal{O}^{\{14\}}, \tag{3.121}$$

$$\mathcal{O}_{v_{2b}} = \mathcal{O}^{\{44\}} - \frac{1}{3}\left(\mathcal{O}^{\{11\}} + \mathcal{O}^{\{22\}} + \mathcal{O}^{\{33\}}\right); \tag{3.122}$$

the first index here is the gamma matrix, and the second index is the derivative. Since v_{2a} and v_{2b} are different representations of the same continuum operator, they should agree in the continuum limit. Similarly,

$$\mathcal{O}_{v_3} = \mathcal{O}^{\{114\}} - \frac{1}{2}\left(\mathcal{O}^{\{224\}} + \mathcal{O}^{\{334\}}\right), \tag{3.123}$$

$$\mathcal{O}_{v_4} = \mathcal{O}^{\{1144\}} + \mathcal{O}^{\{2233\}} - \mathcal{O}^{\{1133\}} - \mathcal{O}^{\{2244\}}, \tag{3.124}$$

provide access to higher moments. For more details on operator construction, see [150].

3.3.3.3 Extracting Moments

Now, we want to extract these moments from calculations of lattice three-point functions (Eq. (3.57)) using the methods outlined in Sect. 3.3.2. Let us take the v_{2a} operator as an example. In Minkowski space this operator takes the indices $\{01\}$

$$\mathcal{O}^M_{v_{2a}} = \mathcal{O}^M_{\{01\}} = \frac{1}{2}\bar{q}\left(\gamma_0^M \overleftrightarrow{D}_1 + \gamma_1^M \overleftrightarrow{D}_0\right) q, \tag{3.125}$$

and the matrix element from Eq. (3.82) can be written then as

$$\frac{i}{4}\left\langle N(p,s') \left| \bar{q}\left(\gamma_0^M \overleftrightarrow{D}_1 + \gamma_1^M \overleftrightarrow{D}_0\right) q \right| N(p,s) \right\rangle = \langle x \rangle^{(q)} \frac{1}{2}\bar{u}(p,s')\left(\gamma_0^M p_1 + \gamma_1^M p_0\right) u(p,s),$$

where we have used the more common notation for $v_2^{(q)} = \langle x \rangle^{(q)}$, denoting the fraction of the nucleon's momentum carried by the quarks with flavour q. After Euclideanisation of this operator,

$$\gamma_0^M = \gamma_4^E, \quad \gamma_i^M = -i\gamma_i^E, \quad p_4^E = ip_0^M \equiv iE(\boldsymbol{p}), \quad p_i^E = -p_i^M, \tag{3.126}$$

$$D_4 = -iD^{(M)_0}, \quad D_i = -D^{(M)_i}, \tag{3.127}$$

we can rewrite it as

$$\frac{i}{4}\left\langle N(p,s')\left|\bar{q}\left(\gamma_0^E \overleftrightarrow{D}_1 + \gamma_1^E \overleftrightarrow{D}_4\right)q\right|N(p,s)\right\rangle$$
$$= \langle x\rangle^{(q)} \frac{1}{2}\bar{u}(p,s')\left(-\gamma_4^E p_1 - \gamma_1^E E_N(\boldsymbol{p})\right)u(p,s)\,. \tag{3.128}$$

Now if we use the standard spin-projector for an unpolarised nucleon, $\Gamma_{\text{unpol}} = (1+\gamma_4)/2$, and

$$\mathcal{J} = \frac{1}{2}\left(-\gamma_4 p_1 - i\gamma_1 E_N(\boldsymbol{p})\right)\langle x\rangle^{(q)}\,, \tag{3.129}$$

in Eq. (3.81), we find that the ratio of three- and two-point functions becomes

$$R(t,\tau;\boldsymbol{p},\boldsymbol{p};\mathcal{O}_{v_{2a}},\Gamma_{\text{unpol}}) = \frac{G_{\Gamma_{\text{unpol}}}(t,\tau;\boldsymbol{p},\boldsymbol{p};\mathcal{O}_{v_{2a}})}{G_2(t,\boldsymbol{p})} = ip_1\langle x\rangle^{(q)}\,. \tag{3.130}$$

Following a similar process for v_{2b} leads to

$$R(t,\tau;\boldsymbol{p},\boldsymbol{p};\mathcal{O}_{v_{2b}}) = -\frac{E_{\boldsymbol{p}}^2 + \frac{1}{3}\boldsymbol{p}^2}{E_{\boldsymbol{p}}}\langle x\rangle^{(q)}\,. \tag{3.131}$$

So we can see that in order to determine $\langle x\rangle$ using the v_{2a} operator we have to work with nonzero momentum, while in case of v_{2b} we can work with zero momentum.

In Fig. 3.13 we present an example of lattice results for these ratios from the QCDSF collaboration [151]. Here we see excellent agreement for the two different representations v_{2a} and v_{2b} of the same continuum operator (here we are considering the up-quark contribution), even though we look at finite lattice spacing, at different choices of proton momentum.

3.3.3.4 Operator Renormalisation

Let us talk now briefly about operator renormalisation, which deserves its own set of lectures (see, for example, [152]); we will consider here just the basic ideas of renormalisation. The lattice itself is a regularisation scheme, and the matrix elements that we measure using lattice operators will be in the lattice scheme; they are so-called bare operators $\mathcal{O}_{\text{bare}}$. In order to compare a lattice calculation of an observable to that in the continuum, i.e. from experiment or phenomenology, we need to switch to a continuum regularisation scheme, e.g. $\overline{\text{MS}}$. This is done by applying some renormalisation constant

$$\mathcal{O}^{\mathcal{S}}(M) = Z_{\mathcal{O}}^{\mathcal{S}}(M)\mathcal{O}_{\text{bare}} \tag{3.132}$$

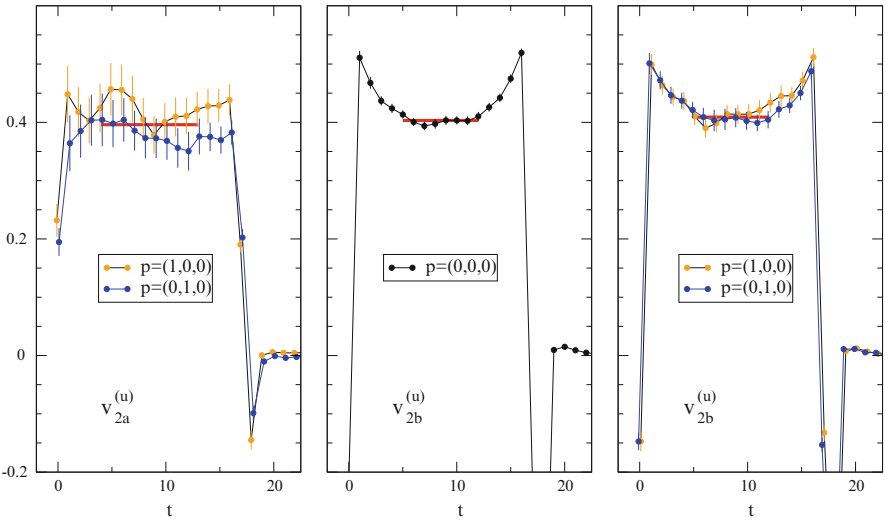

Fig. 3.13 Comparison of the ratios for v_{2a} in Eq. (3.130) and v_{2b} in Eq. (3.131) for a u-quark in the proton for different choices of momentum. Here the proton source and sink are placed at $t = 0$ and $t = 17$, respectively

(renormalise bare lattice operators in scheme $\mathcal{S}$ at scale M). We have mentioned mixing earlier, so if we have more operators with the same quantum numbers, but same or lower dimension, then we need to include mixings between these operators, i.e. we should actually include the sum of all of the contributions from the different lattice operators to get the result for the continuum operator:

$$\mathcal{O}_i^{\mathcal{S}}(M) = \sum_j Z^{\mathcal{S}}_{\mathcal{O}_i\mathcal{O}_j}(M,a)\mathcal{O}_j(a). \tag{3.133}$$

This procedure could in principle be done with lattice perturbation theory [12], however this is well known to be poorly convergent. We are then forced to revert to a nonperturbative method. The two commonly used methods are the Schrödinger functional [153] and the Rome-Southampton method [154].

For recent work computing these renormalisation constants for many lattice operators, see e.g. [155], and for a recent review of nonperturbative renormalisation, see [156].

3.3.4 Generalised Parton Distributions

We have seen in the previous section how parton distribution functions provide a description of the longitudinal momentum distributions of quarks and gluons in the nucleon. Although less well-understood, there is increasing interest in gaining

information on the transverse structure and angular-momentum distribution of partons within the nucleon. Generalised parton distributions (GPDs) [157–159] have opened new ways of studying the complex interplay of longitudinal momentum and transverse coordinate space [160, 161], as well as spin and orbital-angular-momentum degrees of freedom in the nucleon [162]. A full mapping of the parameter space spanned by GPDs is an extremely extensive task, which most probably needs support from nonperturbative techniques like lattice simulations. Given this interest, there has been a large amount of activity within the lattice community in the area of GPDs, and so we will devote some time here to summarising some of the important aspects relevant for lattice simulations.

3.3.4.1 Definition

The generalised parton distributions of quarks are defined at leading twist through the off-forward matrix elements of the light-cone operators

$$\begin{aligned}
&\int \frac{d\lambda}{4\pi}\, e^{i\lambda x}\, \left\langle P' \left| \overline{\psi}\,(-n\lambda/2)\, \gamma^\mu \psi\,(n\lambda/2) \right| P \right\rangle = \\
&\qquad \overline{U}(P') \left(\gamma^\mu H(x,\xi,t) + \frac{i\sigma^{\mu\nu}\Delta_\nu}{2m} E(x,\xi,t) \right) U(P)\,, \\
&\int \frac{d\lambda}{4\pi}\, e^{i\lambda x}\, \left\langle P' \left| \overline{\psi}(-n\lambda/2)\gamma_5\gamma^\mu \psi(n\lambda/2) \right| P \right\rangle = \\
&\qquad \overline{U}(P') \left(\gamma_5\gamma^\mu \tilde{H}(x,\xi,t) + \frac{i\gamma_5\Delta^\mu}{2m} \tilde{E}(x,\xi,t) \right) U(P)\,, \quad (3.134)
\end{aligned}$$

for the helicity-independent and helicity-dependent distributions, respectively. We note that the expressions in Eq. (3.134) are only valid in the light-cone gauge where $n \cdot A = 0$, otherwise we would need to include a gauge link $\exp\left(-ig \int_{-\lambda/2}^{\lambda/2} d\alpha\, n \cdot A(\alpha n)\right)$ between the two quark fields to ensure gauge invariance.

Figure 3.14 shows the electron-proton scattering process relevant for GPDs. Here the proton stays intact as we had earlier for the determination of form factors, but the probe has enough resolution to identify a single quark, as was the case for deep-inelastic scattering. This process is known as deeply virtual Compton scattering (DVCS), and the final states to be detected here are the proton together with the scattered electron and a photon.

It is common to denote the momentum transfer (squared) in the context of GPDs by $\Delta = P' - P$ ($t = \Delta^2$). Using the light-cone vector n, we define the longitudinal momentum transfer by $\xi = -n \cdot \Delta/2$. The proper definition of the twist-2 tensor or quark helicity-flip GPDs H_T, E_T, $\tilde{H}_T$ and $\tilde{E}_T$ can be found in [163]. GPDs provide a solid framework in QCD to relate many different aspects of hadron physics, some of which we have already discussed in earlier sections

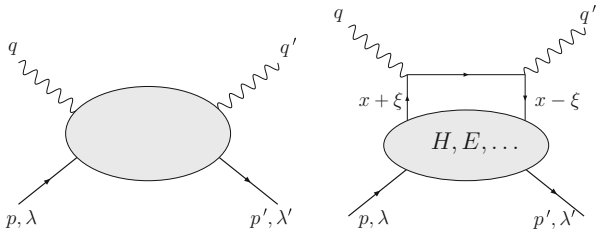

Fig. 3.14 Graphical representation of GPDs as part of a scattering amplitude

- The forward limit $\Delta \to 0$ of certain GPDs reproduces the well known parton distributions, that is $H(x, \xi = 0, t = 0) = q(x) = f_1(x)$, $\tilde{H}(x, 0, 0) = \Delta q(x) = g_1(x)$ and $H_T(x, 0, 0) = \delta q(x) = h_1(x)$.
- The integral over the longitudinal momentum fraction $\int dx$ of the GPDs gives the Dirac, Pauli, axial, pseudo-scalar, tensor etc. form factors, $\int dx\, H(x, \xi, t) = F_1(t)$, $\int dx\, E = F_2(t)$, $\int dx\, \tilde{H} = g_A(t)$, $\int dx\, \tilde{E} = g_P(t)$, $\int dx\, H_T = g_T(t)$ etc.
- The Fourier transforms $(2\pi)^{-2} \int d\Delta_\perp e^{-ib_\perp \cdot \Delta_\perp}$ of the GPDs H, $\tilde{H}$ and H_T at $\xi = 0$ are coordinate-space probability densities in the impact parameter $b_\perp$ [164].
- The forward limit of the x-moment of the GPD E, $\int dx\, x\, E(x, 0, 0) = B_{20}(0)$, allows for the determination of the quark orbital-angular-momentum contribution to the nucleon spin, $L^q = 1/2(\langle x \rangle + B_{20} - \Delta q)$, where $\langle x \rangle$ is the quark momentum fraction [162].

For more information on GPDs, see [165] for a review.

3.3.4.2 Matrix Elements and Moments of GPDs

For a lattice calculation of GPDs, we proceed in a similar way to our earlier discussion of structure functions by working in Mellin space to relate matrix elements of local operators to Mellin moments of the GPDs. But while for the moments of PDFs we considered forward ($t = 0$) matrix elements of the twist-2 operators defined in Eqs. (3.110) and (3.115), here we will use non-forward matrix elements of these same twist-2 operators. These matrix elements will specify the $(n-1)$th moments of the spin-averaged and spin-dependent generalised parton distributions, respectively. In particular, for the unpolarised GPDs, we have

$$\int_{-1}^{1} dx\, x^{n-1}\, H^q(x, \xi, t) = H_n^q(\xi, t)\,,$$
$$\int_{-1}^{1} dx\, x^{n-1}\, E^q(x, \xi, t) = E_n^q(\xi, t)\,, \tag{3.135}$$

where [162]

$$H_n^q(\xi,t) = \sum_{i=0}^{\lfloor\frac{n-1}{2}\rfloor} A_{n,2i}^q(t)(-2\xi)^{2i} + C_n^q(t)(-2\xi)^n|_{n\text{ even}}\,,$$

$$E_n^q(\xi,t) = \sum_{i=0}^{\lfloor\frac{n-1}{2}\rfloor} B_{n,2i}^q(t)(-2\xi)^{2i} - C_n^q(t)(-2\xi)^n|_{n\text{ even}}\,, \tag{3.136}$$

and the generalised form factors $A_{n,2i}^q(t)$, $B_{n,2i}^q(t)$ and $C_n^q(t)$ for the lowest three moments are extracted from the nucleon matrix elements [162]

$$\langle P'|\mathcal{O}_q^{\mu_1}|P\rangle = A_{10}^q(t)\,\bar{u}\,(P')\gamma^{\mu_1}u(P) + B_{10}^q(t)\,\bar{u}(P')\frac{i\sigma^{\mu_1\nu}\Delta_\nu}{2m}u(P)\,, \tag{3.137}$$

$$\langle P'|\mathcal{O}_q^{\{\mu_1\mu_2\}}|P\rangle = A_{20}^q(t)\,\bar{u}\,(P')\gamma^{\{\mu_1}u(P)\overline{P}^{\mu_2\}} \tag{3.138}$$

$$+\,B_{20}^q(t)\,\bar{u}(P')\frac{i\sigma^{\{\mu_1\nu}\Delta_\nu}{2m}u(P)\,\overline{P}^{\mu_2\}} + C_2^q(t)\,\frac{1}{m}\,\bar{u}(P')u(P)\,\Delta^{\{\mu_1}\Delta^{\mu_2\}}\,.$$

Note that the momentum transfer is given by $\Delta = P' - P$ with $t = \Delta^2$, while $\xi = -n\cdot\Delta/2$ denotes the longitudinal momentum transfer, and $\overline{P} = (P'+P)/2$ is the average nucleon momentum. We can construct an overdetermined set of equations to solve Eqs. (3.137), (3.138) for the generalised form factors, $A_{n,2i}^q(t)$, $B_{n,2i}^q(t)$ and $C_n^q(t)$. This technique is described in detail in [166].

For the lowest moment, A_{10} and B_{10} are just the Dirac and Pauli form factors F_1 and F_2, respectively:

$$\int_{-1}^{1} dx\,H^q(x,\xi,t) = A_{10}^q(t) = F_1(t)\,, \tag{3.139}$$

$$\int_{-1}^{1} dx\,E^q(x,\xi,t) = B_{10}^q(t) = F_2(t)\,, \tag{3.140}$$

while $\tilde{A}_{10}$ and $\tilde{B}_{10}$ are the usual axial-vector and pseudoscalar form factors, respectively

$$\int_{-1}^{1} dx\,\tilde{H}^q(x,\xi,t) = \tilde{A}_{10}^q(t) = g_A(t)\,, \tag{3.141}$$

$$\int_{-1}^{1} dx\,\tilde{E}^q(x,\xi,t) = \tilde{B}_{10}^q(t) = g_P(t)\,. \tag{3.142}$$

Similarly, the first moments of $H, E, \tilde{H}, \tilde{E}$ are explicitly

$$\int_{-1}^{1} dx\, x\, H^q(x,\xi,t) = A^q_{20}(t) + \xi^2 C^q_2(t)\,, \tag{3.143}$$

$$\int_{-1}^{1} dx\, x\, \tilde{H}^q(x,\xi,t) = \tilde{A}^q_{20}(t)\,, \tag{3.144}$$

$$\int_{-1}^{1} dx\, x\, E^q(x,\xi,t) = B^q_{20}(t) - \xi^2 C^q_2(t)\,, \tag{3.145}$$

$$\int_{-1}^{1} dx\, x\, \tilde{E}^q(x,\xi,t) = \tilde{B}^q_{20}(t)\,. \tag{3.146}$$

Note that there are no C form factors for the polarised moments.

We also observe that in the forward limit ($t = \xi = 0$) the moments of H_q reduce to the moments of the unpolarised parton distribution $A_{n0}(0) = \langle x^{n-1} \rangle$.

3.3.4.3 Transverse Densities

In the same way as we discussed in Sect. 3.2.1.3 for obtaining charge and magnetisation densities through two-dimensional Fourier transforms of electromagnetic form factors, Burkardt [161] has shown that generalised parton distributions gain a physical interpretation when Fourier transformed to impact parameter space at longitudinal momentum transfer $\xi = 0$. For example,

$$q(x, \boldsymbol{b}_\perp) = \int \frac{d^2\Delta_\perp}{(2\pi)^2}\, e^{-i\boldsymbol{b}_\perp\cdot\Delta_\perp} H(x,0,-\Delta^2_\perp)\,, \tag{3.147}$$

(and similarly for the polarised $\Delta q(x, \boldsymbol{b}_\perp)$) where $q(x, \boldsymbol{b}_\perp)$ is the probability density for a quark with longitudinal momentum fraction x and at transverse position (or impact parameter) $\boldsymbol{b}_\perp$.

Burkardt [161] also argued that $H(x,0,-\Delta^2_\perp)$ becomes $\Delta^2_\perp$-independent as $x \to 1$ since, physically, we expect the transverse size of the nucleon to decrease as x increases, i.e. $\lim_{x\to 1} q(x, \boldsymbol{b}_\perp) \propto \delta^2(\boldsymbol{b}_\perp)$. As a result, we expect the slopes of the moments of $H(x,0,-\Delta^2_\perp)$ in $\Delta^2_\perp$ to decrease as we proceed to higher moments. This is also true for the polarised moments of $\tilde{H}(x,0,-\Delta^2_\perp)$, so from Eq. (3.136) with $\xi = 0$ we expect that the slopes of the generalised form factors $A_{n0}(t)$ and $\tilde{A}_{n0}(t)$ should decrease with increasing n. This was clearly seen in several lattice simulations, e.g. [167, 168].

This idea was extended further to demonstrate how to use the first two moments of proton [169] and pion [170] GPDs to gain insights into the transverse spin distribution of hadrons. These results provided fascinating insights in to the complex interplay between hadron and quark spin orientation and the transverse distribution of quarks inside a hadron.

3.3.4.4 Nucleon Spin

As we have discussed earlier, it has been long known from DIS experiments that only about 30 % of the proton's spin is generated from the intrinsic spin of the quarks. This presents a puzzle as to how the remaining 70 % is generated through quark orbital angular momentum and by gluons.

Ji has provided a way forward by showing that the total quark and gluon angular momenta can be related to the second ($n = 2$) moments of the GPDs H and E [162]

$$J_{q,g} = \frac{1}{2}(A_{20}^{q,g}(0) + B_{20}^{q,g}) \,, \tag{3.148}$$

where $A_{20}(0)$ and $B_{20}(0)$ are the generalised form factors from Eq. (3.138) at zero momentum transfer ($t = 0$). We now have Ji's spin sum rule

$$\frac{1}{2} = \sum_q J_q + J_g \,. \tag{3.149}$$

The matrix elements in Eq. (3.138) can be computed on the lattice, and when combined with the further decomposition

$$J_q = \frac{1}{2}\Delta q + L_q \,, \tag{3.150}$$

together with a lattice determination of the quark spin fractions Δq from Sect. 3.3.2.2, we are able to not only provide a determination for the total amount of the proton's spin provided by the quarks, but also decompose this into quark spin and orbital angular momentum contributions.

As an example, we show in Fig. 3.15 results from QCDSF [171] (left) and LHPC [172] (right) for the total quark angular momentum contribution to the proton's

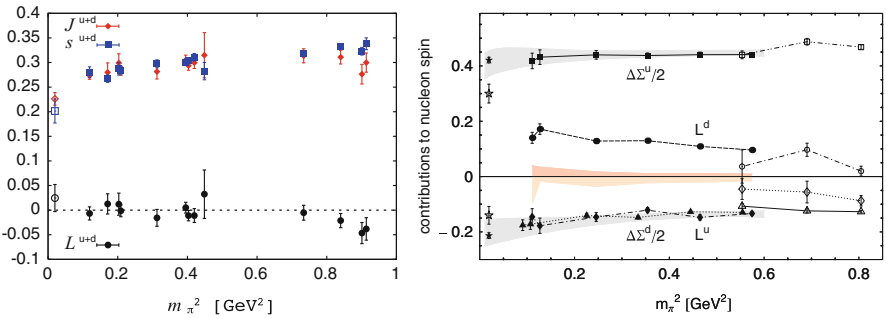

Fig. 3.15 Total angular momentum contribution of the quarks to the spin of the proton. Results are from QCDSF [171] (*left*) and LHPC [172] (*right*)

spin as a function of m_π^2 and its decomposition into helicity and orbital angular momentum contributions.

3.4 Summary

In these notes, we have studied various aspects of hadron structure, focusing on the nucleon, and how they can be studied on the lattice. We started with a discussion of elastic electron-proton scattering and how this leads to the idea of electromagnetic form factors and phenomenological implications for the distribution of charge (quarks) inside the nucleon.

By introducing the idea of deep-inelastic scattering (DIS), we motivated the idea of parton distribution functions (PDFs) and how this leads to description of distribution of momentum. These two ideas were combined into a general picture of the structure of the nucleon through the introduction of generalised parton distributions (GPDs). From these generalised functions, we saw how we can gain insights into transverse densities and decomposition of the spin of the nucleon into its quark and gluon constituents.

From the lattice side, we have learnt how we can determine the nonperturbative matrix elements relevant for these phenomenological quantities on the lattice. To do this, we introduced lattice three-point functions and showed how we can extract these matrix elements via ratios of three-point to two-point functions. We demonstrated the use of these lattice methods by providing some typical examples of recent lattice results of phenomenologically interesting quantities, such as the electromagnetic form factors F_1 and F_2, the average momentum fraction $\langle x \rangle$, the axial coupling constant g_A, and moments of generalised parton distributions.

Acknowledgements We would like to thank the organisers for putting together such a wonderful school. JMZ is supported by the Australian Research Council grant FT100100005.

Chapter 4
Chiral Perturbation Theory

Brian C. Tiburzi

Abstract The era of high-precision lattice QCD has led to synergy between lattice computations and phenomenological input from chiral perturbation theory. We provide an introduction to chiral perturbation theory with a bent towards understanding properties of the nucleon and other low-lying baryons. Four main topics are the basis for this chapter. We begin with a discussion of broken symmetries and the procedure to construct the chiral Lagrangian. The second topic concerns specialized applications of chiral perturbation theory tailored to lattice QCD, such as partial quenching, lattice discretization, and finite-volume effects. We describe inclusion of the nucleon in chiral perturbation theory using a heavy-fermion Euclidean action. Issues of convergence are taken up as our final topic. We consider expansions in powers of the strange-quark mass, and the appearance of unphysical singularities in the heavy-particle formulation. Our aim is to guide lattice practitioners in understanding the predictions chiral perturbation theory makes for baryons, and show how the lattice will play a role in testing the rigor of the chiral expansion at physical values of the quark masses.

4.1 Introductory Remarks

Prior to lattice-QCD computations, chiral perturbation theory (χPT) was the only method for doing high-precision low-energy QCD phenomenology. One crowning achievement of χPT is a procedure for the determination of ratios of the light-quark masses. These ratios can be determined using the experimentally measured hadron spectrum with small effects, such as isospin breaking from both strong and electromagnetic sources, treated in a systematic fashion, see [173]. In essence, χPT provides the tool to study the light-quark mass dependence of low-energy QCD

B.C. Tiburzi (✉)
Department of Physics, The City College of New York, New York, NY 10031, USA

Graduate School and University Center, The City University of New York, New York, NY 10016, USA

RIKEN BNL Research Center, Brookhaven National Laboratory, Upton, NY 11973, USA
e-mail: btiburzi@ccny.cuny.edu

H.-W. Lin, H.B. Meyer (eds.), *Lattice QCD for Nuclear Physics*, Lecture Notes in Physics 889, DOI 10.1007/978-3-319-08022-2_4

observables. As such, it is a tool that furnishes considerable insight for lattice QCD computations. The success of this model-independent description of low-energy QCD is limited in practice by the size of the physical light-quark masses compared to strong interaction scales. Lattice QCD computations are confronting predictions made by χPT. For the strange quark, there has been considerable debate about the efficacy of the $SU(3)$ chiral expansion, even in the meson sector. The chiral dynamics of the nucleon has not been conclusively exposed from lattice QCD computations. As lattice collaborations worldwide attain light quark masses, the chiral dynamics of low-lying hadrons will be rigorously tested.

We undertake the task of making a user-friendly introduction to χPT aimed at lattice practitioners, with a particular focus on the nucleon. From the outset, we stress that this chapter is not meant to be a comprehensive review of the field. By contrast, our aim is to provide a pedagogical introduction that will arm the reader with the tools necessary to investigate further. We hope to familiarize readers with the predictions that χPT makes for hadrons, and to advertise the role lattice QCD will play in assessing the chiral expansion at physical values of the quark masses. It is useful for the reader to be accustomed to the concept of an effective field theory, the study of which is possible through a number of excellent references. We recommend the textbooks [174, 175], and the summer school lectures [176]. For the specific topics covered in this chapter, we will suggest a few references for further study rather than provide an exhaustive list of the possibilities. Various exercises are scattered throughout the presentation. Some are simple and meant only as reminders, whereas others require more thought.

Our presentation is organized around four central topics. The first topic in Sect. 4.2 is key to the entire chapter and concerns the construction of the chiral Lagrangian. We consider the symmetry-breaking pattern of QCD for two light quark flavors, discuss the emergent Nambu-Goldstone bosons, and expose their universal low-energy dynamics through the effective chiral Lagrangian. The second topic is taken up in Sect. 4.3, where applications geared toward lattice QCD are the focus. Beyond providing quark-mass extrapolation formulae, χPT has been extended in various ways that are relevant for lattice gauge theory simulations. In particular, we address extensions needed to account for the partially quenched approximation to QCD, and modifications necessary to describe the effects of finite volume, as well as the effects of lattice discretization. Chiral dynamics of the nucleon is pursued in Sect. 4.4. Using a heavy-fermion Euclidean action, we show how to include the nucleon in χPT. Particular attention is paid to the quark-mass dependence of the nucleon mass, and to the phenomenology of the pion-nucleon sigma term. The issue of convergence is taken up as our final topic in Sect. 4.5. We remind the reader about the nature of asymptotic expansions, and the challenges inherent to assessing the convergence of the chiral expansion using phenomenology and lattice data. With such concerns in mind, we extend χPT to include the strange quark. We investigate how the chiral expansion of certain hyperon properties can be reorganized into a better perturbative expansion by re-summing strange-quark mass contributions. Finally, we address the appearance of unphysical singularities in the heavy-nucleon formulation and the need for threshold re-summations.

4.2 The Chiral Lagrangian

The possibility of building a phenomenological theory of low-energy QCD exists because there are unusually light particles in the hadron spectrum. Pions are the lightest hadrons, and they are well separated in energy from any other states or resonances. There is an elegant explanation, moreover, for the lightness of pions due to spontaneous breakdown of chiral symmetry. The physics underlying this explanation is the Nambu-Goldstone mechanism [177, 178], and allows us to construct systematically a phenomenological theory of pions. Chiral symmetry breaking and the construction of the chiral Lagrangian are the topics of this section.

4.2.1 Symmetries and Symmetry Breaking

The spectrum and properties of low-energy QCD are indicative both of its symmetries, and of its symmetry breaking. We begin with the case of QCD with two massless quark flavors, which will be identified as the up and down quarks. The action density for QCD can be written as the sum of contributions from matter and radiation fields, $\mathcal{L}_{\rm QCD} = \mathcal{L}_\psi + \mathcal{L}_{\rm YM}$, where the latter is the Yang-Mills action, $\mathcal{L}_{\rm YM}$. Our concern lies with the matter part of the action, $\mathcal{L}_\psi$, which has the form

$$\mathcal{L}_\psi = \sum_{i=1}^{2} \overline{\psi}_i \not{D} \psi_i \,. \tag{4.1}$$

Written this way, the action obviously possesses a global $U(2)$ flavor symmetry, but there is a larger symmetry group. To expose the further symmetries of the action, we define chiral projection matrices, $\mathcal{P}_{L,R} = \frac{1}{2}(1 \mp \gamma_5)$, which have all the usual properties expected of projectors. Right- and left-handed quark fields are then defined using chiral projectors, $\psi_{L,R} = \mathcal{P}_{L,R}\psi$. Consequently, the matter part of the QCD action can be written as

$$\overline{\psi} \not{D} \psi = \overline{\psi}_L \not{D} \psi_L + \overline{\psi}_R \not{D} \psi_R, \tag{4.2}$$

for the flavor-doublet quark field. This simple decomposition seems to make a profound statement: the chirality of a massless quark cannot be changed by gluon interactions. This is not exactly the full story, as we shall shortly see.

On account of the handed decomposition of the quark fields in Eq. (4.2), the symmetry group of the massless QCD action is *chiral*, having the form $U(2)_L \otimes U(2)_R$. Specifically for matrices $(L, R) \in U(2)_L \otimes U(2)_R$, we have the transformations $\psi_L \to L\psi_L$ and independently $\psi_R \to R\psi_R$. This transformation appears quite complicated in terms of the original Dirac fermion, $\psi \to (L\mathcal{P}_L + R\mathcal{P}_R)\psi$, but is nonetheless a symmetry of Eq. (4.1). An important subgroup of the chiral symmetry group is the vector subgroup, $U(2)_V$, which is the naïve flavor symmetry of the massless action. For a transformation with $L = R \equiv V$, we have simply $\psi \to V\psi$.

Additional subgroups of the chiral symmetry group are important. Consider the trivial group decomposition, $U(2)_L \otimes U(2)_R = U(1)_L \otimes U(1)_R \otimes SU(2)_L \otimes SU(2)_R$, achieved by removing the overall phase from each $U(2)$ transformation. Under the $U(1)_L \otimes U(1)_R$ subgroup, we have the simple phase transformations $\psi_L \to e^{i\theta_L}\psi_L$, and $\psi_R \to e^{i\theta_R}\psi_R$. In terms of the Dirac fermion field, we see

$$\psi \to \left[\frac{1}{2}\left(e^{i\theta_R} + e^{i\theta_L}\right) + \frac{1}{2}\left(e^{i\theta_R} - e^{i\theta_L}\right)\gamma_5\right]\psi. \tag{4.3}$$

The vector subgroup $U(1)_V \subset U(1)_L \otimes U(1)_R$ is specified by all phase transformations under which the left- and right-handed fields are re-phased identically, $\theta_R = \theta_L \equiv \theta$, and consequently $\psi \to e^{i\theta}\psi$. This global symmetry leads to the conservation of quark number (or equivalently baryon number). The orthogonal choice of phases, namely $\theta_R = -\theta_L \equiv \theta_5$, leads to the axial transformation of the quark field, $\psi \to e^{i\theta_5\gamma_5}\psi$, and generates the $U(1)_A$ symmetry of the action.

1 Consider the non-singlet axial transformation of the quark field, specified by $\psi_i \to (e^{i\phi^a\tau^a\gamma_5})_{ij}\psi_j$, with τ^a as isospin matrices. Is there a corresponding symmetry group for the massless QCD action?

As already alluded to, global symmetries generate classically conserved currents. According to the discussion so far, there should be three non-singlet left-handed currents, $J^a_{\mu,L} = \overline{\psi}_L\tau^a\gamma_\mu\psi_L$, three non-singlet right-handed currents, $J^a_{\mu,R} = \overline{\psi}_R\tau^a\gamma_\mu\psi_R$, in addition to the singlet vector current, $J_\mu = \overline{\psi}\gamma_\mu\psi$, and singlet axial-vector current, $J_{\mu 5} = \overline{\psi}\gamma_\mu\gamma_5\psi$. The regulated theory, however, is not invariant under flavor-singlet axial transformations. This is referred to as the chiral anomaly; because, at the quantum level, the singlet axial current is not conserved:

$$\partial_\mu J_{\mu 5}(x) = \partial_\mu J_{\mu,L}(x) - \partial_\mu J_{\mu R}(x) = -\frac{\alpha_s}{8\pi}\epsilon_{\mu\nu\rho\sigma}F^A_{\mu\nu}F^A_{\rho\sigma}, \tag{4.4}$$

in four dimensions. Of course, this is a subject well-known to lattice QCD. The chiral anomaly presents an essential obstacle in devising chirally invariant lattice regularizations for fermions. We suggest that readers unfamiliar with these issues consult [50].

Due to the chiral *asymmetry* in Eq. (4.4), we shall merely dismiss $U(1)_A$ from our discussion of symmetries. The definition of a regulated theory of massless QCD has a $U(1)_V \otimes SU(2)_L \otimes SU(2)_R$ symmetry, but this is not the final story. Pairing of quark chiralities is preferred by the vacuum state of QCD. This state should be viewed as the ground state of the quantum field theory, and the ground state generally need not respect the symmetries of the underlying theory. While perturbative QCD dynamics does not distinguish between quark chiralities, nonperturbatively, the ground state actually does, through the formation of a nonzero

vacuum expectation value (vev) of the chiral condensate, $\langle\overline{\psi}\psi\rangle = \langle\overline{\psi}_L\psi_R\rangle + \langle\overline{\psi}_R\psi_L\rangle \neq 0$. Indeed, massless quarks can change their chirality by scattering off a vacuum condensate of quarks and antiquarks paired by handedness. In this case, we refer to the chiral symmetry as being spontaneously broken by the vacuum. The formation of the condensate completely breaks the chiral symmetry of the theory, moreover, as the vev $\langle\overline{\psi}\psi\rangle$ is not invariant under any chiral subgroup of $SU(2)_L \otimes SU(2)_R$. The condensate is invariant under the vector subgroup, and thus, we have the symmetry breaking pattern $U(1)_V \otimes SU(2)_L \otimes SU(2)_R \longrightarrow U(1)_V \otimes SU(2)_V$.

At this point, we do not dismiss the non-singlet chiral symmetries as we did with the axial symmetry. It turns out that the case of spontaneously broken symmetries is considerably rich in physics. In fact, spontaneously broken global symmetries lead to massless excitations of the vacuum. This is the Nambu-Goldstone mechanism. In Fig. 4.1, we use a cartoon to elucidate the Nambu-Goldstone mechanism. The cartoon depicts the potential energy of a theory on a group manifold. The lowest-energy states are degenerate and form a circularly symmetric valley that reflects the rotational invariance of this theory; however, the physical vacuum of the theory is located at a particular angle. In this case, the rotational symmetry is spontaneously broken. When quantized, fluctuations about the vacuum state will correspond to particles. There are two distinct types: fluctuations up the hill are energetically costly and will correspond to massive excitations of the theory; on the other hand, fluctuations along the circular valley are energetically free and will correspond to massless excitations. For each of the broken generators, there is a flat direction in the vacuum manifold, and hence a massless particle. In QCD with two massless quarks, there should thus be three Nambu-Goldstone bosons.

Fig. 4.1 Cartoon depicting a spontaneously broken global symmetry. The global symmetry corresponds to rotations in the plane, for which the vacuum manifold exhibits a circular valley of energetically equivalent states. The physical vacuum sits in the valley at a particular angle

4.2.2 Chiral Dynamics

The dynamics governing Nambu-Goldstone modes is universal, depending only on the pattern of spontaneous symmetry breaking. To write down such a theory, we need to parameterize fluctuations associated with the broken generators. Mathematically we are parameterizing a coset of the group manifold. While our presentation is specific to the symmetry-breaking pattern of two-flavor QCD, we keep sufficient generality to allow extension to other cases of interest.

A nonzero value of the condensate specifies the location of the vacuum within the group manifold. Let us write the vev in the form

$$\langle \overline{\psi}_{jR} \psi_{iL} \rangle = -\lambda \delta_{ij}. \tag{4.5}$$

Under an $SU(2)_L \otimes SU(2)_R$ transformation, we see that the condensate is not invariant, $\langle \overline{\psi}_{jR} \psi_{iL} \rangle \to -\lambda (L R^\dagger)_{ij}$. However, the restriction of the condensate to the flavor identity, δ_{ij}, maintains invariance under the vector subgroup, $SU(2)_V$. The preservation of vector symmetries can be argued rigorously [179]. The value of the condensate λ is real, which implies that parity is not spontaneously broken. While we know experimentally that this is the case for QCD, the argument against spontaneous breaking of parity [180] does not have the status of a theorem because known loopholes exist. Nonetheless the form of the condensate in Eq. (4.5) dictates the pattern of spontaneous symmetry breaking.

To describe the Nambu-Goldstone modes, we treat the condensate as a locally valued field $\Sigma(x)$ that picks up a vev. The fluctuations about this value encode the Nambu-Goldstone bosons. Thus we promote

$$\delta_{ij} \longrightarrow \Sigma_{ij}(x) = \delta_{ij} + \cdots . \tag{4.6}$$

Because $\Sigma(x)$ describes the local fluctuations, we must have $\Sigma_{ij}(x) = [L(x) R^\dagger(x)]_{ij} = [e^{i\theta_L^a \tau^a} e^{-i\theta_R^b \tau^b}]_{ij}$ for the most general, local $SU(2)_L \otimes SU(2)_R$ fluctuation. Our concern, however, is not with all fluctuations, but with those corresponding to broken generators. As the vector subgroup remains intact, we seek to parameterize the coset $SU(2)_L \otimes SU(2)_R / SU(2)_V$. This can be achieved by simply restricting $\Sigma(x)$ not to lie in $SU(2)_V$. As such matrices are characterized by $\theta_L^a = \theta_R^a$, choosing the orthogonal combination $\theta_L^a = -\theta_R^a$ produces a parameterization of the coset. Writing $\theta_L^a \tau^a \equiv \phi / f$, we have the desired matrix

$$\Sigma = e^{2i\phi/f} = 1 + \frac{2i\phi}{f} + \cdots . \tag{4.7}$$

The Nambu-Goldstone modes appear in the coset field through ϕ, which is a traceless Hermitian 2×2 matrix, which we write in the form

$$\phi = \begin{pmatrix} \frac{1}{\sqrt{2}}\pi^0 & \pi^+ \\ \pi^- & -\frac{1}{\sqrt{2}}\pi^0 \end{pmatrix}. \tag{4.8}$$

From the transformation property of the coset under global chiral transformations, namely $\Sigma \to L\Sigma R^\dagger$, we can infer the transformation rule of the Nambu-Goldstone modes under the vector subgroup $SU(2)_V$. They transform as $\phi \to V\phi V^\dagger$, which establishes the isospin quantum numbers of ϕ; it contains an isotriplet of pions.

2 Deduce the discrete symmetry properties of the Nambu-Goldstone modes by analyzing the transformations of the coset field Σ.

In describing the vacuum fluctuations, we introduced a dimensionful parameter f. This parameter needs to be determined from experiment, and we will explain how at the end of this section. From a purely theoretical perspective, f controls whether fluctuations about the vacuum are Gaußian, hence, whether the Nambu-Goldstone modes are weakly interacting particles. To see this explicitly, we construct the action for the coset field. It is determined from all possible chirally invariant operators involving Σ, and derivatives of Σ. When the coset is expanded about its vev, the dynamics of massless pions should emerge. Using the transformation rule $\Sigma \to L\Sigma R^\dagger$, and realizing that $\Sigma^\dagger\Sigma = 1$, the chirally invariant combination involving the fewest number of derivatives is

$$\mathcal{L}_{\chi\text{PT}} = \frac{f^2}{8}\,\text{Tr}\left(\partial_\mu\Sigma^\dagger\partial_\mu\Sigma\right) = \frac{1}{2}\partial_\mu\pi^0\partial_\mu\pi^0 + \partial_\mu\pi^+\partial_\mu\pi^- + \mathcal{O}(1/f^2). \tag{4.9}$$

Expanding to quadratic order in the fields, we see that the numerical prefactor appended to the action ensures that the kinetic terms are canonically normalized, and indeed the theory describes three massless pions. This should come as no surprise; it is basically by design. Because the theory is nonlinear, however, expanding to a higher order produces multipion interactions. We will explain shortly how to treat these systematically.

So far our discussion has focused on QCD with two massless quarks, and there appear to be no such quarks found in nature. The up and down quarks have mass, however, their masses are considerably small compared to Λ_{QCD}. We can think about the discussion above as an approximation for the up and down quarks, and the natural question to ask becomes how to address the effect of nonvanishing quark masses. To answer this question, we return to the matter part of the QCD action, which has a mass term of the form

$$\Delta\mathcal{L}_\psi = m_q\overline{\psi}\psi = m_q\left(\overline{\psi}_R\psi_L + \overline{\psi}_L\psi_R\right), \tag{4.10}$$

for degenerate up and down quarks. This term breaks chiral symmetry in precisely the way the chiral condensate does, $SU(2)_L \otimes SU(2)_R \to SU(2)_V$. The theory of the Nambu-Goldstone modes should include terms which encode the explicit symmetry breaking introduced by the quark mass. The correct term to add to Eq. (4.9) is

$$\Delta\mathcal{L}_{\chi\text{PT}} = -m_q\lambda\,\text{Tr}\left(\Sigma^\dagger + \Sigma\right) = 4m_q\lambda\left[-1 + \frac{2}{f^2}\left(\frac{1}{2}\pi^0\pi^0 + \pi^+\pi^-\right)\right] + \cdots . \tag{4.11}$$

A few comments are in order. This term is not chirally invariant but maintains invariance under the vector subgroup, and thus shares precisely the same symmetries as the quark mass term in the QCD action. A new dimensionful parameter λ was introduced when writing down this term. It is not fixed by symmetries. We include here only a term at linear order in the quark mass. While there are terms proportional to m_q^2 which we will meet below, we are considering the perturbative expansion about the chiral limit, $m_q = 0$, and the linear-order term represents the leading contribution. From expanding out $\Delta\mathcal{L}_{\chi\text{PT}}$ to quadratic order in the fields, we see there is a contribution to the vacuum energy, and also a mass term for the pions, $m_\pi^2 = 8\lambda m_q/f^2$. Indeed, the pions are not exact Nambu-Goldstone bosons; the explicit breaking of chiral symmetry introduced by the quark mass term of the QCD action leads to a nonvanishing mass for the pions.

The vacuum energy must be due to the chiral condensate, the existence of which was an essential ingredient in our construction thus far. To expose this fact, we realize that the chiral condensate can be determined from the QCD partition function, $-\partial \log Z_{\text{QCD}}/\partial m_q = \langle\overline{\psi}\psi\rangle$. In order that the chiral Lagrangian be an effective theory for low-energy QCD, it must be that their partition functions match, $Z_{\chi\text{PT}} \simeq Z_{\text{QCD}}$. Of course this relation is not an equality, rather a statement about matching Green functions between the two theories (such foundational aspects to χPT are elucidated in [181]). As a result, we must have

$$\langle\overline{\psi}\psi\rangle = -\partial \log Z_{\chi\text{PT}}/\partial m_q. \tag{4.12}$$

On the left-hand side is the QCD vacuum expectation value, and on the right-hand side is the χPT expression evaluated in terms of the effective pion degrees of freedom. In order that the theories match in the chiral limit, we require $\langle\overline{\psi}\psi\rangle = -2N_f\lambda$. Because of parity and flavor invariance, this condition is simply $\langle\overline{\psi}_{jR}\psi_{iL}\rangle = -\lambda\delta_{ij}$; hence λ is exactly the same parameter introduced in Eq. (4.5) for the chiral condensate. Combining this identification with the expression for the pion mass, we have the Gell-Mann–Oakes–Renner relation, $f^2m_\pi^2 = 2m_q|\langle\overline{\psi}\psi\rangle|$.

4.2.3 Leading Order and Beyond

Let us summarize our findings so far. The dynamics of the approximate Nambu-Goldstone bosons of chiral symmetry breaking is described by the chiral Lagrangian, which has the form

$$\mathcal{L}_{\chi\text{PT}} = \frac{f^2}{8}\,\text{Tr}\left(\partial_\mu \Sigma^\dagger \partial_\mu \Sigma\right) - \lambda m_q\,\text{Tr}\left(\Sigma^\dagger + \Sigma\right) \tag{4.13}$$

and includes the leading terms involving the lowest number of derivatives and a single insertion of the quark mass. Up to quadratic order, we find the vacuum energy due to the chiral condensate and a theory of pions whose masses squared are linear in the quark mass. Beyond quadratic order, there are interaction terms, such as the quartic terms $\sim \frac{m_q\lambda}{f^4}\phi^4$ and $\sim \frac{1}{f^2}(\phi\partial_\mu\phi)^2$. As always, these higher-order interactions renormalize lower-order terms. For example, the four-pion interaction terms lead to a renormalization of the pion mass, which is shown in Fig. 4.2. Using the pion propagator, we schematically evaluate the contribution to the pion self-energy from the four-pion vertex with quark mass insertion,

$$\Delta m_\pi^2 \sim \frac{m_q\lambda}{f^4}\int_k \frac{1}{k^2+m_\pi^2} \sim \frac{m_q\lambda}{f^4}\left[\Lambda^2 + \frac{m_q\lambda}{f^2}\left(\log\Lambda^2 + \text{finite}\right)\right], \tag{4.14}$$

where Λ is a dimensionful ultraviolet cutoff scale. This result features a power-law divergence, which can be absorbed into a definition of the renormalized parameter λ; and, if we use dimensional regularization, this contribution will automatically be subtracted. Additionally, there is a logarithmic divergence which cannot be absorbed into a renormalization of the parameters we have thus far written down. The reason is that the divergence is proportional to the second power of the quark mass. To work at one-loop order, we require additional counterterms than the leading-order chiral Lagrangian can supply.

The requirement of additional terms should not be surprising, since the chiral Lagrangian represents a nonrenormalizable theory. This is not a fundamental limitation, however, because we expect its validity only at low energies. In order to make the theory useful in practice, we desire a scheme for organizing the infinite

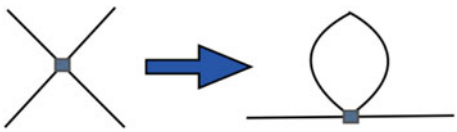

Fig. 4.2 Graphical depiction of the four-pion vertex. Forming a pion loop by contracting two of the external legs produces a divergent self-energy correction

number of local operators needed to renormalize the theory. Without such a power-counting scheme, the theory is of no practical use. In our exploration, we have been tacitly assuming a power counting. We have written down terms with the fewest number of derivatives, and the lowest number of quark mass insertions.

To make this formal, consider p to be a small momentum scale. A consistent loop expansion can be devised by counting the powers of derivatives and quark mass insertions as follows: derivatives count as one power, $\partial_\mu \sim p$, and quark masses count as two powers, $m_q \sim p^2$. The leading chiral Lagrangian written in Eq. (4.9) contains two terms both of order p^2. As a consequence, the pion propagator counts as order p^{-2}, and each of the four-pion interactions counts as order p^2. The remaining powers of momenta in a general Feynman diagram arise from loop integrals, which each contribute p^4 to the counting of powers of p. Now consider a Feynman diagram having L loops, I internal lines, and V vertices from the leading-order Lagrangian. The diagram must scale with the power $p^{4L-2I+2V}$. This power can be simplified using the Euler formula, $L = I - V + 1$, which gives the scaling p^{2L+2}. Thus, there is an ordered expansion in powers of p^2 if we consider the number of loops.

3 What happens to the power-counting argument in $d = 2$ and 6 dimensions? Do the results surprise you? Why is this question not asked about $d = 3$ or 5?

In considering part of the one-loop correction to the pion self-energy in Eq. (4.14), we found the result scales as $m_q^2 \sim p^4$, which is consistent with the general argument. At one-loop order, all contributions are of order p^4. To renormalize one-loop diagrams, we need higher-order local operators that also scale with four powers of p. These operators can only be formed from four derivatives, two derivatives and a quark mass insertion, or two quark mass insertions. At any order in the loop expansion, one requires only a finite number of higher-order counterterms to renormalize the theory. With this power counting, we can hence make sense of the nonrenormalizable theory.

To construct higher-order terms of the chiral Lagrangian with ease, the spurion trick proves useful. Let us first reconsider the leading-order effect of the quark mass in the chiral Lagrangian. The quark mass introduces explicit breaking of chiral symmetry and to include its effects, we wrote down a term which breaks the symmetry in precisely the same manner. Beyond leading-order, this task becomes rather difficult. Instead of this procedure, we promote the quark mass to a complex scalar field, denoted by s

$$\Delta\mathcal{L}_\psi = m_q \left(\overline{\psi}_R \psi_L + \overline{\psi}_L \psi_R\right) \longrightarrow \overline{\psi}_R s^\dagger \psi_L + \overline{\psi}_L s\, \psi_R, \tag{4.15}$$

and endow this field with a spurious transformation rule, $s \to LsR^\dagger$ which renders the quark mass term invariant. The procedure is then to construct all possible operators involving s that are invariant under chiral transformations. For example, with one insertion of s, the term $\mathrm{Tr}\left(\Sigma^\dagger s + s^\dagger \Sigma\right)$ is chirally invariant. At the end of the day, giving the scalar field a vev, $s = m_q + \cdots$, breaks chiral symmetry in precisely the way the quark mass does.

To construct the order p^4 chiral Lagrangian, we have the fields Σ and s, which have the transformations $\Sigma \to L\Sigma R^\dagger$, and $s \to LsR^\dagger$. Using these fields, we write down all possible p^4 terms that are chirally invariant. We also impose Euclidean invariance, and invariance under C, P and T transformations. Finally we replace the spurion field with its vev. The result is an effective Lagrangian encompassing the pattern of spontaneous and explicit symmetry breaking of QCD.

It is easy to construct invariant terms, for example $\left[\mathrm{Tr}\left(\Sigma^\dagger s - s^\dagger \Sigma\right)\right]^2$ is invariant under chiral transformations. When s picks up a vev, however, this term becomes $m_q^2\left[\mathrm{Tr}\left(\Sigma^\dagger - \Sigma\right)\right]^2$, which vanishes because Σ is an $SU(2)$ matrix. The difficult task becomes finding the minimal set of required terms. For two degenerate quarks, the corresponding fourth-order chiral Lagrangian can be written in the form

$$\begin{aligned}\mathcal{L}^{(4)}_{\chi\mathrm{PT}} = {} & L_1\left[\mathrm{Tr}\left(\partial_\mu \Sigma^\dagger \partial_\mu \Sigma\right)\right]^2 + L_2\,\mathrm{Tr}\left(\partial_\mu \Sigma^\dagger \partial_\nu \Sigma\right)\,\mathrm{Tr}\left(\partial_\nu \Sigma^\dagger \partial_\mu \Sigma\right) \\ & + L_3 \frac{m_q \lambda}{f^2}\,\mathrm{Tr}\left(\partial_\mu \Sigma^\dagger \partial_\mu \Sigma\right)\,\mathrm{Tr}\left(\Sigma^\dagger + \Sigma\right) + L_4 \frac{(m_q\lambda)^2}{f^4}\left[\mathrm{Tr}\left(\Sigma^\dagger + \Sigma\right)\right]^2 .\end{aligned} \tag{4.16}$$

The dimensionless coefficients of the operators, $\{L_i\}$, are free parameters referred to as low-energy constants. Often they are also called Gasser-Leutwyler coefficients, because the systematic investigation of chiral perturbation theory to one-loop order was carried out by them, see [182]. It is important to note that our Gasser-Leutwyler coefficients are not Gasser and Leutwyler's coefficients because of our differing parameterization of the coset manifold. The four low-energy constants provide the counterterms necessary to renormalize all one-loop graphs in χPT. When one considers external currents, additional terms become necessary.

4 Determine the effects of strong isospin breaking, $m_d \neq m_u$, on the chiral Lagrangian. At what order does the pion isospin multiplet split?

To illustrate the features of a one-loop computation in χPT, we perform the simplest possible one. This calculation is the chiral correction to the condensate. Beyond leading order, we have the operator expression

$$\langle \overline{\psi}\psi \rangle = -\frac{\partial Z_{\chi\mathrm{PT}}}{\partial m_q} = -4\lambda\left[1 - \frac{1}{f^2}\,\mathrm{Tr}\left(\phi^2\right)\right] + \text{c.t.}, \tag{4.17}$$

where c.t. denotes contributions from counterterms. Contracting the pions to form the bubble diagram yields a correction to the condensate

$$\Delta\langle\overline{\psi}\psi\rangle = \frac{12\lambda}{f^2}\int_k \frac{1}{k^2+m_\pi^2} = -\frac{12\lambda m_\pi^2}{(4\pi f)^2}\left[\frac{1}{\varepsilon} - \gamma_E + \log 4\pi + \log\frac{\mu^2}{m_\pi^2} + 1\right], \tag{4.18}$$

where we have computed the integral in $d = 4 - 2\varepsilon$ dimensions with $\varepsilon \ll 1$. The contribution from the counterterm can be determined using the fourth-order Lagrangian at tree level. Only the L_3 and L_4 terms survive differentiation with respect to the quark mass; furthermore, only the L_4 term contributes to the vacuum energy without requiring pion loops. Assembling the loop and local contributions after $\overline{\text{MS}}$, we arrive at the final result

$$\langle\overline{\psi}\psi\rangle = \langle\overline{\psi}\psi\rangle_{m_q=0}\left[1 + \frac{3m_\pi^2}{(4\pi f)^2}\left(\log\frac{\mu^2}{m_\pi^2} + 1\right) - \frac{m_\pi^2}{f^2}L_4(\mu)\right]. \tag{4.19}$$

Long-range corrections to the chiral-limit value of the condensate come with a chiral logarithm. The renormalization-scale dependence introduced by the logarithm is exactly compensated by the running of the Gasser-Leutwyler coefficient, $L_4(\mu)$; specifically, it must satisfy the renormalization group equation, $\mu^2\frac{d}{d\mu^2}L_4 = \frac{3}{16\pi^2}$.

Generally, χPT can be used to compute the quark-mass corrections to various low-energy observables. Expressions for these observables will involve their chiral-limit values plus chiral logarithms that are calculable from the one-loop (and higher) diagrams. Additionally, there are local contributions from higher-dimensional operators that are required to renormalize the theory. The low-energy constants introduced require experimental data or lattice calculations to determine. Beyond the chiral condensate, which we found has a chiral expansion of the form $\langle\overline{\psi}\psi\rangle = A\left[1 + B\,m_q\left(\log m_q + C\right)\right]$, a few examples are the pion mass, which has a chiral expansion of the form $m_\pi^2 = A\,m_q\left[1 + B\,m_q\left(\log m_q + C\right)\right]$, and the scattering length for $I = 2$ pion scattering, which has a chiral expansion of the form $a_{\pi\pi}^{I=2} = A\sqrt{m_q}\left[1 + B\,m_q\left(\log m_q + C\right)\right]$.

4.2.4 External Fields

The determination of further quantities, such as electroweak observables, requires the inclusion of external fields. To accomplish this, we return to the QCD action and use the gauge principle to include external left- and right-handed fields

$$\mathcal{L}_\psi = \overline{\psi}_L \not{D}_L \psi_L + \overline{\psi}_R \not{D}_R \psi_R, \tag{4.20}$$

with the handed gauge-covariant derivatives specified by $(D_\mu)_L = \partial_\mu + igA_\mu + iL_\mu$, and $(D_\mu)_R = \partial_\mu + igA_\mu + iR_\mu$. For example, an external electromagnetic field is

included by choosing the left- and right-handed gauge fields as $L_\mu = R_\mu = QeA_\mu^{\rm em}$, with $A_\mu^{\rm em}$ the photon field, Q the electric-charge matrix, and e the unit of electric charge. The gauged theory has a local chiral invariance under which the quark fields transform as $\psi_L \to L(x)\psi_L$, and $\psi_R \to R(x)\psi_R$. The external fields must correspondingly transform according to the rules: $L_\mu \to L(x)L_\mu L^\dagger(x) + i[\partial_\mu L(x)]L^\dagger(x)$ for the left-handed gauge field, and $R_\mu \to R(x)R_\mu R^\dagger(x) + i[\partial_\mu R(x)]R^\dagger(x)$ for the right-handed gauge field.

To include external fields in χPT, we promote the global chiral invariance to a local one. The coset field consequently has the transformation $\Sigma \to L(x)\Sigma R^\dagger(x)$, and it becomes efficacious to define a chirally covariant derivative that satisfies the transformation rule $D_\mu\Sigma \to L(x)[D_\mu\Sigma]R^\dagger(x)$. Using the transformations of the external gauge fields, the chirally covariant derivative must have the form

$$D_\mu\Sigma = \partial_\mu\Sigma + iL_\mu\Sigma - i\Sigma R_\mu^\dagger. \tag{4.21}$$

If we count the external gauge fields as order p in the power counting, then $D_\mu \sim p$, and the leading-order chiral Lagrangian has exactly the same form as in Eq. (4.9), with the replacement $\partial_\mu \to D_\mu$. At higher orders, one carries out this replacement to ensure gauge invariance; however, there are additional operators that are required too.

As an application of including external fields in χPT, we shall consider the weak decay of the pion. The charged pion decay process, $\pi \to \mu + \nu_\mu$, arises from the W-boson of the weak interaction, as shown in Fig. 4.3. The left-handed quark current that couples to the weak boson is contained in the interaction Lagrangian

$$\Delta\mathcal{L}_W = W_\mu^- J_{\mu,L}^+, \quad \text{with} \quad J_{\mu,L}^+ = \overline{\psi}_L \tau^+ \gamma_\mu \psi_L. \tag{4.22}$$

The strong interaction part of the decay factorizes into a matrix element between the left-handed current and the pion,

$$\langle 0|J_{\mu,L}^+|\pi(\boldsymbol{p})\rangle = ip_\mu f_\pi, \tag{4.23}$$

where we have parameterized the matrix element based on Euclidean invariance and discrete symmetries. As a result, the parameter f_π, known as the pion decay constant, is a real-valued parameter. While the weak interaction occurs at the scale $\mu \sim M_W$, the nonperturbative QCD matrix element should be evaluated at a scale $\mu \sim \Lambda_{\rm QCD}$. In quark-mass–independent renormalization schemes, however, the non-singlet left-handed current is conserved and, therefore, has vanishing anomalous dimension. Consequently, the pion decay constant is independent of scale.

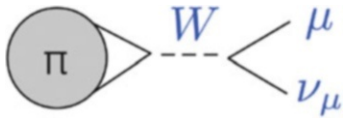

Fig. 4.3 Weak decay of the charged pion through the W-boson and its subsequent decay

With the nonperturbative physics parameterized, evaluating the decay process is a standard quantum field theory exercise, which gives the decay width

$$\Gamma_{\pi\to\mu+\nu_\mu} = \frac{G_F^2}{8\pi} f_\pi^2 \, m_\mu^2 m_\pi |V_{ud}|^2 \left(1 - \frac{m_\mu^2}{m_\pi^2}\right)^2 , \tag{4.24}$$

from which we infer the value $f_\pi = 132\,\text{MeV}$. We can use this value to fix one of the low-energy constants of χPT. The left-handed quark current matches onto operators in the effective theory. Using the order-p^2 chiral Lagrangian, we have

$$J^a_{\mu,L} = \frac{\partial \mathcal{L}_{\chi\text{PT}}}{\partial L^a_\mu}\Big|_{L_\mu = R_\mu = 0} = \frac{f^2}{4} \operatorname{Tr}\left(i\tau^a \Sigma \partial_\mu \Sigma^\dagger\right) = \frac{f}{2} \operatorname{Tr}\left(\tau^a \partial_\mu \phi\right) + \cdots \tag{4.25}$$

Computing the pion decay constant in the effective theory at tree level gives us the matching condition, $f_\pi = f$. A one-loop computation will produce chiral corrections to the matching of the form $f_\pi = f\left[1 + Bm_q\left(\log m_q + C\right)\right]$, whereby we see f is the chiral-limit value of the pion decay constant.

While f happens to show up in the weak decay of the charged pion, this parameter plays an important role in strong-interaction physics. The size of f controls the efficacy of the chiral expansion, because it governs the size of non-Gaußian fluctuations about the vacuum. Let us define the chiral symmetry breaking scale $\Lambda_\chi = 2\sqrt{2}\pi f \approx 1.2\,\text{GeV}$. Because our power-counting scheme gives us an expansion in the number of loops, we see each loop in four dimensions will be accompanied by a factor of $1/\Lambda_\chi^2$. Thus dimensionless parameters governing the size of chiral corrections are m_π^2/Λ_χ^2, and p^2/Λ_χ^2, where p is the momentum involved in a typical process.

5 The masses of hadrons are affected by electromagnetism (Fig. 4.4). Construct all leading-order electromagnetic mass operators by promoting the electric charge matrix to fields transforming under the chiral group. (Notice that no photon fields will appear in the electromagnetic mass operators, because there are no *external* photon lines.) Which pion masses are affected by the leading-order operators? Finally, give an example of a next-to-leading-order operator, or find them all.

Fig. 4.4 Feynman diagrams depicting long-range QED corrections to the pion mass

4.3 Applications Tailored to Lattice QCD

Above, we have detailed the construction of the chiral Lagrangian, and investigated the computation of low-energy QCD observables using this effective theory. The results of such computations are parametrizations of the quark-mass dependence of low-energy observables, with coefficients that must ultimately be determined from phenomenology or lattice QCD computations. The parameterizations, moreover, can be used for the extrapolation of lattice-QCD data at unphysical light-quark masses to their physical values. There are additional applications of chiral perturbation theory tailored to lattice QCD. In this section, we consider the partially quenched approximation to QCD, effects of finite lattice volumes, and effects of finite lattice spacings.

4.3.1 Partially Quenched QCD

Treating the valence and sea quarks in QCD differently is unphysical; however, it can be quite natural from a practical, numerical point of view. Consider the evaluation of the matrix element of an operator $\mathcal{O}$ between hadron states H and H'. On the lattice, one computes Wick contractions between source and sink, which schematically have the form

$$\langle H'|\mathcal{O}|H\rangle_{\mathrm{QCD}} = \int \mathcal{D}A_\mu \ \mathrm{Det}\left(\not{D} + m_q\right) e^{-S[A_\mu]} \frac{1}{\not{D} + m_q} \cdots \frac{1}{\not{D} + m_q}. \tag{4.26}$$

In the early days of lattice QCD, one encountered the quenched approximation, in which the above matrix element is calculated without the quark determinant,

$$\langle H'|\mathcal{O}|H\rangle_{\mathrm{QQCD}} = \int \mathcal{D}A_\mu \ e^{-S[A_\mu]} \frac{1}{\not{D} + m_q} \cdots \frac{1}{\not{D} + m_q}. \tag{4.27}$$

This approximation has various theoretical complications; however, a number of physical observables are insensitive to effects of the QCD vacuum polarization. One way to view the quenched approximation to QCD is a version of QCD with valence and sea quarks, where the latter have masses that are above the ultraviolet cutoff scale. This view suggests another approximation to QCD, the partially quenched approximation, in which the hadronic matrix element of $\mathcal{O}$ is calculated as

$$\langle H'|\mathcal{O}|H\rangle_{\mathrm{PQQCD}} = \int \mathcal{D}A_\mu \ \mathrm{Det}\left(\not{D} + m_{\mathrm{sea}}\right) e^{-S[A_\mu]} \cdot \frac{1}{\not{D} + m_{\mathrm{val}}} \cdots \frac{1}{\not{D} + m_{\mathrm{val}}}. \tag{4.28}$$

Matrix elements calculated in this approximation reduce to QCD matrix elements by choosing the valence and sea quark masses to be degenerate, $m_{\text{val}} = m_{\text{sea}}$. The partially quenched paradigm is useful to have in mind when considering mixed-action simulations, where in essence one replaces $\text{Det}\left(\not{D} + m_q\right) \to \text{Det}\left(\not{D}_{\text{sea}} + m_q\right)$, and when considering the effects of neglecting quark-disconnected diagrams.

For PQQCD computations, the natural questions are whether the quark-mass dependence can be addressed in a model-independent fashion, and whether artifacts of the approximation can be removed in order to connect with QCD physics. The theoretical technique to address such questions was first suggested for QQCD in [183]. The basic idea is as follows. A theory that reproduces the matrix element in Eq. (4.28) contains bosonic quarks, $\tilde{\psi} = \begin{pmatrix} \tilde{u} \\ \tilde{d} \end{pmatrix}$, in addition to fermionic quarks, the valence quarks $\psi = \begin{pmatrix} u \\ d \end{pmatrix}$, and the sea quarks $\psi' = \begin{pmatrix} u' \\ d' \end{pmatrix}$, namely

$$\begin{aligned} \mathcal{L}_{\text{PQQCD}} &= \overline{\psi}\left(\not{D} + m_{\text{val}}\right)\psi + \overline{\psi}'\left(\not{D} + m_{\text{sea}}\right)\psi' + \overline{\tilde{\psi}}\left(\not{D} + m_{\text{val}}\right)\tilde{\psi} \\ &\equiv \overline{\Psi}\left(\not{D} + m_{\text{PQ}}\right)\Psi, \end{aligned} \tag{4.29}$$

where Ψ is the graded vector, $\Psi = \begin{pmatrix} \psi \\ \psi' \\ \tilde{\psi} \end{pmatrix}$, whose upper components ψ and ψ' are Grassmann fields, and lower components $\tilde{\psi}$ are bosonic fields. The bosonic functional integration produces a factor of $\text{Det}\left(\not{D} + m_{\text{val}}\right)^{-1}$ which cancels the determinant produced from the fermionic valence quark functional integration. As a result, a net determinant factor is produced only from the sea quarks. In computing operator matrix elements, the external sources are built from valence quarks, and their contribution to the vacuum polarization is exactly canceled by the degenerate bosonic quarks. The vacuum polarization arises solely from sea quarks, see Fig. 4.5.

These observations were employed to construct PQχPT [184–186]. The relation of parameters in the partially quenched chiral Lagrangian to those in χPT was rigorously established in [187, 188], where further technical details can be found. As a caveat, we will summarize the approach with less rigor, and the careful reader will want to review the technical details in order to confidently utilize the results.

Fig. 4.5 Partially quenched QCD vacuum polarization at one loop. *Thin lines* depict valence quarks ψ, *dashed lines* depict bosonic quarks $\tilde{\psi}$, and *thick lines* depict sea quarks ψ'. Due to mass degeneracy between valence and bosonic quarks, the net contribution arises solely from the sea

In the massless limit, the partially quenched Lagrangian exhibits graded symmetries. These are symmetries under which bosonic and fermionic fields transform into one another. We write the partially quenched quarks as $\Psi_A = \begin{pmatrix} \psi_a \\ \phi_\alpha \end{pmatrix}$, with all fermionic quarks packaged in ψ_a, and bosonic quarks in ϕ_α. Under a graded unitary transformation, $\mathcal{U} \in U(4|2)_V$, we have the quark transformation $\Psi_A \to \mathcal{U}_{AB}\Psi_B$. Written in blocks, $\mathcal{U}$ must have the form

$$\mathcal{U}_{AB} = \begin{pmatrix} \mathcal{A}_{4\times4} & \mathcal{B}_{4\times2} \\ \mathcal{C}_{2\times4} & \mathcal{D}_{2\times2} \end{pmatrix}_{AB}, \tag{4.30}$$

where $\mathcal{A}$ and $\mathcal{D}$ are ordinary matrices, while $\mathcal{B}$ and $\mathcal{C}$ are matrices with Grassmann entries. This grading ensures that the transformed fermionic fields, for example, remain fermionic. Suppose $\mathcal{M}_{AB}$ is a supermatrix transforming under the adjoint, $\mathcal{M}_{AB} \to [\mathcal{U}\mathcal{M}\mathcal{U}^\dagger]_{AB}$, then the invariant graded trace (supertrace) is given by

$$\mathrm{Str}\,(\mathcal{M}) \equiv \sum_A (-)^{g(A)}\mathcal{M}_{AA} = \sum_a \mathcal{M}_{aa} - \sum_\alpha \mathcal{M}_{\alpha\alpha}, \tag{4.31}$$

where the grading factors are defined by $g(a) = 0$ and $g(\alpha) = 1$.

6 Show that the graded trace is invariant under graded unitary transformations.

The partially quenched χPT Lagrangian is constructed by taking into account the pattern of spontaneous and explicit breaking of chiral symmetry in PQQCD. Schematically the massless PQQCD Lagrangian possesses a graded chiral symmetry of the form $SU(4|2)_L \otimes SU(4|2)_R$ that we assume is spontaneously broken down to the vector subgroup, $SU(4|2)_V$. The emerging Nambu-Goldstone bosons live in the coset, $\Sigma = e^{2i\Phi/f}$, where we take Φ to be a $U(4|2)$ matrix

$$\Phi = \begin{pmatrix} \phi_{\bar{\psi}\psi} & \phi_{\bar{\psi}\psi'} & \phi_{\bar{\psi}\tilde{\psi}} \\ \phi_{\bar{\psi}'\psi} & \phi_{\bar{\psi}'\psi'} & \phi_{\bar{\psi}'\tilde{\psi}} \\ \phi_{\tilde{\bar{\psi}}\psi} & \phi_{\tilde{\bar{\psi}}\psi'} & \phi_{\tilde{\bar{\psi}}\tilde{\psi}} \end{pmatrix}, \tag{4.32}$$

which contains both bosonic and fermionic mesons. Taking into account the explicit chiral symmetry breaking due to the PQQCD mass matrix m_{PQ}, we arrive at the chiral Lagrangian

$$\mathcal{L}_{\mathrm{PQ}\chi\mathrm{PT}} = \frac{f^2}{8}\,\mathrm{Str}\left(D_\mu\Sigma^\dagger D_\mu\Sigma\right) - \lambda\,\mathrm{Str}\left(m_{\mathrm{PQ}}\Sigma^\dagger + \Sigma m_{\mathrm{PQ}}\right) + \frac{1}{2}\mu_0^2\left[\mathrm{Str}\,(\Phi)\right]^2. \tag{4.33}$$

Notice we retain the singlet meson in the theory, $\Phi_0 = \mathrm{Str}\,(\Phi) = \eta'_{\mathrm{val}} + \eta'_{\mathrm{sea}} - \tilde{\eta}'$. This is only a convenient device. In PQQCD, the $U(1)_A$ symmetry is anomalous just as in QCD, and the flavor-singlet meson needs to be integrated out of the low-energy theory. Computation of the flavor-neutral meson two-point functions can be carried out easily with the mass term, μ_0^2, treated as an interaction and summed to all orders. The limit $\mu_0 \to \infty$ produces the correct theory corresponding to $SU(4|2)_L \otimes SU(4|2)_R$. The resulting neutral-meson propagators have double poles, which indicate unitary violation in the partially quenched theory. Unitarity is never demanded of an effective theory, and the claim is that the peculiar lack of unitarity of PQQCD is captured at low energies by PQχPT.

After the singlet meson has been integrated out, one can establish that the parameters f and λ of the leading-order PQχPT Lagrangian are numerically identical to those in χPT. The proof utilizes a trick. One considers the computation of quantities involving mesons flavored only with sea quarks. In this sector of the theory, PQQCD Green functions are identical to QCD Green functions with $m_q = m_{\mathrm{sea}}$. As a result, the exact parameters of χPT must appear in PQχPT, although the latter also contains additional parameters. These further terms must be accounted for, and their effects removed to recover QCD physics from PQQCD. Additionally, the valence- and sea-quark mass dependence is described by PQχPT, and must be utilized to extrapolate lattice data to the unitary point, $m_{\mathrm{sea}} = m_{\mathrm{val}}$.

7 Find the tree-level masses of all charged mesons using partially quenched chiral perturbation theory.

4.3.2 Effects of Finite Volume

Lattice QCD computations by necessity utilize finite volumes. Because pions are the lightest hadrons, the long-range physics of low-energy QCD is modified predominantly due to pion effects. In considering finite-volume field theories, we must specify boundary conditions and choose them to be periodic for simplicity. Such boundary conditions lead to a number of salient features: the finite volume action is single valued on a hypertorus, consequently there are no surface terms; discrete translational symmetry is maintained, consequently periodic boundary conditions are not renormalized.

Let ϕ be a generic field satisfying $\phi(x + L) = \phi(x)$, where L is the length of each spacetime direction. The Fourier-mode expansion, $\phi(x) = \int_k e^{ikx}\phi_k$, coupled with periodicity leads to momentum quantization, $k = \frac{2\pi n}{L}$, where n is any integer. This simplicity is quite profound. All of the effects of finite volume follow from the quantization condition. As an example, consider Euclidean $SO(4)$ invariance.

On a finite periodic volume, this continuous invariance is reduced to a discrete permutation symmetry. The rest-frame matrix element measuring the electric charge of a particle, $\langle\phi(0)|J_\mu|\phi(0)\rangle = Q\delta_{\mu 4}$, does not lead to the usual current in a frame moving with velocity $\boldsymbol{v}$, so that $\langle\phi(v)|\boldsymbol{J}|\phi(v)\rangle \neq Q\boldsymbol{v}$, due to the lack of boost covariance. This may seem paradoxical, because gauge invariance, the Ward-Takahashi identity, and the Ward identity place constraints on the matrix elements of conserved currents. Ordinarily these three notions are used interchangeably; however, the Ward identity ceases to be valid. This finite-volume effect is exposed in [189]. Here, we explore finite-volume effects on pion dynamics in two distinct regimes.

4.3.2.1 Zero Pion Momentum

Strictly speaking, spontaneous symmetry breaking does not occur in finite volume. The reason is that spontaneous symmetry breaking is a classical phenomenon requiring infinitely many degrees of freedom. In quantum mechanics, a state prepared in one of a few degenerate ground states will acquire an admixture of the other states due to quantum tunneling. The dynamics of the theory governs tunneling, and over time the state will end up in a symmetric superposition of the degenerate ground states. In quantum field theory, the tunneling probability depends on the transition from two configurations on the group manifold, a and b. For uniform configurations, the tunneling probability, $\mathcal{P} \sim \exp\left(-V\int_a^b \mathcal{V}(\phi)d\phi\right)$, is exponentially suppressed by the infinite spacetime volume V. At finite volume, such tunneling occurs, and the vacuum state will tunnel symmetrically, thereby completely respecting the symmetric dynamics of the underlying action. In QCD, chiral symmetry can be restored at finite volume, and the effect can be deduced by carefully considering the effect of momentum quantization on pion dynamics.[1]

To expose the mechanism behind chiral symmetry restoration, we consider the computation of the chiral condensate in finite-volume χPT at one-loop order. To use χPT in a finite volume, the box size cannot be smaller than the chiral symmetry breaking scale, that is $L \gg \Lambda_\chi^{-1}$, otherwise there is no low-energy dynamics in the theory. Above, in Eq. (4.19), we calculated the infrared chiral logarithm, $\sim m_\pi^2 \log m_\pi^2$, which modifies the value of the chiral condensate away from the chiral limit. In finite volume, the one-loop diagram now requires a momentum mode sum rather than a momentum integral:

[1] Analogous to the situation at finite volume is the finite-temperature case, $\beta = 1/T < \infty$. The equilibrium quantum field theory has a path-integral representation in terms of the QCD action defined with a compact Euclidean time, $0 < x_4 < \beta$. Statistics demands periodic boundary conditions for bosons, and anti-periodic boundary conditions for fermions. In χPT, the restoration of chiral symmetry at finite temperature is linked with the Matsubara modes of the pions.

$$\frac{1}{f^2L^4}\sum_{n_\mu=-\infty}^{\infty}\frac{1}{\left(\frac{2\pi n_\mu}{L}\right)^2+m_\pi^2}=\frac{1}{(fL)^2}\left[\frac{1}{(m_\pi L)^2}+\sum_{n_\mu\neq 0}\frac{1}{4\pi^2 n_\mu^2+(m_\pi L)^2}\right]. \tag{4.34}$$

In the sum, we have separated out the contribution from the zero-momentum mode, $n_\mu = (0,0,0,0)$. The one-loop correction vanishes in infinite volume when $m_\pi = 0$, while in finite volume the zero mode leads to singular behavior in the infrared.

The longest-range piece of the pions, their zero-momentum mode, has become strongly coupled. The effect must be treated nonperturbatively and requires reformulating the power counting at finite volume [190]. Let ε denote a generically small quantity. We assign the counting of physical parameters as follows. The length L is considered large, and so $\frac{1}{L}$ counts as ε. The pion mass is chosen to count as $m_\pi \sim \varepsilon^2$. This creates a dichotomy in the leading-order Lagrangian: the derivative vertices count as $\partial_\mu\partial_\mu \sim \varepsilon^2$, unless they are zero modes, whereas the quark mass insertion is considered smaller, $m_q \sim m_\pi^2 \sim \varepsilon^4$. As a consequence, the pion propagator has two very distinct pieces. The propagation of zero modes counts as ε^{-4}, while nonzero modes count as ε^{-2}. The enhancement of zero modes over nonzero modes in the power counting encapsulates the chiral limit at finite volume.

To count powers of ε for a generic Feynman diagram, we further require the counting of loop factors. Each loop requires the mode summation $\frac{1}{L^4}\sum_{n_\mu}$ which counts as ε^4. For a diagram with I internal lines, V vertices from the leading-order Lagrangian, and L loops, we have now various scalings with ε possible depending on whether derivatives or quark mass insertions are at each vertex, and whether zero or nonzero modes are propagating. Diagrams having a quark-mass insertion at each vertex and only zero modes propagating count as $\varepsilon^{4L+4V-4I}$, which simplifies dramatically to ε^4 on account of the Euler identity. On the other hand, diagrams with only derivative vertices and nonzero modes propagating count as $\varepsilon^{4L+2V-2I} = \varepsilon^{2L+2}$. The nonzero momentum modes of the pion still obey a loop expansion. Diagrams with only zero modes, however, are all equally important.

8 Do the leading-order four-pion interactions allow mixing of zero and nonzero modes? Draw all one- and two-loop diagrams for the chiral condensate and count powers of ε.

The ε-regime power counting requires that the zero-momentum mode be treated nonperturbatively. Fortunately, the zero-momentum mode is the simplest mode, and can be separated out from the coset using the decomposition $\Sigma(x) = \Sigma_0 e^{2i\tilde{\phi}(x)/f}$, where Σ_0 is the zero mode, and the nonzero modes reside in $\tilde{\phi}(x)$. Taking into account only the zero mode, the partition function for χPT becomes a matrix model,

$$Z_{\chi\mathrm{PT}} = \int \mathcal{D}\Sigma_0 \, e^{\frac{1}{2}s\,\mathrm{Tr}\left(\Sigma_0^\dagger + \Sigma_0\right)}, \tag{4.35}$$

where the matrix integral represents averaging the direction of the chiral condensate over the coset manifold. The scaling variable s includes the spacetime volume V, and is defined by $s = 2m_q\lambda V = \frac{1}{4}(fL)^2(m_\pi L)^2$. In $SU(2)$, the matrix integral can be evaluated in terms of a modified Bessel function, $Z_{\chi\mathrm{PT}} = \frac{1}{s}I_1(2s)$. This result, in turn, can be used to find the behavior of the chiral condensate as a function of s in the ε-regime via Eq. (4.12). We plot this dependence in Fig. 4.6. If one takes the chiral limit at finite volume, chiral symmetry is restored. Chiral symmetry breaking can be achieved in a finite volume provided the pion Compton wavelength is small compared to the lattice size, $\frac{1}{m_\pi} \ll L$, for which s is large and the identity matrix becomes the preferred direction for the condensate to point.

4.3.2.2 Zero Pion Winding

To avoid finite-volume restoration of chiral symmetry, we require $m_\pi L \gg 1$ to ensure the zero-momentum modes of pions do not become strongly coupled. Provided this condition is met, finite-volume corrections should be perturbatively small, as pions only interact weakly with their periodic images. With small pion Compton wavelengths, we need to focus on corrections near zero pion winding number, rather than on zero pion momentum. This can be achieved systematically using p-regime power counting [191].

In the p-regime, we no longer distinguish between zero and nonzero momentum modes of pions. As a result, we count the pion mass and derivatives at the same order, $m_\pi \sim p$, and $\partial_\mu \sim \frac{1}{L} \sim p$. This is the same power counting as in infinite volume. The only exception is that the quantization condition restricts available momenta. Consequently, the pion propagator and leading-order vertices scale with the same power of p as in infinite volume. Each loop brings along the momentum mode sum, $\frac{1}{L^4}\sum_{n_\mu}$, and counts as p^4. A general Feynman diagram with I internal lines, V leading-order vertices, and L loops counts as $p^{4L-2I+2V} = p^{2L+2}$. This power counting leads to a loop expansion identical to that in infinite volume. The

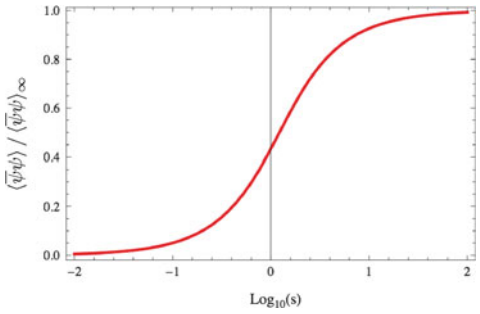

Fig. 4.6 Modification of the chiral condensate in the ε-regime. Shown as a function of the scaling variable, $s = \frac{1}{4}(fL)^2(m_\pi L)^2$, is the finite-volume depletion of the chiral condensate

essential difference is that the evaluation of Feynman graphs requires momentum-mode sums rather than momentum integrals.

Now in the p-regime, momentum-mode sums are not ideal. We prefer that contributions from loop graphs be expressed in a winding number expansion, rather than in terms of periodic momentum modes. Indeed, the external states are assumed to be projected onto good momenta; however, virtual quantum fluctuations span the range of all available momenta. Their contribution to observables is best expressed in position space. The Poisson re-summation formula allows us to recast the momentum mode sums into an expansion in winding number. Before deriving this formula, we recall the definition of the Dirac-delta function on a compact space,

$$\delta_L(x-y) = \frac{1}{L}\sum_{n=-\infty}^{\infty} e^{2\pi i n(x-y)/L}, \quad \text{for} \quad x, y \in \left(-\frac{L}{2}, \frac{L}{2}\right), \tag{4.36}$$

which by inspection has the correct $L \to \infty$ limit.

In considering loop sums, we can enforce the quantization of momentum using the Dirac comb,

$$\frac{1}{L}\sum_{n-\infty}^{\infty} \delta(k - 2\pi n/L) = \int_{-\infty}^{\infty} \frac{dx}{2\pi} e^{-ikx} \frac{1}{L}\sum_{n=-\infty}^{\infty} e^{2\pi i n x/L}, \tag{4.37}$$

where k is a continuous variable, and accordingly has a Fourier transform in terms of a noncompact variable x. We can partition the real line in terms of an infinite number of cells having length L, that is $\int_{-\infty}^{\infty} f(x)dx = \sum_{\nu=-\infty}^{\infty} \int_{\nu L - L/2}^{\nu L + L/2} f(x)dx$. Translating the latter integrals so that they are all centered about $x = 0$, we have $\int_{-\infty}^{\infty} f(x)dx = \sum_{\nu=-\infty}^{\infty} \int_{-L/2}^{+L/2} f(x - \nu L)dx$. Applying this partition to the Dirac comb, we have the Poisson formula

$$\begin{aligned}\frac{1}{L}\sum_{n-\infty}^{\infty} \delta(k - 2\pi n/L) &= \int_{-\frac{L}{2}}^{+\frac{L}{2}} \frac{dx}{2\pi} e^{-ikx} \sum_{\nu=-\infty}^{\infty} e^{ik\nu L}\, \delta_L(x) \\ &= \frac{1}{2\pi}\sum_{\nu=-\infty}^{\infty} e^{ik\nu L}.\end{aligned} \tag{4.38}$$

To utilize the Poisson formula to compute finite-volume corrections, we first observe the momentum-mode expansion of the finite-volume propagator

$$D_{\mathrm{FV}}(x,0) = \frac{1}{L}\sum_{n=-\infty}^{\infty} e^{2\pi i n x/L} G(2\pi n/L), \tag{4.39}$$

where $G(k) = [k^2 + m^2]^{-1}$ is the Euclidean momentum-space propagator in infinite volume. In light of Eq. (4.38), we have the winding-number expansion

$$D_{\mathrm{FV}}(x,0) = \sum_{\nu=-\infty}^{\infty} D_{\infty}(x+\nu L,0), \tag{4.40}$$

in terms of the infinite-volume coordinate-space propagator $D_{\infty}(x,0)$. The infinite-volume limit arises from $\nu = 0$, whereas nonzero winding numbers account for volume corrections from periodic images.

The functional form of the coordinate-space propagator is all we need to derive finite-volume corrections in the p-regime. In Euclidean space, we have the propagator

$$D_{\infty}(x,0) = \frac{m}{4\pi^2\sqrt{x^2}} K_1(m\sqrt{x^2}) \overset{x^2\to\infty}{\longrightarrow} \frac{m^2}{2(2\pi m\sqrt{x^2})^{3/2}} e^{-m\sqrt{x^2}} + \cdots \tag{4.41}$$

To compute the finite-volume modification to the chiral condensate, for example, we realize that the bubble diagram is proportional to $D_{\mathrm{FV}}(0,0)$, which can be written in the winding-number expansion using Eq. (4.40). Taking into account the $\nu = \pm 1$ images in each spatial direction gives us the result

$$\langle\overline{\psi}\psi\rangle = \langle\overline{\psi}\psi\rangle^{\infty}_{m_q=0}\left[1 + \frac{3m_\pi^2}{(4\pi f)^2}\left(\log\frac{\mu^2}{m_\pi^2} + 1 - 12\sqrt{2\pi}\frac{e^{-m_\pi L}}{(m_\pi L)^{3/2}}\right) - \frac{m_\pi^2}{f^2}L_4(\mu)\right]. \tag{4.42}$$

In this regime, corrections to the condensate are exponentially suppressed due to the propagation of pions around the world.

9 In addressing finite-volume corrections, one typically considers lattices with a finite spatial volume and infinite temporal extent. Why is this done? How would the above results be modified? Now consider the pion mass. How does it scale with volume for asymptotically large spatial volumes?

4.3.3 *Lattice Discretization Effects*

As a final application of χPT tailored to lattice QCD, we consider effects of the lattice discretization. In order to connect lattice data to QCD physics, one needs to take the continuum limit. Because χPT is a low-energy effective theory, taking the lattice spacing to zero naïvely does not play a role in the long-range physics. Most solutions to the fermion doubling problem, however, break chiral symmetry at zero

quark mass. In this way, properties of the theory's most infrared modes results from the nature of the short-distance regularization.

Near the continuum, the lattice spacing is small compared to strong-interaction scales, $a \ll \Lambda_{\rm QCD}^{-1}$, and the lattice action can be described by an effective continuum theory, know as the Symanzik effective action [18]. This theory shares all of the symmetries of the lattice action (gauge invariance, hypercubic invariance, C, P, T, ...), but is written in terms of continuum operators and organized in powers of the lattice spacing:

$$S_{\rm Symanzik} = S_0 + aS_1 + a^2 S_2 + \cdots . \tag{4.43}$$

At each order, there is a finite set of operators, $S_i = \sum_j c_j^{(i)} \mathcal{O}_j^{(i)}$, with contributions from higher-dimensional operators becoming less relevant in the continuum limit. Coefficients $c_j^{(i)}$ run weakly with logarithms of the lattice spacing. The leading-order term is just the QCD action, namely $S_0 = \overline{\psi}\left(\not{D} + m_q\right)\psi$, although fine tuning may be required to remove relevant contributions of the form $\frac{1}{a}S_{-1}$, so that the continuum limit exists. By writing Eq. (4.43), we assume any necessary fine tuning has been carried out. Notice that at leading order, Euclidean invariance accidentally appears. Operators breaking Euclidean invariance, e.g. $\overline{\psi}\gamma_\mu D_\mu D_\mu D_\mu \psi$, become irrelevant in the continuum limit.

To account for the effects of discretization on low-energy physics, we must understand how operators of the Symanzik effective action map into χPT. For illustrative early references on the subject, see [192, 193]. The Wilson action, for example, eliminates fermion doubling at the cost of explicitly breaking chiral symmetry. As a result, chiral symmetry is not imposed on the operators of Symanzik's effective action. This allows for a relevant operator, $\frac{1}{a}\overline{\psi}\psi$, that necessitates fine tuning in order to attain light quarks. After such tuning, the leading chiral symmetry breaking operator is contained in the term [194]

$$S_1 = c_{\rm SW}\left(\overline{\psi}_L \sigma_{\mu\nu} F_{\mu\nu} \psi_R + \overline{\psi}_R \sigma_{\mu\nu} F_{\mu\nu} \psi_L\right). \tag{4.44}$$

This term breaks chiral symmetry precisely the way the quark mass does, and its effects can be incorporated into χPT by including the operator

$$\Delta\mathcal{L}_{\chi\rm PT} = -a c_{\rm SW} \lambda_a \,{\rm Tr}\left(\Sigma^\dagger + \Sigma\right). \tag{4.45}$$

As a result, the pion mass depends on the lattice spacing,

$$m_\pi^2 = \tfrac{8}{f^2}\left(m_q \lambda + a\, c_{\rm SW} \lambda_a\right).$$

Infrared enhancements due to chiral logarithms now take the form

$$\sim \log[m_\pi^2(m_q, a)].$$

One should note that improvement of the action will diminish the size of the coefficient $c_{\rm SW}$, and hasten the approach to the continuum limit. Furthermore, our discussion tacitly assumes the product $c_{\rm SW}\lambda_a$ is positive, otherwise one can enter the Aoki phase [195].

Another example of discretization effects concerns mixed-action simulations. For computational economy, one can employ different lattice fermion actions for valence and sea quarks. Lattice collaborations have chosen various options so far: domain-wall valence quarks on staggered sea quarks, overlap valence quarks on domain-wall sea quarks, *etc*. The effects of a mixed action on low-energy physics can be deduced by accounting for the symmetry breaking pattern [196]. Because mixed actions distinguish between valence and sea quarks, the Symanzik effective action is a partially quenched theory. In the combined chiral and continuum limits, the partially quenched theory possesses a graded chiral symmetry, $SU(4|2)_L \otimes SU(4|2)_R$. At finite lattice spacing, however, this chiral symmetry is explicitly broken because no symmetry relates valence and sea quarks. Dimension-6 operators in the Symanzik action lead to a reduction of the chiral symmetry down to $SU(2|2)_L \otimes SU(2|2)_R \otimes SU(2)_L \times SU(2)_R$. Consequently the masses of mesons formed from one valence and one sea quark, $\phi_{\overline{\psi}\psi'}$ and $\phi_{\overline{\psi}'\psi}$ from Eq. (4.32), are not protected from additive renormalization. As a result their masses have a shift

$$\Delta(m^2_{\phi_{\overline{\psi}\psi'}}) = \Delta(m^2_{\phi_{\overline{\psi}'\psi}}) = a^2\Delta_{\rm mix} \tag{4.46}$$

that depends quadratically on the lattice spacing. The behavior of chiral logarithms is modified, but only for those generated by valence-sea meson propagation. Mixed-action χPT can be employed to understand the combined quark-mass and lattice-spacing dependence of mixed-action lattice-QCD data. For a general discussion of applications, see [197, 198].

10 Write down all dimension-6 four-quark operators in the Symanzik effective action for a general mixed-action theory. Classify the operators according to symmetry. Which ones are absent in a theory describing Wilson valence quarks and overlap sea quarks?

4.4 Including the Nucleon

To include the nucleon and other baryons in χPT, we are confronted with a puzzle. The nucleon mass is not a low-energy scale. By contrast, it is on the order of the chiral symmetry breaking scale, $M_N \approx \Lambda_\chi$. The presence of this large scale would seem to complicate the inclusion of the nucleon into χPT. One is not deriving the nucleon from chiral dynamics, however, one is investigating the effect chiral dynamics has on the nucleon. With this view in mind, we include the nucleon as an

external source of isospin and describe small energy fluctuations *about* the nucleon mass, $p \ll M_N \sim \Lambda_\chi$, as first suggested in [199].

To account for the quark-mass dependence of nucleon properties using χPT, we require the chiral-limit value of the nucleon mass, M. This quantity requires a digression. How can the chiral-limit mass M arise from nothing? In QCD, we have the energy-momentum tensor $T_{\mu\nu}$, whose matrix element between nucleon states must have the form

$$\langle N(\boldsymbol{k})|T_{\mu\nu}|N(\boldsymbol{k})\rangle = -\frac{k_\mu k_\nu}{M_N} \tag{4.47}$$

on account of Euclidean invariance and dimensional analysis. The trace of the energy-momentum tensor thus has a matrix element equal to the nucleon mass, $\langle N(\boldsymbol{k})|T_{\mu\mu}|N(\boldsymbol{k})\rangle = M_N$. At the classical level, the energy-momentum tensor's trace is simply $T_{\mu\mu} = m_q\overline{\psi}\psi$. Consequently, $M = 0$ in the chiral limit.

While these considerations apply at the classical level, QCD exhibits a trace anomaly, which is tied to the fact that QCD cannot be defined without a scale. Taking into account quantum corrections, the trace of the energy momentum tensor has the form

$$T_{\mu\mu} = \frac{\beta}{2g^3}F^A_{\mu\nu}F^A_{\mu\nu} + m_q\overline{\psi}\psi \tag{4.48}$$

with β as the QCD beta function. Due to the trace anomaly, the chiral-limit mass is nonvanishing, $M = \langle N(\boldsymbol{k})|\frac{\beta}{2g^3}F^A_{\mu\nu}F^A_{\mu\nu}|N(\boldsymbol{k})\rangle$. The Higgs mechanism does not have a monopoly over all the mass in the universe. Furthermore, on account of the trace of the energy-momentum tensor's form, we can hazard a guess about the quark-mass dependence of the nucleon mass, $M_N = M + \sigma\, m_q + \sigma_2\, m_q^2 + \cdots$, which corresponds to pion-mass dependence of the form $M_N = M + A\, m_\pi^2 + B\, m_\pi^4 + \cdots$ up to logarithms. This guess is not too far off, however, we will find further non-analytic dependence on the quark mass.

11 Is the trace of the energy-momentum tensor the divergence of a current?

4.4.1 Heavy Fermions

To work with small fluctuations about the chiral-limit value of the nucleon mass, we treat M as a large energy scale and write the nucleon momentum as $k_\mu = Mv_\mu + p_\mu$, with $p \ll M$. The uncertainty relation $\Delta k \Delta x \geq \frac{1}{2}$ becomes $\Delta v \Delta x \geq \frac{1}{2M}$ for particles of large mass, and simultaneously specifying position and velocity becomes possible.

We can see the consequences at the level of the nucleon propagator. For the free action, we have

$$\frac{1}{i\not{k}+M}=\frac{-iM\not{v}+M-i\not{p}}{2Mv\cdot p+p^2}=\frac{1}{v\cdot p}\mathcal{P}_+ +\mathcal{O}\left(\frac{p}{M}\right) \tag{4.49}$$

with the nonrelativistic projectors given by $\mathcal{P}_\pm = \frac{1}{2}(1\mp i\not{v})$. These projectors can be used to simplify the spin algebra; for example, one can easily demonstrate the identity $-\mathcal{P}_\pm\gamma_\mu\mathcal{P}_\pm = \pm iv_\mu\mathcal{P}_\pm$. Heavy-fermion propagators lead to dramatic simplifications in Feynman diagrams. Rather than rediscover these simplifications for each diagram, it is convenient to separate out the nonrelativistic modes directly at the level of the nucleon action. The relativistic fluctuations can then be integrated out of the functional integral.

To make explicit the separation of scales, we decompose the nucleon field into two parts,

$$N(x)=e^{iMv\cdot x}\left[\mathcal{P}_+ N_v(x)+\mathcal{P}_-\mathcal{N}_v(x)\right]. \tag{4.50}$$

Because of the explicit phase factor, derivatives acting on the nucleon field will produce either the large momentum, Mv_μ, or the small residual momentum p_μ. At the level of the free nucleon action, we have

$$\begin{aligned}\mathcal{L}&=\overline{N}\left(\not{\partial}+M\right)N\\&=\overline{N}_v iv\cdot\partial\mathcal{P}_+N_v-\overline{\mathcal{N}}_v\left(iv\cdot\partial-2M\right)\mathcal{P}_-\mathcal{N}_v+\text{mixing}.\end{aligned} \tag{4.51}$$

The positive projection of the nucleon, N_v, corresponds to a nonrelativistic nucleon whose energy is measured relative to zero. The negative projection, $\mathcal{N}_v$, on the other hand, corresponds to the negative-energy solution which lies $2M$ away from the positive-energy solution, see Fig. 4.7. The mixing terms between these two fields give rise to a tower of recoil corrections after the field $\mathcal{N}_v$ is integrated out.

12 Integrate out the remaining massive component of the nucleon field to find the first-order correction to the static-nucleon Lagrangian. The result should not surprise you.

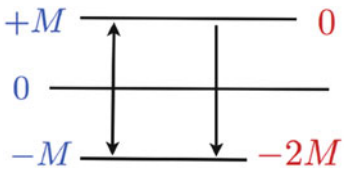

Fig. 4.7 The heavy-fermion approach repositions the zero energy level at the fermion mass M

13 The nonrelativistic projectors reduce the spin algebra to that of Pauli matrices. Show that the axial-vector fermion bilinear reduces to the spin density operator up to a constant, that is $\overline{N}_v \gamma_\mu \gamma_5 N_v = c \overline{N}_v S_\mu N_v$. The relation $\mathcal{P}_+ N_v = N_v$ will prove useful, as will the definition of the spin vector $S_\mu = -\frac{i}{4M} \varepsilon_{\mu\nu\rho\sigma} \sigma_{\nu\rho} k_\sigma$, which satisfies $S_\mu S_\mu = \frac{1}{2}\left(\frac{1}{2}+1\right)$. What are $v_\mu S_\mu$ and $[S_\mu, S_\nu]$?

4.4.2 Heavy-Nucleon χPT

With the large chiral-limit mass of the nucleon M phased away, the derivative expansion is valid: $\partial_\mu N_v \sim p$ with $p \ll M \sim \Lambda_\chi$. From this point forward, we work exclusively with the heavy-nucleon field N_v, and for notational simplicity we strip away the velocity subscript. The goal is to combine the heavy-nucleon limit with chiral perturbation theory to build a tool with which we can address the quark-mass dependence of nucleon properties, pion-nucleon interactions, and so forth.

The nucleon field is an isodoublet of the proton and neutron, $N = \begin{pmatrix} p \\ n \end{pmatrix}$. This translates into the transformation property, $N_i \to V_{ij} N_j$ under an $SU(2)_V$ transformation. On the surface, it appears that we need to know how the nucleon transforms under $SU(2)_L \otimes SU(2)_R$ in order to take into account the pattern of spontaneous and explicit chiral symmetry breaking in QCD. This situation would be unfortunate, because it is unknown to which chiral multiplets the nucleon belongs. A nice discussion and a conjecture are given in [200].

Let us temporarily assume a simple scenario for the nucleon. In the chiral limit, imagine that the nucleon has the charge assignment $(\frac{1}{2}, 0) \oplus (0, \frac{1}{2})$ under $SU(2)_L \otimes SU(2)_R$. That is, the nucleon can be written as the sum of left- and right-handed fields, N_L and N_R, which transform as $N_L \to L N_L$ and $N_R \to R N_R$ under chiral transformations. These fields can then be dressed with pions. For example, taking $\tilde{N}_L \equiv \Sigma N_R$, and $\tilde{N}_R \equiv \Sigma^\dagger N_L$, we have defined fields with exactly the same transformation properties as the original nucleon. Because pions are massless in the chiral limit, moreover, it is not possible to discern between these two possibilities. The nucleon will always be dressed with soft pion radiation, and this presents an infrared ambiguity in distinguishing between a nucleon, and a nucleon plus any number of soft pions.

To exploit the infrared ambiguity, we define the field $\xi = \sqrt{\Sigma}$. Under a chiral transformation, we have $\xi \to \sqrt{L \xi^2 R^\dagger} \equiv L \xi U^\dagger$, where U is a complicated coordinate-dependent matrix, $U = (L, R, \xi(x))$. It is simple to show that $L\xi U^\dagger = U \xi R^\dagger$. Under the vector subgroup of transformations, we have $\xi \to V \xi V^\dagger$. Now one can use the ξ field to dress the nucleon differently with pions. From our original chiral multiplet, we can define the fields $\check{N}_L = \xi N_R$ and $\check{N}_R = \xi^\dagger N_L$,

which both transform the same way, $\check{N}_L \to U\check{N}_L$ and $\check{N}_R \to U\check{N}_R$ under $SU(2)_L \otimes SU(2)_R$. Thus to whichever chiral multiplets the nucleon belongs, we can always suitably dress with pions to define a physically indistinguishable nucleon field that transforms as $N \to UN$ under chiral transformations. This transformation, moreover, respects the known vector transformation of the nucleon doublet.

We are now in a position to build the χPT Lagrangian including a heavy nucleon field. The theory described by this Lagrangian is heavy-nucleon chiral perturbation theory (HNχPT). To aid in its construction, we form the parity even and odd combinations

$$\begin{aligned}\mathcal{A}_\mu &= \frac{i}{2}\left(\xi^\dagger\partial_\mu\xi - \xi\partial_\mu\xi^\dagger\right) \to U\mathcal{A}_\mu U^\dagger \\ \mathcal{V}_\mu &= \frac{1}{2}\left(\xi^\dagger\partial_\mu\xi + \xi\partial_\mu\xi^\dagger\right) \to U\mathcal{V}_\mu U^\dagger + U\partial_\mu U^\dagger,\end{aligned} \tag{4.52}$$

where their chiral transformations are also given. From the vector-field built from mesons, $\mathcal{V}_\mu$, we can form a covariant derivative that acts on the nucleon, $D_\mu N \equiv \partial_\mu N + \mathcal{V}_\mu N$, which satisfies $D_\mu N \to U(D_\mu N)$. The $\mathcal{O}(p)$ HNχPT Lagrangian is specified by two terms

$$\mathcal{L}_{\text{HN}\chi\text{PT}} = N^\dagger iv\cdot D\, N + 2g_A N^\dagger S\cdot\mathcal{A}N. \tag{4.53}$$

The first term is the chirally covariant static-nucleon operator, which contains vector couplings of the nucleon to even numbers of pions. These couplings are exactly fixed by chiral symmetry. The second term contains spin-dependent axial-vector couplings to odd numbers of pions. These couplings are not uniquely determined in χPT, and therefore, we have assigned a low-energy constant g_A to this term (Fig. 4.8).

There are two further invariant terms at $\mathcal{O}(p)$ that we did not write down. These are $N^\dagger v_\mu N\ \text{Tr}\left(\mathcal{V}_\mu\right)$ and $N^\dagger S_\mu N\ \text{Tr}\left(\mathcal{A}_\mu\right)$. These happen to vanish, but could become relevant when flavor-singlet external fields are turned on. To include external fields, we promote the global symmetries to local ones. From left- and right-handed gauge fields, L_μ and R_μ, we form the left- and right-handed gauge-covariant derivatives, $D_{L,\mu} = \partial_\mu + iL_\mu$, and $D_{R,\mu} = \partial_\mu + iR_\mu$. These are then used to gauge the vector and axial-vector fields built from mesons:

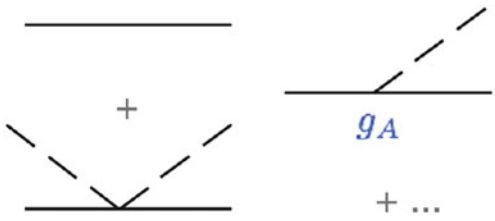

Fig. 4.8 Graphical depiction of terms from the HNχPT Lagrangian expanded to $\mathcal{O}\left(\frac{1}{f^2}\right)$. *Solid lines* denote nucleons, while the *dashed lines* denote pions

$$\mathcal{A}_\mu = \frac{i}{2}\left(\xi^\dagger D_{L,\mu}\xi - \xi D_{R,\mu}\xi^\dagger\right) \to U\mathcal{A}_\mu U^\dagger$$
$$\mathcal{V}_\mu = \frac{1}{2}\left(\xi^\dagger D_{L,\mu}\xi + \xi D_{R,\mu}\xi^\dagger\right) \to U\mathcal{V}_\mu U^\dagger + U\partial_\mu U^\dagger, \tag{4.54}$$

which have the same transformation properties as their zero-field counterparts. The leading-order HNχPT Lagrangian in external fields thus has exactly the same form up to possible flavor-singlet couplings. Turning on flavor-singlet external fields, we have simply $\mathrm{Tr}\left(\mathcal{V}_\mu\right) = \frac{i}{2}\mathrm{Tr}\left(L_\mu + R_\mu\right) = i\,\mathrm{Tr}\left(V_\mu\right)$ with V_μ the flavor-singlet vector field, and $\mathrm{Tr}\left(\mathcal{A}_\mu\right) = -\frac{1}{2}\mathrm{Tr}\left(L_\mu - R_\mu\right) = \mathrm{Tr}\left(A_\mu\right)$ with A_μ the flavor-singlet axial-vector field. The flavor-singlet vector coupling is exactly fixed by the nucleon charge assignments, $D_\mu N = \left[\partial_\mu + \mathcal{V}_\mu + \mathrm{Tr}\left(\mathcal{V}_\mu\right)\right]N$.

14 In the chiral limit, the isovector axial current is a conserved current. Is there a constraint on the quark isovector axial charge due to the non-renormalization of this current? What about on the nucleon axial charge g_A?

4.4.3 Quark-Mass Dependence of the Nucleon

To include explicit chiral symmetry breaking introduced by the quark mass, we follow the spurion trick above. It is convenient to introduce the operators

$$\mathcal{M}_\pm = \frac{1}{2}\left(\xi s^\dagger \xi \pm \xi^\dagger s\,\xi^\dagger\right) \to U\mathcal{M}_\pm U^\dagger, \tag{4.55}$$

which have the simple chiral transformations in terms of U listed. When the spurion picks up a vev, the operators become $\mathcal{M}_\pm = m_q(\Sigma \pm \Sigma^\dagger)$. The leading effects of the quark mass on the nucleon are contained in the $\mathcal{O}(p^2)$ term

$$\mathcal{L}_\mathcal{M} = \sigma\, N^\dagger \mathcal{M}_+ N. \tag{4.56}$$

Expanding this term to tree level, we find the expected linear quark-mass dependence of the nucleon mass, $M_N = M + \sigma\, m_q + \cdots$. Beyond tree-level, there are spin-independent nucleon interactions with an even number of pions contained in the above term. Pion-nucleon scattering provides an avenue to determine σ.

15 Write down all strong-isospin–breaking mass operators up to second order in the quark mass. What effect does isospin breaking in the pion mass have on the nucleon mass? Deduce the behavior of the nucleon mass splitting as a function of the quark masses.

The coefficient σ is related to an important parameter called the pion-nucleon sigma-term, which is defined by

$$\sigma_N = \frac{1}{2M_N}\langle N(\boldsymbol{k})|m_q\overline{\psi}\psi|N(\boldsymbol{k})\rangle. \tag{4.57}$$

In HNχPT, we have just established that $\sigma_N = \frac{\sigma m_q}{2M_N} + \cdots$. Determination of the sigma term is relevant for the nucleon-mass spectrum, the strangeness content of the nucleon, quark mass ratios, pion-nucleon scattering, and new-physics searches.

The sigma term is at the heart of the quark-mass dependence of the nucleon mass. Using the Feynman-Hellmann theorem, we have the relation $\sigma_N = \frac{m_q}{2M_N}\frac{\partial M_N}{\partial m_q}$, which expresses the sigma term as the incremental change in nucleon mass with respect to the quark mass. A quantity not-too-distantly related to the sigma term is the strangeness fraction in the nucleon. This fraction is defined from the ratio of matrix elements of scalar quark bilinear operators

$$y = \frac{\langle N(\boldsymbol{k})|\overline{s}s|N(\boldsymbol{k})\rangle}{\frac{1}{2}\langle N(\boldsymbol{k})|\overline{u}u + \overline{d}d|N(\boldsymbol{k})\rangle}. \tag{4.58}$$

With some algebraic rearrangement, we can produce the relation

$$\left(\frac{m_s}{m_q} - 1\right)(1-y)\,\sigma_N = \frac{m_s - m_q}{2M_N}\langle N(\boldsymbol{k})|\overline{u}u + \overline{d}d - 2\overline{s}s|N(\boldsymbol{k})\rangle \tag{4.59}$$

between quark masses, the strangeness fraction, and the pion-nucleon sigma term. The strange quark will be considered further in the next section, and we will estimate the matrix element on the right-hand side from phenomenology.

The sigma term makes an appearance in pion-nucleon scattering. In the isospin zero channel, the scattering amplitude is constrained by low-energy theorems at the Cheng-Dashen point, namely

$$\frac{1}{2}f^2 D^{I=0}(\nu = 0, t = 2m_\pi^2) - \text{Born} = \sigma_N + \text{large corrections}, \tag{4.60}$$

where the Born subtraction refers to removing contributions from nucleon intermediate states, $\pi N \to N \to \pi N$, and the large corrections scale as $\sqrt{m_q}$. The low-energy theorem can be reformulated in a faster-converging form by considering the form factor of the sigma term, $\sigma_N(t)$. In this case [201], the right-hand side can

be replaced by $\sigma_N(t = 2m_\pi^2) + \Delta_R$, where $\Delta_R \sim m_q^2$, and can be estimated using HNχPT [202]. The problem is then to compute $\sigma_N(2m_\pi^2) - \sigma_N(0)$ in order to extract the sigma term from data.

Finally, the sigma term is relevant for the detection of dark matter. In a typical direct-detection experiment, one seeks to measure the recoil of nuclei that have scattered elastically with dark matter. The scattering could be mediated through a spin-independent interaction of the form $\sim (\overline{\chi}\chi)\left(\overline{\psi}\psi\right)$, where by the dark matter particle χ is coupled to light quarks. Another potential mechanism is from dark matter coupling to the Higgs, and nuclear recoil arises from the Higgs coupling to heavy quarks, $\sim m_Q\left(\overline{Q}Q\right)H$. The Higgs coupling grows with quark mass, however, the heavy-quark scalar density in the nucleon decreases with the mass of the heavy quark. As a result, the product of the two is roughly constant for the heavy quark flavors:

$$\langle N|m_Q\overline{Q}Q|N\rangle \sim 80\ \text{MeV}\left[1 - 2\sigma_N\left(1 + \int_0^{m_s/m_q} y(x)dx\right)\right], \tag{4.61}$$

where the dominant uncertainty is not from perturbative treatment of the heavy quarks but rather from subtracting out the contribution from light quarks, see [203] for a clear discussion.

4.4.4 Beyond Leading Order

The linear quark-mass dependence of the nucleon mass is at $\mathcal{O}(p^2)$, and quadratic dependence enters at $\mathcal{O}(p^4)$ from higher-order local operators. Loop diagrams will produce non-analytic dependence on the quark mass, and the leading such contribution arises from the sunset diagram, which counts at $\mathcal{O}(p^3)$, see Fig. 4.9.

To evaluate the sunset diagram, we recall the form of the heavy-nucleon propagator in the rest frame, $v_\mu = (0, 0, 0, i)$, namely

$$D_N(x, 0) = e^{-Mx_4}\delta(\boldsymbol{x})\theta(x_4)\mathcal{P}_+, \quad \text{with} \quad \theta(x_4) = \int_{-\infty}^{\infty}\frac{dp_4}{2\pi i}\frac{e^{ip_4x_4}}{p_4 - i\epsilon}, \tag{4.62}$$

which is thus nonvanishing only for $x_4 > 0$. For the heavy-particle formulation, the pole prescription is required in Euclidean space. The heavy-nucleon propagator must be treated as $\frac{1}{p\cdot v} = \frac{-i}{p_4 - i\epsilon} = -i\mathcal{PV}\frac{1}{p_4} + \pi\delta(p_4)$ for nucleons to propagate forward in time. From this observation, we can evaluate the sunset diagram

Fig. 4.9 One-loop diagram contributing to the nucleon self energy at $\mathcal{O}(p^3)$

$$\propto \frac{g_A^2}{f^2}\int_p \frac{(p\cdot S)^2}{p\cdot v\,[p^2+m_\pi^2]} \propto \int_p \frac{(\boldsymbol{p}\cdot\boldsymbol{S})^2}{\boldsymbol{p}^2+m_\pi^2} \propto \int_p 1 - m_\pi^2 \int_p \frac{1}{\boldsymbol{p}^2+m_\pi^2}$$
$$\sim \Lambda^3 + m_\pi^2\,\Lambda + m_\pi^3, \quad (4.63)$$

where in the second line, we have introduced an ultraviolet cutoff Λ. The cubic divergence can be absorbed into the renormalized chiral-limit nucleon mass M, while the linear divergence can be absorbed into the renormalization of σ. Both of these power-law divergences are automatically subtracted in dimensional regularization. The finite piece makes a contribution to the nucleon mass that is $m_\pi^3 \propto m_q^{3/2}$. Exhibiting this contribution, we see the nucleon mass has the expansion

$$M_N = M + A\,m_\pi^2 - \frac{3\pi g_A^2}{(4\pi f)^2} m_\pi^3 + B\,m_\pi^4 \left(\log\frac{\mu^2}{m_\pi^2} + C\right) + \cdots \quad (4.64)$$

away from the chiral limit. From lattice-QCD computations of the nucleon mass, it has proven challenging to expose this behavior, see Fig. 4.10.

Chiral perturbation theory can be used to compute chiral corrections to a variety of nucleon observables, we refer the reader to an early review on the subject [205]. Of particular importance are matrix elements of quark bilinear operators, $\overline{\psi}\Gamma\psi$. These matrix elements can be parameterized in terms of various form factors, which we generically denote by $\mathcal{G}(\boldsymbol{q}^2)$, where $\boldsymbol{q}$ is a spacelike momentum transfer. The value at zero momentum transfer, $\mathcal{G}(0)$, is often a charge or a moment. The slope of the form factor away from zero momentum transfer can be used to define an *rms* radius, $\mathcal{G}(\boldsymbol{q}^2) = \mathcal{G}(0) - \frac{1}{6}\boldsymbol{q}^2\langle r_{\mathcal{G}}^2\rangle + \cdots$.

One such bilinear operator is the isovector vector current, J_μ^+. Matrix elements of this current are parameterized by

$$\langle N(\boldsymbol{p}')|J_\mu^+|N(\boldsymbol{p})\rangle = u'^\dagger\left[v_\mu G_E^+(\boldsymbol{q}^2) + \frac{i\varepsilon_{ijk}q_j\sigma_k}{2M_N}G_M^+(\boldsymbol{q}^2)\right]u, \quad (4.65)$$

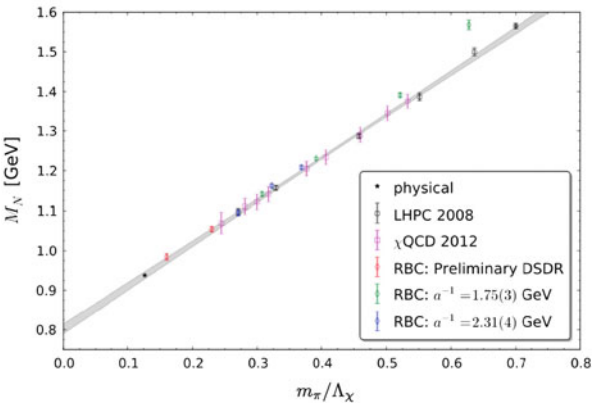

Fig. 4.10 Pion mass dependence of the nucleon mass calculated with lattice QCD. To a very good approximation, the lattice data lie along the straight line $M_N = 0.80\ \text{GeV} + m_\pi$. We thank A. Walker-Loud for providing an updated version of the plot in [204]

where G_E^+ and G_M^+ are just differences between proton and neutron electric and magnetic form factors, respectively. The isovector charge is protected from renormalization by the Ward identity. The isovector electric radius has the behavior $\langle r_E^2 \rangle = A \left(\log m_q + B \right)$ and diverges in the chiral limit. The isovector magnetic moment has the expansion $\mu_I = \mu_0 + A\, m_q^{1/2} + B\, m_q \left(\log m_q + C \right)$, while the isovector magnetic radius $\langle r_M^2 \rangle = A\, m_q^{-1/2} + B \left(\log m_q + C \right)$ also diverges in the chiral limit.

One can carry out the same analysis for the isovector axial-vector current, $J_{\mu 5}^+$. Nucleon matrix elements of this current can be parameterized in terms of two form factors, G_A and G_P,

$$\langle N(\boldsymbol{p}') | J_{\mu 5}^+ | N(\boldsymbol{p}) \rangle = 2\, u'^{\dagger} \left[S_\mu G_A(\boldsymbol{q}^2) - q_\mu \boldsymbol{S} \cdot \boldsymbol{q}\, G_P(\boldsymbol{q}^2) \right] u. \tag{4.66}$$

The axial charge of the nucleon, $G_A \equiv G_A(0)$, has a chiral expansion of the form $G_A = g_A + A\, m_q \left(\log m_q + B \right)$, while the axial radius has the expansion $\langle r_A^2 \rangle = r^2 + A\, m_q \left(\log m_q + B \right)$. The pseudoscalar form factor $G_P(\boldsymbol{q}^2)$ exhibits a pion pole

$$G_P(\boldsymbol{q}^2) = \frac{g_A}{\boldsymbol{q}^2 + m_\pi^2} - \frac{1}{6} \langle r_A^2 \rangle + \mathcal{O}\left(m_\pi^2 \right), \tag{4.67}$$

because the derivative of the isovector axial-vector current has the quantum numbers of a charged pion. Conservation of this current in the chiral limit, moreover, produces a relation between $G_A(\boldsymbol{q}^2)$ and $G_P(\boldsymbol{q}^2)$ at vanishing quark mass [206]. To contrast the behavior of axial-vector and vector form factors, we see the axial-vector size of the nucleon should be smaller than the vector size as one nears the chiral limit. The axial-vector size arises from local interactions, whereas the vector size is dominated by long-distance, charged pion loop contributions. Some credence to this picture is provided by the experimental values: $\langle r_A^2 \rangle = 0.42\ \text{fm}^2$, and $\langle r_E^2 \rangle^{p-n} = 0.88\ \text{fm}^2$.

The low-energy expansion of hadronic observables is limited by the nearest-lying states that have been excluded. For pions, such higher-lying states are reasonably well separated in energy; however, for the nucleon, the nearby $\Delta(1232)$ resonances often undermine the expansion of certain nucleon observables. The mass splitting, $\Delta \equiv M_\Delta - M_N = 290\ \text{MeV}$, is not considerably greater than the pion mass. If one imagines the strict chiral limit, $m_\pi \ll \Delta$, then these resonances can be integrated out to arrive at HNχPT. On the other hand, for physical values of the parameters, we might imagine $m_\pi \sim \Delta$, and these degrees of freedom should be retained. The size of the axial couplings $g_{\Delta N}$ and $g_{\Delta\Delta}$ gives a further phenomenological reason to include Delta-resonance degrees of freedom explicitly. Systematic inclusion of the $\Delta(1232)$ in χPT is reviewed in [207]. While one might expect the inclusion of further higher-lying resonances would improve the description of observables, these higher resonances cannot be included in a low-energy theory. Such resonances have strong decays which produce energetic pions that necessarily preclude a power-counting scheme.

4.5 Issues of Convergence

To begin this section, we remind the reader that perturbative expansions are assumed asymptotic until proven otherwise. In expanding about the chiral limit, changing the sign of the quark mass leads to vacuum instability from which we infer the chiral expansion has zero radius of convergence. This is further evidenced by the non-analyticities of χPT expressions. While the success of QED perturbation theory is set by the smallness of $\alpha = \frac{1}{137}$, the chiral expansion is far from this ideal. Often one is confronted with the need, either from lattice QCD or from phenomenology, to consider expansion parameters not considerably less than unity. For this reason, one should be aware of the limitations inherent to asymptotic series.

To illustrate these limitations, we consider a toy model provided by the integral

$$F(x) = \int_0^\infty ds \frac{e^{-s}}{1+sx}, \tag{4.68}$$

where it is assumed that $0 < x \ll 1$. For negative values of x, the integrand has a non-integrable singularity, thus any expansion about $x = 0$ has zero radius of convergence. Ignoring this fact and blindly expanding the integrand gives the series

$$F_N(x) = \sum_{n=0}^{N} (-)^n n!\, x^n, \tag{4.69}$$

which diverges as $N \to \infty$. Depending on the size of x, however, the first few terms nevertheless give a good approximation to the function $F(x)$, as shown in Fig. 4.11.

For small values of x, namely $x < \frac{1}{4}$, increasing the number of terms in the expansion from $N = 1$ to $N = 3$ gives a better approximation to the function $F(x)$. Adding further terms, however, eventually breaks the trend. Because the series has zero radius of convergence, adding further terms to the expansion limits one to a smaller range of x for which a good approximation can be obtained. For

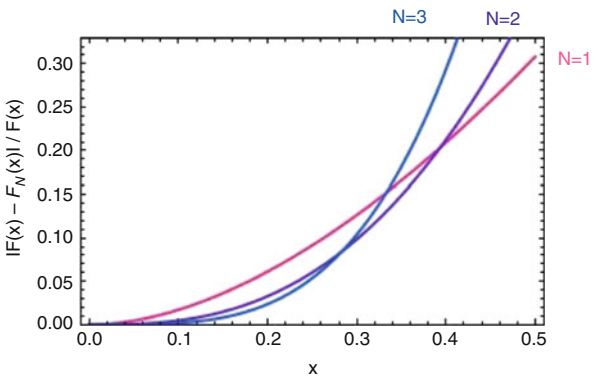

Fig. 4.11 Relative error in approximating $F(x)$ by its asymptotic expansion $F_N(x)$ for $N = 1$–3

the function at hand, the best approximation is attained for $N \sim \frac{1}{x}$. Thus to make a better approximation for larger values of x, one should actually drop higher-order terms in the expansion.

In χPT, one often goes to higher orders in the power counting to test the convergence of the expansion. Doing so, however, brings along unknown low-energy constants. If one knew the chiral-limit values of these parameters *a priori*, then one could assess the convergence. When one uses phenomenology or lattice data to fit the parameters, this task becomes considerably challenging.

In two-flavor χPT, we found that the chiral expansion of pion dynamics is governed by the small parameter $m_\pi^2/\Lambda_\chi^2 \sim 0.02$, which should still be suitably small for pion masses larger than physical. This is too idealistic in certain channels where there are resonance contributions, and more realistic expansion parameters that underlie χPT are $m_\pi^2/m_\rho^2 \sim 0.03$ and $m_\pi^2/m_\sigma^2 \sim 0.08$. When considering the chiral dynamics of the nucleon, we need the chiral limit value of the nucleon mass, which is $M = 0.80$ GeV, see Fig. 4.10. The heavy-nucleon expansion is controlled by $m_\pi/M \sim 0.2$, and Delta-resonance contributions are controlled by $m_\pi/\Delta \sim 0.5$ if excluded, and $\sqrt{\Delta^2 - m_\pi^2}/M \sim 0.3$ if included. We now investigate the state of the three-flavor chiral expansion.

4.5.1 Including Strange Mesons

The strange-quark mass is smaller than the strong-interaction scale, $m_s/\Lambda_{\rm QCD} \sim 0.3$, but not considerably so. Nevertheless, we can understand the low-energy dynamics of QCD that emerges from having three nearly massless quarks, and compare with nature.

Returning to the analysis of Sect. 4.2, the pattern of symmetry breaking in the massless three-flavor case is $SU(3)_L \otimes SU(3)_R \to SU(3)_V$, due to the formation of the chiral condensate $\langle \overline{\psi}\psi \rangle \neq 0$. The coset $SU(3)_L \otimes SU(3)_R/SU(3)_V$ is parameterized similarly to before, $\Sigma = e^{2i\phi/f}$, where $\Sigma \to L\Sigma R^\dagger$ under a three-flavor chiral transformation. The vector transformation can be used to deduce, $\phi \to V\phi V^\dagger$, and so ϕ describes an octet of mesons. These are conventionally packaged as

$$\phi = \begin{pmatrix} \frac{1}{\sqrt{2}}\pi^0 + \frac{1}{\sqrt{6}}\eta & \pi^+ & K^+ \\ \pi^- & -\frac{1}{\sqrt{2}}\pi^0 + \frac{1}{\sqrt{6}}\eta & K^0 \\ K^- & \overline{K}^0 & -\frac{2}{\sqrt{6}}\eta \end{pmatrix}. \tag{4.70}$$

The quark masses, m_q and m_s, explicitly break chiral symmetry from $SU(3)_L \otimes SU(3)_R$ down to $SU(2)_V \otimes U(1)_V$. This effect can be accounted for by the spurion trick used above. Treating each of the quark masses as $\mathcal{O}(p^2)$, the leading-order chiral Lagrangian has the form

$$\mathcal{L}_{\chi\mathrm{PT}} = \frac{f^2}{8}\,\mathrm{Tr}\left(\partial_\mu \Sigma^\dagger \partial_\mu \Sigma\right) - \lambda\,\mathrm{Tr}\left(m\,\Sigma^\dagger + m\,\Sigma\right), \tag{4.71}$$

where $m = \mathrm{diag}\,(m_q, m_q, m_s)$. Aside from this difference, the form of the Lagrangian is the same as that in the two-flavor case, although the values of the low-energy parameters f and λ are different. Their values are now determined by the three-flavor chiral limit. At $\mathcal{O}(p^4)$, there are seven Gasser-Leutwyler coefficients, and a few more when external gauge fields are included [208].

16 In the isospin limit, there are two different quark masses but three different meson masses in the pseudoscalar octet. Use the three-flavor chiral Lagrangian to derive the constraint,

$$\Delta_{\mathrm{GMO}} = \frac{4}{3}m_K^2 - m_\eta^2 - \frac{1}{3}m_\pi^2 = 0, \tag{4.72}$$

which was originally found by Gell-Mann and Okubo. What happens away from the isospin limit?

The tree-level masses of the pseudoscalar mesons lead to the relation $\Delta_{\mathrm{GMO}} = 0$ in Eq. (4.72). Inserting the neutral-meson masses and dividing by the average octet-meson mass, we see that experimentally $\Delta_{\mathrm{GMO}}/\overline{m}_\phi^2 \sim 0.15$. Beyond tree level, this relation is modified by one-loop mass corrections, and local counterterms from the $\mathcal{O}(p^4)$ Lagrangian. Estimating the size of such corrections leads to $\Delta_{\mathrm{GMO}} \sim \frac{m_\phi^4}{\overline{m}_\phi^2 \Lambda_\chi^2}$. In $SU(3)$ χPT, the η meson is the most worrisome. Fourth-order contributions from the η should be $\sim 35\,\%$. This is about the size of corrections needed for the Gell-Mann–Okubo relation, but notice that a factor of two can seriously upset the situation.

To expand about the three-flavor chiral limit, we must add to $m_\pi^2/\Lambda_\chi^2 \sim 0.02$ two further expansion parameters, $m_K^2/\Lambda_\chi^2 \sim 0.23$ and $m_\eta^2/\Lambda_\chi^2 \sim 0.27$. Pending unfortunate numerical factors, $\mathcal{O}(p^6)$ contributions to meson quantities (which include two-loop diagrams) should be $\sim 10\,\%$. To work at this order, one must introduce ~ 100 low-energy constants, which makes it difficult to address issues of convergence. The comprehensive study of χPT predictions at next-to-next-to-leading order allows one to form relations sensitive to only $\mathcal{O}(p^6)$ low-energy constants. While most are not well known, one can use these relations to assess the convergence of the three-flavor expansion, with the result that the expansion "mostly works" [209].

17 Revisit electromagnetic mass corrections in three-flavor χPT. Find all leading- and next-to-leading-order electromagnetic mass operators. Ignoring the up- and down-quark masses, which octet-meson masses are affected by leading and next-to-leading operators?

18 Accounting for strong and electromagnetic isospin breaking to leading order, compute the mass spectrum of the meson octet using χPT. Devise a way to determine the quark mass ratios m_u/m_d and m_d/m_s using the experimentally measured meson masses.

4.5.2 Including Strange Baryons

The lowest-lying baryons form an octet under $SU(3)_V$ and can be packaged in the matrix

$$B = \begin{pmatrix} \frac{1}{\sqrt{2}}\Sigma^0 + \frac{1}{\sqrt{6}}\Lambda & \Sigma^+ & p \\ \Sigma^- & -\frac{1}{\sqrt{2}}\Sigma^0 + \frac{1}{\sqrt{6}}\Lambda & n \\ \Xi^- & \Xi^0 & -\frac{2}{\sqrt{6}}\Lambda \end{pmatrix}, \tag{4.73}$$

which accordingly transforms as $B \to VBV^\dagger$. While the chiral multiplets for these baryons in the chiral limit are unknown, we are free to choose the $SU(3)_L \otimes SU(3)_R$ transformation $B \to UBU^\dagger$ due to the ambiguity in resolving a baryon, and a baryon plus any number of soft octet mesons.

In the three-flavor chiral limit, the octet baryons are degenerate, with a mass we denote by M_B. This mass must be treated as a large scale, and the baryon fields decomposed into heavy baryon fields. Their interactions with octet mesons are constrained by the form of spontaneous and explicit breaking of chiral symmetry. Construction of the heavy-baryon chiral perturbation theory (HBχPT) Lagrangian proceeds similarly to that for the heavy nucleon. To aid in the construction, we appeal to the vector and axial-vector fields built from mesons, $\mathcal{V}_\mu$ and $\mathcal{A}_\mu$ in Eq. (4.52). The former can be used to build a chirally covariant derivative, $D_\mu B \equiv \partial_\mu B + \big[\mathcal{V}_\mu, B\big]$, which transforms as $D_\mu B \to U\left(D_\mu B\right)U^\dagger$.

To $\mathcal{O}(p)$, we have the gauged static-baryon term and two independent axial interactions,

$$\mathcal{L}_{\text{HB}\chi\text{PT}} = \text{Tr}\left(B^\dagger iv\cdot D\, B\right) + 2D\,\text{Tr}\left(B^\dagger S_\mu\{\mathcal{A}_\mu, B\}\right) + 2F\,\text{Tr}\left(B^\dagger S_\mu[\mathcal{A}_\mu, B]\right). \tag{4.74}$$

Further terms are required at $\mathcal{O}(p)$ because of the nearness of spin-$\frac{3}{2}$ baryon resonances. These baryons form a decuplet under $SU(3)_V$, so that $T_{ijk} \to V_i^{i'} V_j^{j'} V_k^{k'} T_{i'j'k'}$, with T_{ijk} completely symmetric. The size of the average mass splitting between the octet and decuplet baryons, $\Delta \equiv M_T - M_B = 270\,\text{MeV}$, necessitates inclusion of the decuplet because $\Delta \sim \overline{m}_\phi$. Their leading-order Lagrangian is given by

$$\mathcal{L}^{(\Delta)}_{\text{HB}\chi\text{PT}} = T^\dagger_\mu \left(iv\cdot D + \Delta\right) T_\mu + 2H\, T^\dagger_\mu S\cdot \mathcal{A} T_\mu + 2C\, \left(T^\dagger_\mu \mathcal{A}_\mu B + B^\dagger \mathcal{A}_\mu T_\mu\right) \tag{4.75}$$

and includes an axial coupling of pions to the decuplet H, as well as an axial transition coupling of pions to octet and decuplet baryons C. Notice the large mass scale M_B has been removed from the chiral-limit decuplet mass rather than M_T. While we could remove the mass of the decuplet fields, the splitting Δ would then show up in time-dependent factors for the axial baryon transition, and these factors would ultimately incorporate the baryon mass difference in Feynman diagrams which involve both octet and decuplet baryons.

To include the leading-order effects of quark masses, we need terms of the $\mathcal{O}(p^2)$ Lagrangian. Focusing on the quark-mass dependence of the octet baryons, we have three leading-order terms

$$\mathcal{L}_m = b_D\,\text{Tr}\left(B^\dagger\{\mathcal{M}_+, B\}\right) + b_F\,\text{Tr}\left(B^\dagger[\mathcal{M}_+, B]\right) + b_\sigma\,\text{Tr}\left(B^\dagger B\right)\,\text{Tr}\left(\mathcal{M}_+\right). \tag{4.76}$$

Because there are three parameters and four octet baryon masses in the isospin symmetric limit, there is a relation between the masses implied by leading-order HBχPT, which has the form

$$M_{\text{GMO}} = M_\Lambda + \frac{1}{3}M_\Sigma - \frac{2}{3}M_N - \frac{2}{3}M_\Xi = 0. \tag{4.77}$$

Experimentally, this relation is very well satisfied. Normalizing to the average octet-baryon mass, we have $M_{\text{GMO}}/\overline{M}_B \sim 1\,\%$. Corrections to this relation can be computed in HBχPT and first arise at $\mathcal{O}(p^3)$ from one-loop diagrams. Because these contributions are non-analytic in the quark masses, there are no additional parameters required beyond the various axial couplings entering the one-loop diagrams.

To compute the one-loop corrections, we require the octet-baryon sunset diagram, shown in Fig. 4.9. This diagram evaluates similarly to before. Additionally, we require the sunset diagram shown in Fig. 4.12. The anatomy of this intermediate-state decuplet contribution is as follows. By angular momentum, the virtual meson must be in a relative p-wave, which at low energies requires the momentum suppression factor $\boldsymbol{p}^{2\ell}$ with $\ell = 1$. This factor automatically appears in the numerator when evaluating the Feynman diagram:

Fig. 4.12 One-loop octet-baryon (B) self-energy diagram with intermediate-state decuplet (T) baryon

$$\sim \frac{C^2}{f^2}\int_p \frac{\boldsymbol{p}^2}{[ip_4+\Delta][(p_4)^2+\boldsymbol{p}^2+m_\phi^2]}. \tag{4.78}$$

The energy integral can be done by contour integration, which puts the meson on shell with $E_\phi = \sqrt{\boldsymbol{p}^2+m_\phi^2}$. The diagram is then proportional to

$$\frac{C^2}{f^2}\int_{\boldsymbol{p}} \frac{\boldsymbol{p}^2}{E_\phi(E_\phi+\Delta)} \sim \frac{C^2}{f^2}\int_{m_\phi}^{\Lambda} dE_\phi \frac{(E_\phi^2-m_\phi^2)^{3/2}}{E_\phi+\Delta}, \tag{4.79}$$

where the numerator factor is a combination of p-wave suppression, $\boldsymbol{p}^2 = E_\phi^2 - m_\phi^2$, and the available two-body phase space near threshold, $\sqrt{E_\phi^2-m_\phi^2}$. In changing variables, we have included an ultraviolet cutoff Λ to regulate the divergences. For large meson energies, there are multiple divergences,

$$\begin{aligned}&\int^{\Lambda} dE\, E^2 \left(1-\frac{\Delta}{E}+\frac{\Delta^2}{E^2}-\frac{\Delta^3}{E^3}+\cdots\right)\left(1-\frac{3}{2}\frac{m_\phi^2}{E^2}+\cdots\right)\\ &\sim \Lambda^3+\Delta\Lambda^2+\Delta^2\Lambda+\Delta^3\log\Lambda+m_\phi^2\,\Lambda+m_\phi^2\,\Delta\log\Lambda+\text{finite}.\end{aligned} \tag{4.80}$$

The first four terms are removed by the chiral-limit baryon-mass renormalization condition, $M_{N,\Sigma,\Lambda,\Xi}\Big|_{m_q=m_s=0} = M_B$. The remaining two divergences are proportional to the quark masses. The first is a power-law divergence which can be removed by a renormalization of the parameters $b_{D,F,\sigma}$. The logarithmic divergence produces running of these couplings, which is possible due to treating Δ as a small parameter. After renormalization, what remains is described by $\mathcal{F}(m_\phi,\Delta,\mu)$, which is a non-analytic function of m_ϕ and Δ that is given by

$$\begin{aligned}\mathcal{F}(m,\delta,\mu) = (m^2-\delta^2)\left[\sqrt{\delta^2-m^2}\log\left(\frac{\delta-\sqrt{\delta^2-m^2+i\epsilon}}{\delta+\sqrt{\delta^2-m^2+i\epsilon}}+\delta\log\frac{\mu^2}{m^2}\right)\right]\\ +\frac{1}{2}\delta m^2\log\frac{\mu^2}{m^2}+\delta^3\log\frac{\mu^2}{4\delta^2}.\end{aligned} \tag{4.81}$$

For $\delta > -m$, the function $\mathcal{F}(m,\delta,\mu)$ is real valued.

Table 4.1 Estimated one-loop correction to the baryon Gell-Mann–Okubo relation

Source	D	F	C	$M_{\rm GMO}/\overline{M}_B$
χPT [210]	0.61	0.40	1.2	0.79 %
Lattice QCD [211]	0.72	0.45	1.6	1.12 %
SU(6) Quark Model	3/4	1/2	3/2	1.29 %

Combining results for the two sunsets, and forming the linear combination of octet baryon masses in Eq. (4.77), we have the one-loop result

$$M_{\rm GMO} = \frac{4}{3(4\pi f)^2}\left[\pi(D^2-3F^2)\Delta_{\rm GMO}(m_\phi^3) - \frac{1}{6}C^2\Delta_{\rm GMO}[\mathcal{F}(m_\phi,\Delta,\mu)]\right], \tag{4.82}$$

where $\Delta_{\rm GMO}(x_\phi) = \frac{4}{3}x_K - x_\eta - \frac{1}{3}x_\pi$ for any octet-baryon quantity x, and consequently the μ dependence is only superficial. The one-loop correction is determined using various estimates of the axial couplings, see Table 4.1, and is in line with the experimental value for $M_{\rm GMO}$. This agreement is actually quite surprising if we analyze the expansion of individual octet baryon masses. The one-loop corrections are particularly large: for the nucleon, $\delta M_N(\mu = \Lambda_\chi)/M_N = -39\,\%$; for the Lambda hyperon, $\delta M_\Lambda(\mu = \Lambda_\chi)/M_\Lambda = -67\,\%$; for the Sigmas, $\delta M_\Sigma(\mu = \Lambda_\chi)/M_\Sigma = -89\,\%$; and finally for the cascade baryons, $\delta M_\Xi(\mu = \Lambda_\chi)/M_\Xi = -98\,\%$. The expansion is worse with increasing strangeness because of larger couplings to strange mesons. The expansion parameters governing the heavy-octet-baryon expansion are not considerably less than unity, m_K/M_B and m_η/M_B are both ~ 0.5. The success of three-flavor HBχPT to describe certain observables seems to require a deeper explanation.

19 Recall the relation between the nucleon sigma term and strangeness, Eq. (4.59). Using the baryon chiral Lagrangian at tree level, calculate the matrix element on the right-hand side and express it in terms of the octet baryon masses. Finally, obtain a rough estimate the size of the sigma term.

4.5.3 Excluding Strangeness

In the three-flavor chiral expansion, we treat the quark masses equally $m_q \sim m_s \ll \Lambda_{\rm QCD}$. Unless one is exceptionally lucky, the strange-quark mass is probably too large to be considered a perturbation about the chiral limit. With notable exceptions, baryon observables exhibit poor convergence, and even meson properties determined with lattice QCD extrapolate better without the constraints of $SU(3)$ χPT [212].

One approach to the problematic strange quark is to integrate it out in order to use a two-flavor chiral expansion. This corresponds to the mass hierarchy $m_q \ll m_s \sim \Lambda_{\rm QCD}$. For the nucleon and pion, integrating out the strange quark results in $SU(2)$ χPT developed above. For the nucleon, we treated it as an external source of isospin, and nothing stops us from having external sources with nonvanishing strangeness quantum number. As a result, one can consider $SU(2)$ χPT for strange hadrons [213–215]. This description has limited predictive power, but is ideally suited for lattice applications.

To exhibit the idea behind two-flavor chiral expansions for strange hadrons, consider the kaon mass. At tree level in $SU(3)$, one has the expression

$$m_K^2 = \frac{4\lambda}{f^2}\left(m_q + m_s\right) = \frac{1}{2}m_\pi^2 + M_K^2 = M_K^2\left(1 + \frac{m_\pi^2}{2M_K^2} + \cdots\right), \tag{4.83}$$

where we have separated out dependence on the strange quark mass by defining the two-flavor chiral-limit value of the kaon mass, $M_K = m_K\big|_{m_q=0}$. From the physical kaon mass, $m_{K^0} = 0.497$ GeV, we can estimate M_K using $SU(3)$ χPT at one-loop order. Not surprisingly, the overwhelming majority of the kaon mass arises from the strange quark, $M_K = 0.486(5)$ GeV, where the uncertainty corresponds to that from the fourth-order low-energy constants.

Now we extend the idea to hyperons. Consider for simplicity kaon contributions to the mass of the Σ baryon. These contributions schematically take the form

$$\begin{aligned} M_\Sigma &= M_B + a\, m_K^2 + b\, m_K^3 + \cdots \\ &= M_B + a' M_K^2 + a'' m_\pi^2 + b' M_K^3 + b'' M_K m_\pi^2 + b''' \frac{1}{M_K} m_\pi^4 + \cdots, \end{aligned} \tag{4.84}$$

where, in the second line, we have expanded out the contributions from the strange-quark mass. This expression can then be reorganized into an $SU(2)$ chiral-limit expansion,

$$M_\Sigma = M_\Sigma^{(2)} + A\, m_\pi^2 + B\, m_\pi^3 + C\, m_\pi^4 \left(\log m_\pi + D\right) + \cdots, \tag{4.85}$$

where $M_\Sigma^{(2)}$ denotes the Σ baryon mass in the two-flavor chiral limit. In the $SU(2)$ expansion, the all-orders strange-quark mass dependence is contained in the parameters, $M_\Sigma^{(2)}, A, B, \ldots$

The price to pay for a better converging expansion is a mild proliferation of low-energy constants. Table 4.2 summarizes the various parameters entering the two-flavor expansion of baryon properties. Computing the one-loop contributions to baryon masses in two-flavor χPT and evaluating these at a scale of $\mu = \Lambda_\chi$ shows perturbatively small corrections over a range of pion masses, see Fig. 4.13. The dimensionless parameters underlying the two-flavor chiral expansion are m_π^2/Λ_χ^2 and m_π^2/M_K^2, and $m_\pi/M^{(2)}$ from the heavy-baryon expansion. Baryons

Table 4.2 Comparison of $SU(3)$ and $SU(2)$ χPT for baryons. Listed for each theory are the quantities required to be small for the perturbative expansion, the baryon multiplets entering the theory, and their associated axial couplings

	$SU(3)$	$SU(2)_{S=0}$	$SU(2)_{S=1}$	$SU(2)_{S=2}$	$SU(2)_{S=3}$
Expansion	p	p	p	p	p
Parameters	m_π, m_K, m_η	m_π	m_π	m_π	m_π
	Δ	$\Delta_{\Delta N}$	$\Delta_{\Sigma\Lambda}, \Delta_{\Sigma^*\Sigma}$	$\Delta_{\Xi^*\Xi}$	
Baryon	**8** B	**2** N	**1** Λ, **3** Σ	**2** Ξ	
Multiplets	**10** T	**4** Δ	**3** Σ^*	**2** Ξ^*	**1** Ω
Axial	D, F	g_A	$g_{\Lambda\Sigma}, g_{\Sigma\Sigma}$	$g_{\Xi\Xi}$	
Couplings	C	$g_{\Delta N}$	$g_{\Lambda\Sigma^*}, g_{\Sigma\Sigma^*}$	$g_{\Xi\Xi^*}$	
	H	$g_{\Delta\Delta}$	$g_{\Sigma^*\Sigma^*}$	$g_{\Xi^*\Xi^*}$	

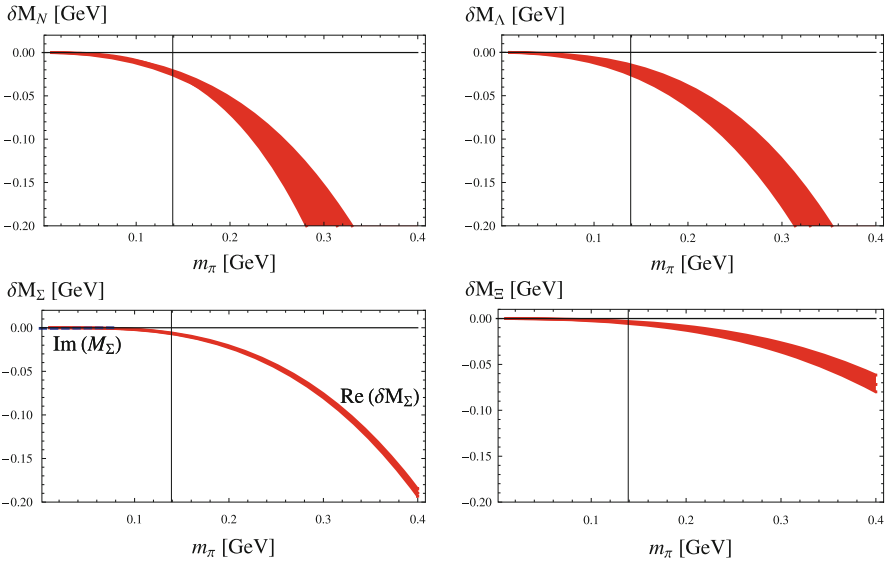

Fig. 4.13 One-loop corrections to baryon masses as functions of pion mass in $SU(2)$ HBχPT. The bands are generated by varying the renormalization scale μ within $\pm 25\,\%$ of Λ_χ

with increasing strangeness perform correspondingly better in $SU(2)$ χPT for two reasons. The first reason is that the axial couplings decrease with increasing strangeness. Secondly the heavy baryon approximation depends on the $SU(2)$ chiral-limit masses, and these increase with increasing strangeness. As a result, the approximation works better the stranger the hyperon. Lattice QCD will ultimately reveal whether this is a successful description of hyperons, and whether $SU(3)$ relations among couplings emerge.

20 Use $SU(2)$ χPT to construct a low-energy theory of kaons. Do the same for the η.

21 Find a process involving strange baryons for which a description in terms of $SU(2)$ χPT must certainly fail.

4.5.4 Not-So-Heavy Baryons

Treating baryons as heavy is required to have a power counting scheme, however, the static approximation is often severe. Recoil corrections can be treated in perturbation theory, but this approach will not allow one to exactly capture the correct analytic structure of amplitudes. Most unnerving, furthermore, is that the heavy-baryon approximation can lead to unphysical singularities. In such cases, one needs all-orders re-summation of recoil corrections, and this can be achieved through relativistic-baryon χPT [216].

We will use the nucleon's scalar form factor as an illustrative example. Using relativistic nucleon spinors, this form factor is defined from the matrix element

$$\langle N(\boldsymbol{p}')|m_q\left(\overline{u}u+\overline{d}\,d\right)|N(\boldsymbol{p})\rangle=\overline{u}(\boldsymbol{p}')\sigma(t)u(\boldsymbol{p}) \tag{4.86}$$

and differs by a trivial normalization factor from the scalar form factor we used in Sect. 4.4, namely $\sigma_N(t)=\frac{1}{2M_N}\sigma(t)$. Computing this matrix element at the Cheng-Dashen point ($t=2m_\pi^2$) with HNχPT, we obtain the result $\sigma(t=2m_\pi^2)-\sigma(t=0)=\frac{3\pi g_A^2 m_\pi^3}{2\Lambda_\chi^2}$ with corrections at $\mathcal{O}(m_\pi^4)$. This result does not indicate anything problematic about the heavy-nucleon approach.

For a general t-channel momentum transfer, the analytic properties of the amplitude allow for a once-subtracted dispersion relation,

$$\sigma(t)-\sigma(0)=\frac{t}{\pi}\int_{4m_\pi^2}^{\infty}dt'\,\frac{\mathcal{I}[\sigma(t')]}{t'(t'-t)}, \tag{4.87}$$

where the integration proceeds along the two-pion cut. The fully relativistic computation at one loop can be obtained using the imaginary part of the form-factor diagrams with relativistic kinematics and the dispersion integral above. The result has the form

$$\sigma(t)-\sigma(0)=\frac{3\pi g_A^2 m_\pi}{4\Lambda_\chi^2} \tag{4.88}$$
$$\left[(t-2m_\pi^2)\left[\frac{1}{2\sqrt{\tau}}\log\frac{1+\sqrt{\tau}}{1-\sqrt{\tau}}-\log\left(1+\frac{m_\pi}{2M_N\sqrt{1-\tau}}\right)\right]\right.$$
$$\left.+2m_\pi^2\left[1-\log\left(1+\frac{m_\pi}{2M_N}\right)\right]\right].$$

Above, τ is the threshold parameter defined by $\tau=\frac{t}{4m_\pi^2}$.

One can perform the same computation using HNχPT. This result agrees with the heavy-nucleon limit, $m_\pi/M_N \ll 1$, of the fully relativistic expression, which is given by

$$\sigma(t)-\sigma(0)=\frac{3\pi g_A^2 m_\pi}{4\Lambda_\chi^2}\left[(t-2m_\pi^2)\left[\frac{1}{2\sqrt{\tau}}\log\frac{1+\sqrt{\tau}}{1-\sqrt{\tau}}\right]+2m_\pi^2\right], \tag{4.89}$$

where the second term survives at the Cheng-Dashen point. The problem with the above expression, however, is that it becomes singular at the two-pion threshold. This unphysical behavior is due to the factor $\frac{1}{2}\log\frac{1+\sqrt{\tau}}{1-\sqrt{\tau}} \to -\frac{1}{2}\log(1-\tau)$, as $\tau \to 1$. Physically, we expect a branch cut to start at threshold, whereas HNχPT produces an unphysical singularity right at threshold.

The fully relativistic expression has the correct analytic structure. As one approaches threshold, the unphysical singularity is exactly canceled by the additional logarithm in Eq. (4.88), namely $-\log\left(1+\frac{m}{2M_N\sqrt{1-\tau}}\right) \to +\frac{1}{2}\log(1-\tau)$. This logarithm, moreover, is responsible for the branch cut above threshold. The complications with the heavy-nucleon approach can be linked to the emergence of a large parameter as one nears threshold. This parameter is $\frac{m_\pi}{M_N\sqrt{1-\tau}}$, which is small in the heavy-nucleon approach, $m_\pi/M_N \ll 1$, but the strict heavy-nucleon power counting is spoiled as one nears threshold, $\tau \to 1$. Consequently re-summation of m_π/M_N terms becomes necessary to produce the physically correct analytic behavior of the form factor.

If one requires χPT amplitudes in the vicinity of multiparticle thresholds, one must be careful to perform re-summations to produce the correct non-analyticities. On the other hand, when one is far from such thresholds, their effect can be captured in a tower of analytic terms. This is the principle underlying the construction of every effective field theory.

4.6 Final Remarks

To conclude, we will summarize the results detailed in this chapter in just a few sentences. χPT provides the tool to systematically account for the light-quark–mass dependence of low-energy QCD observables. This effective field theory is written in terms of the approximate Nambu-Goldstone modes that emerge from spontaneous breaking of chiral symmetry. Their interactions, and interactions with low-lying baryons are constrained by the symmetries and symmetry-breaking pattern of QCD. The perturbative expansion of χPT is limited in practice by the size of the physical quark masses relative to strong interaction scales. The nonrelativistic-baryon approximation, and, in particular, the size of the strange-quark mass put strain on the expansion.

Prior to lattice-QCD computations, χPT was the only way to do precision low-energy QCD phenomenology. The era of high-precision lattice QCD has altered the situation. Lattice gauge theory and chiral dynamics have been used in conjunction as an essential way to extract physics from QCD. In the next era, we see lattice computations testing the rigor of the chiral expansion directly, with the power of resolving long-standing puzzles. As our understanding progresses beyond the single-nucleon sector, we additionally may hope to expose the chiral dynamics of light nuclei from first principles.

Acknowledgements Work supported by a joint City College of New York – RIKEN/Brookhaven Research Center fellowship, an award of the Professional Staff Congress of the City University of New York, the Alfred P. Sloan foundation through a City University of New York Junior Faculty Research Award in Science and Engineering, and by the U.S. National Science Foundation, under grant number PHY12-05778.

Chapter 5
Nuclear Physics from Lattice QCD

William Detmold

Abstract I present a pedagogical overview of the application of lattice QCD to the physics of multi-hadron systems. This is a relatively new area of research in which progress has been significant in the last few years and the aim of these lectures is to provide a perspective on the current and future scope of this emerging frontier. After reviewing the recent developments that are beginning to enable nuclear physics to be studied from the underlying theory of the Standard Model, I discuss the recent results that have been obtained in the study of two-hadron and multi-hadron systems. I also explore the difficulties particular to lattice QCD calculations of such systems and emphasise the issues that remain to be resolved.

5.1 Introduction

At a fundamental level, nuclei and other systems of relevance to nuclear physics arise from the Standard Model of particle physics that describes how matter interacts through Quantum Chromodynamics (QCD) and the electromagnetic and weak (electroweak) forces. At the relatively low energies that are relevant for much of nuclear physics, only a few parameters of the Standard Model are relevant, namely the light quark and electron masses, the QCD scale, $\Lambda_{\rm QCD}$, and the coupling to electromagnetism, $\alpha_{f.s}$. From these five inputs, the whole complexity of nuclear physics emerges, with all its remarkable fine-tunings and intricate structure. However, calculations involving the strong interaction are enormously challenging, and demonstrating this emergence by computing the properties and interactions of an arbitrary nucleus from the Standard Model is beyond our current abilities. While enormous advances have been made over the years in developing both phenomenological descriptions of nuclei [217–221] and effective field theory-based descriptions of low energy nuclear physics constrained by the symmetries of the Standard Model [222–224], these approaches must be tuned to experimental data, and their predictive power in realms where there is no such data is limited.

W. Detmold (✉)
Center for Theoretical Physics, Massachusetts Institute of Technology, Cambridge, MA 02139, USA
e-mail: wdetmold@mit.edu

H.-W. Lin, H.B. Meyer (eds.), *Lattice QCD for Nuclear Physics*, Lecture Notes in Physics 889, DOI 10.1007/978-3-319-08022-2_5

To date, the only tool with which to perform QCD calculations in a systematically improvable way is lattice QCD (LQCD). In this approach, space-time is discretised and QCD is numerically solved on a space-time lattice; for realistic calculations, this requires highly optimised algorithms and cutting-edge supercomputing resources. LQCD calculations have led to important insights in particle physics and are critical ingredients in the determination of many of the parameters of the Standard Model. In recent years, the application of LQCD to the intrinsically more complex realm of nuclear physics has begun in earnest. This is a challenging task as nuclei are complicated systems with many relevant energy scales, ranging from nuclear excitations that can be just a few tens of keV through nuclear bindings of a few MeV per nucleon, to hadronic energies and excitations at the typical QCD scale, $\Lambda_{\rm QCD} \sim 300$ MeV, all the way to the total energy of the system (a few hundred GeV). Nevertheless, this is an important endeavour as it will allow ab initio predictions and ultimately place nuclear physics on the firm foundation of the Standard Model.

Progress over the last few years has been significant, and the primary goal of these lecture notes is to highlight this in the context of light nuclei and other multi-hadron systems. The main body of these lectures presents a discussion of our theoretical understanding of multi-hadron systems and overviews recent numerical studies, starting with two-body systems and then moving on to nuclei and multi-meson systems. After summarising the current state of the field, I discuss current issues and future challenges that must be faced in order to provide a truly ab initio approach to nuclear physics.

5.2 Approaching Nuclear Physics in Lattice QCD

Of the various components of the Standard Model, the most challenging piece to deal with in the low energy regime is the strong interaction, described by QCD. The difficulties arise because of the non-perturbative nature of strong interactions at long distances, $r > 0.1$ fm, that means that the perturbative techniques that work well for many calculations in the electroweak sector and in QCD at high energies are inapplicable. For the majority of our discussion, we shall consequently ignore the electroweak interactions and focus on QCD which is defined in Euclidean space-time by the partition function

$$\begin{aligned} \mathcal{Z} &= \int \mathcal{D}A_\mu \mathcal{D}\overline{q}\mathcal{D}q e^{-S_{\rm QCD}[A,\overline{q},q]} \\ &= \int \mathcal{D}A_\mu \det[\mathcal{M}] e^{-S_{\rm g}[A]}\,, \end{aligned} \tag{5.1}$$

where A_μ and q are the gluon and quark fields respectively and, defining $D_\mu = \partial_\mu - igA_\mu$ and $F_{\mu\nu} = [D_\mu, D_\nu]$,

$$S_{\rm QCD}[A,\overline{q},q] = \int d^4x \left[-\frac{1}{2}{\rm tr}F^{\mu\nu}F_{\mu\nu} + \overline{q}(\not{D}+m)q \right] , \tag{5.2}$$

is the QCD action. In the second line of Eq. (5.1), we have integrated over the quark degrees of freedom where $S_g[A]$ is the purely gluonic part of the action and $\mathcal{M}[A]$ is the Dirac operator, which depends on the gauge field. A pedagogical introduction to lattice QCD is provided in the literature [6, 80, 82] and in other contributions in this volume and we refer the reader to this for many details; here we briefly present elements that will be germane to our discussion. The main focus of these lectures will turn out to be on spectroscopy; this is enabled by measurement of two-point correlation functions defined for some set of quantum numbers $\{Q\}$ by

$$\begin{aligned} C_{\{Q\}}(t) &= \frac{1}{\mathcal{Z}} \int \mathcal{D}A_\mu \mathcal{D}\overline{q}\mathcal{D}q \tilde{\mathcal{O}}_Q(t)\mathcal{O}^\dagger_Q(0) e^{-S_{\rm QCD}[A,\overline{q},q]} \\ &= \frac{1}{\mathcal{Z}} \int \mathcal{D}A_\mu \mathcal{F}\left[\tilde{\mathcal{O}}_Q(t), \mathcal{O}^\dagger_Q(0)\right] {\rm det}[\mathcal{M}] e^{-S_{\rm g}[A]} , \end{aligned} \tag{5.3}$$

where the composite operators $\mathcal{O}^\dagger_Q$ and $\tilde{\mathcal{O}}_Q$ create and annihilate states with the quantum numbers Q and are separated in Euclidean time. The functional $\mathcal{F}$ is the result of performing the fermion integrations of the interpolating operators and is generally defined in terms of the quark propagator (the inverse of the Dirac operator). For brevity, we have suppressed the spatial structure of these operators which may be used to project to a fixed momentum for example. The Euclidean time behaviour of such correlation functions is determined by the energies of the QCD eigenstates with the requisite quantum numbers and by the specific forms of the interpolating operators. By determining $C_{\{Q\}}(t)$ numerically, we can attempt to extract information about a subset of the eigen-energies.

To render the calculation finite, we discretise space-time and impose boundary conditions that we take to be periodic in spatial directions and periodic (anti-periodic) in time for bosons (fermions). The gluon degrees of freedom are implemented through SU(3)-valued link variables $U_\mu(x) = \exp[i\ A_\mu(x)]$; for details of the various discretised forms of the QCD action we refer the reader to the literature [6,80,82]. In order to perform the requisite functional integrals over the gluon fields, we use importance sampling, recognising that the factor $\mathcal{P}[U] = \det \mathcal{M}[U] E^{-S_{\rm g}[U]}$ can be interpreted as a Boltzmann weight as we use the Euclidean metric. By generating an ensemble of configurations of the gluon link variables according to this probability measure, we are able to estimate the correlation function $C_{\{Q\}}$ reliably. For an ensemble of N configurations, $\{U_\mu^{[1]},\ U_\mu^{[2]}, \ldots,\ U_\mu^{[N]}\}$,

$$C_{\{Q\}}(t) = \frac{1}{N}\sum_{c=1}^{N} \mathcal{F}\left[\tilde{\mathcal{O}}_Q(t)\mathcal{O}^\dagger_Q(0)\right]\left[U_\mu^{[c]}\right] + \mathcal{O}\left(N^{-1/2}\right) , \tag{5.4}$$

with uncertainties that decrease as the size of the ensemble increases.

To generate such ensembles requires algorithms that efficiently and effectively explore the space of possible gluon configurations and, because of the four-dimensional nature of space-time and the non-locality of $\mathcal{P}[U]$, this is a challenging problem, requiring supercomputing resources. The necessary machinery has been developed over the last few decades, culminating, for example, in the last few years in increasingly precise LQCD determinations of many quantities of importance to particle physics and of the baryon number $B = 0, 1$ ground state hadron spectrum with fully controlled statistical and systematic uncertainties [92] (these results have been nicely reviewed recently in [225, 226]). This is an important achievement as, when compared to experimental measurements, it demonstrates that QCD describes the strongly interacting regime of the strong interaction and that lattice QCD provides a systematic and reliable tool for the computation of hadronic contributions to Standard Model observables. It also demonstrates that the field of LQCD is at a point where more computationally challenging problems, such as many of those encompassed by nuclear physics, can begin to be tackled. A number of groups have recently taken up the task of applying LQCD to the nuclear physics of few hadron systems and significant progress has been made. A discussion of this progress and the issues that still remain is the subject of these lectures.

5.3 Two-Hadron Systems

We begin by investigating systems that, in the infinite volume, non-relativistic sense, correspond to two-hadron systems.

5.3.1 Scattering Information from Finite Volume Energy Eigenvalues

In order to describe reality, we are fundamentally interested in physics in infinite volume Minkowski space-time. However, by necessity, current importance-sampling lattice QCD calculations are performed with a Euclidean metric and in a finite space-time volume. The restriction to Euclidean space-time places fundamental constraints on the physics that can be extracted [120], or at least constrains the way in which we can access particular physical observables. Similarly, the imposition of boundary conditions to reduce the system to a finite volume modifies the system in the infrared regime and must be accounted for. Nevertheless, for many single hadron observables, the analytic structure of the relevant correlation functions is such that Wick rotation does not present an obstruction. It is also the case that for single hadron correlation functions in the low energy regime, chiral perturbation theory (χPT) allows a model-independent extrapolation to infinite

volume. However, for infinite volume extrapolations of higher energy observables, such as form factors at momentum transfers, $Q > 1$ GeV, we must rely on more empirical studies of the volume dependence.

Multi-hadron systems present a more complex problem, and one in which effective field theory plays an important role. Understanding systems with the quantum numbers of multiple hadrons can be viewed as a matching of QCD correlations onto equivalent correlation functions in an effective hadronic description and this hadronic description is important in defining the observables that can be extracted. Hadrons are emergent collective degrees of freedom that arise from QCD dynamics, but they are the degrees of freedom that we are necessarily interested in because they define the asymptotic states of the infinite volume theory. QCD correlations that are amenable to an *effective* hadronic description are those in which it makes sense to consider dominant contributions from a finite, preferably small, number of hadronic degrees of freedom. Chiral perturbation theory provides such a description at low energy, but the concept is more general. For example, an effective hadronic description of the nucleon matrix element of the vector current at multi-GeV momentum transfer exists, but a chiral expansion of the process is not useful because of the large momentum that renders the power-counting useless. In lattice calculations of the three point functions that probe such a matrix element, the dominant contribution at large Euclidean times comes from transitions between single nucleon states at rest and boosted to the given momentum transfer (up to lattice artifacts that we ignore at present). Contributions from internal excitations of the nucleon and from nucleon+pion multi-hadron states[1] are suppressed in the Euclidean correlation functions by the relevant energy gap and only become important at early times.

For multi-hadron systems, an effective hadronic description allows us to understand the connection between Euclidean space lattice calculations and the Minkowski space hadronic quantities of the real world. Provided an effective hadronic description exists, physical information can be extracted by understanding the analytic structure of the hadronic theory. If the hadronic description is too complex to determine cleanly through matching to Euclidean QCD correlations, analytic continuation, or other methods of connecting to Minkowski space physics, become ambiguous. An example is provided by correlators with the quantum numbers of a minimum of two stable[2] hadrons (for example, $I = 2$, $J = 0$, even parity, corresponding most simply to two pion systems). In a finite volume, and at energies far below the inelastic threshold, the long time behaviour of the hadronic theory is dominated by two-body states of the lightest hadrons that can produce the required quantum numbers. In the absence of bound states, the most important contribution at large Euclidean times is from the two-hadrons at rest in the corresponding centre-of-mass (CoM) frame, but sub-leading contamination arises

[1] This is very loose terminology as the ground state should not be thought of as a bare object to which pions are added to get an excited state.

[2] At a minimum, stable under the strong interaction.

from two hadron state moving back-to-back in the CoM frame and from internal excitations of the hadrons. By careful analysis of multiple different correlators with the given quantum numbers, it is possible to extract information about these states. Crucially, the hadronic description allows us to understand the analytic structure of the two-hadron correlators in this regime and determinations of the energies of these states translate to extractions of the scattering phase shift through the Lüscher formalism [117, 125, 227] (see also [228]) to be discussed below. At earlier times, or with more complicated sets of correlation functions, contributions from higher energy states of the given quantum numbers begin to be resolved and eventually more complex $N > 2$ hadron states make significant contributions, resulting in different analytic structure in the correlation function. If we can construct an effective hadronic description in this regime and determine enough information (at high enough precision) about the various contributions by matching to the finite-volume, Euclidean QCD correlators, we can in principle determine infinite volume Minkowski space information in the inelastic regime. If such an hadronic description is ambiguous, then model dependence necessarily arises. It should be noted that the effectiveness of a hadronic description is volume dependent; as the volume increases, the number of finite volume states in a given energy range increases making a hadronic description more cumbersome. If one is interested in information about states other than the ground state, this becomes increasingly difficult to reliably extract—an important part of the obstruction discussed by Maiani and Testa [120].

For two-particle interactions, the constraints that the Euclidean formulation imposes have been famously circumvented by the work of Lüscher [117, 125, 227] which showed that the finite volume two-hadron energy spectrum below the inelastic threshold depends in a calculable way on the phase-shift in the appropriate scattering channel. The allowed energies are quantised, with the quantisation condition depending explicitly on the two-particle phase shift. As a corollary, calculations of these energies can be used to extract the phase-shift up to the inelastic thresholds. This result has been known for many years in the context of quantum mechanical systems [229–231] but Lüscher demonstrated that this remains true in the context of relativistic quantum field theory up to corrections that are exponentially suppressed in the large volume limit. We shall first discuss this classic result before turning to more recent generalisations in subsequent subsections.

In general, systems confined in any kind of finite volume have momentum modes that are restricted or quantised in some way. For free particles in one-dimension, of size L with periodic boundary conditions, the allowed modes are plane-waves of momentum $k_n = \frac{2\pi n}{L}$ for integer n. In the presence of finite range interactions these are modified. Using translational invariance, we can consider the two particle system as one particle moving in a potential generated by the other particle, and since the interaction is of finite range, the potential is non-zero only in some finite region which we assume to be in the interior of the finite volume. The quantisation condition is then modified in a way that is encapsulated in the phase shift induced by the potential as we require that the wavefunction in the interior of the potential

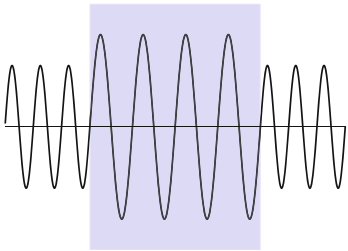

Fig. 5.1 One-dimensional scattering wavefunction amplitude. The *shading* shows the interaction region in which the wavefunction is modified

must match on to the plane-wave wavefunction in the region outside the interaction, as well as being periodic. That is, the quantisation condition becomes

$$k_n\, L + 2\,\delta(k_n) = 2\,\pi\, n\,. \tag{5.5}$$

with an example wavefunction shown in Fig. 5.1 for a simple square-well potential.

Proceeding to a three-dimensional cubic spatial volume of periodicity L in each direction, the allowed modes are again quantised, but the quantisation condition is more complicated. This is most easily derived in the context of effective field theory as first expounded in [232],[3] and that is the approach we take here. Consider a non-relativistic,[4] spin-less species of particles, ϕ, whose dynamics are described by the Lagrangian

$$\mathcal{L} = \mathcal{L}_0 + C_0(\mu)(\phi^\dagger\phi)^2 + C_2(\mu)(\phi^\dagger\nabla\phi)^2 + \ldots \tag{5.6}$$

where $\mathcal{L}_0$ is the free Lagrangian and the couplings, C_{2n}, depend on the renormalisation scale μ. For this simple example, we will assume that the allowed couplings are only s-wave in nature. The scattering amplitude is given by the geometric series shown in Fig. 5.2 which can be resummed as

$$\begin{aligned}\mathcal{A} &= \left[\sum_n C_{2n}(\mu)\,p^{2n}\right] + \left[\sum_n C_{2n}(\mu)\,p^{2n}\right] I_0 \left[\sum_n C_{2n}(\mu)\,p^{2n}\right] \\ &\quad + \left[\sum_n C_{2n}(\mu)\,p^{2n}\right] I_o \left[\sum_n C_{2n}(\mu)\,p^{2n}\right] I_o \left[\sum_n C_{2n}(\mu)\,p^{2n}\right] + \ldots \\ &= \frac{\left[\sum_n C_{2n}(\mu)\,p^{2n}\right]}{1 - I_0\left[\sum_n C_{2n}(\mu)\,p^{2n}\right]}\,,\end{aligned} \tag{5.7}$$

[3] See also the original derivation [125, 227] or [123] for a particularly clear alternate derivation.

[4] Working with relativistic particles does not modify the resulting expressions. In the non-relativistic context, the relativistic corrections can be accounted for by changes in higher-derivative operators.

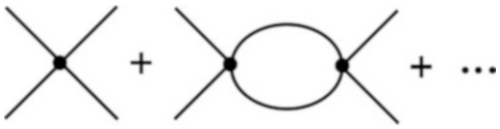

Fig. 5.2 Contributions to the two particle scattering amplitude. The blobs represents the insertion of the interactions

where the infinite volume loop integral is given by

$$\begin{aligned} I_0(\mu) &= \left(\frac{\mu}{2}\right)^{4-d} \int \frac{d^{d-1}\mathbf{q}}{(2\pi)^{d-1}} \frac{1}{E - |\mathbf{q}|^2/M + i\,\epsilon} \\ &\xrightarrow{PDS} -\frac{M}{4\pi}(\mu + i\,p) + \mathcal{O}(d-4)\,, \end{aligned} \tag{5.8}$$

E is the centre-of-mass energy of the system and M is the mass of the particles. In the second line of Eq. (5.8), we have chosen the PDS subtraction scheme [233] to define the integral and couplings and set $p = \sqrt{M\,E}$. The renormalisation scale dependence of the loop integrals is exactly cancelled by that of the couplings $C_{2n}(\mu)$. In terms of the scattering phase shift, $\delta(p)$, the infinite volume scattering amplitude is given by

$$\mathcal{A} \equiv \frac{4\pi}{M} \frac{1}{p\,\cot\delta(p) - i\,p}\,. \tag{5.9}$$

Equating this with Eq. (5.7), one can read off that $\mu + \frac{4\pi}{M}\left[\sum C_{2n}(\mu)\,p^{2n}\right]^{-1} = p\,\cot\delta(p)$. For future discussion, it is useful to define the effective range expansion of the phase shift

$$p\,\cot\delta(p) = -\frac{1}{a} + \frac{r}{2}p^2 + \sum_{i=2}^{\infty} q_i\,(p^2)^i\,, \tag{5.10}$$

in terms of the scattering length, a, the effective range, r and the shape parameters, q_i (this form is analytic around $p = 0$). The expansion is valid for momenta below any possible cuts and thresholds and there is a straightforward relationship between the parameters in the effective range expansion and the couplings, C_{2n}, in the Lagrangian.

In a finite volume, the eigen-energies of the system are signalled by poles in the two-particle scattering amplitude. Since the allowed momentum modes are restricted in finite volume, the denominator of Eq. (5.9) is modified and we seek zeros of

$$\frac{1}{\sum C_{2n}(\mu)\,p^{2n}} - Re\left[I_0^{PDS}(L;\mu)\right] = 0 \tag{5.11}$$

using the same subtraction scheme. Here, $I_0^{PDS}(L,\mu)$ is the finite volume form of the regulated integral in Eq. (5.8) that is defined with the intermediate help of a cutoff regulator as

$$I_0^{PDS}(L;\mu) = \frac{1}{L^3}\sum_{\mathbf{k}}^{\Lambda}\frac{1}{E-|\mathbf{k}|^2/M} - \int^{\Lambda}\frac{d^3\mathbf{k}}{(2\pi)^3}\frac{M}{|\mathbf{k}|^2} + \int^{PDS}\frac{d^3\mathbf{k}}{(2\pi)^3}\frac{M}{|\mathbf{k}|^2} \quad (5.12)$$

$$= \frac{1}{L^3}\sum_{\mathbf{k}}^{\Lambda}\frac{1}{E-|\mathbf{k}|^2/M} - 4\pi\Lambda - \frac{M\,\mu}{4\pi}\,, \quad (5.13)$$

which we note is independent of Λ. Combining Eqs. (5.9), (5.11), and (5.13), and writing the sum over allowed momentum modes in terms of the integer triplets $\mathbf{n} = \frac{L}{2\pi}\mathbf{k}$, this reduces to

$$p\,\cot\delta(p) = \frac{1}{\pi L}\left[\sum_{\mathbf{n}}^{\Lambda_n}\frac{1}{|\mathbf{n}|^2-\left(\frac{pL}{2\pi}\right)^2} - 4\pi\Lambda_n\right] \equiv \frac{1}{\pi\,L}S\left(\frac{pL}{2\pi}\right)\,, \quad (5.14)$$

where the integer cutoff $\Lambda_n = \frac{L\,\Lambda}{2\pi}$. This is the quantisation condition that allowed values of the momentum $p = |\mathbf{p}|$ must satisfy. There are two ways in which it can be used. Firstly, if the phase shift is known as a function of momentum, the allowed scattering momenta, p_i, can be predicted, and assuming the validity of the relativistic dispersion relation, thereby the energy spectrum, $E_i = 2\sqrt{m^2+p_i^2}$. Secondly, if one determines some number of the energies of states in the spectrum, E_i from numerical calculations, they determine scattering momenta $p_i = \sqrt{E_i^2/4-m^2}$ for which Eq. (5.14) is satisfied and thereby allow the extraction of the scattering phase shift at those momenta.

A number of comments are in order at this point.

- The quantisation condition above was first derived [125, 227] using analytic continuation to regulate the divergent sum contained in the function $S(\eta)$ whereby it is represented by the three-dimensional Epstein ζ-function,

$$\mathcal{Z}_{00}(s,\eta) = \frac{1}{\sqrt{4\pi}}\sum_{\mathbf{n}}\frac{1}{(|\mathbf{n}|^2-\eta)^s}\,, \quad (5.15)$$

  defined via analytic continuation for $s \leq 3/2$. The original form of the quantisation condition is

$$e^{2\,i\,\delta(p)} = \frac{\mathcal{Z}_{00}\left(1,\frac{p^2L^2}{4\pi^2}\right)+\frac{i\sqrt{\pi}}{2}Lp}{\mathcal{Z}_{00}\left(1,\frac{p^2L^2}{4\pi^2}\right)-\frac{i\sqrt{\pi}}{2}Lp} \quad (5.16)$$

and, as the choice of regularisation does not affect physical quantities, the two quantisation conditions are equivalent. The quantisation condition is valid for volumes large compared to the effective range of the interaction, $L \gg r$. In the effective field theory approach, this stems from requiring locality of the interactions. In the original derivation, the requirement arises from there being a region inside the lattice volume where the two-particle wavefunction takes its asymptotic, non-interacting form.

- The simple form above assumes a single $L = 0$ scattering channel that subduces to the A_1^+ cubic irrep and neglects the effects of mixing of $L = 4, 6, \ldots$ partial waves into the A_1^+ cubic irrep. The equation is also valid only for systems whose centre-of-mass is at rest relative to the spatial boundary conditions. These limitations can be overcome as will be discussed below.
- The relation of the eigen-energies to the scattering momenta above assumes the continuum dispersion relation for the hadronic components. This is modified in an unknown way by the lattice discretisation and necessarily introduces uncertainty into the extracted phase shift. Nevertheless, in many calculations, the single hadron dispersion relations have been investigated numerically (see for example [234]) and, within statistical uncertainties, are well represented by the continuum dispersion relation at the relevant low momenta, so it is likely that such effects are not large.
- For weakly interacting systems, where $a, r \ll L$, it is possible to perform an expansion of the quantisation condition, Eq. (5.14), around the non-interacting momentum poles, $p^2 = \frac{4\pi^2}{L^2}|\mathbf{n}|^2$ [125,227]. This leads to a set of relations such as

$$\Delta E_0 = \frac{4\pi a}{ML^3}\left(1 - c_1\frac{a}{L} + c_2\frac{a^2}{L^2} + \ldots\right), \tag{5.17}$$

  for the ground state energy shift, where $c_1 = -2.837297$ and $c_2 = 6.375183$. Similar relations for excited state energy levels can be constructed.
- The above analysis explicitly encompasses only those effects in which particles are on shell inside the loop integral/sum. Additional quantum contributions from virtual particles (where the sum of the energies of all the particles is larger than the energy of the scattering particles) also occur and give rise to additional volume dependence that is exponentially small. For a virtual particle of mass m, the corrections are $\mathcal{O}(e^{-mL})$, and in most cases the pion is the lightest relevant particle and dominates these sub-leading effects. For $\pi\pi$ and NN scattering, these effects have been investigated to one loop order in [235,236].
- For similar reasons, the analysis above is limited to scattering momenta below the appropriate inelastic threshold where additional intermediate states can go on-shell and information beyond the elastic scattering phase shift is needed.

5.3.2 *Boosted Systems, Asymmetric Systems, and Systems with Unequal Masses*

There have been a number significant generalisations of the Lüscher formalism since its inception, primarily concerning scattering states in less symmetrical cases. There are multiple ways in which the scattering of two hadrons can be less symmetric: the system can have momentum relative to the boundary conditions, the boundary conditions can be asymmetric, one can be interested in higher partial waves/irreducible representations of the cubic group other than the A_1^+ representation, or the two hadrons can be unequal in some regard such as their mass. All of these situations have been addressed at some level and below I only briefly summarise the current understanding.

Eigenstates of the lattice calculation are classified by the irreducible representations of the appropriate symmetry group (for a cubic spatial volume and a spatially isotropic discretisation, this is the octahedral group and its double covering for spinorial representations) and are more constrained than in the continuum, infinite volume limit. Two-particle eigen-energies hence determine a combination of the infinite volume partial wave phase shifts. The symmetries are further reduced when the eigenstates that are studied are boosted relative to the lattice boundary conditions, or when a rectangular rather than cubic spatial volume is considered (see [237, 238] in the latter case). For moving systems, Rummukainen and Gottlieb [122] provided the first analysis and this has been generalised in recent years [123, 124, 130, 239–243]. By performing different boosts of the system, many more energy eigenstates can be accessed in a single lattice calculation, resulting in a more detailed extraction of phases shifts. Boosted systems of unequal mass have been treated in [244, 245] and boosted bound states have been investigated in [246, 247]. Scattering in the case of multiple two-particle channels has been considered in a number of contexts in [130, 241, 242, 248–251] and a detailed investigation of higher partial waves has been recently presented in [252]. A number of other interesting developments in this context have also been reported recently [253–264].

A further way in which phase shifts can be accessed at a larger range of energies is by the use of *twisted boundary conditions* in which quarks pick up an additional phase at one of more of the boundaries [265]. Considering for simplicity a twist in the quark boundary conditions in the z direction alone, quarks satisfy

$$q(\mathbf{x} + \hat{\mathbf{z}}\, L) = e^{i\phi} q(\mathbf{x})\,, \tag{5.18}$$

and in this case, the free two particle energy levels are shifted to $\frac{2\pi}{L}(n_x, n_y, n_z + \frac{\mathcal{N}}{3}\frac{\phi}{2\pi})$, where $\mathcal{N}$ is the baryon number of the scattered particles.[5] Equation (5.18)

[5] With flavour independent boundary conditions, quarks and anti-quarks receive equal and opposite twists so mesonic systems are unaffected. One can introduce *flavour-twisted boundary conditions*

is equivalent to the imposition of a constant vector potential. Correspondingly, the Lüscher quantisation condition, Eq. (5.14), is modified by the replacement

$$S\left(\frac{pL}{2\pi}\right) \longrightarrow S\left(\frac{pL}{2\pi},\phi\right) = \sum_{\mathbf{n}}^{\Lambda_n} \frac{1}{|\tilde{\mathbf{n}}|^2 - \left(\frac{pL}{2\pi}\right)^2} - 4\pi\Lambda_n \tag{5.19}$$

where $\tilde{\mathbf{n}} = (n_x, n_y, n_z + \frac{\mathcal{N}}{3}\frac{\phi}{2\pi})$. In order for the theory to be QCD, the modified boundary conditions must be applied for both the sea quarks used in the lattice generation and the valence quarks used for measurements. This is an expensive task and it is interesting to consider the case of *partially twisted boundary conditions* in which only the valence quarks see the twisted boundary conditions. This theory is a partially-quenched cousin of QCD; it has been shown that for simple cases such as NN or $I = 2\ \pi\pi$ scattering physical information can be obtained, but care must be taken in cases where the unitarity violations that partial twisting induces become evident such as for $I = 0\ \pi\pi$ scattering or $\Delta I = 1/2\ K \to \pi\pi$ decays [271, 272].

5.3.3 Resonances

Most hadrons that are listed in the Review of Particle Properties [72] are in fact not asymptotic states, but occur as resonances in scattering channels of asymptotically stable states.[6] When they are sharply localised in energy, such resonances can be effectively characterised by a mass and a width, or correspondingly a pole position in the complex energy plane (although the full phase shift in the channel contains more information than this simplest parameterisation).

It is of significant interest to investigate what lattice QCD can determine about resonances such as the ρ-meson or the Δ baryon. As in experiment, in lattice QCD resonances manifest as rapid motion of the phase shift in the corresponding scattering channel which in turn gives rise to particular patterns in the energy levels that the system exhibits as a function of the center-of-mass momentum or the lattice volume. This was first investigated in [121, 273, 274] and has been the subject of much attention in recent years because of the phenomenological importance in the context of ongoing and planned experimental spectroscopy efforts in the light and charm sectors [275–277]. The central observation is that the presence of the

[266–270] to modify flavour non-singlet mesonic quantisation conditions, but this introduces difficulties in importance sampling and can only be easily implemented for valence quarks.

[6] Only states that are the lightest state with a given set of quantum numbers are asymptotically stable: for hadrons composed of light and strange quarks, only the pion, kaon, proton and Λ, Ξ and Ω baryons are stable under the strong interaction. Interestingly, at unphysically heavy quark masses and finite volume, a number of other states such as the ρ and Δ become stable because the pion mass increases more rapidly than that of other hadrons as the quark masses increase.

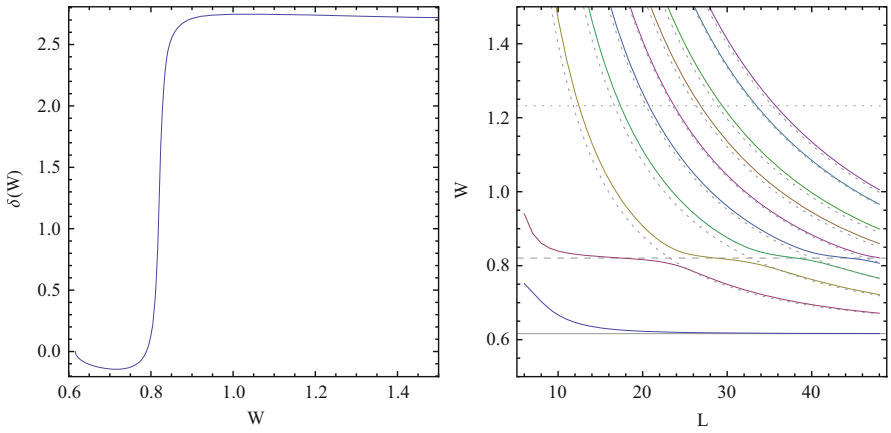

Fig. 5.3 Phase shift and energy spectrum (lowest ten energy levels shown) of the simple model of Eq. (5.20). The *solid, dashed and dotted horizontal lines* correspond to the elastic threshold at $2m_\phi$, to m_ρ, and to the inelastic threshold at $4m_\phi$, respectively. The *dotted curves* show the free particle energy levels

resonance does not manifest in a single energy level, but through the behaviour of multiple energy levels as a function of the lattice volume. This is best illustrated by an example; following [278], we choose a phase shift

$$\delta(p) = -\lambda_R \frac{p}{16\pi W} + \frac{g_R^2}{32\pi W p} \log\left[1 + \frac{4p^2}{m_\rho^2}\right] - \arctan\left[\frac{g_R^2 p}{16\pi W} \frac{1}{W^2 - m_\rho^2}\right], \tag{5.20}$$

where $m_\phi = 0.31$, $m_\rho = 0.82$, $g_R = 1.5$, $\lambda_R = 48$ and $W \equiv 2\sqrt{p^2 + m_\phi^2}$. This phase shift approximately describes $\phi\phi$ scattering in a $3+1$ dimensional model of two coupled Ising spins, ϕ and ρ with an interaction term $\phi^2\rho$ and exhibits a narrow resonance. Figure 5.3 shows the phase shift and the corresponding spectrum in the centre-of-mass frame, with the presence of the additional level associated with the resonance being clear.

In order to determine the resonance position with accuracy, it is important to map out multiple measurements of the phase shift in the resonant energy region. This can be done by making use of extractions of multiple excited state energies from multiple different correlation functions, the use of multiple different volumes, and by determining energies in systems that are boosted relative to the boundary conditions [122]. A recent review of different techniques to analyse these systems is given in [279] and a recent numerical example is discussed below.

5.3.4 Bound Systems

For two-hadron bound states, of energy $E_2 < 2M$, the Lüscher quantisation condition also applies and can be used to ascertain the expected dependence of the bound state energy on the lattice volume. To see this, we note that the $S(\eta)$ function occurring in the quantisation condition has a useful alternative representation for imaginary values of it argument (an imaginary scattering momentum correspond to a two-hadron energy that is less than the sum of the individual hadron masses) that is

$$\begin{aligned} S(i\,\eta) &\equiv \sum_{\mathbf{n}}^{\Lambda_j} \frac{1}{|\mathbf{n}|^2+\eta^2} - 4\pi\Lambda_j \\ &= -2\,\pi^2\,\eta + \pi \sum_{\mathbf{m}\neq 0} \frac{1}{|\mathbf{m}|} e^{-2\pi|\mathbf{m}|\eta}\,. \end{aligned} \tag{5.21}$$

To derive this *Chowla-Selberg form*, the Poisson resummation formula has been used, see [280] for further discussion and extension. From Eq. (5.9), it is clear that a bound state at infinite volume is signalled by a zero of the denominator at $i\,\cot\delta(p) = -1$. Inserting Eq. (5.21) into the quantisation condition, Eq. (5.14), for $p = i\,\kappa$ we see that it reduces to

$$i\,\cot\delta(p)|_{p=i\kappa} = -1 + \sum_{\mathbf{m}\neq 0} \frac{1}{|\mathbf{m}|\kappa L} e^{-|\mathbf{m}|\kappa L}\,, \tag{5.22}$$

showing that the finite volume contamination of bound state energies is exponential in form [232,281]. In the infinite volume limit, this reduces to the expected form and the momentum κ approaches the binding momentum of the system, $\gamma = \sqrt{M\,B_E}$ where $B_E = |E_2 - 2M|$ is the binding energy. As discussed above, the Lüscher analysis does not account for polarisation effects and there are additional finite volume effects arising from virtual states (pions) propagating around the lattice boundary, giving rise to contributions $\sim e^{-m_\pi L}$ as for single hadron systems.[7] For shallow bound states, in which the binding energy and binding momentum become very small, the volume effects $\propto e^{-\gamma L}$ dominate and make it difficult to study such systems in realistic lattice volumes. A notorious example is set by the deuteron which at the physical values of the quark masses has a binding energy of 2.2 MeV, corresponding to a binding momentum $\gamma_d \sim 40$ MeV; in this case, modification of the bound state wavefunction by the boundaries is exponentially worse than the effects of pions propagating around the boundaries. An interesting attempt to reduce these effects is presented in [247] where bound states are considered for

[7] In the strict definition of a hadron as a localised colourless asymptotic state, what we refer to as a multi-hadron bound state is itself a hadron.

different centre-of-mass momenta relative to the boundary conditions and combined to provide an extraction of the infinite volume binding momentum with corrections that are suppressed to $\sim e^{-2\gamma L}$.

5.3.5 *Lattice Wavefunctions and Potentials*

Following the discussion of Bethe-Salpeter (BS) wavefunctions in Lüscher's original works, a method to directly extract information on two-hadron wavefunctions has been developed in [282–284]. The asymptotic form of a two-particle wavefunction is known outside the range of the interaction but is characterised by the scattering phase shift in the respective channel. By determining the large distance part of the wavefunction and fitting to the known form, scattering information can be obtained. This was pioneered for the $I = 2\ \pi\pi$ system in [284] and enabled the extraction of the phase shift.

The HALQCD collaboration has further pursued this approach and produced a method of extracting inter-hadron potentials for two-hadron systems [285] that we briefly overview and discuss (see [286] for a recent review). The method proceeds by defining the BS wavefunction from QCD correlation functions

$$G(\mathbf{r}, t - t_0; J^P) = \sum_{\mathbf{x}} \left\langle 0 \left| h^{(1)}(\mathbf{x}, t) h^{(2)}(\mathbf{x} + \mathbf{r}, t) \overline{J}(t_0; \{Q\}) \right| 0 \right\rangle , \quad (5.23)$$

where $h^{(i)}$ are sink interpolators that annihilate hadrons at time t and $\overline{J}(t_0; \{Q\})$ is a source interpolating function for the two hadron system with quantum numbers, $\{Q\}$, typically specifying the total momentum, angular momentum (or more accurately, the irrep of the lattice symmetry group), parity, and flavour. In our discussion, we suppress indices on the interpolating operators for simplicity (they can be subsumed into the definition of the quantum numbers). The projection to particular quantum numbers at the source is sufficient to define the quantum numbers of states that contribute to the correlation function at all times. We note that while the correlators are labelled by $\mathbf{r}$, this is *not a quantum number*; for short separations, $|\mathbf{r}| < 1/\Lambda_{\text{QCD}}$, the two hadrons overlap significantly and $\mathbf{r}$ is essentially meaningless, while for large $\mathbf{r} \gg 1/\Lambda_{\text{QCD}}$, the separation can only be defined up to a resolution scale of the size of a hadron. For calculations with an infinite temporal extent, this correlator can be written as

$$G(\mathbf{r}, t - t_0; \{Q\}) = \sum_{n=0}^{\infty} A_n \, \psi^{(n)}(\mathbf{r}; \{Q\}) \, e^{-E_n (t - t_0)} \quad (5.24)$$

where the sum is over all eigenstates, $|n\rangle$, with the corresponding quantum numbers and

$$A_n \equiv \langle n|\overline{J}(0;\{Q\})|0\rangle, \tag{5.25}$$
$$\psi^{(n)}(\mathbf{r};\{Q\}) \equiv \sum_{\mathbf{x}} \langle 0|h_a^{(1)}(\mathbf{x},0)h_b^{(2)}(\mathbf{x}+\mathbf{r},0)|n\rangle\,.$$

Up to an irrelevant normalisation, the BS wavefunction $\psi^{(n=0)}(\mathbf{r},\{Q\})$ of the lowest energy state with the requisite quantum numbers can be extracted from the long time behaviour, $t - t_0 \to \infty$ where G behaves as a single exponential. This wavefunction can be used to define a non-local, energy-independent potential, U, below the inelastic threshold of the system through the Schrödinger equation

$$(E_{n=0} - H_0)\,\psi^{(n=0)}(\mathbf{r},\{Q\}) = \int d^3\mathbf{r}'\,U(\mathbf{r},\mathbf{r}')\,\psi^{(n=0)}(\mathbf{r}',\{Q\})\,. \tag{5.26}$$

Here, $H_0 = -\nabla^2/M$ (assuming henceforth that the two hadrons are the same mass, M, for simplicity) and $E_{n=0} \equiv 2\sqrt{|\mathbf{k}|^2 + M^2}$ defines the asymptotic relative scattering momentum $\mathbf{k}$ between the two hadrons. The nonlocal potential can be written in terms of local potentials as

$$U(\mathbf{r},\mathbf{r}') = V(\mathbf{r},-i\,\nabla)\delta^{(3)}(\mathbf{r}-\mathbf{r}')\,, \tag{5.27}$$

where

$$V(\mathbf{r},-i\,\nabla) = V_0(r) + \mathcal{O}(\nabla^2/M^2)\,, \tag{5.28}$$

where $r = |\mathbf{r}|$. Depending on the quantum numbers of the system under consideration, this expansion can also contain terms linear in the derivative operator; an example is for $J = 1$ two nucleons systems, where the spin vector, $\mathbf{S}$, of the system can be used to construct a spin-orbit term, $\mathbf{L}\cdot\mathbf{S}\,V_{LS}(r)$ where $\mathbf{L} = -i\,\mathbf{r}\times\nabla$. The above expansion is a velocity expansion and the corrections are relative to the hadron mass, typically scaling as $\Lambda_{\rm QCD}/M$ that sets the scale for excitations of the single hadrons.[8] With BS wavefunctions determined at many energies, Eq. (5.28) can be used to extract a large subset of local potentials and hence may provide a constrained approximation to the non-local potential, U, for energies where the expansion is convergent. If a single BS wavefunction is determined, the local potential V_0 can be extracted but is energy-dependent because of the neglect of the additional terms in Eq. (5.28). All numerical work so far has used the latter

[8] In the limit that the masses of both hadrons become infinite, only the first term in Eq. (5.28) survives and an energy-independent local potential can be defined [287–292]. In this limit, $\mathbf{r}$ also becomes a well-defined quantum number.

approach (see however [293]). Making this approximation, Eq. (5.26) reduces to (the superscript $n = 0$ is appended to V_0 to indicate the energy dependence)

$$(E_{n=0} + \nabla^2/M)\,\psi^{(n=0)}(\mathbf{r}, \{Q\}) = V_0^{(n=0)}(\mathbf{r})\,\psi^{(n=0)}(\mathbf{r}, \{Q\})\,, \tag{5.29}$$

which can be inverted to extract

$$V_0^{(n=0)}(\mathbf{r}) = \frac{1}{M}\frac{(\nabla^2 + |\mathbf{k}|^2)\psi^{(n=0)}(\mathbf{r}, \{Q\}))}{\psi^{(n=0)}(\mathbf{r}, \{Q\})}\,. \tag{5.30}$$

The BS wavefunction, and hence the potential, can be extracted from numerical lattice calculations of the correlator in Eq. (5.23). These objects are defined in finite volume, but presuming the lattice volume is large compared to the range of the potential (the same constraint that applies to the Lüscher method discussed above), can be extrapolated to infinite volume. The infinite volume potential can then be used in the Schrödinger equation to determine the physical quantity of interest, the scattering phase shift at the energy of the two hadron system in the lattice calculation.

A number of comments on this method and possible extensions are in order:

- As discussed above, in neglecting the non-locality of the potential in Eq. (5.28), energy dependence is introduced into the extracted potential and, from an ab initio point of view, the energy-dependent potential contains exactly the same information as the phase shift evaluated at the lattice energy. With the assumption of slowly varying behaviour of the phase shift, small extrapolations in energy may be justified; however such assumptions are invalid when the system becomes interesting because of resonance structures and threshold effects. Extrapolations of phase shifts to $p \sim 300$ MeV from two-body systems calculated essentially at rest (such as those presented in [286, 294, 295]) should be viewed with caution.
- The extracted potentials depend on the sink-interpolating operators used in the calculation [290, 296, 297] with significant modifications seen at short hadron separations from different smearings of the quark fields [298], for example. This is expected as potentials are not observable quantities. Indeed, the use of different interpolating operators results in the construction of different potentials that should be phase-shift equivalent at the given energy, but will produce different phase shifts at other energies. In [297], Birse reemphasised the ambiguities associated with potentials through the simple example of an attractive square well potential with a repulsive delta function coupling to an excited state at short distance.
- As the box size becomes large, the number of scattering states, which in the absence of interactions have energies $E_n = 2\sqrt{M^2 + 4\pi^2|\mathbf{n}|^2/L^2}$, below the inelastic threshold increases. In an attempt to deal with this pile up of states, [299] introduces a "time-independent" potential method. Returning to Eq. (5.26) and performing a weighted sum including the different n contributions, it is straightforward to see that the ratio

$$R(\mathbf{r}, t-t_0; \{Q\}) = \frac{G(\mathbf{r}, t-t_0; \{Q\})}{[C(t-t_0)]^2} = \frac{\sum_n A_n \psi^n(\mathbf{r}; \{Q\}) e^{-E_n(t-t_0)}}{[\sum_m Z_m e^{-e_m(t-t_0)}]^2}, \tag{5.31}$$

(where $C(t)$ is a zero-momentum-projected single hadron correlator and e_m are the single particle eigen-energies, with $e_0 = M$) satisfies the slightly more complicated Schrödinger-like equation

$$\left(-\frac{\partial}{\partial t} + \frac{1}{4M}\frac{\partial^2}{\partial t^2} - H_0\right) R(\mathbf{r}, t-t_0; \{Q\}) = \int d^3\mathbf{r}'\, U(\mathbf{r}, \mathbf{r}')\, R(\mathbf{r}', t-t_0; \{Q\}), \tag{5.32}$$

for the same $U(\mathbf{r}, \mathbf{r}')$ provided i) that terms other than the ground state in the denominator of Eq. (5.31) are negligible, and ii) that terms in the numerator of Eq. (5.31) that are not purely elastic hadron-hadron scattering states are also negligible. The breakup of terms contributing to the sum in the numerator is into asymptotic elastic scattering states that are two non-interacting hadrons of the type described by the BS wavefunction, and into other states such as three hadron states (for example, $|h_1\rangle|h_2\rangle|\pi\rangle$) or two hadron states of different individual nature (such as $|h_1\rangle|h_2^*\rangle$, where h_2^* is a internal excitation of hadron h_2). Near the chiral limit, the inelastic threshold where the other states become important is set by the addition of a single pion to the system, but for heavier values of the quark masses, internal excitations of single hadrons may give rise to a lower threshold.[9]

In order for this method to apply, one has to be *certain* that the time dependence of G arises purely from elastic scattering states. This is a challenging task as it would require complicated multi-exponential fits that completely describe the correlator in the relevant region by a sum of terms that have energies below the inelastic threshold and rule out the presence of contamination from states with energies above the inelastic threshold. Indeed one can consider interpolators that strongly overlap onto inelastic excited states rather than scattering states, for example, those that centre the two hadrons at the same location. Given this ambiguity, and the intrinsically ill-conditioned nature of multiple exponential fits (see [300]), an "inelastic-state free" extraction cannot be performed in practice, and the use of the "time-independent" method therefore introduces an uncontrolled systematic error in the extracted phase shifts, at least as currently applied. In addition, the contamination from states other than the ground state,

[9] In a finite volume, it is not obvious that any state can be purely an elastic state, a concept that requires asymptotic separations. Nevertheless, for large volumes, it is perhaps enough to invoke the cluster decomposition property.

which depends on the overlap of source and sink interpolators onto such states, introduces dependence on the source interpolator.
- The HALQCD approach has also been extended to consider the extraction of tensor and spin-orbit interactions and to the parity odd sector [301]. Extensions beyond the inelastic threshold are presented in [302], but the same limitations of energy dependence and source dependence and problems with the time-dependent method continue to apply.
- Finally, in [303], the potential method has recently been directly compared to the Lüscher method using the same lattice setup. The systematics of these approaches are different and the comparison is interesting.

5.3.6 Numerical Investigations

The scattering problem has been numerically studied over the years following the first lattice investigations of scattering in the Ising model [304], two-dimensional models [305, 306], four-dimensional O(4) models [307, 308], and quenched QCD [309] and finally in QCD [310]. In the last few years there has been a rapid growth of interest in full QCD calculations of two-hadron systems, and I attempt to summarise this recent work, discussing meson-meson scattering, meson-baryon scattering and baryon-baryon scattering before moving on to discuss dibaryon bound states.

5.3.6.1 Meson-Meson Scattering

There have been a number of recent investigations of various meson-meson scattering channels. For $\pi\pi$ scattering, the $I = 2$ channel is numerically the simplest to study and has received significant attention [311–316], and an important recent achievement has been a first extraction of the d-wave phase shift [126]. The $I = 0$ channel is technically more demanding as it involves quark-line disconnected contractions but it is phenomenologically interesting and is also important in the analysis of $\Delta I = 1/2$ $K \to \pi\pi$ decays and has also been studied recently [313, 317, 318]. The $I = 1$ P-wave $\pi\pi$ channel contains the ρ, the prototypical resonance, and many groups have recently presented investigations [319–323]. A particularly clean study on anisotropic lattices with multiple volumes, showing the structure of the resonance has appeared recently [127]. The phase shift extracted in this last work provides an exemplary demonstration of the finite volume analysis required to understand resonant behaviour and is reproduced in Fig. 5.4. By using multiple volumes and considering systems boosted in various ways with respect to the lattice boundaries, the phase shift has been mapped out over the entire elastic scattering region and clearly demonstrates the resonant nature of the system (the resonance is particularly narrow at the unphysical quark masses used in this study).

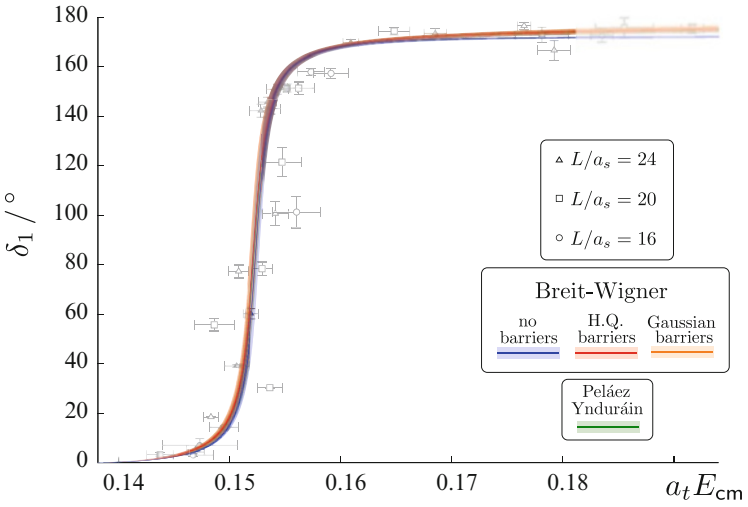

Fig. 5.4 Phase shift extracted for the $I = 1$ P-wave $\pi\pi$ scattering channel that contains the ρ resonance. Figure courtesy of J. J. Dudek following [127]

Systems involving kaons and heavy mesons have also been investigated, with studies of $K\pi$ scattering in $I = 1/2,\ 3/2$ [314, 324–327], KK scattering in $I = 1$ [314], $D\pi$ scattering [328, 329], DK [128], DD scattering [330–332], $J\psi$–ϕ scattering [333] and finally of Υ–π and η_b–π scattering using lattice non-relativistic QCD for bottom quarks [334]. Interestingly, in the case of open charm scattering [332], there are indications of a possible sub-threshold state with the quantum numbers of the phenomenologically interesting X(3872) state, although further studies of volume and lattice spacing dependence are needed.

5.3.6.2 Meson-Baryon Scattering

Meson-baryon systems are of significant phenomenological interest as, at least for πN, they can be studied experimentally. It is also possible that the $K^- n$ interaction plays an important role in the interior of dense stars where a kaon condensed phase may appear [335] depending on the strength of various interactions amongst kaons and nucleons (KK, Kn, Knn,...). In the last few years, there have been relatively few numerical studies of meson-baryon interactions. Following [336], in which various meson-baryon channels were investigated, the only recent studies have been of negative parity πN scattering [337] (see also [338]), and again of the annihilation-less channels [339], although there have been a number of phenomenological investigations referred to above.

5.3.6.3 Baryon-Baryon Scattering

Baryon-baryon scattering is also of great phenomenological interest, and for the nucleon-nucleon system, the results of many decades of experimental investigation offer the possibility of precision tests of lattice methods for two-hadron systems once calculations can be performed at the physical quark masses and the systematics of the lattice method are accounted for. Other baryon-baryon scattering channels are difficult to access experimentally and LQCD offers the prospect of providing more precise determinations of phase shifts than can be made experimentally in many cases and of providing the only determinations in other cases. Such extractions would materially improve our understanding of various aspects of nuclear astrophysics where the interactions of strange hadrons become important. There have been a number of recent investigations of baryon-baryon scattering parameters and phase shifts. In [340], hyperon–nucleon scattering and the consequences for dense nuclear matter were investigated, while [341] presents a study of the NN scattering lengths and effective ranges in $N_f = 3$ LQCD at the physical strange quark mass. All octet-baryon–octet-baryon channels have been investigated by the HALQCD collaboration in $N_f = 3$ [294, 342] and $N_f = 2 + 1$ [295] LQCD using the potential method discussed above and constructing phase shifts by neglecting the energy-dependence of the extracted potentials. LQCD also allows the investigation of more exotic scattering processes such as Ω–Ω scattering, as studied in [343].

5.3.6.4 Dibaryons

The last few years have seen remarkable progress in lattice calculations of baryon number $B = 2$ systems (dibaryons). In [345], the first calculation of a QCD bound-state with $B > 1$ was presented by the NPLQCD collaboration, albeit at unphysical values of the quark masses corresponding to $m_\pi \sim 390$ MeV. That calculation concerned the so-called H-dibaryon postulated many years ago [346]. Subsequent works have considered the H-dibaryon further and have also looked at other $B = 2$ systems including the deuteron, di-neutron and other more exotic channels [234, 294, 344, 347–349]. The results of these calculations are summarised in Fig. 5.5 for the deuteron, di-neutron, H-dibaryon and the strangeness $s = -4$ $\Xi^-\Xi^-$ system (for other channels where there are fewer calculations, the reader is referred to the original works). In both of the two nucleon channels, it is apparent that these systems become more bound as the quark masses increase and a naive linear fit suggests consistency with the bound deuteron and near threshold di-neutron system at the physical quark masses, although calculations at lighter quark masses are clearly required to investigate this quantitatively. The H-dibaryon is predicted, both in simplistic polynomial extrapolations [348] and in χPT-based extrapolations [350–352], to be very close to threshold at the physical values of the quark masses, but further calculations at lighter quark masses are also required

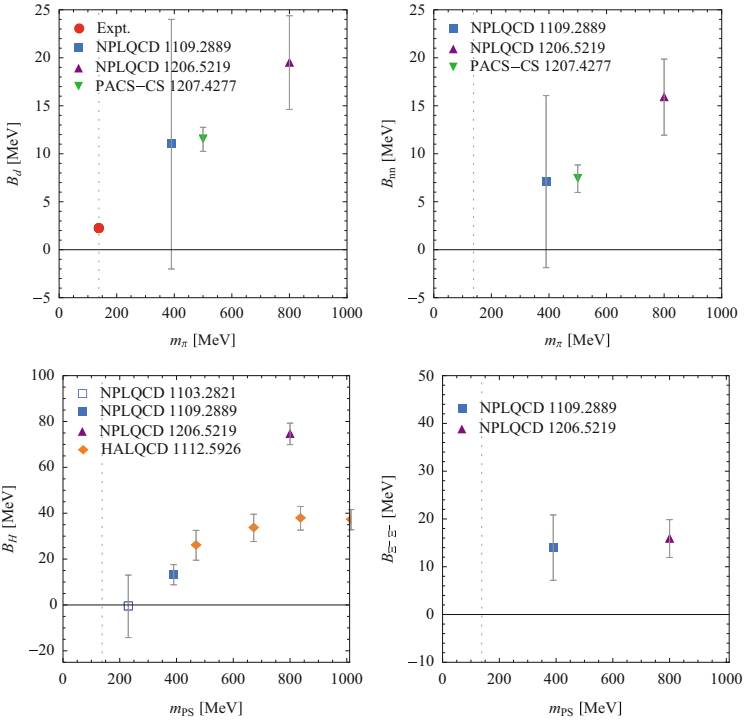

Fig. 5.5 Summary of the results obtained in $n_f = 2 + 1$ or $n_f = 3$ lattice QCD calculations of the binding energies of the deuteron, di-neutron, H-dibaryon and the strangeness $s = -4$ $\Xi^-\Xi^-$ system. In the case of the deuteron, the *red circle* corresponds to the experimentally determined binding energy. For the H-dibaryon, the results labelled HALQCD and NPLQCD 1206.5219 use three degenerate flavours of quarks and the point at $m_\pi = 230$ MeV (NPLQCD 1103.2821) should be treated with caution as no infinite volume extrapolation has been performed

to directly ascertain its nature and, as it appears to be a finely-tuned system, care must be taken to ensure that the effects of discretisation, isospin breaking, and electroweak contributions are correctly accounted for.[10] In the case of the H-dibaryon, it is also apparent that there is a significant discrepancy between the SU(3)$_f$ symmetric NPLQCD and HALQCD calculations at $m_\pi \sim 800$ MeV. This disagreement is further exacerbated by the calculation of bound deuteron and di-neutron states at this mass by the NPLQCD and PACS-CS collaborations, in direct contrast with the non-observation of these states by the HALQCD collaboration [294]. These two sets of calculations have fairly similar lattice discretisations and

[10]We note that all of the calculations discussed here are performed at essentially one lattice spacing, $a \sim 0.1$—0.12 fm in the isospin symmetric limit. It is expected that lattice artifacts, which are typically $\mathcal{O}(a^2)$ in these calculations, and isospin-breaking effects produce sub-leading modifications to dibaryon energies.

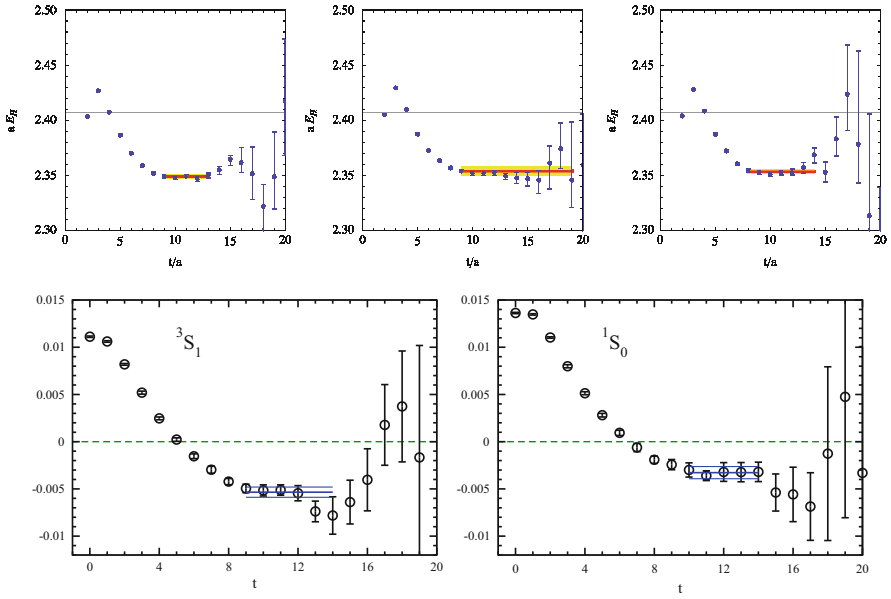

Fig. 5.6 *Upper row*: effective mass plots for one of the H-dibaryon correlators studied in [234] on three different volumes (3.4, 4.5 and 6.7 fm from left to right, respectively) that lead in the infinite volume limit to the result indicated by the upright triangle in the lower left panel of Fig. 5.5. The *horizontal line* indicates the two hadron threshold. *Lower row*: effective mass plots for the deuteron and di-neutron system at one volume (5.8 fm) associated with the PACS-CS data points in Fig. 5.5 (from [344])

volumes and the minor differences are unlikely to account for the discrepancy. These calculations also differ in methodology, with NPLQCD and PACS-CS (in the case of two-nucleon systems) performing spectroscopy in multiple volumes (see Fig. 5.6 for representative effective mass plots from the H-dibaryon study in [234]; also shown are effective mass plots from the two-neutron systems studied in [344]) and HALQCD using the potential method discussed above. These differences suggest that there may be systematic effects that are underestimated in one or both approaches and it is very important to resolve this discrepancy.

5.4 Multi-Hadron Systems: Theoretical Framework

The theoretical tools with which to understand the lattice calculations of systems with the quantum numbers of many hadrons are far less developed than those in the two-hadron sector. Nevertheless, this is an active area of research as the potential impact of such investigations is significant, both in nuclear physics where nuclei

present a plethora of example systems, and in particle physics where multi-hadron decays necessitate an understanding of the final state interactions in such systems.

5.4.1 Three-Body Systems

In the three body sector, investigations based on effective field theory have been presented in [353–360]. Very recently, a fully relativistic analysis based only on the properties of the three-particle scattering amplitude has been presented [361]. The program developed in these works allows three-hadron interactions to be extracted from a detailed analysis of the QCD spectra of two- and three-hadron systems at finite volume. However, such a numerical analysis has only been attempted in the case of pion systems where the interactions are perturbatively weak [314,362–364]. There are also attempts to extend the potential method to three-body systems [365].

5.4.2 Many-Meson Systems: Threshold Expansion

For hadronic systems with perturbatively small interactions, it has been possible to extend the finite-volume analysis to the case of arbitrary numbers of hadrons and provide a direct link between the ground state energies of multi-hadron systems and the underlying two-body, three-body, and, in principle, higher-body interactions. Following the classic works of Lee, Huang and Yang [230,231], and [353,354,366] developed an expansion of the energies of an n-boson system in terms of the particle number, the two- and three-body interactions and the size of the box. Considering spin-less particles, the interactions arise in a Hamiltonian form as

$$
\begin{aligned}
H = & \sum_{\mathbf{k}} h^\dagger_{\mathbf{k}} h_{\mathbf{k}} \left(\frac{|\mathbf{k}|^2}{2M} - \frac{|\mathbf{k}|^4}{8M^3} \right) \\
& + \frac{1}{(2!)^2} \sum_{\mathbf{Q},\mathbf{k},\mathbf{p}} h^\dagger_{\frac{\mathbf{Q}}{2}+\mathbf{k}} h^\dagger_{\frac{\mathbf{Q}}{2}-\mathbf{k}} h_{\frac{\mathbf{Q}}{2}+\mathbf{p}} h_{\frac{\mathbf{Q}}{2}-\mathbf{p}} \cdot \\
& \quad \left(\frac{4\pi a}{M} + \frac{\pi a}{M} \left(a r - \frac{1}{2M^2} \right) \left(|\mathbf{k}|^2 + |\mathbf{p}|^2 \right) \right) \\
& + \frac{\eta_3(\mu)}{(3!)^2} \sum_{\mathbf{Q},\mathbf{k},\mathbf{p},\mathbf{r},\mathbf{s}} h^\dagger_{\frac{\mathbf{Q}}{3}+\mathbf{k}} h^\dagger_{\frac{\mathbf{Q}}{3}+\mathbf{p}} h^\dagger_{\frac{\mathbf{Q}}{3}-\mathbf{k}-\mathbf{p}} h_{\frac{\mathbf{Q}}{3}+\mathbf{r}} h_{\frac{\mathbf{Q}}{3}+\mathbf{s}} h_{\frac{\mathbf{Q}}{3}-\mathbf{r}-\mathbf{s}} ,
\end{aligned}
\tag{5.33}
$$

where the operator $h_{\mathbf{k}}$ annihilates a boson with momentum $\mathbf{k}$ with unit amplitude, the two-body scattering length and effective range are a and r, and the three body momentum independent interaction is characterised by the parameter $\eta_3(\mu)$ which depends on the renormalisation scale, μ.

At $\mathcal{O}(1/L^7)$, the shift in energy of n bosons of mass M from the non-interacting case is given by [354]

$$\begin{aligned}\Delta E_n = \frac{4\pi\,\overline{a}}{M\,L^3}{}^nC_2\Bigg\{1 &- \left(\frac{\overline{a}}{\pi\,L}\right)\mathcal{I} + \left(\frac{\overline{a}}{\pi\,L}\right)^2\left[\mathcal{I}^2 + (2n-5)\mathcal{J}\right] \\ &- \left(\frac{\overline{a}}{\pi\,L}\right)^3\left[\mathcal{I}^3 + (2n-7)\mathcal{I}\mathcal{J} + \left(5n^2-41n+63\right)\mathcal{K}\right] \\ &+ \left(\frac{\overline{a}}{\pi\,L}\right)^4\Big[\mathcal{I}^4 - 6\mathcal{I}^2\mathcal{J} + (4+n-n^2)\mathcal{J}^2 + 4(27-15n+n^2)\mathcal{I}\,\mathcal{K} \\ &\qquad + (14n^3 - 227n^2 + 919n - 1043)\mathcal{L}\Big]\Bigg\} \\ &+ {}^nC_3\left[\frac{192\,\overline{a}^5}{M\pi^3L^7}\left(\mathcal{T}_0 + \mathcal{T}_1\,n\right) + \frac{6\pi\overline{a}^3}{M^3L^7}\,(n+3)\,\mathcal{I}\right] \\ &+ {}^nC_3\,\frac{1}{L^6}\,\overline{\overline{\eta}}_3^L + \mathcal{O}\left(L^{-8}\right) \quad , \end{aligned} \tag{5.34}$$

where the parameter $\overline{a}$ is the inverse phase shift at the given energy and is related to the scattering length and the effective range by

$$a = \overline{a} - \frac{2\pi}{L^3}\overline{a}^3 r\left(1 - \left(\frac{\overline{a}}{\pi L}\right)\mathcal{I}\right) \quad . \tag{5.35}$$

The geometric constants, $\mathcal{I}$, $\mathcal{J}$, $\mathcal{K}$, $\mathcal{L}$, $\mathcal{T}_{0,1}$, that enter into Eq. (5.34) are defined in [354] and ${}^nC_m$ are the binomial coefficients. The three-body contribution to the energy-shift given in Eq. (5.34) is represented by the parameter $\overline{\overline{\eta}}_3^L$ (which is closely related to $\eta_3(\mu)$ in Eq. (5.33), see [354]). This expansion of the energy shifts has been generalised to the case of two different species accurate to $\mathcal{O}(L^{-6})$ in [367].

The expansion above is valid when both the scattering length and effective range are small compared to the size of the box. Unlike the Lüscher analysis of two-body systems, this form is a perturbative approximation that works close to threshold and requires $\overline{a}/L \ll 1$ as well as $r/L \ll 1$ (as also required in the Lüscher approach). It is straightforward to expand the Lüscher result near threshold [125] and show that the $n = 2$ case of the above expression reproduces this expectation. In addition, it can be seen from Eq. (5.34) that this expansion requires that the system is dilute such that $n\overline{a}/L \ll 1$ as the factors in the square brackets in Eq. (5.34) grow with n. The breakdown of the expansion as n increases for fixed L, becoming less dilute, can be seen numerically [315].

5.4.3 *Many Baryon Systems*

Two issues complicate the extension of the above discussion to the case of many baryons. Firstly, the spin degree of freedom carried by baryons (or indeed, higher-spin bosons) complicates the interactions and one may expect a much more elaborate form for such energy shifts. More importantly, in multi-nucleon systems, the interactions are sufficiently strong such that bound states form and the applicability of the perturbative expansion used in Eq. (5.34) is limited. In order to fully understand the spectrum of such systems, a resummation must be performed, but an analytic form for this is not known beyond $n = 2$.

A practical approach to the problem may be to perform a purely numerical matching on to the appropriate hadronic effective theory. That is, to compute the finite volume spectrum of an A baryon system both in lattice QCD and in the effective field theory and to demand that they agree, thereby determining the appropriate low-energy constants of the EFT. While simpler than the A baryon lattice QCD calculations, finite volume A body EFT calculations are non-trivial to perform. A promising approach is perhaps to make use of the methods developed in [368, 369] and perform the calculations using a latticised version of the EFT that can be studied using Monte-Carlo methods.

5.5 Multi-Hadron Systems: Contraction Methods

A major part of the challenge of nuclear physics is in the complexity of the many-body problem that it encompasses. Even at the level of an effective description of nuclei in terms of nucleons, the combinatorics of multi-nucleon systems provide limitations to our ability to perform calculations [221, 370], and for large A, techniques that do not explicitly treat the A nucleons are currently necessary. At the fundamental level of QCD, the problem is seemingly even more difficult as each nucleon is made up of a minimum of three quarks.[11]

The machinery of calculating hadronic observables in LQCD begins with the construction of correlation functions as in Eq. (5.3). For simple quantities such as energies, a source and sink are chosen where, by the choice of appropriate combinations of quark and antiquark fields, states with the quantum numbers of the system in question are created and destroyed, respectively. To evaluate this matrix element, the creation and annihilation operators in the quark fields must be paired in all possible ways, forming various different Wick contractions. For a given nuclear system with atomic number A and proton number Z, the number of such contractions is $N_{\text{contractions}} = \prod_f N_f! \to (2A - Z)!(A + Z)!$ where N_f

[11] It is an interesting and subtle question as to whether a nucleus is indeed more complex than a proton; from the QCD point of view, both are complicated systems made of many quarks, anti-quarks and gluons.

is the number of quarks of flavour f, and the product runs over all such flavours (the second relation only follows for non-strange nuclear systems). Their evaluation consequently seems to be an exponentially difficult task for systems with large numbers of hadrons. The presence of symmetries, Pauli blocking and cancellations amongst contractions means that this counting can be a vast overestimate, but determining the minimal set of contractions, and the optimal way in which to perform them, is a non-trivial task.

5.5.1 Mesonic Systems

For the case of systems with zero baryon number but large isospin charge, I_z (which naively correspond to large numbers of charged pions), efficient algorithms have been developed to perform the required contractions. An important approach that was developed in [364] is recursive and is based on forming partly-contracted hadronic blocks which can then be combined sequentially to produce many pion correlation functions. This is illustrative of the sorts of ideas that can be used to speed up calculations of contractions and we briefly outline the steps involved for the case of a single source location, directing the reader to the original work for a more complete discussion.

A typical correlation function with the quantum numbers of $I = I_z = n$ is given by

$$C_{n\pi+}(t) = \left\langle \left(\sum_{\mathbf{x}} \pi^+(\mathbf{x},t) \right)^n \left(\pi^-(\mathbf{0},0) \right)^n \right\rangle , \tag{5.36}$$

where the quark-level interpolating operator $\pi^+(\mathbf{x},t) = \overline{d}(\mathbf{x},t)\ \gamma_5\ u(\mathbf{x},t)$ and $\pi^- = (\pi^+)^\dagger$. Integration over the fermionic degrees of freedom turns this into an expression involving quark propagators, with $(n!)^2$ terms. For the correlator above, which has identical source interpolators for each of the n terms in the source (the second parentheses), a twelve component anti-commuting Grassmann variable, η, can be introduced in order to write the correlation function as

$$\begin{aligned} C_{n\pi+}(t) &= n!\ \langle\ \left(\ \overline{\eta}_i\ A_{ij}(t)\ \eta_j\ \right)^n\ \rangle\ , \\ A_{ij}(t) &= \sum_{\mathbf{x}} \left[S(\mathbf{x},t;\mathbf{0},0)\right]_{ik} \left[S^\dagger(\mathbf{x},t;\mathbf{0},0)\right]_{kj}\ , \end{aligned} \tag{5.37}$$

after the quark field has been integrated over. Here, $S(x,y) = [\mathcal{M}(x,y)]^{-1}$ is the quark propagator and the indices run over spin and colour. The 12×12 matrix $A(t)$ forms the basis for recursively constructing a series of matrices $R_n(t)$ whose traces are the correlation functions above; formally,

$$[R_n]_{ij} = \overline{u}_i(0) d_k(0) \frac{\delta}{\delta d_k(0)} \frac{\delta}{\delta \overline{u}_j(0)} C_{n\pi+}, \qquad C_{n\pi+} = \langle R_n \rangle , \tag{5.38}$$

where $\langle \ldots \rangle$ indicates a trace over spin-colour indices. In terms of this, the following recursion relation can be readily derived

$$R_{n+1} = \langle\, R_n \,\rangle\, A \;-\; n\, R_n\, A\,, \tag{5.39}$$

with the initial condition that $R_1 = A$. This relation allows the evaluation of the correlators, C_n, with linear complexity.

Recursion relations have also been constructed for systems with multiple source locations and for systems containing different species of mesons. In addition, by making use of the closure of correlation functions when the 12 spin-colour degrees of freedom at a given source location are all used, descending recursion relations can be constructed (see [364] for details). A further version of these relations has been constructed in momentum space in [315]. It is interesting to note that the multiple source location problem can be addressed using the same recursion, Eq. (5.39). For N_s source locations $\mathbf{y}_1, \ldots, \mathbf{y}_{N_s}$, we can enlarge the definition of A to a $12N_s \times 12N_s$ matrix

$$\mathbf{A}(t) = \begin{pmatrix} A^{[11]}(t) & \ldots & A^{[1N_s]}(t) \\ \vdots & \ddots & \vdots \\ A^{[N_s 1]}(t) & \ldots & A^{[N_s N_s]}(t) \end{pmatrix}, \tag{5.40}$$

where

$$A^{[ij]} = \sum_{\mathbf{x}} S(\mathbf{x}, t; \mathbf{y}_j, 0)\; S^\dagger(\mathbf{x}, t; \mathbf{y}_i, 0)\;. \tag{5.41}$$

Using this matrix as the seed for the recursion, that is, taking $R_1 = \mathbf{A}$ and replacing A by $\mathbf{A}$ in Eq. (5.39), we generate $12N_s \times 12N_s$ matrices, R_n, whose traces over colour, spin and source site indices are correlators for the n pion systems for $0 < n < 12N_s$. In contrast to the single source correlators above, and to the multi-source correlators explicitly constructed in [364], these correlators are combinations of correlators of n pions coming from the N_s different source locations in all possible ways. Nevertheless, independent of the precise form of the interpolating operators that create them, the energies of the extracted eigenstates are the n pion system energies.

An number of alternative, even more efficient, approaches to many-meson contractions were developed in [315, 371] and make use of modified fast-Fourier techniques that use a divide-and-conquer approach to evaluate the contractions. These algorithms scale only polynomially with n and allow the investigation of systems with large isospin. The calculations become more involved however, as significant care must be taken in order to avoid numerical roundoff issues and obtain accurate results, necessitating the use of high- or arbitrary- precision libraries such as `qd` [372] and `arprec` [373]. Nevertheless, one of the approaches in [315] has been used in numerical calculations of systems with isospin charge up to $I_z = 72$, as will be discussed below.

By constructing appropriate "blocks" (the equivalent of the objects A in Eq. (5.37)), these approaches can also be applied for more general mesonic systems, including those with different species or with $I_z < |I|$, and to calculating three-point multi-meson correlation functions to study multi-meson matrix elements.

5.5.2 *Baryonic Systems*

In [374–376], algorithms have been developed to perform the more complex contractions that appear in multi-baryon systems with the aim of allowing studies of systems with large numbers of baryons. The fundamental approach used in these works is to perform contractions by iterating over a minimal list of indices of quark fields and corresponding weights.[12] Using the notation of [375], any nuclear two-point correlation function can be expressed as

$$\langle \mathcal{N}_1^h(t)\bar{\mathcal{N}}_2^h(0)\rangle = \frac{1}{\mathcal{Z}}\int \mathcal{D}\mathcal{U}\mathcal{D}q\mathcal{D}\bar{q}\ \mathcal{N}_1^h(t)\bar{\mathcal{N}}_2^h(0)\ e^{-\mathcal{S}_{QCD}}\,, \tag{5.42}$$

where the $\mathcal{N}_i^h$ are nuclear interpolating operators constructed from quark, and possibly gluon, fields. The source and sink interpolating operators must have commensurate quantum numbers, but there is an enormous degree of freedom in defining these operators. Generically, any such definition can be encapsulated in the following form

$$\bar{\mathcal{N}}^h = \sum_{k=1}^{N_w} \tilde{w}_h^{(a_1,a_2\cdots a_{n_q}),k} \sum_{\mathbf{i}} \epsilon^{i_1,i_2,\cdots,i_{n_q}}\,\bar{q}(a_{i_1})\bar{q}(a_{i_2})\cdots\bar{q}(a_{i_{n_q}})\,, \tag{5.43}$$

where the a_j are generalised indices that combine the colour, spin, flavour and space-time indices of the quark, $\mathbf{i}$ represents the n_q-plet $(i_1, i_2 \cdots i_{n_q})$ and $\epsilon^{i_1,i_2,\cdots,i_{n_q}}$ is a totally anti-symmetric tensor of rank n_q. The $\tilde{w}_h^{(a_1,a_2,\ldots a_{n_q})}$ are the weights for the given term in the sum and N_w is the total number of terms in the sum. To perform the contractions most efficiently, the number of weights is reduced to the minimum by applying explicitly the antisymmetrisation implied by the Grassmannian nature of the quark fields and by enforcing the symmetries of the state under consideration.

[12] The methods of [374, 375] differ in the way in which the lists of weights are constructed. Reference [374] iterates over the full, factorially-large set of possible index values, whereas [375] constructs the index lists recursively by building a multi-baryon system up one baryon at a time. In [376], the recursive approach is further developed with a clever definition of the antisymmetrisation operation.

The entire correlation function can then be constructed as

$$\langle \mathcal{N}_1^h(t)\bar{\mathcal{N}}_2^h(0)\rangle = \frac{1}{\mathcal{Z}}\int \mathcal{D}\mathcal{U}\,\det[\mathcal{M}]e^{-S_{\rm g}}\sum_{k=1}^{N_w}\sum_{k'=1}^{N_{w'}}\tilde{w}_{h_1}^{(a_1,a_2\cdots a_{n_q}),k}\,\tilde{w}_{h_2}^{(a'_1,a'_2\cdots a'_{n_q}),k'}$$
$$\times\sum_{\mathbf{i}}\sum_{\mathbf{j}}\epsilon^{i_1,i_2,\cdots,i_{n_q}}\epsilon^{j_1,j_2,\cdots,j_{n_q}}[\mathcal{M}^{-1}]_{a_{i_1}a'_{j_1}}\ldots[\mathcal{M}^{-1}]_{a_{i_{n_q}}a'_{j_{n_q}}}\,, \tag{5.44}$$

where, the quark fields have been integrated over and, as before, $\mathcal{M}$ is the Dirac operator and $S_{\rm g}$ is the gauge action.

This expression can be rewritten in a number of ways. Firstly, defining the matrix

$$G(\mathbf{a}';\mathbf{a})_{j,i} = \begin{cases}[\mathcal{M}^{-1}]_{a'_j;a_i} & \text{for } a'_j\in\mathbf{a}' \text{ and } a_i\in\mathbf{a}\\ \delta_{a'_j,a_i} & \text{otherwise}\end{cases}\,, \tag{5.45}$$

the correlator can be written as a sum of determinants

$$\langle \mathcal{N}_1^h(t)\bar{\mathcal{N}}_2^h(0)\rangle = \frac{1}{\mathcal{Z}}\int \mathcal{D}\mathcal{U}\,\det[\mathcal{M}]e^{-S_{\rm g}}\cdot \tag{5.46}$$
$$\cdot\sum_{k=1}^{N_w}\sum_{k'=1}^{N_{w'}}\tilde{w}_{h_1}^{(a_1,a_2\cdots a_{n_q}),k}\,\tilde{w}_{h_2}^{(a'_1,a'_2\cdots a'_{n_q}),k'}\,\det G(\mathbf{a}';\mathbf{a})\,,$$

where each term in the sum can be evaluated very quickly since the nontrivial part of the matrix G is relatively small. The cost of this approach for generic choices of interpolators is hidden in the number of terms contributing to the sums in Eq. (5.47) which can be very large. However, there are many choices of interpolating operators for which the number of reduced weights is small. As an example, a ^{4}He correlator can be evaluated with a single term in the sum by demanding that the weights are arranged so that they restrict all 12 quarks to be at a single point. By using multiple source locations, this idea can be extended to larger systems and in [375], correlators with the quantum numbers of ^{8}Be, ^{12}C, ^{16}O and ^{28}Si have been constructed and studied numerically.

A second way to make use of the above generic correlator form is to realise that it may be advantageous to construct multi-hadron states from localised colour-singlet single hadron states of particular momenta. While only the total momentum of the multi-hadron system is a quantum number, constructing states in this way appears to provide strong overlap onto scattering states [312, 341]. This can be formulated in terms of quark-level weights, but can be made more compact by defining nuclear interpolators first at a hadronic level:

$$\bar{\mathcal{N}}^h = \sum_{k=1}^{M_w}\tilde{W}_h^{(b_1,b_2\cdots b_A)}\sum_{\mathbf{i}}\epsilon^{i_1,i_2,\cdots,i_A}\bar{B}(b_{i_1})\bar{B}(b_{i_2})\cdots\bar{B}(b_{i_A})\,, \tag{5.47}$$

where M_w is the number of hadronic weights $\tilde{W}_h^{(b_1,b_2\cdots b_A)}$ (reduced to the minimal set through the application of possible symmetries), $B(b_i)$ are baryon interpolating fields and the b_i are generic indices that include parity, angular momentum, isospin, strangeness, and spatial indices. Equations (5.43) and (5.47) can be equated by replacing the baryon interpolating fields by a given quark level expression,

$$\bar{B}(b) = \sum_{k=1}^{N_{B(b)}} \tilde{w}_b^{(a_1,a_2,a_3),k} \sum_{\mathbf{i}} \epsilon^{i_1,i_2,i_3} \bar{q}(a_{i_1})\bar{q}(a_{i_2})\bar{q}(a_{i_3}) \,. \tag{5.48}$$

The original weights, $\tilde{w}_h$ in Eq. (5.43) can be expressed in terms of the hadronic and baryonic weights $\tilde{W}_h$ and $\tilde{w}_b$ through the convolution of Eqs. (5.47) and (5.48). In order to incorporate the quark propagators, we can define baryon blocks

$$\begin{aligned}\mathcal{B}_{a_1'a_2'a_3'}(b) \;&=\; \sum_{k=1}^{N_{B(b)}} \tilde{w}_b^{(a_1,a_2,a_3),k} \sum_{\mathbf{i}} \epsilon^{i_1,i_2,i_3} q(a_1')q(a_2')q(a_3')\bar{q}(a_{i_1})\bar{q}(a_{i_2})\bar{q}(a_{i_3}) \\ &\to \sum_{k=1}^{N_{B(b)}} \tilde{w}_b^{(a_1,a_2,a_3),k} \sum_{\mathbf{i}} \epsilon^{i_1,i_2,i_3} \cdot \\ &\qquad\qquad [\mathcal{M}^{-1}]_{a_{i_1}a_1'} [\mathcal{M}^{-1}]_{a_{i_2}a_2'} [\mathcal{M}^{-1}]_{a_{i_3}a_3'} \,,\end{aligned} \tag{5.49}$$

with the second line holding in a correlation function after integration over the quark fields. The complete correlation function can then be written in terms of these objects. Note that at the source (*or* the sink, but not both), we can uniquely associate the quarks to a particular hadron, but at the sink (or the source), this is not the case and the indices on $\mathcal{B}_{a_1'a_2'a_3'}(b)$ will be contracted amongst the weight factors arising from different hadrons.

In all of these approaches, there is still an intrinsically poor scaling with baryon number implied for all but the simplest choices of multi-baryon operators. For the simplest operators, the cost of contractions in manageable as it scales as A^3, but more complex operators require a larger set of terms (in the worst case, growing factorially with A) to be considered. There is considerable room for further improvements, with the goal being to find choices of operators that are both good interpolators onto the states of interest and are also computationally expedient.

5.6 Many Meson Systems

For many years, the many-body nature of nuclei, and the corresponding complexity of contractions, has dissuaded lattice QCD practitioners from tackling such systems. For this reason, significant effort has been devoted to studying the simplest multi-hadron systems, those with the quantum numbers of many pseudoscalar mesons

[314, 315, 362–364, 377]. Unlike multi-baryon systems, these systems do not suffer from exponentially growing statistical noise problems.[13] As discussed above, these systems have served as a useful testing ground for ideas related to the many-body nature of the multi-hadron systems in general. In terms of physics, pion and kaon gases have also proved interesting as they have enabled investigations of the physics of systems at non-zero isospin/kaon density. Three main avenues have been pursued as discussed below.

The first studies of multi-meson systems focused on $I \leq 5$ [362] and the $I \leq 12$ [363] systems and undertook an extraction of the energies of these states and, using Eq. (5.34), of the zero momentum, $I = 3$ three-pion interaction for the first time, finding it to be repulsive and commensurate with estimates based on naive dimensional analysis. These studies were followed up with investigations of multi-kaon systems [377] and mixed systems containing both pions and kaons [314]. Further studies of systems with even larger isospin charge [315, 378] also investigated the three pion interactions, but did not significantly improve on the previous extractions.

For larger isospin charge, it is more useful to think of the many-pion states that are created as corresponding to statistical systems of fixed isospin charge density (the "number of pions" in the system becomes ambiguous). In this way, it is possible to study the structure of the system as a function of isospin density. An important quantity that can be determined is the ground state energy density of the system as was studied in [315] and is shown in Fig. 5.7. The energy density displays a sharp peak at an isospin density, $\rho_I^{(\text{crit})} \sim 0.5\,\text{fm}^{-3}$ which provides a signal of the transition from a pion gas to a Bose-Einstein condensate (BEC) of pions as expected from analysis of the system in χPT [379]. An "effective isospin chemical potential" (it is the derivative of the ground state energy rather than the free energy) can be defined from the derivative of the energy with respect to the density. The transition to the BEC occurs at an isospin chemical potential $\sim 1.3 m_\pi$, close to the expectation from χPT. For even larger isospin density, the energy density appears to saturate, albeit with growing uncertainties. Based on asymptotic freedom, it is expected [379] that the system should undergo a crossover to a BCS state at large chemical potential. However, it is not clear whether the current numerical investigations reach high enough density to explore this regime.

In addition, the non-zero isospin density medium created by these correlation functions has been used to investigate its influence on other observables. The first such study considered the static quark potential between an infinitely heavy quark and anti-quark [380] where it was found that there is a screening effect caused by the presence of the isospin density. At low densities in the region of constant force (linear rising potential), the effect provides a screening of the force that is proportional to the density and independent of the separation. This work was

[13] For kaons there is a minor problem with the growth of noise.

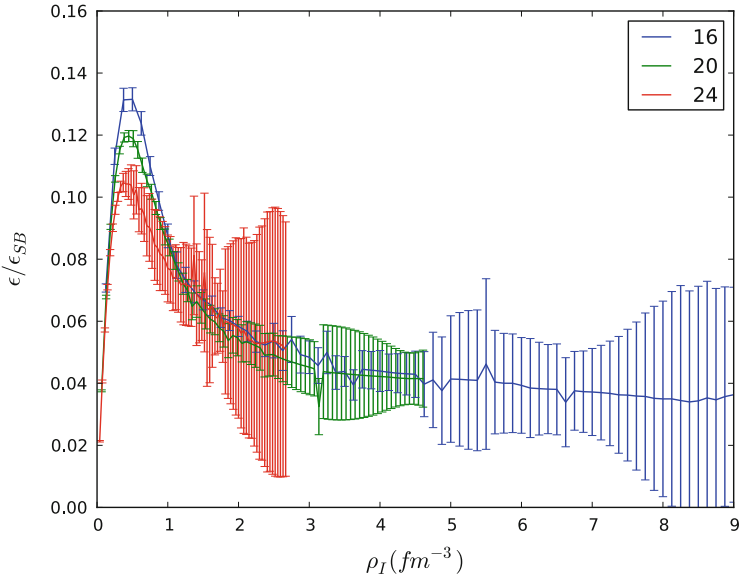

Fig. 5.7 The ratio of the energy density of isospin charged matter to that of a free gas is shown as a function of isospin density for three different lattice volumes (following [315]). The peak is conjectured to correspond to the transition of the system from a pion gas to a Bose-Einstein condensed phase

improved upon in [334] where a non-relativistic QCD formulation of b quarks was used to study correlation functions of bottomonium in the presence of isospin density. Again, a small but noticeable energy shift was extracted and the effects were commensurate with expectations of a potential model in which the above modifications of the potential were included. This study allowed investigations of higher density media than the original work and interesting behaviour was seen at densities corresponding to those where the peak in the energy density of the medium itself was observed.

As many of the important questions we are interested in nuclear physics are encoded in matrix elements rather than simply in the energy spectrum, it is important to understand how to extract multi-hadron matrix elements from QCD. A first attempt at this has been made in [381], where the first moment of the pion parton distribution has been investigated in the presence of a isospin density. Since the operator insertion is local, these results can be interpreted in terms of the modification of the single pion parton distribution in a medium with varying isospin charge and are a direct analogue of the famous EMC effect in nuclei. This is work in progress, and a number of subtleties involving the finite lattice volume and temporal extent remain to be investigated.

5.7 Nuclei and Hypernuclei

The lattice QCD study of nuclei started a few years ago with the high statistics investigation of the $\Xi^0\Xi^0 n$ and triton systems by the NPLQCD collaboration [382] at light quark masses corresponding to $m_\pi \sim 390$ MeV. In the relatively small volume used in this work, both states were consistent with being unbound but the ground state was clearly resolvable. Perhaps most importantly, this study showed that signals could be obtained for these states. As discussed in more detail below, the naive expectation is that multi-baryon correlation functions would have an exponentially decreasing signal-to-noise ratio as a function of Euclidean time [383], prohibiting useful analysis. In contrast, the study of [382] showed that at least for the chosen interpolating operators, there is a region of time (referred to as the "golden window") in which noise remains constant and physical information can be extracted for multi-baryon systems. This first study was followed up and extended by the PACS-CS collaboration who investigated ^{3}He and ^{4}He first in quenched QCD [384] and more recently in QCD with quark masses corresponding to $m_\pi \sim 500$ MeV [344]. After developing new contraction methods as discussed above [375], the NPLQCD collaboration have performed a comprehensive calculation of a large number of phenomenologically relevant nuclei and hyper-nuclei for $A < 5$, albeit at a heavy quark mass corresponding to $m_\pi \sim 800$ MeV [234]. Figure 5.8 shows a summary of the binding energies of the strangeness, $s = 0$ and $s = -1$ three- and four-body systems that have been investigated, and Fig. 5.9 shows results for these and the other more exotic systems investigated in [234]. Figure 5.10, shows representative effective mass plots for energy shifts in various multi-baryon systems; while they are not as clean as those for $A = 2$ in Fig. 5.6, significant negative energy shifts are readily apparent.

Using two body potentials extracted from LQCD, and solving the three- and four-body Schrödinger equations, the HALQCD collaboration have also investigated few-body systems [294]. As noted in this study, this approach neglects three- and four- body interactions, but provides an interesting guide as higher body forces are expected to be small. Indeed, the two-body interaction alone is sufficient to bind the ^{4}He state at SU(3)-symmetric quark masses where the pion masses are in the range $500\ \text{MeV} < m_\pi < 1200\ \text{MeV}$.

The improved contraction methods discussed above have also enabled the construction of correlation functions with the quantum numbers of significantly larger nuclei such as ^{8}Be, ^{12}C, ^{16}O and ^{28}Si [375], opening the way for studies of these systems. Examples of these correlations are shown in Fig. 5.11, and, while the correlators for $A < 20$ show signs of the expected approach to single exponential behaviour, no statistically meaningful binding energies could be extracted at the statistical precision used in this preliminary investigation. Indeed, it appears that the noise is becoming exponentially worse (with a small prefactor) as A increases for these particular choices of interpolators, which involve multiple lower components of quark fields, and further improvements are required. Even with high statistics and improved interpolators, the presence of very closely spaced excitations in these

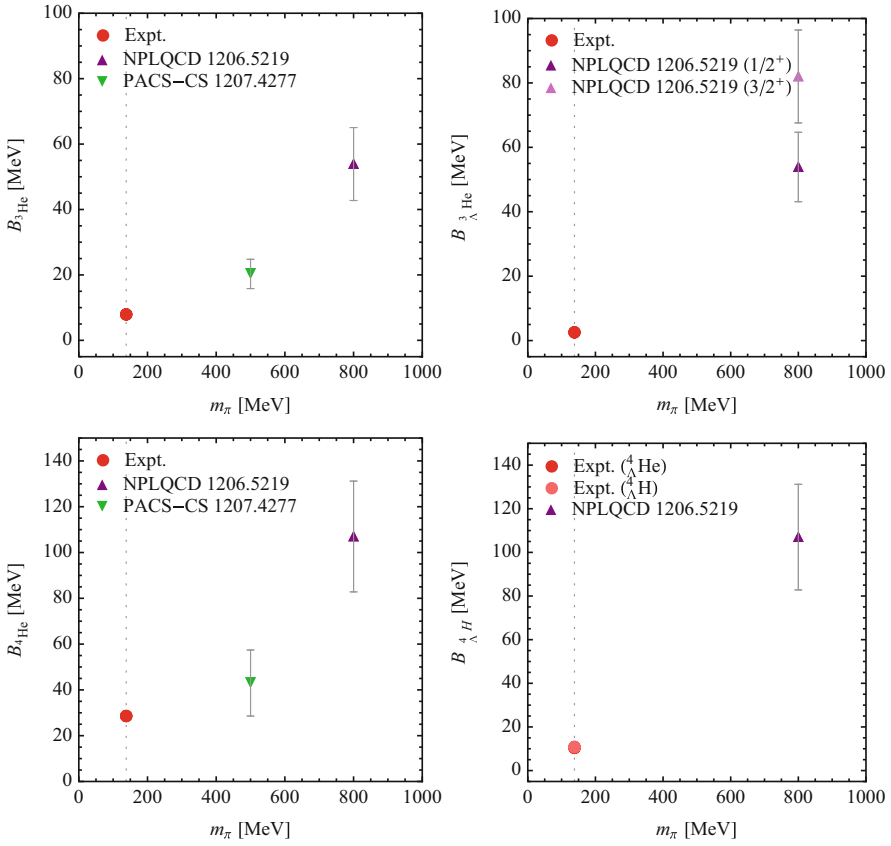

Fig. 5.8 Summary of the results obtained in $n_f = 2 + 1$ or $n_f = 3$ lattice QCD calculations of the binding energies of ^{3}He, $^3_\Lambda$H, ^{4}He and $^4_\Lambda$He. The *red circles* correspond to the physical binding energies (for $^4_\Lambda$He experimental determinations of both iso-doublet states are shown). For $^3_\Lambda$He, both $J = 1/2$ and $3/2$ states were extracted, with the higher spin state being more tightly bound for this SU(3)$_f$ symmetric quark mass

complex systems will make extraction of the ground state energy a challenge as will be discussed below.

From these studies, we can tentatively conclude that light nuclei generically become more deeply bound as the quark masses increase. Clearly there is a long way to go before these calculations make direct contact with experiment, but at least in cases where a trend can be established as a function of quark mass, the trend is towards the experimental result. Even at unphysical quark masses, such as those used in the above studies, it is of broad interest to pursue such calculations as they provide information about possible alternate versions of the Universe. In looking at nuclear physics in a broader context, it is natural to ask how sensitive the structure and evolution of our Universe is to the fundamental parameters (for

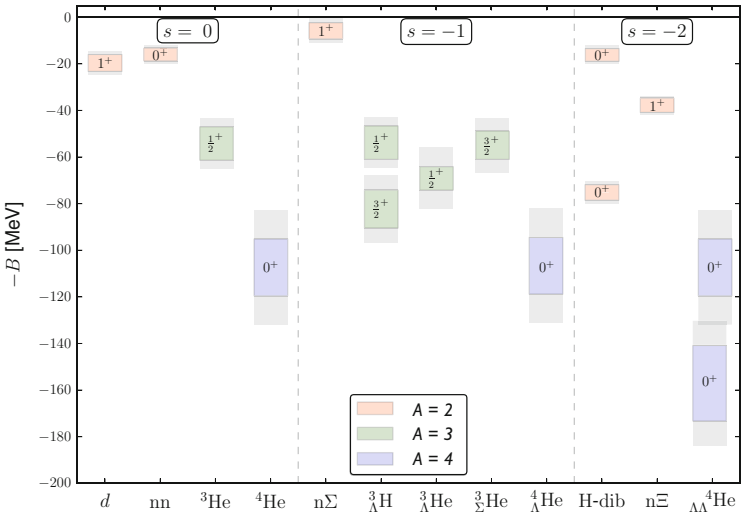

Fig. 5.9 Spectrum of light nuclei and hypernuclei studied in [234]. The SU(3)$_f$ flavour symmetry results in unphysical degeneracies (After [234])

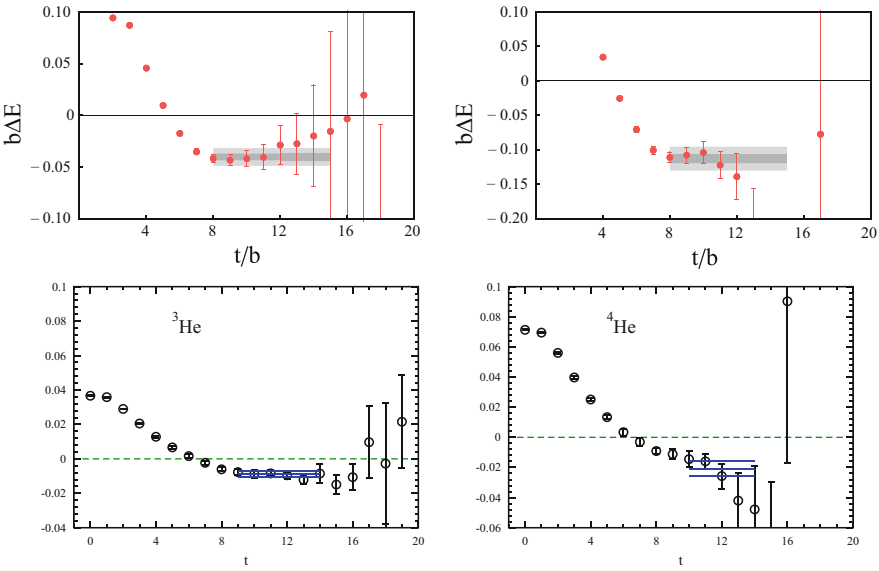

Fig. 5.10 Example effective mass plots for $A > 2$ baryon systems. The top row corresponds to the $^3_\Sigma$He ($J = 3/2$) (*left*) and $^4_{\Lambda\Lambda}$He (*right*) correlators from the NPLQCD study in [234]. The bottom row corresponds to the ^{3,4}He correlators from Yamazaki et al. [344] (From [234, 344])

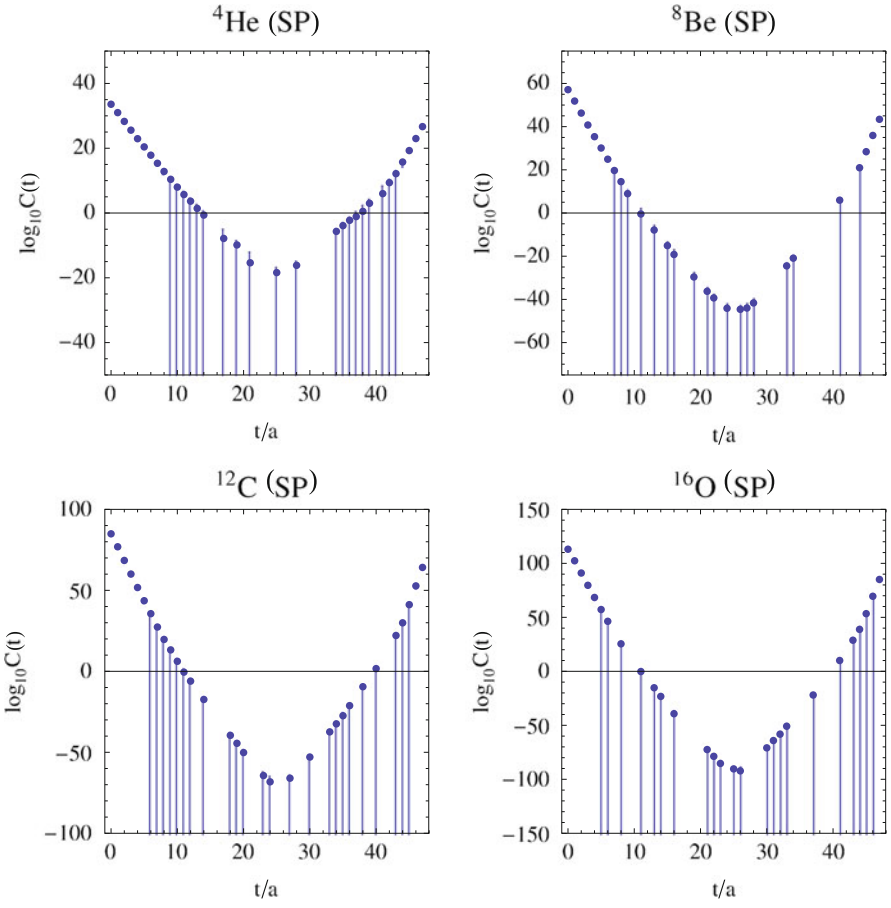

Fig. 5.11 Logarithmic plots of correlators for larger nuclei studied in [375]. The points with error bars reaching the lower axis are consistent with zero at one standard deviation and show where the signal is lost

all but the earliest times, this is the realm of nuclear physics and, as discussed in the introduction, the only relevant parameters are $\Lambda_{\rm QCD}$, the fine structure constant $\alpha_{f.s.} \sim \frac{1}{137}$, and the light quark and electron masses), and it is likely that useful constraints can be determined from ab initio studies. For example, Big Bang Nucleosynthesis is determined by a network of reactions of light nuclei, some of which may plausibly be investigated in future LQCD calculations. Changing the parameters of the Standard Model will modify this network and may make life, at least as we know it, not viable [385, 386]. In addition, such calculations offer the prospect of understanding how finely-tuned processes such as carbon production through the triple-α process are. Studies of smaller A systems in LQCD (which will be computationally feasible in the near future) also have phenomenological impact

as they can be used to constrain effective field theory based approaches and thereby play an important role in predictions for larger systems (see [368, 369, 387, 388] for recent work in this direction). Already, we are gaining surprising insights about such fine-tunings. In [341], the ratios of the scattering lengths to effective ranges of the ${}^3S_1$ and ${}^1S_0$ nucleon-nucleon interactions were studied at $m_\pi \sim 800$ MeV. There it was seen that in the deuteron channel, the fine-tuning of the system that a large value of this ratio characterises is also present at this unphysically large quark mass. It is very interesting to see in which other systems, and for which parameter ranges, such behaviour occurs.

5.8 Current Issues and Future Challenges

As discussed above, significant progress has been made in the last few years, however the current studies are clearly only the beginning of the application of lattice QCD to nuclear physics. A number of important issues remain to be understood and in this section, I summarise these challenges as they appear at the present time.

5.8.1 Statistical Precision

Since nuclear physics entails small energies on the scale typical of QCD, high precision calculations are important, requiring precise statistical sampling of correlation functions. In [383], Lepage pointed out that for single baryon correlation functions, the ratio of signal-to-noise should decay exponentially with Euclidean time (a fact borne out in many numerical investigations). If $C(t)$ is a single nucleon correlation function, with its average falling asymptotically as $\exp(-M_N t)$, its variance is given by

$$\text{var}(C) = \left\langle C(t)C^\dagger(t)\right\rangle - |\,\langle C(t)\rangle\,|^2\,, \tag{5.50}$$

with angle brackets denoting the gauge field ensemble average. The first term in this is a correlation function in its own right with the quantum numbers of the corresponding three quarks and three antiquarks (since fermions are integrated out exactly, the valence fermion content is fixed in C and $C^\dagger$ separately). Since the lightest state with the requisite quantum numbers is a three pion state, the variance will fall off at large times as $\exp(-3m_\pi t)$ (up to shifts due to interactions) and correspondingly, the signal-to-noise ratio will degrade as $\langle C\rangle/\sqrt{\text{var}(C)} \sim \exp(-(M_N - \frac{3}{2}m_\pi)t)$. Generalising to an A baryon system [382], we may expect an exponentially worse behaviour with the signal decaying into noise as $\exp(-A(M_N - \frac{3}{2}m_\pi)t)$. As discussed in [382], the choice of interpolating operators that are used for a particular set of quantum numbers is critical and can be used to some degree

to delay the onset of these noisiest contributions to a given correlation function. It is important to systematise these findings and understand to what extent these and other noise-reducing optimisations (some ideas that may be relevant are discussed in [389–392]) can be implemented.

The sampling of configurations representative of the vacuum encoded in Eq. (5.4) is likely a particularly inefficient way to determine properties of nuclei, states that are very different from the vacuum. It is possible that a reorganisation of the calculation by moving an appropriate part of the multi-nucleon observable into the Boltzmann weight will result in better statistical determination of multi-hadron correlations. However, it is not known how to do this effectively while maintaining positivity of the integration measure, and thereby avoiding the sign-problem that plagues lattice QCD at nonzero quark chemical potential [393]. Such a technique would most likely be implemented on an observable-by-observable basis and would therefore be extremely computationally demanding.

5.8.2 *Beyond Spectroscopy*

While most efforts in lattice QCD for nuclear physics currently focus on the spectroscopy of multi-hadron systems, these systems also present a rich set of more complicated observables that are of phenomenological interest.[14] For example, a precise determination of the matrix elements of the axial current in two-nucleon systems would impact our understanding of the *pp* fusion process that powers the sun and the $\nu\ d \longrightarrow n\ p$ breakup process used as a neutrino detection mode in the Sudbury Neutrino Observatory. In addition, any information from QCD about the interactions of nuclei with dark matter through scalar [394] or other currents would have immediate phenomenological interest. In [238, 395], the problem of determining such matrix elements has begun to be addressed.

For two-body final states, this problem is technically similar to $K \to \pi\pi$ decays induced by weak interactions that are of importance in particle physics [396] (although in the case of $\nu\ d \longrightarrow n\ p$ and various other nuclear processes, the lepton injects energy into the hadronic system). In [397], Lellouch and Lüscher developed the formalism to extract the infinite volume decay matrix elements for $K \to \pi\pi$ (see also [283]). This has recently been generalised to multiple final state channels in [130, 242] and the reader is referred to the original references for details. Extension of this work to final states with more than three particles is a challenging problem, but one that is important to understand before we can consider QCD calculations of the large range of multi-hadron properties and transitions that are of interest to the experimental and phenomenological nuclear physics communities.

[14] As discussed above, in [381], a first numerical investigation of matrix elements of multi-pion systems has been presented. Even in this simplest case, theoretical difficulties remain to be resolved.

Another related topic is the determination of matrix elements of unstable states such as the Δ or ρ resonances (although care needs to be applied in the definition of such matrix elements). In [398], a possible approach to this problem was suggested.

5.8.3 How Large Is a Large Volume?

In the analysis of two particle systems in finite volume, a requirement for the validity of the Lüscher approach discussed above is that the system size is large compared to the range of the interaction which is typically set by the Compton wavelength of the pion for light pions (at large quark masses, other scales $\sim \Lambda_{\rm QCD}$ become important [341]). For bound states, the lattice volume must additionally be large compared to the size of the bound state, the scale of which is set by the binding momentum, γ; this second constraint is more stringent for shallow bound states which can be large even on the scale of the pion Compton wavelength. As discussed in [283], the Lüscher method also requires volumes large enough that the finite volume spectrum of states is sufficiently dense so that finite volume sums provide a good approximation to infinite volume integrals. Similar constraints exist in the case of the potential method and will also arise for higher-body systems. There remains a question as to what large means: does $m_\pi L,\ \gamma L > 4$ suffice, or are the requirements more stringent? Precise calculations are needed to address this question, both at "large" volumes in the region where asymptotic behaviour can be clearly confirmed, but also in "small" volumes where deviations from theoretical expectations can be demonstrated. For precise results, it is important to mark out the region in which systematics such as these are well controlled.

It is likely that a number of earlier calculations with $m_\pi L \sim 4$ have additional systematic uncertainties from volume dependence that is not controlled by the Lüscher approach (particularly in cases where there is a shallow bound state). For example, in the NPLQCD calculations of bound states at $m_\pi \sim 390$ MeV [345, 348], data for $L = 2.0$ and 2.5 fm (corresponding to $m_\pi L = 3.9$ and 4.9, respectively) were dropped for this reason, and similar exclusions may need to be made elsewhere.

5.8.4 Spectral Gaps, Large Volumes and the Approach to the Chiral Limit

At finite volume, hadron-hadron two-point correlation functions for large Euclidean times are dominated by exponentials corresponding to a series of poles in energy arising from states is which the two hadrons move with back-to-back momenta in their CoM frame (as discussed above, four- and higher-particle contributions are expected to dominate eigenstates of higher energy). For weakly interacting states,

the gaps between these states are approximately given by the difference between E_n and E_{n+1} where $E_n = 2\{M^2 - \frac{4\pi^2}{L^2} n\}^{1/2}$ for two identical hadrons (since $n = |\mathbf{n}|$ for integer triplets $\mathbf{n}$, there are some levels that are not allowed, for example $n = 7$). As L increases, these gaps shrink rapidly (quadratically in the case of two hadrons) and it becomes hard to isolate the different levels. Variational approaches can help to some degree, but as the states collapse towards each other, they are by definition becoming more and more alike, so diagonalisation of correlator matrices will become an almost degenerate problem. Characterisations of this increasing level density for increasing volume are given in an appendix of [234] for ^{4}He. As pointed out in [341], in the two-body sector this is further manifest in that the poles in the Lüscher eigenvalue equation accumulate at threshold and thus extracted energy levels of a given precision start to straddle these singularities, making extraction of phase shifts difficult in these energy regimes.

This problem is not unique to the large volume limit. As the quark masses are decreased toward the chiral limit, pions become lighter. Consequently, the spectrum becomes denser as, for a given choice of quantum numbers, the energy gap between the ground state and states that include additional pions (see footnote 1) tends to zero. The problem is compounded by the fact that one needs to take the infinite volume limit before, or at least in combination with, the chiral limit so that finite-volume distortions of individual hadrons remain exponentially small.

This issue is one of the major challenges that must be addressed to open a path towards nuclear physics at the physical quark masses and seems to require a significant conceptual advance.

5.8.5 *Electroweak Effects*

None of the calculations discussed above include the effects of the electroweak interaction. For simple quantities such at the ratio of pion and kaon decay constants, f_π / f_K, lattice calculations are attaining the level of precision where electromagnetic effects are important and attempts are being made to include them (see [399] for a recent review). In the future, such effects must also be included in calculations relevant for nuclear physics. Indeed, as the number of protons increases, so does the charge and thus the importance of electromagnetic effects, eventually overcoming the smallness of $\alpha_{f.s.} \sim \frac{1}{137}$, and making inclusion of electromagnetism even more important in nuclei.

Conclusions

Over the last decade, the numerical implementation of lattice QCD has realised its potential and become a precision tool for the calculation of hadronic quantities in particle physics. It has become a crucial part of our

(continued)

understanding of the Standard Model and an indispensable component in the search for physics beyond it through precision flavour physics. For many quantities, current calculations are either already reaching levels of precision comparable to experiment, or the path toward such precision is clear [400]. More complicated observables and/or effects remain to be, and must be, considered (examples being the complete inclusion of electromagnetism and the calculation of so-called long-distance contributions [401]). However, the first phase of calculations is being successfully completed. In the intrinsically more complex realm of nuclear physics, lattice QCD is only now making inroads into our understanding, and represents a new frontier for the field and also for lattice QCD. As well as providing tests of the Standard Model in a new regime, the ab initio approach to nuclear physics from the underlying Standard Model offers exciting opportunities to make reliable predictions for quantities that are difficult, or even impossible, to access experimentally. In many areas of terrestrial nuclear physics and in nuclear astrophysics, input from well constrained calculations is important for guiding and understanding both experiments and observations. In the context of nuclear physics, lattice QCD also presents new challenges, both conceptual and numerical, that we are just beginning to uncover.

Acknowledgements I warmly thank Stefan Meinel, Zhifeng Shi, Brian Tiburzi and my colleagues in the NPLQCD collaboration for many interesting discussions on the topics of these lectures and Zhifeng Shi for producing Fig. 5.7. I also thank Huey-Wen Lin, Harvey Meyer and David Richards for their hard work in organising this very successful summer school. Finally, I thank the students, in particular Raul Briceno and Zoreh Davoudi, for making the lectures enjoyable. This work was supported by the U.S. Department of Energy through Outstanding Junior Investigator Award DE-SC0001784 and Early Career Award DE-SC0010495 and by the Solomon Buchsbaum Fund at MIT.

Chapter 6
High Temperature and Density in Lattice QCD

Carleton DeTar

Abstract These lectures provide an introduction to lattice gauge theory calculations of the properties of strongly interacting matter at high temperatures and densities. Such an environment is produced in heavy ion collisions and was most likely present in the early universe. Emphasis is placed, not on formalism, rather on an intuitive understanding of the nature of the crossover from the confined, chiral-symmetry-broken phase to the deconfined, chiral-symmetry-restored phase. Illustrations are taken from results of recent numerical simulations. Connections with phenomenology are discussed.

Lecture 1: The strong-coupling, high-temperature limit and the Potts model paradigm

In this first lecture we survey the phenomenology and offer an intuitive understanding of the phase transitions by appealing to approximate models of lattice QCD applicable at high temperature, strong coupling, and large mass.

6.1 Introduction

6.1.1 Why Study High T and High Density QCD?

Moments after the "big bang", before the formation of hadrons, the universe passed through a phase in which quarks and gluons (as well as leptons and photons) existed in a plasma-like phase. It is conceivable that, even today, a deconfined state of matter occurs at the cores of very dense stars. This form of strongly interacting matter is not well understood and surely holds interesting surprises. Understanding the properties of matter under such extreme conditions involves both experiment

C. DeTar (✉)
Department of Physics and Astronomy, University of Utah, Salt Lake City, UT 84112, USA
e-mail: detar@physics.utah.edu

H.-W. Lin, H.B. Meyer (eds.), *Lattice QCD for Nuclear Physics*, Lecture Notes in Physics 889, DOI 10.1007/978-3-319-08022-2_6

and theory. To study strongly interacting matter under these conditions, we try to recreate it in a microcosm in heavy-ion accelerator laboratories at the Relativistic Heavy Ion Collider at Brookhaven, the Large Hadron Collider at CERN, and at the Facility for Antiproton and Ion Research (FAIR) in Darmstadt, Germany. What we learn provides insights into the origin of matter and the phenomenology of dense stars.

6.1.2 Phenomenology of the Quark-Gluon Plasma

Theoretical studies of the "quark-gluon plasma" have used approximate models, resummed perturbation theory, and nonperturbative numerical simulation to develop some understanding of the properties and behavior of quark-gluon matter at high temperature and density. Some of what we know is well founded in theory and experiment, but much is speculative. Here is a list of the main phenomenologocial properties:

- **Deconfinement**. At high temperature or density, quarks and gluons are no longer confined in distinct color-singlet combinations.
- **Phase transition or crossover**. The transition between confined and deconfined matter at zero baryon density is only a crossover and not a true phase transition at physical values of the quark masses.
- Chiral symmetry restoration. The loss of confinement is accompanied by an approximate restoration of chiral symmetry.
- **Phase diagram 1**. Figure 6.1 gives a speculative phase diagram as a function of temperature and baryonic chemical potential. The figure indicates a phase boundary between confined matter (hadron gas) and deconfined matter (quark-gluon plasma) as well as some unusual and highly speculative phases at very high density. Sketched are the paths taken as matter evolves in a heavy-ion collision and in the cooling of the early universe.
- **Phase diagram 2**. Figure 6.2 shows the phase structure as a function of quark mass at zero chemical potential. In this case the regions show for what ranges of quark masses a phase transition of any sort is possible at some temperature. One should imagine a third, temperature axis extending out of the plane. Then what is shown is a projection of phase diagram surfaces onto the quark mass plane. What we see is that at very high quark masses, a first-order phase transition occurs at some temperature. This region is bounded by a second-order line in the $Z(2)$ universality class. At quite low quark masses, there is, again, a first-order phase transition, also bounded by a second order line. This line merges with the m_s axis and extends to infinity. Between these first-order regions there is only a crossover.

As we have emphasized, these figures mix some solid theoretical results with considerable speculation. So far, there is fairly good agreement about what happens at low baryon number density. There are several open questions: (1) What happens at high density is not well established. (2) At moderately low density, Fig. 6.1

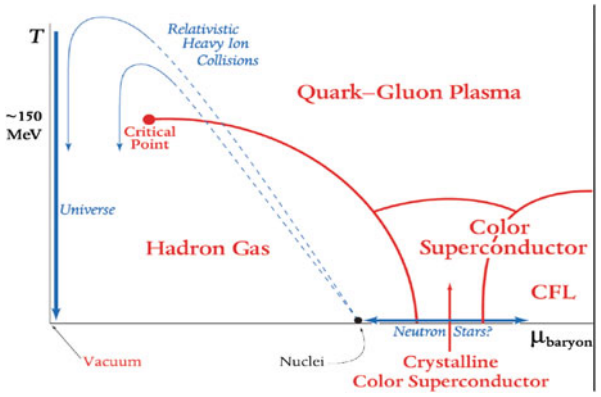

Fig. 6.1 Speculative phase diagram for QCD as a function of temperature and baryonic chemical potential. (*right*) phase structure as a function of the degenerate up/down quark mass and the strange quark mass

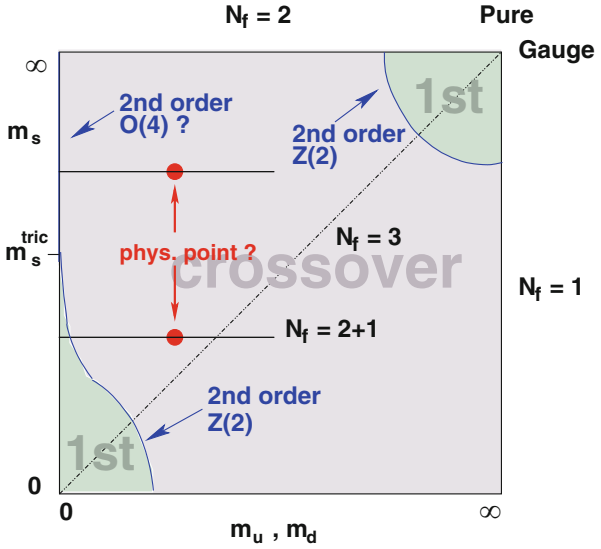

Fig. 6.2 Speculative phase structure for QCD as a function of the degenerate up/down quark mass and the strange quark mass

shows a critical point at the end of the first-order line. Is this correct? Is it experimentally accessible? (3) At low up and down quark masses, Fig. 6.2 indicates some uncertainty about whether, at fixed physical strange quark mass, we should encounter a first order phase transition at a nonzero value of the up/down quark mass. Present indications are that, if so, that mass is quite small.

How can we make further progress addressing these questions? They all require a nonperturbative treatment of quantum chromodynamics (QCD). Although the

underlying field theory for QCD is well-known and widely accepted, the only reliable method we have for answering nonperturbative questions is through numerical simulation via lattice QCD. This approach is properly called *ab initio*, since the reliability of its results can be improved indefinitely by decreasing the lattice size (and finding a larger computer!). The lattice version of QCD is not just an approximation. It is a well-defined regularization procedure with a high-momentum cut off that can be removed in the same way as in any standard regularization scheme.

Some disclaimers are in order, however. The numerical methods used to date have their limitations. First, lattice QCD is most naturally designed to describe matter in thermal equilibrium with small perturbations from there. But heavy ion collisions are naturally dynamic. Thus, for example, lattice QCD is not designed for modeling the expansion and cooling of the quark-gluon plasma. Instead, lattice QCD can provide the equilibrium properties of the plasma, which then become inputs to phenomenological models (e.g. hydrodynamic models) of the expansion.

These lectures are intended to give an overview of lattice QCD applied to quark and gluon matter at high temperature and high density. To help develop some intuition about high-temperature lattice QCD, we begin in this lecture by discussing the strong-coupling, high-temperature limit of the theory, making connection with the statistical mechanical three-state, three-dimensional Potts model.

6.2 Lattice QCD at Strong Coupling

We assume familiarity with the basics of lattice gauge theory from chapter "Lattice QCD: A Brief Introduction".

6.2.1 Partition Function

The imaginary-time Feynman path integral formulation is ideally suited for thermodynamics. With suitable boundary conditions in the imaginary (Euclidean) time dimension, namely, periodic for bosonic fields and antiperiodic for fermionic fields, the integration over classical histories naturally gives us the quantum partition function

$$Z = \mathrm{Tr}\exp(-H/T) = \int [dU][d\psi d\bar{\psi}]\exp(-S)\,. \tag{6.1}$$

In this notation H is the QCD hamiltonian, T is the temperature, $[dU]$ is the Haar measure over the gauge-field (gluon) links, $[d\psi d\bar{\psi}]$ is the Grassmann measure over the quark and antiquark fields, and S is the classical Euclidean action for QCD.

The temperature is related to the Euclidean time extent of the lattice:

$$T = 1/(N_\tau a)\,, \tag{6.2}$$

where the lattice spacing is a and the number of lattice sites in the Euclidean time direction is N_τ. Thus we can vary the temperature by varying N_τ and by varying a. The latter approach is most widely used.

6.2.2 Wilson Action and Noether Current

The Wilson lattice action S consists of a gauge-field part and a fermion part:

$$S = S_G + S_F\,, \tag{6.3}$$

where[1]

$$S_G = \frac{6}{g^2} \sum_{x,\mu<\nu} [1 - \mathrm{Re}\,\mathrm{Tr} U_P(x;\mu,\nu)/3]\,, \tag{6.4}$$

$$S_F = \sum_x \bar{\psi}(x)\psi(x) \tag{6.5}$$

$$- \kappa \sum_{x,\mu} [\bar{\psi}(x)(1+\gamma_\mu)U_\mu(x)\psi(x+\hat{\mu}) + \bar{\psi}(x+\hat{\mu})(1-\gamma_\mu)U_\mu^\dagger(x)\psi(x)]\,.$$

The gauge coupling is denoted by g, the lattice sites, by the four-vector x, the coordinate directions by μ and ν, the plaquette at site x and plane μ,ν, by $U_P(x;\mu,\nu)$ and the hopping parameter, by κ, which is related to the bare quark mass M through the relationship $\kappa = 1/(2aM+8)$.

As discussed in chapter "Lattice QCD: A Brief Introduction", the fermion action is bilinear in the fields, so it can be written in compact form as

$$S_F = \sum_{x,x'} \bar{\psi}(x') M(x',x) \psi(x)\,. \tag{6.6}$$

We saw that the path integral over the fermion fields in Eq. (6.1) could be carried out explicitly, resulting in the determinant of the fermion matrix $M(U)$, leading to an integral over just the gauge field:

$$Z_W = \int [dU] \exp[-S_G(U)] \det[M(U)]\,, \tag{6.7}$$

[1]Note that the fermion field has been rescaled by a factor $\sqrt{2\kappa}$ relative to the notation of chapter "Lattice QCD: A Brief Introduction". This normalization is convenient for numerical implementations.

For Monte Carlo integration it is important that the fermionic determinant be real and positive so it can be used as a probability weight for importance sampling. This is true for all fermion formulations commonly used in numerical simulation. The Wilson action in Eq. (6.5) satisfies $M^\dagger = \gamma_5 M \gamma_5$, from which we can infer that $\det M = \det M^\dagger$ so the determinant is, indeed, real.

For later reference we write the conserved Noether current for Wilson fermions, which follows in the usual way from the $U(1)$ symmetry of the action:

$$J_\mu(x) = \kappa[\bar{\psi}(x)(1+\gamma_\mu)U_\mu(x)\psi(x+\hat{\mu}) - \bar{\psi}(x+\hat{\mu})(1-\gamma_\mu)U_\mu^\dagger(x)\psi(x)]\,. \tag{6.8}$$

6.2.3 External Point Current

Let us consider introducing an external point charge g in the fundamental representation of SU(3) into the action. Let it move along the world line C. It modifies the continuum action through the source term

$$\delta S = \int d^4x A_a^\mu(x) J_\mu^a(x) = -ig \oint_C \lambda^a A_a^\mu dx_\mu\,. \tag{6.9}$$

Gauge invariance requires that C be closed. When this term is inserted into the path integral for the partition function we get a path-ordered exponential of the integral over the vector potential.

$$P \exp[-ig \oint_C \lambda^a A_a^\mu dx_\mu]\,. \tag{6.10}$$

On the lattice this turns into a path-ordered product of gauge links:

$$Z = \int [dU][d\psi d\psi] \exp(-S) L_C \tag{6.11}$$

$$L_C = \mathrm{Tr} \prod_{x,\mu \in C} (1+\gamma_\mu) U_{x,\mu}\,. \tag{6.12}$$

(For backward hopping we use the convention, $\gamma_{-\mu} = -\gamma_\mu$ and $U_{-\mu}(x) = U_\mu^\dagger(x-\hat{\mu})$.)

Now we consider placing a static charge in the statistical ensemble. The static charge worldline C is fixed at $\mathbf{x}$, moving forward only in imaginary time τ. The term L_C is then

$$L_C \propto \mathrm{Tr} \prod_{\tau=0}^{N_\tau - 1} U_{\mathbf{x},\tau;0}\,. \tag{6.13}$$

It is called a "Polyakov loop" (also, sometimes "Wilson line").

6.2.4 Gauge Theory at Strong Coupling, High T

Taking soluble limits provides insights into the workings of a theory. We recount an old story that bears repeating for its intuitive value: [402, 403]. We consider the strong-coupling, high-temperature limit of the Wilson action for just the gluons, in other words, pure $SU(3)$ Yang-Mills theory.

The temperature is the inverse of the lattice extent in the imaginary time direction, as in Eq. (6.2). To get a very high temperature we consider an anisotropic lattice, i.e., with different lattice constants in time and space ($a_t \neq a_s$). Then the Wilson action takes the form

$$S_G = \frac{6a_s}{a_t g^2} \sum_{x,i} [1 - \mathrm{Tr} U_P(x;0,i)/3] + \frac{6a_t}{a_s g^2} \sum_{x,i>j} [1 - \mathrm{Tr} U_P(x;i,j)/3] \,, \tag{6.14}$$

where the space-time oriented plaquettes (first term) get a larger weight than the space-space ones (second term). For high temperature we set $N_\tau = 1$ so $a_t = 1/T$, and we want $a_t/a_s \ll 1$. So we may drop the space-space term. We then have only $U_P(\mathbf{x}, 0)$ and $U_P(\mathbf{x}, i)$ and the space-time-oriented plaquette becomes

$$\mathrm{Tr} U_P(x;0,i) = \mathrm{Tr} U_0(\mathbf{x},0) U_i(\mathbf{x}) U_0^\dagger(\mathbf{x}+\hat{\mathbf{i}}) U_i^\dagger(\mathbf{x}) \,. \tag{6.15}$$

The trace takes its maximum value of 3 when $U_0(\mathbf{x}, 0) = z_\mathbf{x} I \in Z(3)$, the center of $SU(3)$: $\{1, \exp(\pm 2\pi i/3)\}$. The center elements commute with the space-like link matrices, which then cancel, leaving only the $Z(3)$ elements. So we approximate the integral over the gauge fields by a sum over elements of $Z(3)$:

$$Z = \int \prod_{x,\mu} [dU_\mu(x)] \exp(S_G) \to \sum_{z_\mathbf{x}} \exp\left[\frac{6a_s}{g^2 a_t} \sum_{\mathbf{x},\mathbf{i}} \mathrm{Re}\left(z_\mathbf{x}^* z_{\mathbf{x}+\hat{i}} \right) \right] . \tag{6.16}$$

Our approximation has become the classical three-state, three-dimensional Potts model, a popular toy model in statistical mechanics.

The Potts model is a generalization of the familiar Ising model, but here there are three orientations of each spin, rather than just two. Note that the model has a global $Z(3)$ symmetry: $z_\mathbf{x} \to Y z_\mathbf{x}$ for $Y \in Z(3)$. Just as with the Ising model, the Potts model has a ferromagnetic phase transition from a magnetized (ordered) phase at low temperature where the global symmetry is spontaneously broken to a disordered phase at high temperature. The order parameter is the magnetization, proportional to the expectation value of the spins, $\langle z \rangle$. In this Potts model the phase transition is first order.

In the spin system, we interpret the factor $6a_s/(g^2 a_t)$ as the ratio J/T_{Potts} where J is the coupling strength between neighboring spins, and T_{Potts} is the spin-lattice temperature. So the Potts temperature T_{Potts} is proportional to g^2 at fixed a_t/a_s. Now in QCD the renormalization group tells us that the lattice spacings a_t and a_s must

decrease as we decrease g. So at fixed a_t/a_s, small g^2 corresponds to a high QCD temperature $T_{\rm QCD} = 1/a_t$ and a low Potts model temperature $T_{\rm Potts}$.

So from these considerations we expect to find a first order phase transition in $SU(3)$ Yang-Mills theory with an ordered phase at high (QCD) temperature and a disordered phase at low temperature. The order parameter of the transition is $\mathrm{Tr}U_0(\mathbf{x})$, the Polyakov loop in this $N_\tau = 1$ example. For a more extended lattice, it is still the "Polyakov loop":

$$L(\mathbf{x}) = P \exp\left[\int igA_0(\mathbf{x},\tau)d\tau\right]. \tag{6.17}$$

This quantity should have a zero expectation value in the low-temperature, disordered phase and a nonzero expectation value in the spontaneously broken, ordered high-temperature phase.

6.2.5 Chemical Potential

Before extending the strong-coupling, high-temperature analysis to fermions, we show how to introduce chemical potentials so we can discuss the high temperature approximation at nonzero baryon number density as well.

The conserved charges on the lattice are the flavor numbers (Q_f) (including baryon number). In the grand canonical ensemble, the partition function is

$$Z_W = \mathrm{Tr}\exp\left(-H/T + \sum_f \mu_f Q_f/T\right). \tag{6.18}$$

The Noether current in Eq. (6.8) gives us the conserved charge density

$$\rho_f(x) = \kappa[\bar\psi_f(x)(1+\gamma_0)U_0(x)\psi_f(x+\hat 0) - \bar\psi_f(x+\hat 0)(1-\gamma_0)U_0^\dagger(x)\psi_f(x)], \tag{6.19}$$

from which we may calculate the contribution to the exponential in the partition function as

$$\mu_f Q_f/T = \mu_f \int \sum_\tau Q_f = \sum_x \mu_f \rho_f(x). \tag{6.20}$$

Note that this term is just like the time-like kinetic term in the action except for a sign. We get a factor $(1+a\mu)$ for forward hopping and $(1-a\mu)$ for backward. It is more natural to use $e^{\pm\mu a}$ for these factors. So we replace

$$\bar\psi(x)(1+\gamma_0)U_0(x)\psi(x+\hat 0) \to \bar\psi(x)(1+\gamma_0)U_0(x)\psi(x+\hat 0)e^{\mu a}, \tag{6.21}$$

$$\bar\psi(x+\hat 0)(1-\gamma_0)U_0^\dagger(x)\psi(x) \to \bar\psi(x+\hat 0)(1-\gamma_0)U_0^\dagger(x)\psi(x)e^{-\mu a}. \tag{6.22}$$

An important consequence of a nonzero chemical potential is that the fermionic determinant $\det M(\mu)$ is no longer real. We can guess this would happen if we observe that the γ_5 symmetry we used to prove reality now reads $M^\dagger(\mu) = \gamma_5 M(-\mu)\gamma_5$. So $\det[M(\mu)]^* = \det[M(-\mu)]$. It cannot be used directly as a Monte Carlo probability weight. A common expedient is to use the magnitude of the determinant as a probability weight and average over the phase. But the phase oscillations grow with the volume of the system V. So one cannot take the thermodynamic limit $V \to \infty$ with that method.

This vexing problem is called the "sign" problem. It appears in strongly-coupled electron systems as well, when one considers doping to move away from a half-filled conduction band.

6.2.6 *Fermions at Strong Coupling, Large Mass, High T*

Let's see what happens to the Potts model approximation when we include fermions. We write the Wilson fermion action for an anisotropic lattice ($a_t \neq a_s$), and we include the chemical potential μ for completeness:

$$\begin{aligned} S_F = & \sum_x \bar{\psi}(x)\psi(x) \\ & - \kappa \sum_x [\bar{\psi}(x)(1+\gamma_0)U_0(x)e^{-\mu a_t}\psi(x+\hat{0}) \\ & \qquad + \bar{\psi}(x+\hat{0})(1-\gamma_0)U_0^\dagger(x)e^{\mu a_t}\psi(x)] \\ & - \frac{\kappa a_t}{a_s} \sum_{x,i} [\bar{\psi}(x)(1+\gamma_i)U_i(x)\psi(x+\hat{i}) + \bar{\psi}(x+\hat{i})(1-\gamma_i)U_i^\dagger(x)\psi(x)] \,. \end{aligned} \tag{6.23}$$

The relationship between bare quark mass and hopping parameter is now

$$1/\kappa = 6a_t/a_s + 2 + 2Ma_t \,. \tag{6.24}$$

At very high temperature with $N_\tau = 1$ we have $a_t/a_s = 1/(a_s T) \to 0$, so we drop the space-like term in the action. The fermion matrix is then diagonal in space-time with values on each spatial site

$$1 - \kappa(1+\gamma_0)ze^{-\mu a_t} - \kappa(1-\gamma_0)z^* e^{\mu a_t} \,, \tag{6.25}$$

where we have introduced the $Z(3)$ variable as before.

At large mass (small κ) the fermionic determinant becomes

$$\exp\left[h_0(\kappa,\mu) + h(\kappa,\mu)\sum_{\mathbf{x}} \mathrm{Re} z_{\mathbf{x}} + ih'(\kappa,\mu)\sum_{\mathbf{x}} \mathrm{Im} z_{\mathbf{x}} \right] , \tag{6.26}$$

where

$$h(\kappa,\mu) \approx 24\kappa\cosh(a_t\mu)\,, \qquad h'(\kappa,\mu) \approx 24\kappa\sinh(a_t\mu)\,. \tag{6.27}$$

So our modified Potts model is now

$$H = -J\sum_{\mathbf{x},\mathbf{i}} \mathrm{Re}\left(z^*_{\mathbf{x}} z_{\mathbf{x}+\hat{i}}\right) - \sum_{\mathbf{x}} [h\,\mathrm{Re} z_{\mathbf{x}} - ih'\,\mathrm{Im} z_{\mathbf{x}}] \tag{6.28}$$

for values of h, h' given by Eq. (6.27). So the fermions introduce "external" magnetic fields into the spin system. In the Ising system there is only one magnetic field, but because there are three states in this Potts model, we can have two. In this case the two fields combine to make a complex field. The quark mass introduces an external real magnetic field, and the chemical potential gives rise to an imaginary magnetic field. In the Ising system any nonzero external magnetic field removes the continuous phase transition, resulting in a crossover. At zero field the Potts system has a first order transition, which weakens as the external field is turned on. Eventually, it, too becomes a continuous transition at a critical point and, at higher fields, a crossover. These properties are demonstrated in a numerical simulation of the Potts model [403]. Results are shown in Fig. 6.3. The imaginary field further weakens the transition.

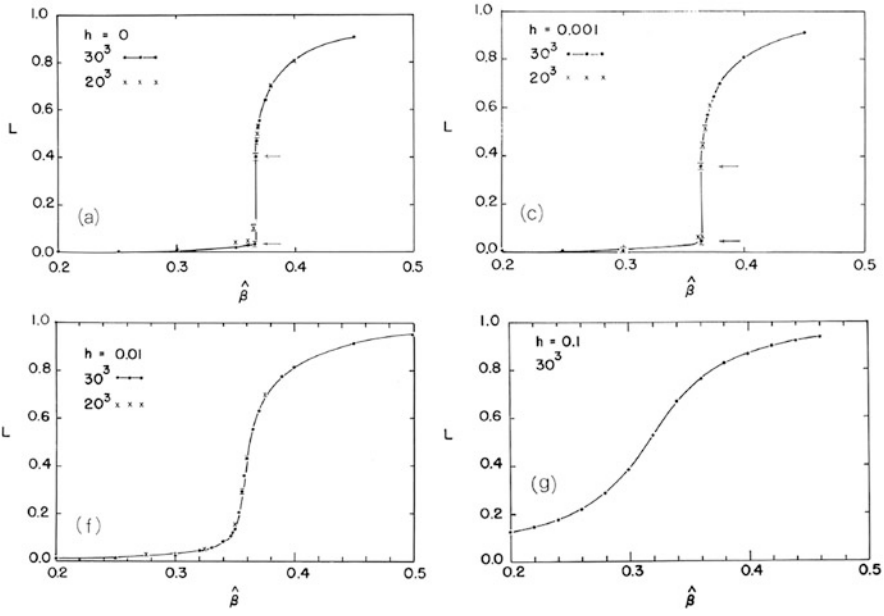

Fig. 6.3 Magnetization *vs.* inverse Potts temperature in the presence of an external field h. Notice that the first order phase transition disappears with increasing field [403]

The Potts model gives a good understanding of the large-mass portion (upper right corner) of the phase diagram of Fig. 6.2. The first order phase transition degrades into a crossover as the quark masses are decreased. These suggestive features of the approximate model are confirmed in simulations of QCD [404].

6.2.7 Three-Dimensional Flux-Tube Model of QCD

Some years ago, Appoorva Patel introduced an intuitively appealing toy model that imitates strong-coupling, large mass, high-temperature lattice QCD [405, 406], called the "flux-tube model". The model is equivalent to the three-dimensional three-state Potts model that we have been discussing, but the degrees of freedom are quite different.

The flux-tube model on a cubic lattice places quantized $Z(3)$ electric fluxes $\ell_{\mathbf{x},i}$ on next-neighbor links and $Z(3)$ charges $n_{\mathbf{x}}$ on sites. A charge of $+1$ on a site represents a quark, -1, an antiquark, and 0 is an empty site. Fluxes and charges are required to satisfy Gauss' law mod 3:

$$\sum_i (\ell_{\mathbf{x},i} - \ell_{\mathbf{x},-i}) \mod 3 = n_{\mathbf{x}} \,. \tag{6.29}$$

The hamiltonian is, then simply

$$H = \sigma \sum_{\mathbf{x},\mathbf{i}} |\ell_{\mathbf{x}}, i| + m \sum_{\mathbf{x}} |n_{\mathbf{x}}| \,. \tag{6.30}$$

where σ is the energy of a flux link and m is the mass of a quark. States of the model must be "singlets" because of the Gauss' law constraint. As illustrated in Fig. 6.4, there are meson-like states, baryon-like states, and glueball-like states consisting of only a flux loop.

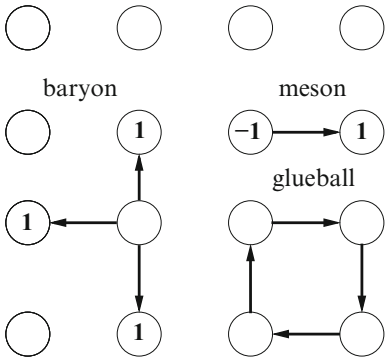

Fig. 6.4 Possible "hadrons" in the flux tube model. Shown are a "meson", "baryon", and "glueball"

The grand-canonical ensemble for this classical flux-tube model is defined by the partition function

$$Z = \sum_{n_{\mathbf{x}}, \ell_{\mathbf{x}\mathbf{i}}} \exp[-(H - \mu N)/T] \,, \tag{6.31}$$

where the sum is over configurations that satisfy Gauss' law and $N = \sum_{\mathbf{x}} n_{\mathbf{x}}$. Note that there is no complex phase problem at nonzero chemical potential in this representation.

The equivalence between the flux-tube model and three-dimensional three-state Potts model is easy to show. The essential step in the derivation replaces the Gauss' Law constraint in the partition function with the $Z(3)$ identity on each lattice site:

$$\frac{1}{3} \sum_{z} z^{\ell} = \delta_{\ell,0} \,. \tag{6.32}$$

The z's become the Potts spins. The flux-tube parameters σ, m, and μ map to the Potts model parameters.

There are some amusing features of the deconfined phase of the flux-tube model. At very large quark mass, most of the configurations consist of a continuous fabric of flux links. At low temperature, there are not enough flux links to create a continuous fabric. So one could say at low temperature we have a gas of hadrons, which grow in size as the temperature increases until they connect, leading to the deconfined phase. Quarks terminate flux lines. At lower quark mass there are enough quarks that the fabric is not connected at any temperature, so the phase transition is lost.

We learn from this example that we can solve at least part of the sign problem by a change of basis. In the field basis (gauge links), the complex phase comes from the imbalance between forward time-like and backward time-like hopping, combined with the presence of complex time-like gauge links. Integration over the time-like gauge links enforces Gauss' Law at each lattice site. Changing from the field basis to the hadron basis eliminates the complex phase.

With $SU(3)$ it is much more difficult to formulate the path integral with a basis change because there are an infinite number of irreducible representations of $SU(3)$. Moreover, there will still be a fermion sign problem, just as with electrons in condensed matter physics. Our simple models don't expose it. Finally, and probably most importantly, while the Potts and flux-tube models capture the deconfinement aspects of the high temperature phase transition, the strong coupling and large mass approximation doesn't capture chiral symmetry or its restoration, aspects of the transition that are most important for high temperature physics at physical quark masses.

Exercise 1 In mean field theory we consider the statistical mechanics of a single site, assuming that the neighbors of the site take on the same mean value. So for the Potts model we have a single-site partition function

$$Z(\bar{z}) = \sum_z \exp[-H(z,\bar{z})/T_{\rm Potts}]\,, \tag{6.33}$$

where the single-site $H(z,\bar{z})$ is obtained from the full H by setting all spins to the mean value $\bar{z}$, except for one site, which carries variable spin z.

We then impose self-consistency by calculating the output mean value of the spin on the single site and requiring that it equal the input mean value.

Do this for the 3D 3-state Potts model with $h = h' = 0$, and show that there is one real solution for low J/T and three real nonzero solutions for sufficiently high J/T. (In the latter case, the middle one happens to be unstable.) Then show that the transition is first order.

Maple, Mathematica, or gnuplot can help with the numerics here.

Lecture 2: Deconfining transition

In this second lecture we consider a variety of deconfinement features of the high temperature transition, including the free energy of a static charge, the strange quark number susceptibility, insights from dimensional reduction, and the survivability of hadrons at high temperature. The equation of state is another, but we defer discussion of that to the last lecture.

6.3 Signals for Deconfinement

6.3.1 Free Energy of a Static Charge

The free energy of a static charge at position **x** is measured through the expectation value of the Polyakov loop operator, which we introduced in the first lecture:

$$L(\mathbf{x}) = P \exp\left[\int igA_0(\mathbf{x},\tau)d\tau\right]$$

Here $A_0(\mathbf{x}) = \sum_a \lambda_a A_0^a(\mathbf{x})/2$ is the time component of the color vector potential and P represents path ordering. Its expectation value on the lattice is

$$\langle L(\mathbf{x})\rangle = \int [dU] L(\mathbf{x})\, \exp[-S_{\rm eff}(U)] / \int [dU] \exp[-S_{\rm eff}(U)]\,. \tag{6.34}$$

As we observed in the first lecture, this operator inserts a static external point source at position **x**, so its expectation value gives the difference F_0 in free energy between the ensemble plus an additional static charge and the unmodified ensemble:

$$\exp(-F_0/T) = \langle L\rangle\ . \tag{6.35}$$

Actually $F_0 = F_0(a,T)$ depends on the lattice spacing and temperature. It is ultraviolet divergent ($\sim \text{const}/a$), just as in quantum electrodynamics. Usually, we renormalize it so

$$F_0(T) \equiv F_0(a,T) - F_0(a,T_0) + \text{const}\,. \tag{6.36}$$

Exercise 2 The Wilson fermion action for a fermion of bare mass m is

$$S_F = \sum_{x,x'} \bar{\psi}(x) M(x,x') \psi(x') = \sum_x \bar{\psi}(x)\psi(x) \tag{6.37}$$
$$- \kappa \sum_{x,\mu} [\bar{\psi}(x)(1+\gamma_\mu) U_\mu(x) \psi(x+\hat{\mu}) + \bar{\psi}(x+\hat{\mu})(1-\gamma_\mu) U_\mu^\dagger(x) \psi(x)]\,,$$

where $\kappa = 1/(8+2ma)$. The fermion propagator is $M^{-1}(x,x')$.

Note that $M = 1 - \kappa H$, where H is called the "hopping matrix". For large bare mass (small κ) the propagator, $[1-\kappa H]^{-1}$, can be evaluated as a geometric series (hopping parameter expansion). Find the propagator in leading order in κ for a static quark over the time interval $[0,t]$.

The partition function in the presence of a static quark at $\mathbf{x}$ is

$$\int [dU] \exp[-S_{\text{eff}}(U)] \,\text{Tr} M^{-1}(\mathbf{x}, 1/T; \mathbf{x}, 0)\,, \tag{6.38}$$

where the trace of the propagator is over color and spin.

So show that $\exp(-F_0/T)$ is proportional to the Polyakov loop operator, where F_0 is the free energy of a static quark, i.e., the difference in the free energies of the ensembles with the static quark and without.

6.3.2 *Free Energy of a Pair of Static Charges*

The free energy of a pair of static charges is constructed in an obvious way from the product of Polyakov loops:

$$\exp[-F(\mathbf{R},T,a)/T] = \langle L(\mathbf{x}) L^*(\mathbf{x}+\mathbf{R}) \rangle\,. \tag{6.39}$$

At zero T this is the same as the potential $V(R)$ of separation of a static quark/antiquark pair. Numerical results are shown in Fig. 6.5. If there are no sea quark-antiquark pairs, confinement requires that at large separation

$$\lim_{R\to\infty} F(R) = \sigma R\,. \tag{6.40}$$

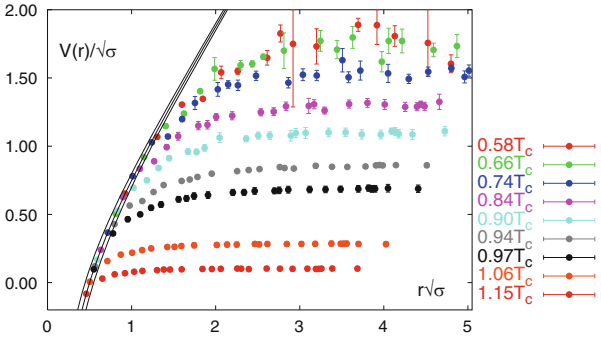

Fig. 6.5 Free energy of a static quark/antiquark pair as a function of separation in units of the string tension $R\sqrt{\sigma}$ for a variety of temperatures [407]. Results were calculated with three degenerate flavors of light quarks with masses $am_q = 0.1$ fixed in lattice units. σ is the string tension. The band of lines indicates the Cornell phenomenological heavy quark potential, appropriate at zero temperature. Deviations from this potential with increasing temperature can be interpreted as a weakening of confinement

This form of the free energy is equivalent to the statement that the expectation value of the product of two Polyakov loops at separation R falls exponentially with the area of the region between the loops. Since they are as long as the temporal extent $1/T$ of the lattice, the area is R/T. So $\exp[-F(\mathbf{R}, T, a)/T] \to \exp(-\sigma R/T)$.

When sea quark-antiquark pairs are included in the ensemble, they screen the static charges, as illustrated in Fig. 6.6 (upper left), so we always have, asymptotically, twice the free energy of a single static quark. The result is finite at any temperature:

$$F(R, T, a) \to 2F_0(a, T)\,. \tag{6.41}$$

When sea quark-antiquark pairs are absent, as in pure Yang-Mills theory, there is no screening, as sketched in Fig. 6.6 (lower right) so $F_0(a, T)$ is infinite at low temperature. Above the deconfinement temperature the free energy is finite. In pure Yang-Mills theory there is a first-order phase transition separating the deconfined and confined phases. The static quark free energy is an order parameter for the transition.

If we introduce dynamical sea quarks into the ensemble, the static quark free energy is finite at any temperature, but, as long as the quark masses are large, we still see a dramatic decrease in the free energy as we cross the transition temperature. For sufficiently large masses, the transition is still first-order, but as the sea quark masses are decreased, the transition weakens, and eventually there is only a crossover, as shown in Fig. 6.7. In that case the static quark free energy is only a qualitative indicator of deconfinement.

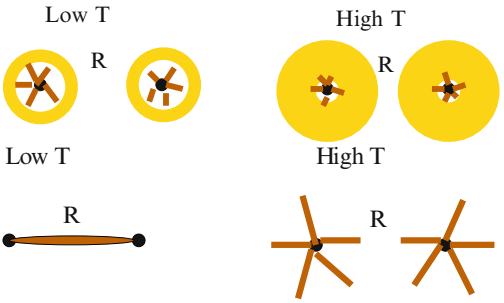

Fig. 6.6 *Yellow* indicates sea quarks. *Brown lines* indicate color electric flux. *Left, upper*: static quarks screened in the presence of sea quarks and lower, unscreened in the absence of sea quarks. *Right, upper*: static quark at high temperature, screened in the presence of sea quarks and lower, screened by thermal gluon fluctuations in the absence of sea quarks

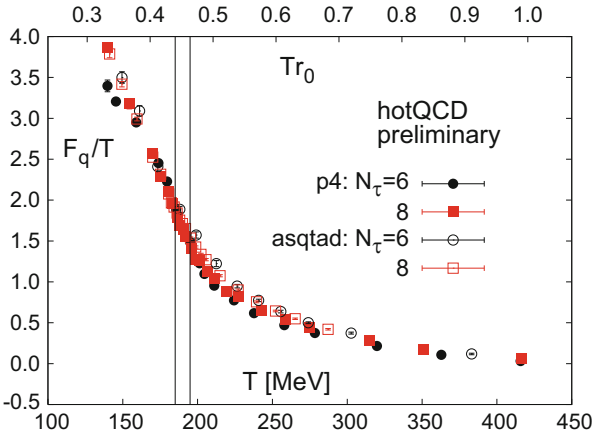

Fig. 6.7 Free energy of a static quark $F_q(T)$ as a function of temperature in the presence of sea quarks [408]. It drops steadily through the transition temperature between 150 and 200 MeV. There are light sea quarks, so the transition is only a crossover

6.3.3 *Strange Quark Number Susceptibility*

The number of strange quarks in the ensemble N_s can fluctuate. A measure of fluctuation is the strange quark number susceptibility,

$$\chi_s = \left\langle N_s^2 \right\rangle / (VT) \,. \tag{6.42}$$

It is another qualitative indicator of deconfinement, since fluctuations are controlled by the Boltzmann factor. In the low temperature, confined phase, strangeness fluctuations come from fluctuations in the number of strange hadrons. At high temperature they come from fluctuations in the number of strange quarks. Since

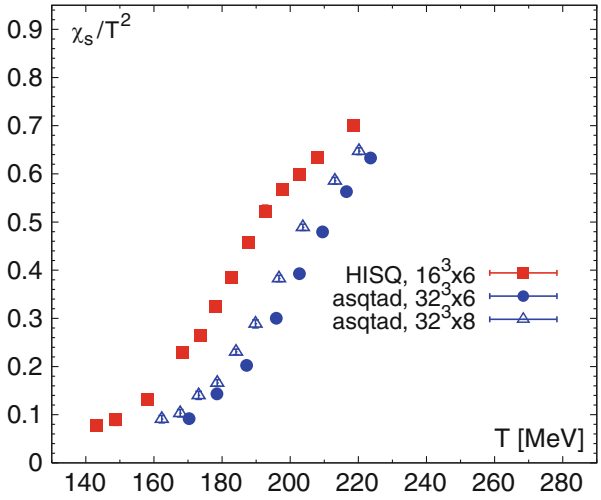

Fig. 6.8 Strange quark number susceptibility [408], showing a rapid rise in the transition region between 150 and 200 MeV

strange hadrons are heavier than strange quarks, we expect the fluctuations to increase with deconfinement. Results from a numerical simulation are shown in Fig. 6.8.

6.3.4 Dimensional Reduction

Since temperature is determined by the inverse temporal extent of the lattice, high temperature corresponds to a small temporal extent. At sufficiently high temperature, the four-dimensional Euclidean space-time lattice becomes, effectively, a three-dimensional Euclidean lattice. This is called "dimensional reduction."

Euclidean time boundary conditions

$$A^a_\mu(\mathbf{x},\tau) = A^a_\mu(\mathbf{x},\tau + 1/T) \quad \text{periodic} \tag{6.43}$$

$$q(\mathbf{x},\tau) = -q(\mathbf{x},\tau + 1/T) \quad \text{antiperiodic}\,, \tag{6.44}$$

lead to different behavior for bosons and fermions in the dimensionally reduced lattice. This can be seen from a Fourier decomposition in imaginary time τ:

$$A^a_\mu(\mathbf{x},\tau) = \sum_{n=-\infty}^{\infty} \exp(i\,\omega_{b,n}\,\tau) A^a_{\mu,n}(\mathbf{x}) \quad \text{for } \omega_{b,n} = 2\pi\, n\, T \tag{6.45}$$

$$q(\mathbf{x},0) = \sum_{n=-\infty}^{\infty} \exp(i\omega_{f,n}\tau) q_n(\mathbf{x}) \quad \text{for } \omega_{f,n} = 2\pi(n+\tfrac{1}{2})\,T\,. \tag{6.46}$$

For free fields the mass-shell condition becomes

$$p_x^2 + p_y^2 + p_z^2 + \omega_n^2 + m^2 = 0\,, \tag{6.47}$$

where the fermion Matsubara frequencies are $\omega_{f,n}$, and the boson Matsubara frequencies are ω_{bn}.

In a Euclidean world, any direction can be called imaginary time. So we swap z and τ and let $E = ip_z$. Then the free-field mass-shell condition becomes

$$E^2 = p_x^2 + p_y^2 + \omega_n^2 + m^2\,. \tag{6.48}$$

We get a tower of 3D bosonic fields, one for each Matsubara frequency:

$$E_n^2 = p_x^2 + p_y^2 + m_b^2 + (2\pi nT)^2\,. \tag{6.49}$$

Likewise, we get a tower of 3D fermionic fields, one for each Matsubara frequency:

$$E_n^2 = p_x^2 + p_y^2 + m_f^2 + [2\pi(n+\tfrac{1}{2})T]^2\,. \tag{6.50}$$

The result is a three-dimensional Euclidean field theory in which the original time components of the vector potentials $A^a_{n,0}$ become scalar fields, the original spatial components $A^a_{n,i}$ become 3D vector fields and the fermions q_n have effective masses that increase with T. At high T all fermion fields have high mass regardless of m_f, and they are rare. Only the $n = 0$ bosons are massless when $m_b = 0$.

So at high temperature we get a confining zero-temperature 3D Euclidean gauge-Higgs field theory! The 3D coupling is $g\sqrt{T}$. Since it is confining, we get an area law for the Wilson loop, which corresponds to a space-like Wilson loop in 4D. We expect confinement effects for momenta less than g^2T. The confined states in 3D correspond to spatial screening in 4D:

$$\langle A(0)B(\mathbf{r})\rangle \to \exp(-\mu r)/r\,. \tag{6.51}$$

For a quark bilinear, $A = \bar{q}\Gamma q$, the screening mass at high T is twice the effective mass of the lightest 3D quark ($n = 0$), or $\mu \approx 2\pi T$. Note, also that QCD exhibits "spatial confinement" even at the highest T!

The thermodynamic potential can be calculated in low order QCD perturbation theory. It has the form

$$\Omega(T) = c_0(T) + \alpha_s c_1(T) + \alpha_s^{3/2} c_{3/2}(T) + \alpha_s^2 c_2(T) + \ldots\,. \tag{6.52}$$

Because of spatial confinement, we expect nonperturbative contributions to enter at order α_s^3. A simple way to see that is to note that confinement affects states moving with low momenta, such that $p < g^2 T$. The corresponding volume of phase space goes like $g^6 T^3$.

6.3.5 Hadrons in the Thermal Medium

Another anticipated aspect of deconfinement is that hadrons dissociate. Given that the transition is a crossover, the dissolution should occur gradually as the temperature is increased through the transition. Indeed hadrons might persist as quasi-bound states or resonances at temperatures above the transition. (In a statistical ensemble at any temperature, there are no true bound states because scattering with the medium destroys any initial state.)

The static quark potential in Fig. 6.5 shows short-range attraction even at $1.15 T_c$. Of course these results are for static quarks, so they do not account for the response of the medium to the motion of light quarks. Still, they suggest, at least, that heavy quarks might bind, since they move slowly in a bound state, in which case the Born-Oppenheimer approximation might apply.

There is a way, albeit difficult, to study the survival of a hadronic state in a thermal plasma without making the Born-Oppenheimer approximation. This method involves extracting the real-frequency spectral response from the Euclidean time correlator that excites the hadronic state in question. We start with the thermal correlator

$$\left\langle \mathcal{O}^\dagger(\mathbf{x}, 0) \mathcal{O}(\mathbf{y}, \tau) \right\rangle \tag{6.53}$$

and do the spatial Fourier transform (using momentum conservation)

$$C(p, \tau, T) = \left\langle \mathcal{O}^\dagger(\mathbf{p}, 0) \mathcal{O}(\mathbf{p}, \tau) \right\rangle . \tag{6.54}$$

where $p = |\mathbf{p}|$. The real-frequency spectral decomposition of the correlator reads

$$C(p, \tau) = \frac{1}{2\pi} \int_0^\infty d\omega \, \rho(\omega, p, T) K(\omega, \tau, T) , \tag{6.55}$$

where the kernel function is

$$K(\omega, \tau, T) = \frac{\cosh \omega(\tau - 1/2T)}{\sinh(\omega/2T)} . \tag{6.56}$$

The spectral density $\rho(\omega, p, T)$ has peaks in ω marking resonances that couple to the operators in the correlator. An example for the J/ψ is shown in Fig. 6.9.

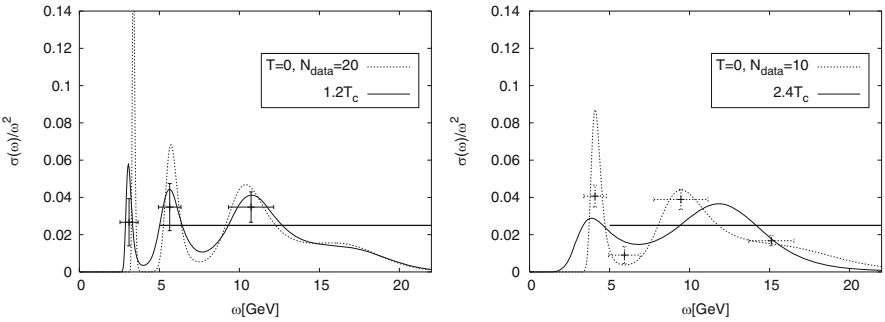

Fig. 6.9 Charmonium spectral density as a function of frequency (energy) at $1.2T_c$ (*left*) and $2.4T_c$ (*right*) from [409], suggesting that charmonium survives at $1.2T_c$, but possibly not at $2.4T_c$

Although the method is interesting, it is numerically extremely challenging. The correlator $C(p, \tau, T)$ is measured only for discrete $\tau = 0, 1, \ldots, N_\tau - 1$. In fact, because of symmetries under $\tau \to N_\tau - \tau$, there are only $N_\tau/2 + 1$ independent points (for even N_τ). But $\rho(\omega, p, T)$ has values on the real ω line. Thus solving for the spectral density is an ill-posed problem. To get a meaningful resolution in frequency, one needs a high precision determination of the correlator and *many* imaginary time points. (An anisotropic lattice with $a_t \ll a_s$ helps.) To reduce the ambiguity in the result, it is popular to add extra constraints. A common one goes by the name "maximum entropy" [410]. Essentially, it favors a spectral density that deviates from a default spectral density only as much as required by the data – essentially an Occam's razor or Bayesian prior. Of course, the result then depends to some extent on the choice of the default spectral density.

The same method is used to extract transport coefficients, such as the electrical conductivity and shear and bulk viscosity, important for hydrodynamics [411, 412]. These quantities control the behavior of the spectral density of the correlator of the electromagnetic current and the stress-energy tensor, respectively, close to zero frequency.

Lecture 3: Chiral symmetry restoration

In this third lecture we consider features of the high temperature transition related to the partial restoration of chiral symmetry, including the behavior of the chiral condensate, the chiral susceptibility, and the hadron spectrum. Also discussed is the question of the restoration of the gauge anomaly and an analysis of the universal critical behavior.

6.4 Signals for Chiral Symmetry

Let us recall what is meant by "chiral symmetry". We start with the continuum Euclidean fermion action for N_f flavors in the presence of a color vector field:

$$S_F = \sum_{f=1}^{N_f} \int d^4x [\bar{\psi}_f(x)\gamma_\mu(\partial_\mu + igA^a_\mu \lambda^a/2)\psi_f(x) + m_f \bar{\psi}_f(x)\psi_f(x)] \,. \tag{6.57}$$

If all masses are degenerate, the action is invariant under an $SU(N_f) \times U(1)$ transformation. That is, the action is invariant under an infinitesimal change in the fermion fields $\psi(x) \to \psi(x) + \delta\psi(x)$, given by

$$\delta\psi(x) = \left(i\theta^0/2 + i\theta^k \tau^k/2\right)\psi(x) \,, \tag{6.58}$$

where τ^k are generators of $SU(N_f)$. A consequence of this symmetry is that hadrons appear in degenerate flavor multiplets.

When the fermion masses are zero the symmetry increases to $SU(N_f)_L \times SU(N_f)_R \times U(1) \times U_A(1)$. The action is invariant under the infinitesimal change

$$\delta\psi(x) = \left(i\theta^0/2 + i\theta^k\tau^k/2 + i\phi^0\gamma_5/2 + i\phi^k\tau^k\gamma_5/2\right)\psi(x) \,, \tag{6.59}$$

$$\delta\bar{\psi}(x) = \bar{\psi}(x)\left(-i\theta^0/2 - i\theta^k\tau^k/2 + i\phi^0\gamma_5/2 + i\phi^k\tau^k\gamma_5/2\right) \,. \tag{6.60}$$

One might expect larger hadron multiplets as a consequence of this symmetry, but how it is realized in the hadron spectrum depends on mechanisms that break it, as we discuss next.

At zero temperature the $U_A(1)$ symmetry (ϕ^0 term) is broken by the gauge anomaly, a quantum effect that appears at one-loop order. Then the axial chiral symmetry (ϕ^k terms) is broken spontaneously at zero temperature. The breaking of the symmetry results in a nonvanishing expectation value of the "chiral condensates" for each flavor:

$$\left\langle \bar{\psi}_f \psi_f \right\rangle \neq 0 \,. \tag{6.61}$$

The spontaneous breaking of the ϕ^k symmetry gives rise to $N_f^2 - 1$ Goldstone bosons. Had the $U_A(1)$ symmetry been spontaneously broken, we would have had one more Goldstone boson.

Since, in nature, the up and down quarks are nearly massless, let us examine in more detail the $N_f = 2$ case and consider the transformation of quark bilinears under the chiral symmetry. We define the interpolating operators ($f_0 \equiv \sigma$; $a_0 \equiv \delta$)

$$\pi^k = \bar{\psi}\tau^k\gamma_5\psi \,, \quad f_0 = \bar{\psi}\psi \,, \tag{6.62}$$

$$a_0^k = \bar{\psi}\tau^k\psi \,, \quad \eta = \bar{\psi}\gamma_5\psi \,. \tag{6.63}$$

Table 6.1 Mixing pattern of quark bilinears for two flavors under $SU(2)_L \times SU(2)_R$ and $U_A(1)$ transformations

	$SU(2)_L \times SU(2)_R$		
$U_A(1)$	$\pi : \bar{\psi}\tau\gamma_5\psi$	$\leftrightarrow$	$f_0 : \bar{\psi}\psi$
	$\updownarrow$		$\updownarrow$
	$a_0 : \bar{\psi}\tau\psi$	$\leftrightarrow$	$\eta : \bar{\psi}\gamma_5\psi$

Then under an $SU(2)$ axial transformation

$$\delta\pi^k = i\phi^k f_0\,, \quad \delta f_0 = i\phi^k \pi^k\,, \tag{6.64}$$

$$\delta a_0^k = i\phi^k \eta\,, \quad \delta\eta = i\phi^k a_0^k\,, \tag{6.65}$$

and under a $U_A(1)$ (axial) transformation

$$\delta\pi^k = i\phi^0 a_0^k\,, \quad \delta f_0 = i\phi^0 \eta\,, \tag{6.66}$$

$$\delta a_0^k = i\phi^0 \pi^k\,, \quad \delta\eta = i\phi^0 f_0\,. \tag{6.67}$$

The mixing of the bilinears under both transformations is mapped in Table 6.1.

6.4.1 Chiral Effective Theory and Symmetry Restoration

When quark masses are not zero, but only small, the Goldstone bosons still have small masses, and they dominate the physics of QCD at low temperature and long wavelength. This observation leads to a low-energy description of QCD, the "chiral effective theory" based on $N_f^2 - 1$ Goldstone bosons, π^k. The nonlinear version of this theory is usually formulated in terms of the $SU(N_f)$ fields:

$$U = \exp\left(i\hat{\pi}_k \tau_k / f\right)\,. \tag{6.68}$$

Here f is a low energy constant (closely related to the pion decay constant). In terms of these fields the chiral effective Lagrange density is

$$\mathcal{L} = \frac{f^2}{4}\,\mathrm{Tr}\left(\partial_\mu U\, \partial_\mu U^\dagger\right) + f^2 B\,\mathrm{Re}\,\mathrm{Tr}(MU)\,, \tag{6.69}$$

where $M = \mathrm{diag}\{m_1, m_2, \dots\}$ contains the quark masses. B is another low-energy constant. When $M = 0$, the Lagrange density is invariant under the chiral transformation

$$U \to V_R U V_L^\dagger\,. \tag{6.70}$$

If we put the low energy theory on a lattice with spacing a and make the masses degenerate, we can approximate the partial derivatives with

$$\partial_\mu U(x) \approx [U(x + a\hat{\mu}) - U(x - a\hat{\mu})]/(2a) . \tag{6.71}$$

If for $N_f = 2$ we write $U(x) = u_0(x) + i \sum_{k=1}^{3} u_k(x)\sigma_k$, where $u \cdot u = 1$, then the kinetic energy term in the Lagrange density becomes

$$\frac{f^2}{4a}\left[2 - 2\sum_{\mu} u(x) \cdot u(x + a\hat{\mu})\right] + 2f^2 B m u_0(x) . \tag{6.72}$$

This is the Lagrange density for a 3D $O(4)$ ferromagnet. The external field is proportional to the quark mass m, and the magnetization is proportional to $u_0 = \mathrm{Tr}U/2$. These observations lead to some important consequences for the chiral effective theory and, therefore, for QCD:

1. The chiral model behaves like a ferromagnetic spin system. For $N_f = 2$ it is equivalent to an $O(4)$ model.
2. Quark masses play the role of a magnetic field. $\mathrm{Re\,Tr}U$ plays the role of magnetization. It is the analog of $\langle\bar{\psi}\psi\rangle$.
3. At low temperatures we expect spontaneous symmetry breaking, and at high temperatures we expect symmetry restoration, just as with a ferromagnet.
4. Restoration of $SU(N_f)_L \times SU(N_f)_R$ at high T in QCD, therefore seems certain.
5. Restoration of the chiral symmetry is certainly associated with a phase transition. At nonzero quark masses there need not be a phase transition, and the restoration is found to be gradual (a 'crossover'); at sufficiently high mass we expect no chiral phase transition.

Whether the $U_A(1)$ symmetry is restored is a separate question and depends on the fate of the anomaly at high T. We have not included this symmetry in the simple chiral effective theory above. Pisarski and Wilczek [413] did this and concluded that the nature of the chiral phase transition depends on N_f and on whether the $U_A(1)$ symmetry is simultaneously restored:

1. For $N_f \geq 3$ the phase transition is first order.
2. The $U_A(1)$ symmetry should be restored at least asymptotically at high T, but its restoration need not occur at the same temperature as that of $SU(N_f)_L \times SU(N_f)_R$.
3. For $N_f = 2$, the nature of the phase transition depends on what happens with $U_A(1)$.
4. If $U_A(1)$ is effectively restored at the same temperature as $SU(N_f)_L \times SU(N_f)_R$, the transition can be a fluctuation-driven first-order transition.
5. Otherwise, it is continuous (second order).

These observations allow us to characterize the QCD high temperature phase transition as a function of the light quark masses, as shown in Fig. 6.10. The figure

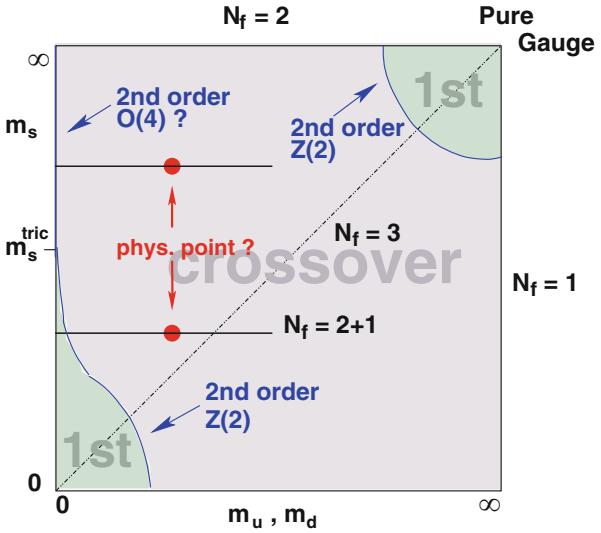

Fig. 6.10 A cartoon showing the character of the QCD high temperature phase transition as a function of the light, degenerate (up and down) quark masses and the strange quark mass [414]. Key features are the expected first-order phase transition when all three quark masses are small, the second-order phase transition at zero light quark masses (left axis) when the strange quark mass is large, the first order deconfinement transition when the quark masses are so large, we recover, approximately, the Yang-Mills theory, and the crossover region for intermediate quark masses. Where the physical masses are located in this picture is uncertain, as indicated. In one case, at fixed strange quark mass, there is a first order phase transition at low light quark mass. In the other case there is only a second order transition at zero light quark mass

is only a sketch. To make it quantitative requires a lattice QCD simulation, which can tell us (1) whether there is a phase transition at the physical (nonzero) values of the light (up and down) quark masses or only at zero quark masses, (2) how large the masses can be before the phase transition is lost, and (3) at what temperature the $U_A(1)$ symmetry is (at least effectively) restored?

6.4.2 *Signals of Chiral Symmetry Restoration*

We list a variety of indicators of chiral symmetry restoration:

1. **Chiral condensates** $\langle\bar{\psi}_f\psi_f\rangle$ The light quark chiral condensate is an order parameter for chiral symmetry. At zero mass it should vanish when the symmetry is restored. If quark masses are not zero, we can still use it as an indicator, even if it is not, strictly, an order parameter.
2. **Chiral susceptibility** $\chi_f = \partial\langle\bar{\psi}_f\psi_f\rangle/\partial m$ The susceptibility should peak at the transition (or crossover) temperature.

3. **Hadron correlators** Hadron correlators, which imply, also, hadron masses, should become equal. For $SU(2)_L \times SU(2)_R$ we have $C_\pi(x) = C_{f_0}(x)$.

$$C_{f_0}(x) = \langle f_0(x) f_0(0) \rangle \tag{6.73}$$

$$C_\pi(x)\delta_{k,k'} = \left\langle \pi^k(x)\pi^{k'}(0) \right\rangle . \tag{6.74}$$

Similarly $C_\eta(x) = C_{a_0}(x)$. With restoration of $U_A(1)$ we also have $C_\pi(x) = C_{a_0}(x)$ and $C_{f_0}(x) = C_\eta(x)$.

We turn, now, to results from lattice simulations that reflect restoration of chiral symmetry. The lattice implementation of chiral symmetry depends on the fermion formulation: The Wilson/clover fermionic actions break chiral symmetry explicitly. The staggered (asqtad, HISQ) fermions preserve a remnant of chiral symmetry. Finally, the overlap and domain wall fermions aim to treat chiral symmetry exactly. For illustration, here, we discuss results for staggered fermions.

The chiral condensate at nonzero quark mass is ultraviolet divergent, which can be seen at one-loop order in QCD perturbation theory:

$$\left\langle \bar{\psi}_f \psi_f \right\rangle = m_f/a^2 + \dots . \tag{6.75}$$

Since this divergence appears for each flavor, it can be removed at this order by subtracting the light quark ($m_u = m_d$) and strange quark condensates, leading to the "subtracted condensate".

$$D_{ud,s}(T) = [\left\langle \bar{\psi}\psi \right\rangle_{ud} - m_{ud}/m_s \left\langle \bar{\psi}\psi \right\rangle_s] . \tag{6.76}$$

The chiral condensate is also subject to a multiplicative renormalization (independent of temperature). This effect can be removed in the ratio

$$\Delta_{ud,s}(T) = D_{ud,s}(T)/D_{ud,s}(T=0) , \tag{6.77}$$

before comparing results from different calculations. The resulting quantity from a lattice simulation is shown in Fig. 6.11. We see a rapid decrease in the chiral condensate as temperature is increased through the crossover region. Results for the chiral susceptibility are shown in Fig. 6.12.

As we have remarked above the restoration of the $U_A(1)$ symmetry leads to the equality of the π and a_0 correlators (of the corresponding local bilinears), $C_\pi(x)$ and $C_{a_0}(x)$. There is a particularly useful connection between the symmetry of the correlators and the spectral density of the Dirac matrix at zero eigenvalue [416]. This is seen by considering the related susceptibilities,

$$\chi_S = \left\langle \int C_{a_0}(x) d^4x \right\rangle , \quad \chi_P = \left\langle \int C_\pi(x) d^4x \right\rangle , \tag{6.78}$$

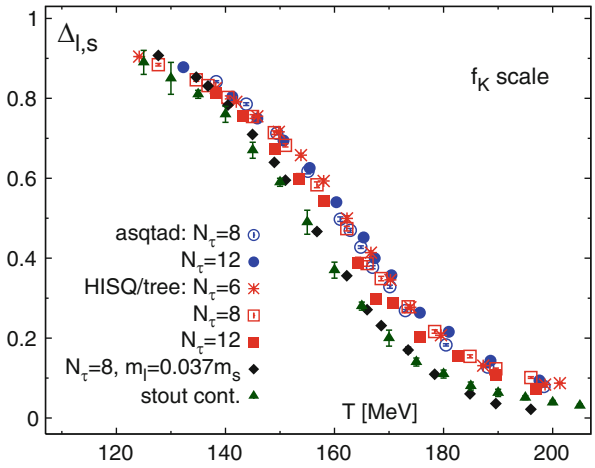

Fig. 6.11 Subtracted, normalized chiral condensate as a function of temperature [415]. We see a rapid decrease in the crossover region 150–180 MeV, indicating a partial restoration of chiral symmetry

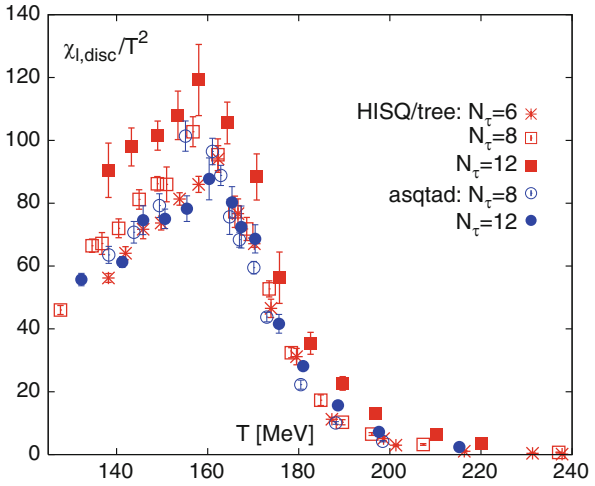

Fig. 6.12 Unrenormalized chiral (disconnected) susceptibility as a function of temperature [415]. We see a peak in the crossover region 150–180 MeV, an indication of partial restoration of chiral symmetry

which must also be equal. The susceptibilities are particularly useful, because they are related to the eigenspectrum of the lattice Dirac matrix:

$$\langle \bar{\psi}\psi \rangle = -m \int_{-\infty}^{\infty} d\lambda \frac{\rho(\lambda)}{\lambda^2 + m^2} \tag{6.79}$$

$$\chi_P - \chi_S = \int_{-\infty}^{\infty} d\lambda \frac{2m^2\rho(\lambda)}{(\lambda^2 + m^2)^2} \tag{6.80}$$

where m is the degenerate up and down quark mass and $\rho(\lambda)$ is the eigenvalue density. These expressions can be derived from a spectral decomposition of the quark propagators involved in the correlators. As the quark masses are decreased to zero, we get

$$\lim_{m\to 0} \langle \bar{\psi}\psi \rangle = -\pi\rho(0)\,, \tag{6.81}$$

also known as the Banks-Casher relation [31]. Restoration of the $SU(2)_L \times SU(2)_R$ symmetry implies that $\langle \bar{\psi}\psi \rangle = 0$, so then $\rho(0) = 0$. If a gap opens in the spectrum at $\lambda = 0$, then certainly $\chi_P - \chi_S = 0$ in the limit of zero mass. If, instead, the spectral density vanishes as $\rho(\lambda) = A\lambda^\alpha$, with suitable α, we can have vanishing $\langle \bar{\psi}\psi \rangle$ and nonvanishing $\chi_P - \chi_S$.

Thus a study of the eigenvalue density at small eigenvalue can help in testing the restoration of the $U_A(1)$ symmetry. An example of a numerical test of these ideas is given in Figs. 6.13 and 6.14 [416]. Lattice results thus far suggest that the $U_A(1)$ symmetry is not restored at the same temperature as $SU(2)_L \times SU(2)_R$, but more work is needed [417]. For a recent domain wall study on smaller lattices, see [418].

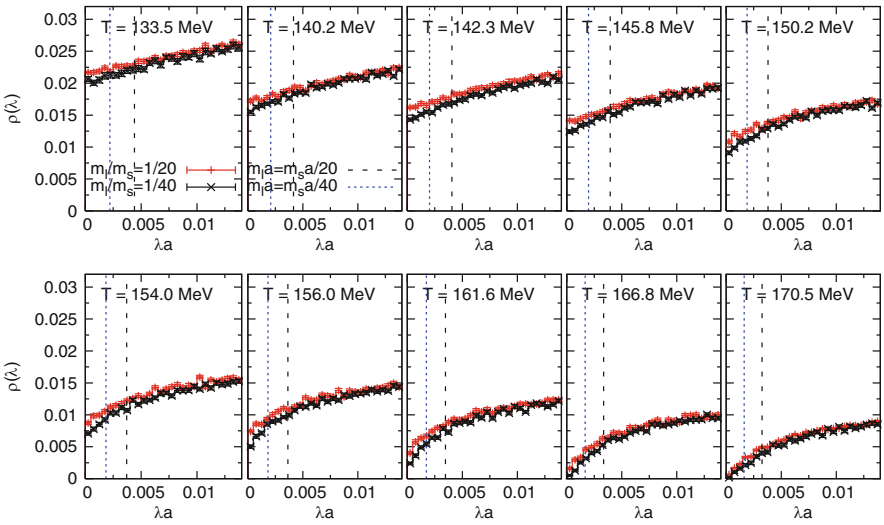

Fig. 6.13 Eigenvalue density as a function of eigenvalue for various temperatures [416]. There appears to be a zero for $T > 168$ MeV indicating restoration of the $SU(2)_L \times SU(2)_R$ chiral symmetry

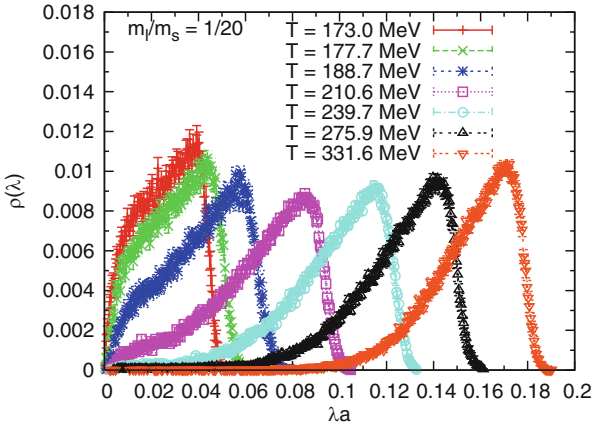

Fig. 6.14 Eigenvalue density as a function of eigenvalue for various temperatures [416]. Whether the apparent gap for $T > 240$ MeV is significant remains to be studied further [417]

Exercise 3 In terms of the Euclidean Dirac matrix $M = m + \not{D}$, the chiral condensate is

$$\langle \bar{\psi}\psi \rangle = \mathrm{Tr} M^{-1} . \tag{6.82}$$

The eigenvalues and eigenvectors of $\not{D}$ satisfy $Mu_n = i\lambda_n u_n$. Assume that the antihermitian $\not{D}$ operator also satisfies the anticommutation relation $\{\not{D}, \gamma_5\} = 0$.

Prove that (Banks-Casher)

$$\langle \bar{\psi}\psi \rangle = -m \int_{-\infty}^{\infty} d\lambda \frac{\rho(\lambda)}{\lambda^2 + m^2} . \tag{6.83}$$

where the spectral density is constructed from $1/V \sum_n \to \int d\lambda \rho(\lambda)$.

Then show that at zero mass $\langle \bar{\psi}\psi \rangle = -\pi\rho(0)$.

6.4.3 *Universality and Critical Behavior*

The theory of critical phenomena places systems in universality classes according to their symmetries and spatial dimension. They alone determine the critical exponents and universal scaling functions that control scaling and the functional dependence of key quantities close to the critical point.

For the remainder of this lecture we will assume that the critical point appears only at $T = T_c^0$ and $m_{ud} = 0$. Since the relevant chiral symmetry is $SU(2)_L \times SU(2)_R$, equivalent to $O(4)$, QCD is expected to fall into the 3D $O(4)$ universality

class. Staggered fermion implementations preserve a reduced symmetry, suggesting an $O(2)$ behavior at nonzero lattice spacing. The critical behavior of these two universality classes is very similar.

We discuss the critical behavior in QCD by rescaling T and m_{ud} to give t and h:

$$t = \frac{1}{t_0}\frac{T - T_c^0}{T_c^0}\,, \tag{6.84}$$

$$h = \frac{1}{h_0}H \quad \text{for } H = m_{ud}/m_s\,, \tag{6.85}$$

where m_{ud}/m_s is the ratio of light to strange quark masses. The quantities t_0 and h_0 are constants. These variables correspond to the temperature and magnetic field in the $O(4)$ spin system.

The free energy density as a function of quark masses and temperature in the vicinity of a critical point has two contributions, a universal singular part and a regular part.

$$f = -\frac{T}{V}\log Z \equiv f_{\text{sing}}(t,h) + f_{\text{reg}}(T, m_{ud}, m_s)\ . \tag{6.86}$$

Up to a rescaling of the variables (via h_0 and t_0), the singular part is universal. It can be expressed in terms of a universal function of a single scaling variable $z = t/h^{1/\beta\delta}$ where δ and β are universal critical exponents. The singular part is then

$$f_{\text{sing}}(t,h) = h^{1/\delta} f_s(z)\,, \tag{6.87}$$

where $f_s(z)$ is universal. (In the condensed matter literature, it is often called the "equation of state".) So, for example, the scaling function $f_s(z)$ in the 3D $O(4)$ model is the same as the QCD scaling function.

The free energy is thermodynamically fundamental, since most physical observables can be expressed as derivatives of the free energy. For many observables the singular part dominates over the regular part close to the critical point. Where this happens is called the Landau region. The size of this region is not universal.

The chiral condensate plays the role of magnetization in QCD. We define

$$M_b \equiv \frac{m_s \left\langle \bar{\psi}\psi \right\rangle_{ud}}{T^4}\,, \tag{6.88}$$

where

$$\left\langle \bar{\psi}\psi \right\rangle_{ud} = T/V\,\partial \log Z/\partial m_{ud}\,. \tag{6.89}$$

Then

$$M_b(T,H) = h^{1/\delta} f_G(t/h^{1/\beta\delta}) + f_{M,\text{reg}}(T,H)\,, \tag{6.90}$$

where the function f_G is universal. The chiral susceptibility is the derivative

$$\chi_{ud} = \frac{\partial}{\partial m_{ud}} \langle \bar{\psi}\psi \rangle_{ud} \ . \tag{6.91}$$

We get a scaling expression for it by differentiation

$$\frac{\chi_{ud}}{T^2} = \frac{T^2}{m_s^2} \left(\frac{1}{h_0} h^{1/\delta - 1} f_\chi(z) + \frac{\partial f_{M,reg}(T,H)}{\partial H} \right) , \tag{6.92}$$

where

$$f_\chi(z) = \frac{1}{\delta} \left[f_G(z) - \frac{z}{\beta} f_G'(z) \right] . \tag{6.93}$$

So the behavior of $\langle \bar{\psi}\psi \rangle_{ud}$ and χ_{ud} is governed by the same singular function.

A fit to lattice measurements using this analysis is shown in Fig. 6.15. The universal scaling function used in the fit was taken from a separate study of the $O(4)$ spin model. To obtain the agreement shown, it was necessary to include a regular part, parameterized with its leading-order Taylor expansion in the scaling variables. A byproduct of this analysis was the value $T_c = 154(9)$ MeV for the crossover temperature at physical quark masses

Lecture 4: Connection with phenomenology

In this fourth and last lecture we consider a variety of observables of more direct interest to the phenomonology of heavy ion collisions, including the equation of state at zero and nonzero density, the charm quark contribution to the equation of state, and fluctuations in conserved charges.

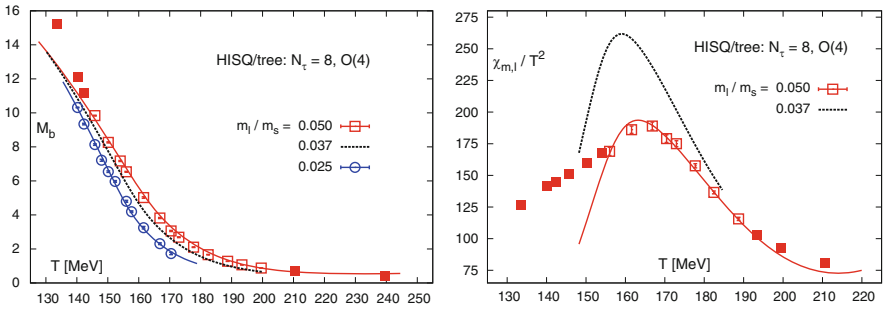

Fig. 6.15 Fit to the chiral condensate (left) and susceptibility (right) to the same scaling function plus a small regular part [415]

6.5 Equation of State

6.5.1 Models at Low and High Temperature

At extremes of temperatures some approximations are possible. We discuss the hadron resonance gas model, applicable at low temperature and the Stefan-Boltzmann gas model, at high temperature.

6.5.1.1 Hadron Resonance Gas Model

The hadron resonance gas model is a simple (simple-minded!) model often used as an approximation to the low temperature behavior of QCD. Introduced by Hagedorn, it approximates the QCD ensemble as a noninteracting gas of mesons and baryons, including resonances. All particles (and resonances) listed in the Particl Data Group summary are included. One stops at some cut off mass M. Interactions are treated only in the sense that resonances are included. One expects the model to be good for $T \ll m_\pi$, the lowest mass. If the density of states grows as $dN/dm = C\exp(m/T_c)$ then the partition function diverges for $T > T_c$ (Hagedorn limiting temperature). At this point one has to change the model by switching to quark and gluon degrees of freedom for $T > T_c$.

In the low temperature limit we get an explicit expression for the partition function for mesons/baryons (M/B):

$$\log \mathcal{Z} = \sum_i \log \mathcal{Z}^{\mathcal{M}} + \sum_i \log \mathcal{Z}^{\mathcal{B}} . \tag{6.94}$$

For the ith meson or baryon we have

$$\begin{aligned} \log \mathcal{Z}_{M_i}^{M/B} &= \mp \frac{V d_i}{2\pi^2} \int_0^\infty dk k^2 \log(1 \mp z_i e^{-\varepsilon_i/T}) \\ &= \frac{VT^3}{2\pi^2} d_i \left(\frac{M_i}{T}\right)^2 \sum_{k=1}^{\infty} (\pm 1)^{k+1} \frac{z_i^k}{k^2} K_2(kM_i/T) , \end{aligned} \tag{6.95}$$

where d_i is a multiplicity factor.

6.5.1.2 Stefan-Boltzmann Limit

In the high temperature limit the QCD running coupling is expected to be small, so we can treat the quarks and gluons as approximately noninteracting and massless, leading to the relativistic ideal gas limit (Stefan-Boltzmann gas). In the presence

of a chemical potential μ_f for conserved flavor number N_f, the Stefan-Boltzmann pressure is

$$\frac{p_{SB}}{T^4} = \frac{8\pi^2}{45} + \frac{7\pi^2}{20} + \sum_{f=u,d,s} \left[\frac{1}{2} \left(\frac{\mu_f}{T} \right)^2 + \frac{1}{4\pi^2} \left(\frac{\mu_f}{T} \right)^4 \right] . \tag{6.96}$$

6.5.2 Equation of State at Zero Density

More generally, at any temperature thermodynamic identities relate the energy density and pressure to the partition function as follows:

$$\varepsilon = \frac{T^2}{V} \left. \frac{\partial \log Z}{\partial T} \right|_V \tag{6.97}$$

$$p = T \left. \frac{\partial}{\partial V} \log Z \right|_T . \tag{6.98}$$

To calculate them separately on the lattice is a bit involved. It is more convenient to calculate the "interaction measure"

$$I = \varepsilon - 3p = -\frac{T}{V} \frac{d \log Z}{d \log a} . \tag{6.99}$$

For the Wilson gauge action we get

$$I = -T/V (d \log g^2 / d \log a) \langle S_G \rangle . \tag{6.100}$$

We must subtract the vacuum value to remove an ultraviolet divergence. From now on, we assume this has been done and drop the Δ.

$$\Delta I = I(T) - I(0) . \tag{6.101}$$

Exercise 4 The previous discussion gives the thermodynamic identities that relate the energy density and pressure to derivatives of the ensemble free energy with respect to temperature and volume, respectively. On a lattice of a fixed number of sites $N_s^3 \times N_t$, the volume is given in terms of the spatial and temporal lattice constants a_s and a_t by $N_s^3 a_s^3$, and the inverse temperature is given by $a_t N_t$. So we can relate the derivatives in the thermodynamic identities to derivatives with respect to a_s and a_t. To relate these derivatives to the lattice action, one must take care to include the appropriate factors of a_s and a_t in the expression for the lattice action and to remember that the gauge coupling g^2 also depends on the lattice constants.

With these preliminaries in mind, show that

$$I \equiv \varepsilon - 3p = -T/V(d \log g^2/d \log a) \langle S_G \rangle \ . \tag{6.102}$$

For sufficiently large volume the pressure is independent of volume:

$$\log Z = pV/T \ . \tag{6.103}$$

so the interaction measure is

$$I = -\frac{T}{V} \frac{d(pV/T)}{d \log a} \ , \tag{6.104}$$

and, if the temperature is varied by varying a with fixed N_τ, we can determine the pressure from it by integrating from low temperature (large $a = a_0$) to high temperature (small a).

$$p(a)a^4 - p(a_0)a_0^4 = -\int_{\log a_0}^{\log a} \Delta I(a')(a')^4 \, d \log a' \ . \tag{6.105}$$

At sufficiently low T_0 we may take $p(a_0) = 0$, or take its small value from the hadron resonance gas model.

Exercise 5 Derive the integral expression for the pressure in Eq. (6.105).

For illustration we show some lattice results for a variety of thermodynamic quantities obtained in the past few years. To find the most recent results, the proceedings of the annual Lattice conferences are a good place to start.[2]

Results for the interaction measure are shown in Fig. 6.16. The corresponding energy density and pressure are shown in Fig. 6.17. Next, the entropy density $s = (\varepsilon + p)/T$ is shown in Fig. 6.18. Finally, the speed of sound is

$$c_s^2 = \frac{\mathrm{d}p}{\mathrm{d}\epsilon} = \epsilon \frac{\mathrm{d}(p/\epsilon)}{\mathrm{d}\epsilon} + \frac{p}{\epsilon} \ . \tag{6.106}$$

[2]Recent proceedings of the Lattice conference series are published by SISSA: http://pos.sissa.it/ and can be found under the search term "Lattice Field Theory."

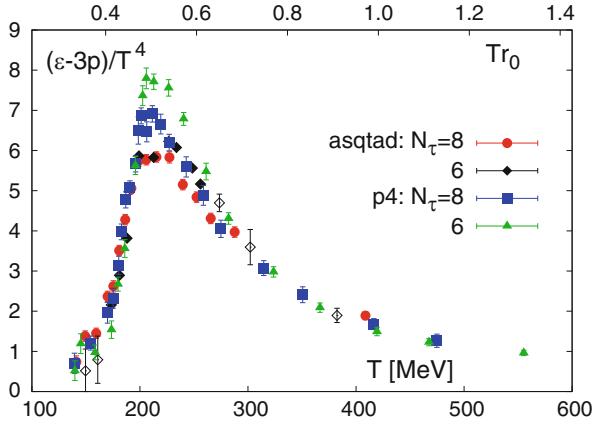

Fig. 6.16 Interaction measure $\varepsilon - 3p$ as a function of temperature [408]. As the lattice spacing is decreased the peak softens a bit

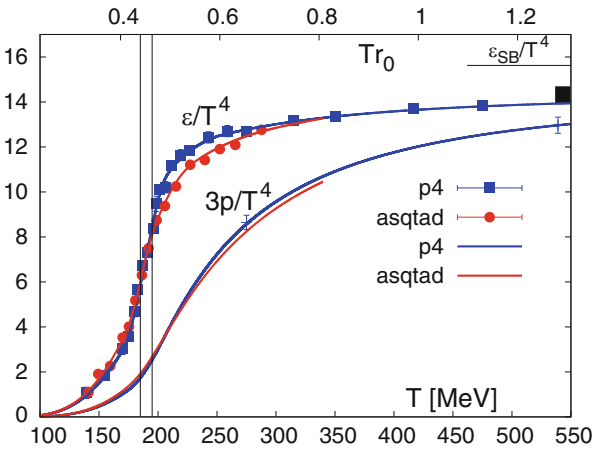

Fig. 6.17 Energy density and three times pressure as a function of temperature from [408]. We see a strong increase in the temperature range 150–200 MeV. These results are for higher than physical mass and for nonzero lattice spacing

It is illustrated in Fig. 6.19. All of these quantities are of importance for hydrodynamic modeling of the quark-gluon plasma. However, it should be noted that these results are for higher than physical mass and for nonzero lattice spacing and require extrapolation to physical values to be realistic.

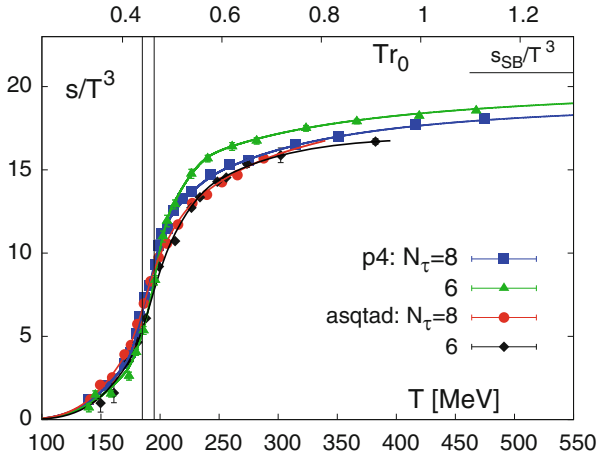

Fig. 6.18 Entropy density as a function of temperature from [408]

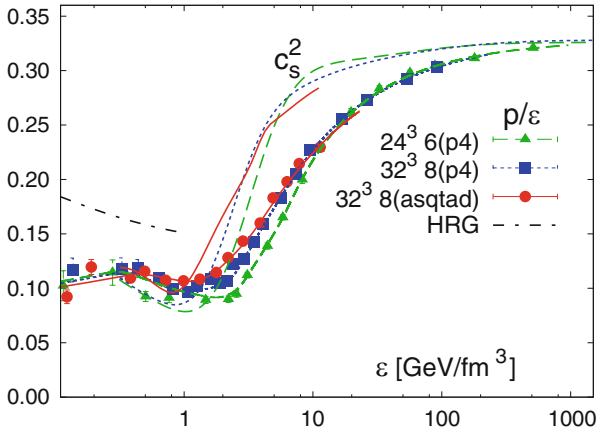

Fig. 6.19 Speed of sound from [408]

6.5.3 Equation of State at Nonzero Density

We observed in the first lecture that we cannot simulate directly at $\mu \neq 0$, because the fermion determinant is complex. For heavy ion collisions, the chemical potentials are small. Therefore, one is led to a Taylor series expansion for small μ. For the $2+1$ flavor case, the expansion reads

$$\frac{p}{T^4} = \sum_{n,m=0}^{\infty} c_{nm}(T) \left(\frac{\mu_{ud}}{T}\right)^n \left(\frac{\mu_s}{T}\right)^m , \tag{6.107}$$

The coefficients are evaluated at $\mu_{ud} = \mu_s = 0$

$$c_{nm}(T) = \frac{1}{n!}\frac{1}{m!}\frac{1}{T^3 V}\frac{\partial^{n+m}\log Z}{\partial(\mu_{ud}/T)^n \partial(\mu_s/T)^m}\bigg|_{\mu_{ud,s}=0}. \tag{6.108}$$

The derivatives are expectation values of combinations of traces of the inverse of the lattice Dirac matrix. An example of a calculation at nonzero chemical potential is given in Fig. 6.20. As in this figure, the results are often shown at fixed ratios of entropy density to baryon density. Since in heavy ion collisions the strange number density n_s is zero, it is necessary to tune $\mu_\ell = \mu_u = \mu_d$ and μ_s to get $n_s = 0$ at fixed s/n_B. The tuned trajectories are shown in Fig. 6.21. One often assumes an isentropic formation and expansion of the plasma. The equation of state at constant entropy along the trajectories plotted in Fig. 6.21 is shown in Fig. 6.20.

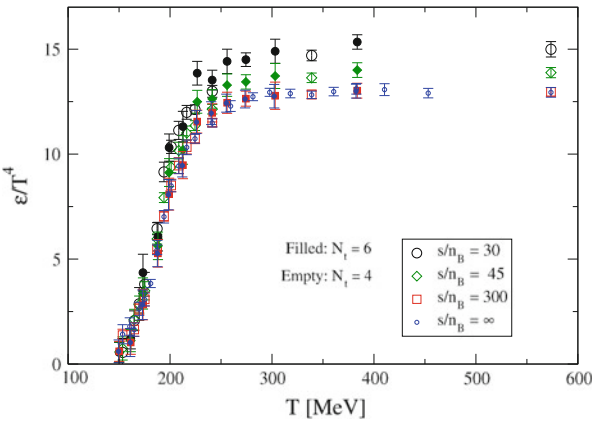

Fig. 6.20 Isentropic equation of state: energy density as a function of temperature at three constant ratios s/n_B of entropy density to baryon number density from [419]

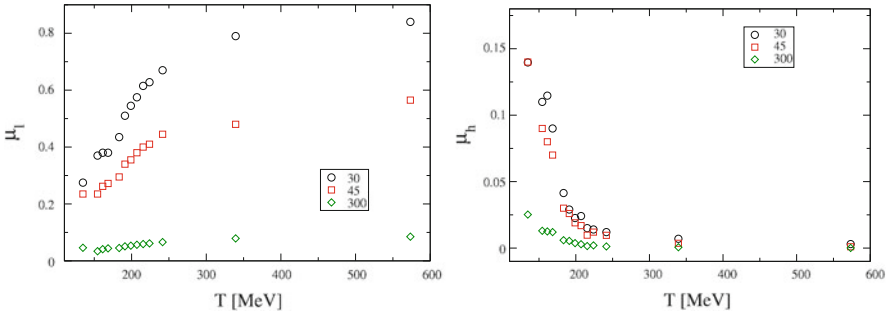

Fig. 6.21 Tuned values of the light quark chemical potential μ_ℓ and strange quark chemical potential μ_h as a function of temperature giving zero strangeness density at three fixed ratios s/n_B of entropy density to baryon number density [420]

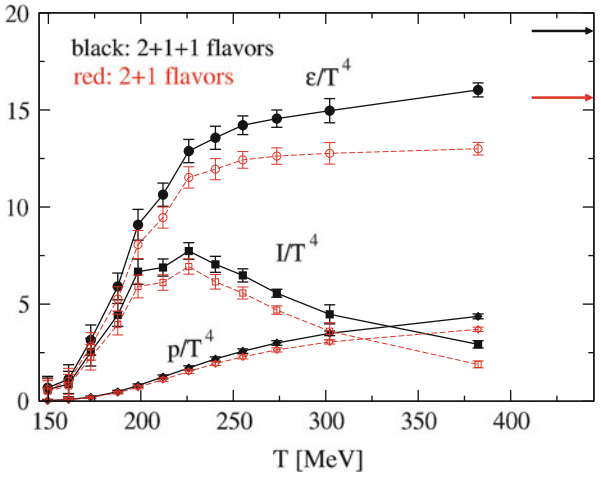

Fig. 6.22 Contribution of the charm quark to the equation of state [419]

6.5.4 Charm Quark Contribution

It is interesting to consider how charm quarks contribute to the equation of state. Whether the quark plasma in a heavy ion collision has time to equilibrate charm is an open question, but in the early universe it certainly does. The charm contribution to the equation of state can be done without including charm quarks explicitly in the statistical ensemble (quenched charm) with the result shown in Fig. 6.22. We see that charm effects start to become visible above about $T = 200$ MeV. The stout and p4 action results are a bit smaller than the result from the asqtad action.

6.6 Fluctuations of Conserved Charges

In a neutral ensemble, conserved charges still fluctuate about zero.

$$\delta N_X \equiv N_X - \overline{N_X}\,. \tag{6.109}$$

So we define susceptibilities of the generic form,

$$\chi_2^X = \langle (\delta N_X)^2 \rangle / (VT^3)\,, \tag{6.110}$$

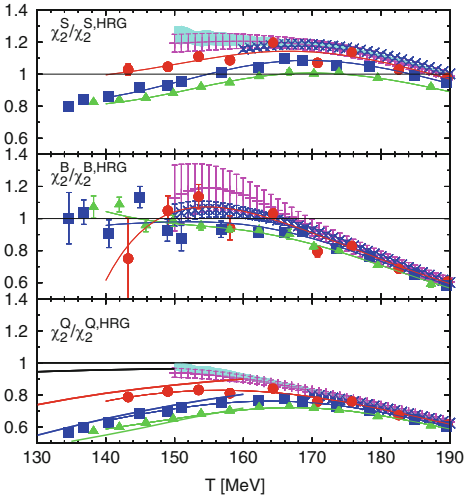

Fig. 6.23 Fluctuations in baryon number B, electric charge Q, and strangeness S as a function of temperature from [421]. Plotted is the lattice susceptibility divided by the hadron-resonance-gas susceptibility. The *magenta bars and cyan bands* show results of two extrapolations to zero lattice spacing. We see that the HRG agrees reasonably well for B and Q, but not S

for X = baryon number B, strangeness S, and electric charge Q. They can be derived from the second-order Taylor coefficients in the expansion of the pressure in terms of the chemical potentials:

$$\chi_2^X = \left.\frac{\partial^2 p/T^4}{\partial \hat{\mu}_X^2}\right|_{\boldsymbol{\mu}=0}, \tag{6.111}$$

$$\chi_{11}^{XY} = \left.\frac{\partial^2 p/T^4}{\partial \hat{\mu}_X \partial \hat{\mu}_Y}\right|_{\boldsymbol{\mu}=0}, \tag{6.112}$$

where $\hat{\mu}_X = \mu_X/T$. Results for these quantities are shown in Fig. 6.23.

Conclusions
What has lattice QCD taught us about the behavior of QCD at high temperature and density?

1. We have learned a great deal about the qualitative behavior of QCD in thermal equilibrium at low chemical potential for a few flavors and nonzero quark masses. This reach of lattice QCD is illustrated in Fig. 6.24.
2. We have fairly good control of a variety of important quantities needed for hydrodynamic modeling.
3. We have good quantitative predictions for fluctuations in conserved charges.

(continued)

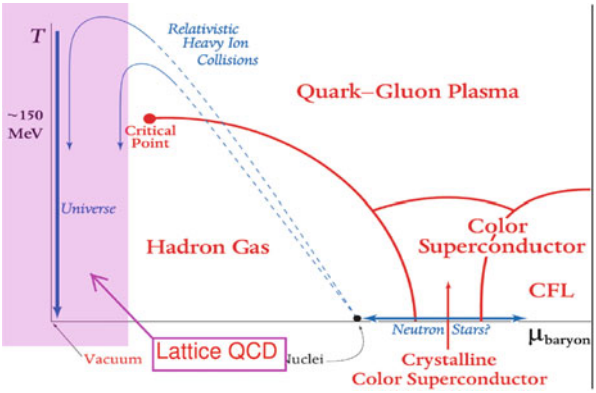

Fig. 6.24 A speculative phase diagram for high temperature and density QCD. The *shaded region* indicates the current reach of lattice QCD

What might lattice QCD still teach us?

1. We need better ideas/methods for dealing with higher baryon density.
2. We hope to learn more about whether the critical endpoint is accessible to experiment.
3. We expect to learn more about transport properties: viscosity, electric conductivity, etc. This is difficult, though.
4. We do not yet have a completely satisfactory understanding of what happens at the chiral critical point at low $m_u = m_d$, but this will come.
5. We expect to learn more about the behavior of the QGP in strong magnetic fields.

Acknowledgements I thank the organizers of the summer school for their hospitality and excellent organization. I am grateful to Ludmila Levkova for critical comments.

References

1. K.G. Wilson, Phys. Rev. **D10**, 2445 (1974)
2. M. Creutz, Phys. Rev. **D21**, 2308 (1980)
3. I. Montvay, G. Munster, *Quantum Fields on a Lattice* (Cambridge University Press, Cambridge, 1994)
4. H.J. Rothe, World Sci. Lect. Notes Phys. **74**, 1 (2005)
5. J. Smit, Cambridge Lect. Notes Phys. **15**, 1 (2002)
6. C. Gattringer, C.B. Lang, Lect. Notes Phys. **788**, 1 (2010)
7. C. Itzykson, J. Zuber, *Quantum Field Theory* (Mcgraw-Hill, New York, 1980)
8. L. Susskind, Phys. Rev. **D16**, 3031 (1977)
9. G. Kilcup, S.R. Sharpe, Nucl. Phys. **B283**, 493 (1987)
10. HPQCD Collaboration, UKQCD Collaboration, E. Follana et al., Phys. Rev. **D75**, 054502 (2007). arXiv:hep-lat/0610092
11. M. Lüscher, Lectures given at Summer School 'Fields, Strings and Critical Phenomena', Les Houches, France, Jun 28–Aug 5, 1988
12. S. Capitani, Phys. Rept. **382**, 113 (2003). arXiv:hep-lat/0211036
13. M. Lüscher, P. Weisz, Nucl. Phys. **B266**, 309 (1986)
14. C. Becchi, A. Rouet, R. Stora, Ann. Phys. **98**, 287 (1976)
15. C. Monahan, PoS **LATTICE2013**, 021 (2014). arXiv:1310.4536
16. HPQCD Collaboration, C. Davies et al., Phys. Rev. **D78**, 114507 (2008). arXiv:0807.1687
17. P. Weisz, (2010). arXiv:1004.3462
18. K. Symanzik, Nucl. Phys. **B226**, 187 (1983)
19. W. Bietenholz, U. Gerber, M. Pepe, U.-J. Wiese, JHEP **1012**, 020 (2010). arXiv:1009.2146
20. M. Lüscher, S. Sint, R. Sommer, P. Weisz, Nucl. Phys. **B478**, 365 (1996). arXiv:hep-lat/9605038
21. M. Lüscher, (1998). arXiv:hep-lat/9802029
22. M. Lüscher, S. Sint, R. Sommer, P. Weisz, U. Wolff, Nucl. Phys. **B491**, 323 (1997). arXiv:hep-lat/9609035
23. R. Sommer, Nucl. Phys. **B411**, 839 (1994). arXiv:hep-lat/9310022
24. R. Sommer, PoS **LATTICE2013**, 015 (2014). arXiv:1401.3270
25. M. Lüscher, P. Weisz, JHEP **0207**, 049 (2002). arXiv:hep-lat/0207003
26. H. Meyer, M. Teper, JHEP **0412**, 031 (2004). arXiv:hep-lat/0411039
27. M. Lüscher, K. Symanzik, P. Weisz, Nucl. Phys. **B173**, 365 (1980)
28. M. Lüscher, G. Munster, P. Weisz, Nucl. Phys. **B180**, 1 (1981)
29. O. Aharony, Z. Komargodski, JHEP **1305**, 118 (2013). arXiv:1302.6257
30. A. Athenodorou, B. Bringoltz, M. Teper, JHEP **1102**, 030 (2011). arXiv:1007.4720

H.-W. Lin, H.B. Meyer (eds.), *Lattice QCD for Nuclear Physics*, Lecture Notes in Physics 889, DOI 10.1007/978-3-319-08022-2

31. T. Banks, A. Casher, Nucl. Phys. **B169**, 103 (1980)
32. L. Giusti, M. Lüscher, JHEP **03**, 013 (2009). arXiv:0812.3638
33. M. Lüscher, JHEP **1304**, 123 (2013). arXiv:1302.5246
34. S. Aoki et al., Eur. Phys. J. C74(9), 2890 (2014). arXiv:1310.8555
35. QCDSF Collaboration, M. Göckeler et al., Nucl. Phys. **B688**, 135 (2004). arXiv:hep-lat/0312032
36. M. Bochicchio, L. Maiani, G. Martinelli, G.C. Rossi, M. Testa, Nucl. Phys. **B262**, 331 (1985)
37. M. Lüscher, S. Sint, R. Sommer, H. Wittig, Nucl. Phys. **B491**, 344 (1997). arXiv:hep-lat/9611015
38. ALPHA, S. Capitani, M. Lüscher, R. Sommer, H. Wittig, Nucl. Phys. **B544**, 669 (1999). arXiv:hep-lat/9810063
39. L. Giusti, H.B. Meyer, JHEP **1301**, 140 (2013). arXiv:1211.6669
40. H.B. Nielsen, M. Ninomiya, Phys. Lett. **B105**, 219 (1981)
41. H.B. Nielsen, M. Ninomiya, Nucl. Phys. **B185**, 20 (1981)
42. H.B. Nielsen, M. Ninomiya, Nucl. Phys. **B193**, 173 (1981)
43. M. Lüscher, Phys. Lett. **B428**, 342 (1998). arXiv:hep-lat/9802011
44. F. Wilczek, Phys. Rev. Lett. **59**, 2397 (1987)
45. P.H. Ginsparg, K.G. Wilson, Phys. Rev. **D25**, 2649 (1982)
46. H. Neuberger, Phys. Lett. **B417**, 141 (1998). arXiv:hep-lat/9707022
47. P. Hasenfratz, V. Laliena, F. Niedermayer, Phys. Lett. **B427**, 125 (1998). arXiv:hep-lat/9801021
48. M. Lüscher, (2000). arXiv:hep-th/0102028
49. S. Chandrasekharan, U. Wiese, Prog. Part. Nucl. Phys. **53**, 373 (2004). arXiv:hep-lat/0405024
50. D.B. Kaplan, 223 (2009). arXiv:0912.2560
51. D.B. Kaplan, Phys. Lett. **B288**, 342 (1992). arXiv:hep-lat/9206013
52. Y. Shamir, Nucl. Phys. **B406**, 90 (1993). arXiv:hep-lat/9303005
53. V. Furman, Y. Shamir, Nucl. Phys. **B439**, 54 (1995). arXiv:hep-lat/9405004
54. M. Lüscher, Phys. Lett. **B593**, 296 (2004). arXiv:hep-th/0404034
55. L. Del Debbio, L. Giusti, C. Pica, Phys. Rev. Lett. **94**, 032003 (2005). arXiv:hep-th/0407052
56. B. Lucini, M. Teper, JHEP **06**, 050 (2001). arXiv:hep-lat/0103027
57. L. Del Debbio, H. Panagopoulos, E. Vicari, JHEP **0208**, 044 (2002). arXiv:hep-th/0204125
58. M. Lüscher, R. Narayanan, P. Weisz, U. Wolff, Nucl. Phys. **B384**, 168 (1992). arXiv:hep-lat/9207009
59. G. de Divitiis, R. Frezzotti, M. Guagnelli, R. Petronzio, Nucl. Phys. **B422**, 382 (1994). arXiv:hep-lat/9312085
60. M. Lüscher, R. Sommer, P. Weisz, U. Wolff, Nucl. Phys. **B413**, 481 (1994). arXiv:hep-lat/9309005
61. ALPHA Collaboration, M. Della Morte et al., Nucl. Phys. **B713**, 378 (2005). arXiv:hep-lat/0411025
62. PACS-CS Collaboration, S. Aoki et al., JHEP **0910**, 053 (2009). arXiv:0906.3906
63. ALPHA Collaboration, F. Tekin, R. Sommer, U. Wolff, Nucl. Phys. **B840**, 114 (2010). arXiv:1006.0672
64. ALPHA Collaboration, M. Della Morte et al., Nucl. Phys. **B729**, 117 (2005). arXiv:hep-lat/0507035
65. S. Borsanyi, G. Endrodi, Z. Fodor, S. Katz, K. Szabo, JHEP **1207**, 056 (2012). arXiv:1204.6184
66. L. Giusti, M. Pepe, Phys. Rev. Lett. **113**, 031601 (2014). arXiv:1403.0360
67. M. Lüscher, (2010). arXiv:1002.4232
68. H.B. Meyer, (2004). arXiv:hep-lat/0508002
69. S. Duane, A. Kennedy, B. Pendleton, D. Roweth, Phys. Lett. **B195**, 216 (1987)
70. A. Kennedy, (2006). arXiv:hep-lat/0607038
71. S. Schaefer, PoS **LATTICE2012**, 001 (2012). arXiv:1211.5069
72. Particle Data Group, J. Beringer et al., Phys. Rev. **D86**, 010001 (2012)
73. T. Appelquist et al., (2013). arXiv:1309.1206

74. D. Lee, B. Borasoy, T. Schaefer, Phys. Rev. **C70**, 014007 (2004). arXiv:nucl-th/0402072
75. B. Borasoy, E. Epelbaum, H. Krebs, D. Lee, U.-G. Meißner, Eur. Phys. J. **A35**, 357 (2008). arXiv:0712.2993
76. A. Bulgac, J.E. Drut, P. Magierski, Phys. Rev. **A78**, 023625 (2008). arXiv:0803.3238
77. C.J. Morningstar, M.J. Peardon, Phys. Rev. **D60**, 034509 (1999). arXiv:hep-lat/9901004
78. E. Gregory et al., JHEP **1210**, 170 (2012). arXiv:1208.1858
79. BESIII Collaboration, M. Ablikim et al., Phys. Rev. Lett. **106**, 072002 (2011). arXiv:1012.3510
80. H. Rothe, Lattice gauge theories: An introduction. World Sci. Lect. Notes Phys. **43**, 1 (1992)
81. M. Creutz, *Quarks, Gluons and Lattices*. Cambridge University Press, Cambridge (1984)
82. T. DeGrand, C.E. Detar, *Lattice Methods for Quantum Chromodynamics*. World Scientific, Singapore (2006)
83. D. Vautherin, F. Lenz, J.W. Negele, NATO Adv. Study Inst. Ser. B Phys. **228**, 1 (1990)
84. R. Gupta, *Introduction to Lattice QCD: Course*, vol. 83 (1997). arXiv:hep-lat/9807028
85. G.P. Lepage, *Lattice QCD for Novices*. arXiv:hep-lat/0506036
86. H. Wittig, *QCD on the Lattice*, in Schopper, H. (ed.), The Landolt-Börnstein Database. Springer, New York (2008)
87. C. Hoelbling, PoS **LATTICE2010**, 011 (2010). arXiv:1102.0410
88. PACS-CS Collaboration, S. Aoki et al., Phys. Rev. **D81**, 074503 (2010). arXiv:0911.2561
89. European Twisted Mass Collaboration, C. Alexandrou et al., Phys. Rev **D80**, 114503 (2009). arXiv:0910.2419
90. European Twisted Mass Collaboration, C. Alexandrou et al., Phys. Rev. **D78**, 014509 (2008). arXiv:0803.3190
91. A. Bazavov et al., Rev. Mod. Phys. **82**, 1349 (2010). arXiv:0911.2561
92. S. Durr et al., Science **322**, 1224 (2008). arXiv:0906.3599
93. B. Blossier, M. Della Morte, G. von Hippel, T. Mendes, R. Sommer, JHEP **0904**, 094 (2009). arXiv:0902.1265
94. T.A. DeGrand, M. Hecht, Phys. Lett. **B275**, 435 (1992)
95. T. Draper, C. McNeile, Nucl. Phys. Proc. Suppl. **34**, 453 (1994). arXiv:hep-lat/9401013
96. UKQCD Collaboration, C. Allton et al., Phys. Rev. **D47**, 5128 (1993). arXiv:hep-lat/9303009
97. S. Gusken et al., Phys. Lett. **B227**, 266 (1989)
98. APE Collaboration, M. Albanese et al., Phys. Lett. **B192**, 163 (1987)
99. A. Hasenfratz, F. Knechtli, Phys. Rev. **D64**, 034504 (2001). arXiv:hep-lat/0103029
100. C. Morningstar, M.J. Peardon, Phys. Rev. **D69**, 054501 (2004). arXiv:hep-lat/0311018
101. Hadron Spectrum Collaboration, M. Peardon et al., Phys. Rev. **D80**, 054506 (2009). arXiv:0905.2160
102. J. Foley et al., Comput. Phys. Commun. **172**, 145 (2005). arXiv:hep-lat/0505023
103. J.J. Dudek et al., Phys. Rev. **D83**, 111502 (2011). arXiv:1102.4299
104. C. Morningstar et al., Phys. Rev. **D83**, 114505 (2011). arXiv:1104.3870
105. J. Foley et al., PoS **LATTICE2010**, 098 (2014). arXiv:1011.0481
106. J. Cornwell, *Group Theory in Physics*, vol. 1. Academic Press, London (1985)
107. J. Cornwell, *Group Theory in Physics*, vol. 2. Academic Press, London (1985)
108. H. Jones, *Groups, Representations and Physics*. Hilger, Bristol (1990)
109. R. Gilmore, *Lie Groups, Lie Algebras, and Some of Their Applications* (2006)
110. C.E. Thomas, R.G. Edwards, J.J. Dudek, Phys. Rev. **D85**, 014507 (2012). arXiv:1107.1930
111. C. Morningstar et al., Phys. Rev. **D88**, 014511 (2013). arXiv:1303.6816
112. Bern-Graz-Regensburg Collaboration, T. Burch et al., Phys. Rev. **D70**, 054502 (2004). arXiv:hep-lat/0405006
113. Hadron Spectrum Collaboration, J. Bulava, R. Edwards, C. Morningstar, PoS **LATTICE2008**, 124 (2008). arXiv:0810.1469
114. J.J. Dudek, R.G. Edwards, N. Mathur, D.G. Richards, Phys. Rev. **D77**, 034501 (2008). arXiv:0707.4162
115. Z. Davoudi, M.J. Savage, Phys. Rev. **D86**, 054505 (2012). arXiv:1204.4146
116. Hadron Spectrum Collaboration, L. Liu et al., JHEP **1207**, 126 (2012). arXiv:1204.5425

117. M. Lüscher, U. Wolff, Nucl. Phys. **B339**, 222 (1990)
118. C. Michael, Nucl. Phys. **B259**, 58 (1985)
119. H. Wittig and others (Eds), In: Proceedings of Science, pos.sissa.it
120. L. Maiani, M. Testa, Phys. Lett. **B245**, 585 (1990)
121. M. Lüscher, Nucl. Phys. **B364**, 237 (1991)
122. K. Rummukainen, S.A. Gottlieb, Nucl. Phys. **B450**, 397 (1995). arXiv:hep-lat/9503028
123. C. Kim, C. Sachrajda, S.R. Sharpe, Nucl. Phys. **B727**, 218 (2005). arXiv:hep-lat/0507006
124. N.H. Christ, C. Kim, T. Yamazaki, Phys. Rev. **D72**, 114506 (2005). arXiv:hep-lat/0507009
125. M. Lüscher, Commun. Math. Phys. **105**, 153 (1986)
126. J.J. Dudek, R.G. Edwards, C.E. Thomas, Phys. Rev. **D86**, 034031 (2012). arXiv:1203.6041
127. J.J. Dudek, R.G. Edwards, C.E. Thomas, Phys. Rev. **D87**, 034505 (2013). arXiv:1212.0830
128. D. Mohler, C. Lang, L. Leskovec, S. Prelovsek, R. Woloshyn, Phys. Rev. Lett. **111**, 222001 (2013). arXiv:1308.3175
129. G. Moir, M. Peardon, S.M. Ryan, C.E. Thomas, L. Liu, (2013). arXiv:1312.1361
130. M.T. Hansen, S.R. Sharpe, Phys. Rev. **D86**, 016007 (2012). arXiv:1204.0826
131. HERMES Collaboration, A. Airapetian et al., Phys. Rev. **D75**, 012007 (2007). arXiv:hep-ex/0609039
132. COMPASS Collaboration, V.Y. Alexakhin et al., Phys. Lett. **B647**, 8 (2007). arXiv:hep-ex/0609038
133. J. Arrington, P. Blunden, W. Melnitchouk, Prog. Part. Nucl. Phys. **66**, 782 (2011). arXiv:1105.0951
134. A. Akhiezer, M. Rekalo, Sov. Phys. Dokl. **13**, 572 (1968)
135. A. Akhiezer, M. Rekalo, Sov. J. Part. Nucl. **4**, 277 (1974)
136. N. Dombey, Rev. Mod. Phys. **41**, 236 (1969)
137. R. Arnold, C.E. Carlson, F. Gross, Phys. Rev. **C23**, 363 (1981)
138. A. Puckett et al., Phys. Rev. **C85**, 045203 (2012). arXiv:1102.5737
139. G.A. Miller, Phys. Rev. Lett. **99**, 112001 (2007). arXiv:0705.2409
140. X. Zhan et al., Phys. Lett. **B705**, 59 (2011). arXiv:1102.0318
141. R. Pohl et al., Nature **466**, 213 (2010)
142. W. Wilcox, T. Draper, K.-F. Liu, Phys. Rev. **D46**, 1109 (1992). arXiv:hep-lat/9205015
143. T. Yamazaki et al., Phys. Rev. **D79**, 114505 (2009). arXiv:0904.2039
144. S. Collins et al., Phys. Rev. **D84**, 074507 (2011). arXiv:1106.3580
145. J. Kelly, Phys. Rev. **C70**, 068202 (2004)
146. J. Green et al., PoS **LATTICE2013**, 276 (2014). arXiv:1310.7043
147. H.-W. Lin, PoS **LATTICE2012**, 013 (2012). arXiv:1212.6849
148. S. Capitani et al., Phys. Rev. **D86**, 074502 (2012). arXiv:1205.0180
149. R. Horsley et al., (2013). arXiv:1302.2233
150. M. Göckeler et al., Phys. Rev. **D54**, 5705 (1996). arXiv:hep-lat/9602029
151. QCDSF Collaboration, M. Göckeler et al., Nucl. Phys. Proc. Suppl. **140**, 399 (2005). arXiv:hep-lat/0409162
152. R. Sommer, (2006). arXiv:hep-lat/0611020
153. K. Jansen et al., Phys. Lett. **B372**, 275 (1996). arXiv:hep-lat/9512009
154. G. Martinelli, C. Pittori, C. T. Sachrajda, M. Testa, A. Vladikas, Nucl. Phys. **B445**, 81 (1995). arXiv:hep-lat/9411010
155. M. Göckeler et al., Phys. Rev. **D82**, 114511 (2010). arXiv:1003.5756
156. Y. Aoki, PoS **LAT2009**, 012 (2009). arXiv:1005.2339
157. D. Müller, D. Robaschik, B. Geyer, F.-M. Dittes, J. Horejsi, Fortsch. Phys. **42**, 101 (1994). arXiv:hep-ph/9812448
158. A. Radyushkin, Phys. Rev. **D56**, 5524 (1997). arXiv:hep-ph/9704207
159. M. Diehl, T. Gousset, B. Pire, J.P. Ralston, Phys. Lett. **B411**, 193 (1997). arXiv:hep-ph/9706344
160. M. Diehl, Eur. Phys. J. **C25**, 223 (2002). arXiv:hep-ph/0205208
161. M. Burkardt, Int. J. Mod. Phys. **A18**, 173 (2003). arXiv:hep-ph/0207047
162. X.-D. Ji, Phys. Rev. Lett. **78**, 610 (1997). arXiv:hep-ph/9603249

163. M. Diehl, Eur. Phys. J. **C19**, 485 (2001). arXiv:hep-ph/0101335
164. M. Burkardt, Phys. Rev. **D62**, 071503 (2000). arXiv:hep-ph/0005108
165. M. Diehl, Phys. Rept. **388**, 41 (2003). arXiv:hep-ph/0307382
166. LHPC collaboration, SESAM collaboration, P. Hägler et al., Phys. Rev. **D68**, 034505 (2003). arXiv:hep-lat/0304018
167. LHPC Collaboration, SESAM Collaboration, LHPC et al., Phys. Rev. Lett. **93**, 112001 (2004). arXiv:hep-lat/0312014
168. M. Göckeler et al., Nucl. Phys. Proc. Suppl. **153**, 146 (2006). arXiv:hep-lat/0512011
169. QCDSF Collaboration, UKQCD Collaboration, M. Göckeler et al., Phys. Rev. Lett. **98**, 222001 (2007). arXiv:hep-lat/0612032
170. QCDSF Collaboration, UKQCD Collaboration, D. Brommel et al., Phys. Rev. Lett. **101**, 122001 (2008). arXiv:0708.2249
171. QCDSF-UKQCD Collaboration, D. Brommel et al., PoS **LAT2007**, 158 (2007). arXiv:0710.1534
172. LHPC Collaborations, P. Hägler et al., Phys. Rev. **D77**, 094502 (2008). arXiv:0705.4295
173. J. Gasser, H. Leutwyler, Phys. Rept. **87**, 77 (1982)
174. J. Donoghue, E. Golowich, B.R. Holstein, Camb. Monogr. Part. Phys. Nucl. Phys. Cosmol. **2**, 1 (1992)
175. A.V. Manohar, M.B. Wise, Camb. Monogr. Part. Phys. Nucl. Phys. Cosmol. **10**, 1 (2000)
176. D.B. Kaplan, nucl-th/0510023 (2005)
177. Y. Nambu, G. Jona-Lasinio, Phys. Rev. **122**, 345 (1961)
178. J. Goldstone, Nuovo Cim. **19**, 154 (1961)
179. C. Vafa, E. Witten, Nucl. Phys. **B234**, 173 (1984)
180. C. Vafa, E. Witten, Phys. Rev. Lett. **53**, 535 (1984)
181. H. Leutwyler, Ann. Phys. **235**, 165 (1994). arXiv:hep-ph/9311274
182. J. Gasser, H. Leutwyler, Ann. Phys. **158**, 142 (1984)
183. A. Morel, J. Phys. (France) **48**, 1111 (1987)
184. C.W. Bernard, M.F. Golterman, Phys. Rev. **D49**, 486 (1994). arXiv:hep-lat/9306005
185. S.R. Sharpe, Phys. Rev. **D56**, 7052 (1997). hep-lat/9707018
186. M.F. Golterman, K.-C. Leung, Phys. Rev. **D57**, 5703 (1998). arXiv:hep-lat/9711033
187. S.R. Sharpe, N. Shoresh, Phys. Rev. **D62**, 094503 (2000). arXiv:hep-lat/0006017
188. S.R. Sharpe, N. Shoresh, Phys. Rev. **D64**, 114510 (2001). arXiv:hep-lat/0108003
189. J. Hu, F.-J. Jiang, B.C. Tiburzi, Phys. Lett. **B653**, 350 (2007). arXiv:0706.3408
190. J. Gasser, H. Leutwyler, Phys. Lett. **B188**, 477 (1987)
191. J. Gasser, H. Leutwyler, Phys. Lett. **B184**, 83 (1987)
192. S.R. Sharpe, R.L. Singleton, Phys. Rev. **D58**, 074501 (1998). arXiv:hep-lat/9804028
193. W.-J. Lee, S.R. Sharpe, Phys. Rev. **D60**, 114503 (1999). arXiv:hep-lat/9905023
194. B. Sheikholeslami, R. Wohlert, Nucl. Phys. **B259**, 572 (1985)
195. S. Aoki, Phys. Rev. **D30**, 2653 (1984)
196. O. Bär, G. Rupak, N. Shoresh, Phys. Rev. **D67**, 114505 (2003). arXiv:hep-lat/0210050
197. J.-W. Chen, D. O'Connell, A. Walker-Loud, JHEP **0904**, 090 (2009). arXiv:0706.0035
198. J.-W. Chen, M. Golterman, D. O'Connell, A. Walker-Loud, Phys. Rev. **D79**, 117502 (2009). arXiv:0905.2566
199. E.E. Jenkins, A.V. Manohar, Phys. Lett. **B255**, 558 (1991)
200. S.R. Beane, M.J. Savage, Phys. Lett. **B556**, 142 (2003). arXiv:hep-ph/0212106
201. L.S. Brown, W. Pardee, R. Peccei, Phys. Rev. **D4**, 2801 (1971)
202. V. Bernard, N. Kaiser, U.-G. Meißner, Phys. Lett. **B389**, 144 (1996). arXiv:hep-ph/9607245
203. A. Kryjevski, Phys. Rev. **D70**, 094028 (2004). arXiv:hep-ph/0312196
204. A. Walker-Loud et al., Phys. Rev. **D79**, 054502 (2009). arXiv:0806.4549
205. V. Bernard, N. Kaiser, U.-G. Meißner, Int. J. Mod. Phys. **E4**, 193 (1995). arXiv:hep-ph/9501384
206. S.L. Adler, Y. Dothan, Phys. Rev. **151**, 1267 (1966)
207. T.R. Hemmert, B.R. Holstein, J. Kambor, J. Phys. **G24**, 1831 (1998). arXiv:hep-ph/9712496
208. J. Gasser, H. Leutwyler, Nucl. Phys. **B250**, 465 (1985)

209. J. Bijnens, I. Jemos, Eur. Phys. J. **C64**, 273 (2009). arXiv:0906.3118
210. M.N. Butler, M.J. Savage, R.P. Springer, Nucl. Phys. **B399**, 69 (1993). arXiv:hep-ph/9211247
211. H.-W. Lin, K. Orginos, Phys. Rev. **D79**, 074507 (2009). arXiv:0812.4456
212. RBC-UKQCD Collaboration, C. Allton et al., Phys. Rev. **D78**, 114509 (2008). arXiv:0804.0473
213. A. Roessl, Nucl. Phys. **B555**, 507 (1999). arXiv:hep-ph/9904230
214. B.C. Tiburzi, A. Walker-Loud, Phys. Lett. **B669**, 246 (2008). arXiv:0808.0482
215. F.-J. Jiang, B.C. Tiburzi, A. Walker-Loud, Phys. Lett. **B695**, 329 (2011). arXiv:0911.4721
216. T. Becher, H. Leutwyler, Eur. Phys. J. **C9**, 643 (1999). arXiv:hep-ph/9901384
217. S.C. Pieper, R.B. Wiringa, Ann. Rev. Nucl. Part. Sci. **51**, 53 (2001). arXiv:nucl-th/0103005
218. D. Dean, M. Hjorth-Jensen, Phys. Rev. **C69**, 054320 (2004). arXiv:nucl-th/0308088
219. S. Bogner, R. Furnstahl, A. Schwenk, Prog. Part. Nucl. Phys. **65**, 94 (2010). arXiv:0912.3688
220. B.R. Barrett, P. Navratil, J.P. Vary, Prog. Part. Nucl. Phys. **69**, 131 (2013)
221. S. Bogner et al., Comput. Phys. Commun. **184**, 2235–2250 (2013). arXiv:1304.3713
222. S.R. Beane, P.F. Bedaque, W.C. Haxton, D.R. Phillips, M.J. Savage, (2000). arXiv:nucl-th/0008064
223. R. Machleidt, D. Entem, Phys. Rept. **503**, 1 (2011). arXiv:1105.2919
224. E. Epelbaum, H.-W. Hammer, U.-G. Meißner, Rev. Mod. Phys. **81**, 1773 (2009). arXiv:0811.1338
225. A.S. Kronfeld, (2012). arXiv:1209.3468
226. Z. Fodor, C. Hoelbling, Rev. Mod. Phys. **84**, 449 (2012). arXiv:1203.4789
227. M. Lüscher, Nucl. Phys. **B354**, 531 (1991)
228. H. Hamber, E. Marinari, G. Parisi, C. Rebbi, Nucl. Phys. **B225**, 475 (1983)
229. E. Beth, G. Uhlenbeck, Physica **4**, 915 (1937)
230. K. Huang, C. Yang, Phys. Rev. **105**, 767 (1957)
231. T. Lee, K. Huang, C. Yang, Phys. Rev. **106**, 1135 (1957)
232. S.R. Beane, P.F. Bedaque, A. Parreño, M.J. Savage, Phys. Lett. **B585**, 106 (2004)
233. D.B. Kaplan, M.J. Savage, M.B. Wise, Phys. Lett. **B424**, 390 (1998). arXiv:nucl-th/9801034
234. S. Beane et al., Phys. Rev. **D87**, 034506 (2013). arXiv:1206.5219
235. P.F. Bedaque, I. Sato, A. Walker-Loud, Phys. Rev. **D73**, 074501 (2006). arXiv:hep-lat/0601033
236. I. Sato, P.F. Bedaque, Phys. Rev. **D76**, 034502 (2007). arXiv:hep-lat/0702021
237. X. Li, C. Liu, Phys. Lett. **B587**, 100 (2004). arXiv:hep-lat/0311035
238. W. Detmold, M.J. Savage, Nucl. Phys. **A743**, 170 (2004). arXiv:hep-lat/0403005
239. X. Feng, K. Jansen, D.B. Renner, PoS **LAT2010**, 104 (2010). arXiv:1104.0058
240. M. Göckeler et al., Phys. Rev. **D86**, 094513 (2012). arXiv:1206.4141
241. N. Li, C. Liu, Phys. Rev. **D87**, 014502 (2013). arXiv:1209.2201
242. R.A. Briceno, Z. Davoudi, Phys. Rev. **D88**9, 094507 (2013). arXiv:1204.1110
243. M. Döring, U.G. Meißner, E. Oset, A. Rusetsky, Eur. Phys. J. **A48**, 114 (2012)
244. Z. Fu, Phys. Rev. **D85**, 014506 (2012). arXiv:1110.0319
245. L. Leskovec, S. Prelovsek, Phys. Rev. **D85**, 114507 (2012). arXiv:1202.2145
246. S. Bour, S. Koenig, D. Lee, H.W. Hammer, U.-G. Meißner, Phys. Rev. **D84**, 091503 (2011)
247. Z. Davoudi, M.J. Savage, Phys. Rev. **D84**, 114502 (2011). arXiv:1108.5371
248. C. Liu, X. Feng, S. He, Int. J. Mod. Phys. **A21**, 847 (2006). arXiv:hep-lat/0508022
249. M. Lage, U.-G. Meißner, A. Rusetsky, Phys. Lett. **B681**, 439 (2009). arXiv:0905.0069
250. V. Bernard, M. Lage, U.-G. Meißner, A. Rusetsky, JHEP **1101**, 019 (2011). arXiv:1010.6018
251. S. He, X. Feng, C. Liu, JHEP **07**, 011 (2005). arXiv:hep-lat/0504019
252. T. Luu, M.J. Savage, Phys. Rev. **D83**, 114508 (2011). arXiv:1101.3347
253. J. M.M. Hall et al., PoS **LATTICE2012**, 145 (2012)
254. E. Berkowitz, T.D. Cohen, P. Jefferson, (2012). arXiv:1211.2261
255. E. Oset, Eur. Phys. J. **A49**, 32 (2013). arXiv:1211.3985
256. I. Montvay, C. Urbach, Eur. Phys. J. **A48**, 38 (2012). arXiv:1105.5009
257. T. Luu, M.J. Savage, A. Schwenk, J.P. Vary, Phys. Rev. **C82**, 034003 (2010). arXiv:1006.0427

258. M. Doring, U.-G. Meißner, E. Oset, A. Rusetsky, Eur. Phys. J. **A47**, 139 (2011). arXiv:1107.3988, 15 pages, 17 figures
259. H.-X. Chen, E. Oset, Phys. Rev. **D87**, 016014 (2013). arXiv:1202.2787
260. M. Albaladejo, J.A. Oller, E. Oset, G. Rios, L. Roca, JHEP **08**, 071 (2012). arXiv:1205.3582
261. L. Roca, E. Oset, Phys. Rev. **D85**, 054507 (2012). arXiv:1201.0438
262. J.-J. Xie, E. Oset, Eur. Phys. J. **A48**, 146 (2012). arXiv:1201.0149
263. M. Döring, U. G. Meißner, JHEP **01**, 009 (2012). arXiv:1111.0616
264. E. Oset, M. Döring, U.G. Meißner, A. Rusetsky, (2011). arXiv:1108.3923
265. P.F. Bedaque, Phys. Lett. **B593**, 82 (2004). arXiv:nucl-th/0402051
266. B.C. Tiburzi, Phys. Lett. **B617**, 40 (2005). arXiv:hep-lat/0504002
267. B.C. Tiburzi, Phys. Lett. **B641**, 342 (2006). arXiv:hep-lat/0607019
268. F.-J. Jiang, B. Tiburzi, Phys. Lett. **B645**, 314 (2007). arXiv:hep-lat/0610103
269. F.-J. Jiang, B.C. Tiburzi, Phys. Rev. **D78**, 037501 (2008). arXiv:0806.4371
270. F.-J. Jiang, B. Tiburzi, Phys. Rev. **D78**, 114505 (2008). arXiv:0810.1495
271. C. Sachrajda, G. Villadoro, Phys. Lett. **B609**, 73 (2005). arXiv:hep-lat/0411033
272. P.F. Bedaque, J.-W. Chen, Phys. Lett. **B616**, 208 (2005). arXiv:hep-lat/0412023
273. U. Wiese, Nucl. Phys. Proc. Suppl. **9**, 609 (1989)
274. T.A. DeGrand, Phys. Rev. **D43**, 2296 (1991)
275. P. Eugenio, PoS **ConfinementX**, 349 (2012)
276. S. Marcello, Hyperfine Interact. **209**, 93 (2012)
277. P. Wang, Nucl. Phys. Proc. Suppl. **225–227**, 97 (2012)
278. S.A. Gottlieb, K. Rummukainen, Nucl. Phys. Proc. Suppl. **47**, 819 (1996). arXiv:hep-lat/9509088
279. D. Mohler, PoS **LATTICE2012**, 003 (2012). arXiv:1211.6163
280. E. Elizalde, Commun. Math. Phys. **198**, 83 (1998). arXiv:hep-th/9707257
281. S. Sasaki, T. Yamazaki, Phys. Rev. **D74**, 114507 (2006). arXiv:hep-lat/0610081
282. J. Balog et al., Phys. Rev. **D60**, 094508 (1999). arXiv:hep-lat/9903036
283. C. Lin, G. Martinelli, C.T. Sachrajda, M. Testa, Nucl. Phys. **B619**, 467 (2001). arXiv:hep-lat/0104006
284. CP-PACS Collaboration, S. Aoki et al., Phys. Rev. **D71**, 094504 (2005). arXiv:hep-lat/0503025
285. N. Ishii, S. Aoki, T. Hatsuda, Phys. Rev. Lett. **99**, 022001 (2007). arXiv:nucl-th/0611096
286. S. Aoki et al., PTEP **2012**, 01A105 (2012). arXiv:1206.5088
287. A. Mihaly, H. Fiebig, H. Markum, K. Rabitsch, Phys. Rev. **D55**, 3077 (1997)
288. UKQCD Collaboration, C. Michael, P. Pennanen, Phys. Rev. **D60**, 054012 (1999). arXiv:hep-lat/9901007
289. T. Doi, T.T. Takahashi, H. Suganuma, AIP Conf. Proc. **842**, 246 (2006). arXiv:hep-lat/0601008
290. W. Detmold, K. Orginos, M.J. Savage, Phys. Rev. **D76**, 114503 (2007). arXiv:hep-lat/0703009
291. Z.S. Brown, K. Orginos, Phys. Rev. **D86**, 114506 (2012). arXiv:1210.1953
292. P. Bicudo, M. Wagner, Phys. Rev. **D87**, 114511 (2013). arXiv:1209.6274
293. K. Murano, N. Ishii, S. Aoki, T. Hatsuda, Prog. Theor. Phys. **125**, 1225 (2011). arXiv:1103.0619
294. T. Inoue et al., Nucl. Phys. **A881**, 28 (2012). arXiv:1112.5926
295. N. Ishii, (2012), presentation at *Chiral Dynamics 2012*,http://www.jlab.org/conferences/CD12/thursday/Ishii.pdf
296. S.R. Beane, W. Detmold, K. Orginos, M.J. Savage, Prog. Part. Nucl. Phys. **66**, 1 (2011)
297. M.C. Birse, (2012). arXiv:1208.4807
298. S. Aoki, (2009), lectures at *13^{th} Taiwan Nuclear Physics Summer School*, Hsinchu, Taiwan, http://phys.cts.ntu.edu.tw/nuclear/2009/Aoki3.pdf
299. HAL QCD Collaboration, N. Ishii et al., Phys. Lett. **B712**, 437 (2012). arXiv:1203.3642
300. M. Osborne, G.K. Smyth, SIAM J. Sci. Comput. **16**, 119 (1995)
301. K. Murano et al., Phys. Lett. **B735**, 19–24 (2014). arXiv:1305.2293

302. S. Aoki et al., Phys. Rev. **D87**, 034512 (2013). arXiv:1212.4896
303. T. Kurth, N. Ishii, T. Doi, S. Aoki, T. Hatsuda, JHEP **1312**, 015 (2013). arXiv:1305.4462
304. I. Montvay, P. Weisz, Nucl. Phys. **B290**, 327 (1987)
305. C. Gattringer, C. Lang, Phys. Lett. **B274**, 95 (1992)
306. C. Gattringer, C. Lang, Nucl. Phys. **B391**, 463 (1993). arXiv:hep-lat/9206004
307. J. Nishimura, Nucl. Phys. Proc. Suppl. **26**, 542 (1992)
308. M. Göckeler, H.A. Kastrup, J. Westphalen, F. Zimmermann, Nucl. Phys. **B425**, 413 (1994). arXiv:hep-lat/9402011
309. S.R. Sharpe, R. Gupta, G.W. Kilcup, Nucl. Phys. **B383**, 309 (1992)
310. CP-PACS Collaboration, T. Yamazaki et al., Phys. Rev. **D70**, 074513 (2004). arXiv:hep-lat/0402025
311. J.J. Dudek et al., Phys. Rev. **D83**, 071504 (2011)
312. S.R. Beane et al., Phys. Rev. **D85**, 034505 (2012). arXiv:1107.5023
313. Z. Fu, Commun. Theor. Phys. **57**, 78 (2012). arXiv:1110.3918
314. W. Detmold, B. Smigielski, Phys. Rev. **D84**, 014508 (2011). arXiv:1103.4362
315. W. Detmold, K. Orginos, Z. Shi, Phys. Rev. **D86**, 054507 (2012). arXiv:1205.4224
316. T. Yagi, S. Hashimoto, O. Morimatsu, M. Ohtani, (2011). arXiv:1108.2970
317. Q. Liu, PoS **LAT2009**, 101 (2009). arXiv:0910.2658
318. T. Blum et al., Phys. Rev. **D84**, 114503 (2011). arXiv:1106.2714
319. J. Frison et al., PoS **LATTICE2010**, 139 (2010). arXiv:1011.3413
320. X. Feng, K. Jansen, D.B. Renner, Phys. Rev. **D83**, 094505 (2011). arXiv:1011.5288
321. C. Lang, D. Mohler, S. Prelovsek, M. Vidmar, Phys. Rev. **D84**, 054503 (2011). arXiv:1105.5636
322. CS Collaboration, S. Aoki et al., Phys. Rev. **D84**, 094505 (2011). arXiv:1106.5365
323. C. Pelissier, A. Alexandru, Phys. Rev. **D87**, 014503 (2013). arXiv:1211.0092
324. K. Sasaki, N. Ishizuka, T. Yamazaki, M. Oka, Prog. Theor. Phys. Suppl. **186**, 187 (2010)
325. Z. Fu, Phys. Rev. **D85**, 074501 (2012). arXiv:1110.1422
326. C.B. Lang, L. Leskovec, D. Mohler, S. Prelovsek, Phys. Rev. **D86**, 054508 (2012)
327. Z. Fu, K. Fu, Phys. Rev. **D86**, 094507 (2012). arXiv:1209.0350
328. D. Mohler, S. Prelovsek, R. Woloshyn, Phys. Rev. **D87**, 034501 (2013). arXiv:1208.4059
329. K. Liu, Sci. China Phys. Mech. Astron. **55**, 2326 (2012)
330. G.-Z. Meng et al., Phys. Rev. **D80**, 034503 (2009). arXiv:0905.0752
331. S. Prelovsek, L. Leskovec, Phys. Lett. **B727**, 172–176 (2013). arXiv:1308.2097
332. S. Prelovsek, L. Leskovec, Phys. Rev. Lett. **111**, 192001 (2013). arXiv:1307.5172
333. S. Ozaki, S. Sasaki, Phys. Rev. **D87**, 014506 (2013). arXiv:1211.5512
334. W. Detmold, S. Meinel, Z. Shi, Phys. Rev. **D87**, 094504 (2013). arXiv:1211.3156
335. D. Kaplan, A. Nelson, Nucl. Phys. **A479**, 273 (1988)
336. A. Torok et al., Phys. Rev. **D81**, 074506 (2010). arXiv:0907.1913
337. C. Lang, V. Verduci, Phys. Rev. **D87**, 054502 (2013). arXiv:1212.5055
338. S.R. Beane et al., Phys. Rev. **D79**, 114502 (2009). arXiv:0903.2990
339. W. Detmold, A.N. Nicholson, Phys. Rev. **D88**, 074501 (2013). arXiv:1308.5186
340. S.R. Beane et al., Phys. Rev. Lett. **109**, 172001 (2012). arXiv:1204.3606
341. S. Beane et al., Phys. Rev. **C88**(2), 024003 (2013). arXiv:1301.5790
342. HAL QCD collaboration, T. Inoue et al., Prog. Theor. Phys. **124**, 591 (2010). arXiv:1007.3559
343. M.I. Buchoff, T.C. Luu, J. Wasem, Phys. Rev. **D85**, 094511 (2012). arXiv:1201.3596
344. T. Yamazaki, K.-i. Ishikawa, Y. Kuramashi, A. Ukawa, Phys. Rev. **D86**, 074514 (2012)
345. S.R. Beane et al., Phys. Rev. Lett. **106**, 162001 (2011). arXiv:1012.3812
346. R.L. Jaffe, Phys. Rev. Lett. **38**, 195 (1977). [Erratum-ibid. **38**, 617 (1977)]
347. T. Inoue et al., Phys. Rev. Lett. **106**, 162002 (2011). arXiv:1012.5928
348. S.R. Beane et al., Mod. Phys. Lett. **A26**, 2587 (2011). arXiv:1103.2821
349. T. Yamazaki, Y. Kuramashi, A. Ukawa, Phys. Rev. **D84**, 054506 (2011). arXiv:1105.1418
350. P. Shanahan, A. Thomas, R. Young, Phys. Rev. Lett. **107**, 092004 (2011). arXiv:1106.2851
351. J. Haidenbauer, U.-G. Meißner, Phys. Lett. **B706**, 100 (2011). arXiv:1109.3590
352. P. Shanahan, A. Thomas, R. Young, (2013). arXiv:1308.1748

353. S.R. Beane, W. Detmold, M.J. Savage, Phys. Rev. **D76**, 074507 (2007). arXiv:0707.1670
354. W. Detmold, M.J. Savage, Phys. Rev. **D77**, 057502 (2008). arXiv:0801.0763
355. T. Luu, PoS **LATTICE2008**, 246 (2008). arXiv:0810.2331
356. S. Kreuzer, H.W. Hammer, Phys. Lett. **B694**, 424 (2011). arXiv:1008.4499
357. S. Kreuzer, H.W. Grießhammer, Eur. Phys. J. **A48**, 93 (2012). arXiv:1205.0277
358. P. Guo, J. Dudek, R. Edwards, A.P. Szczepaniak, Phys. Rev. **D88**(1), 014501 (2013). arXiv:1211.0929
359. R.A. Briceno, Z. Davoudi, Phys. Rev. **D87**(9), 094507 (2013). arXiv:1212.3398
360. K. Polejaeva, A. Rusetsky, Eur. Phys. J. **A48**, 67 (2012). arXiv:1203.1241
361. M.T. Hansen, S.R. Sharpe, (2013). arXiv:1311.4848
362. S.R. Beane et al., Phys. Rev. Lett. **100**, 082004 (2008). arXiv:0710.1827
363. W. Detmold et al., Phys. Rev. **D78**, 014507 (2008). arXiv:0803.2728
364. W. Detmold, M.J. Savage, Phys. Rev. **D82**, 014511 (2010). arXiv:1001.2768
365. HAL QCD Collaboration, T. Doi, PoS **LATTICE2011**, 151 (2011). arXiv:1112.4103
366. S. Tan, Phys. Rev. **A78**, 013636 (2008). arXiv:0709.2530
367. B. Smigielski, J. Wasem, Phys. Rev. **D79**, 054506 (2009). arXiv:0811.4392
368. B. Borasoy, E. Epelbaum, H. Krebs, D. Lee, U.-G. Meißner, Eur. Phys. J. **A31**, 105 (2007). arXiv:nucl-th/0611087
369. E. Epelbaum, H. Krebs, D. Lee, U.-G. Meißner, Eur. Phys. J. **A41**, 125 (2009). arXiv:0903.1666
370. E. McCutchan et al., Phys. Rev. Lett. **103**, 192501 (2009). arXiv:0907.3688
371. Z. Shi, W. Detmold, PoS **LATTICE2011**, 328 (2011). arXiv:1111.1656
372. Y. Hida, X.S. Li, D.H. Bailey, Algorithms for quad-double precision floating point arithmetic, in *Proceedings. 15th IEEE Symposium on Computer Arithmetic, 2001*, pp. 155–162. IEEE (2001)
373. D.H. Bailey, Y. Hida, X.S. Li, B. Thompson, Arprec an arbitrary precision computation package (2002)
374. T. Doi, M.G. Endres, Comput. Phys. Commun. **184**, 117 (2013). arXiv:1205.0585
375. W. Detmold, K. Orginos, Phys. Rev. **D87**, 114512 (2013). arXiv:1207.1452
376. J. Gunther, B.C. Toth, L. Varnhorst, Phys. Rev. **D87**, 094513 (2013). arXiv:1301.4895
377. W. Detmold, K. Orginos, M.J. Savage, A. Walker-Loud, Phys. Rev. **D78**, 054514 (2008). arXiv:0807.1856
378. Z. Shi, Multi-meson systems form Lattice Quantum Chromodynamics. PhD thesis, College of William & Mary (2013)
379. D.T. Son, M.A. Stephanov, Phys. Rev. Lett. **86**, 592 (2001). arXiv:hep-ph/0005225
380. W. Detmold, M.J. Savage, Phys. Rev. Lett. **102**, 032004 (2009). arXiv:0809.0892
381. W. Detmold, H.-W. Lin, PoS **LATTICE2011**, 149 (2011). arXiv:1112.5682
382. S.R. Beane et al., Phys. Rev. **D80**, 074501 (2009). arXiv:0905.0466
383. G.P. Lepage, Invited lectures given at TASI'89 Summer School, Boulder, CO, Jun 4–30, 1989
384. T. Yamazaki, Y. Kuramashi, A. Ukawa, Phys. Rev. **D81**, 111504 (2010). arXiv:0912.1383
385. J.D. Barrow, F.J. Tipler, *The Anthropic Cosmological Principle*. Clarendon Press, Oxford (1986)
386. B. Carr, (ed.), *Universe of Multiverse?* Cambrige University Press, Cambrige (2007)
387. E. Epelbaum, H. Krebs, T.A. Lahde, D. Lee, U.-G. Meißner, Phys. Rev. Lett. **112502**, 110 (2013). arXiv:1212.4181
388. N. Barnea, L. Contessi, D. Gazit, F. Pederiva, U. van Kolck, (2013). arXiv:1311.4966
389. M. Lüscher, P. Weisz, JHEP **09**, 010 (2001). arXiv:hep-lat/0108014
390. M. Della Morte, L. Giusti, Comput. Phys. Commun. **180**, 819 (2009). arXiv:0806.2601
391. G.S. Bali, S. Collins, A. Schäfer, Comput. Phys. Commun. **181**, 1570 (2010). arXiv:0910.3970
392. T. Blum, T. Izubuchi, E. Shintani, Phys. Rev. **D88**(9), 094503 (2013). arXiv:1208.4349
393. P. de Forcrand, PoS **LAT2009**, 010 (2009). arXiv:1005.0539
394. S. Beane, S. Cohen, W. Detmold, H.W. Lin, M. Savage, (2013). arXiv:1306.6939
395. H.B. Meyer, (2012). arXiv:1202.6675

396. T. Blum et al., Phys. Rev. **D86**, 074513 (2012). arXiv:1206.5142
397. L. Lellouch, M. Lüscher, Commun. Math. Phys. **219**, 31 (2001). arXiv:hep-lat/0003023
398. V. Bernard, M. Lage, U.-G. Meißner, A. Rusetsky, JHEP **08**, 024 (2008). arXiv:0806.4495
399. B. Tiburzi, PoS **LATTICE2011**, 020 (2011). arXiv:1110.6842
400. T. Blum et al., USQCD whitepaper: Lattice qcd at the intensity frontier, http://www.usqcd.org/documents/13flavor.pdf, 2013
401. N. Christ, T. Izubuchi, C. Sachrajda, A. Soni, J. Yu, Phys. Rev. **D88**(1), 014508 (2013). arXiv:1212.5931
402. L.G. Yaffe, B. Svetitsky, Phys. Rev. **D26**, 963 (1982)
403. T.A. DeGrand, C.E. DeTar, Nucl. Phys. **B225**, 590 (1983)
404. WHOT-QCD Collaboration, S. Ejiri et al., Central Eur. J. Phys. **10**, 1322 (2012). arXiv:1203.3793
405. A. Patel, Nucl. Phys. **B243**, 411 (1984)
406. A. Patel, Phys. Lett. **B139**, 394 (1984)
407. F. Karsch, E. Laermann, A. Peikert, Nucl. Phys. **B605**, 579 (2001). arXiv:hep-lat/0012023
408. A. Bazavov et al., Phys. Rev. **D80**, 014504 (2009). arXiv:0903.4379
409. A. Jakovac, P. Petreczky, K. Petrov, A. Velytsky, Phys. Rev. **D75**, 014506 (2007). arXiv:hep-lat/0611017
410. M. Asakawa, T. Hatsuda, Y. Nakahara, Prog. Part. Nucl. Phys. **46**, 459 (2001). arXiv:hep-lat/0011040
411. F. Karsch, E. Laermann, P. Petreczky, S. Stickan, I. Wetzorke, Phys. Lett. **B530**, 147 (2002). arXiv:hep-lat/0110208
412. H.B. Meyer, Phys. Rev. Lett. **100**, 162001 (2008). arXiv:0710.3717
413. R.D. Pisarski, F. Wilczek, Phys. Rev. **D29**, 338 (1984)
414. E. Laermann, O. Philipsen, Ann. Rev. Nucl. Part. Sci. **53**, 163 (2003). arXiv:hep-ph/0303042
415. A. Bazavov et al., Phys. Rev. **D85**, 054503 (2012). arXiv:1111.1710
416. H. Ohno, U. Heller, F. Karsch, S. Mukherjee, PoS **LATTICE2011**, 210 (2011). arXiv:1111.1939
417. H. Ohno, U. Heller, F. Karsch, S. Mukherjee, PoS **LATTICE2012**, 095 (2012). arXiv:1211.2591
418. HotQCD Collaboration, A. Bazavov et al., Phys. Rev. **D86**, 094503 (2012). arXiv:1205.3535
419. C. DeTar et al., Phys. Rev. **D81**, 114504 (2010). arXiv:1003.5682
420. C. Bernard et al., Phys. Rev. **D77**, 014503 (2008). arXiv:0710.1330
421. HotQCD Collaboration, A. Bazavov et al., Phys. Rev. **D86**, 034509 (2012). arXiv:1203.0784